Effects of powder conditioning on the quality, microstructure and mechanical properties of sintered titanium alloys

A thesis

submitted in fulfilment

of the requirements for the degree

of

Doctor of Philosophy in Engineering

at

The University of Waikato

by

Jia Lou

THE UNIVERSITY OF
WAIKATO
Te Whare Wānanga o Waikato

2015

Abstract

A small amount of internal lubricant (Stearic acid (SA) or Magnesium stearate (MgSt)) was added to Ti powder for the purpose of improving the compressibility and the green density homogeneity. Lubrication improved the compressibility of Ti powder compacts, especially in the low pressure region (<400MPa), yet at higher pressures, lubricants hindered further improvement. An addition of up to 0.3wt.% SA improved the green density. MgSt showed a better lubrication effect and an addition of up to 0.6wt.% improved the density. The difference in the lubrication effect between SA and MgSt was due to their mixing or blending characteristics. A homogenous mixing of lubricant led to an increased lubricated area and the effectiveness of the lubrication. Lubricants had a strong influence on shape retention, green strength and ejection behaviour of Ti powder compacts.

The green density distribution was improved by adding a lubricant. The density profiles were measured experimentally using a coloured layer method. SA gave better results compared with MgSt, with 0.6wt.% of SA considered to be the optimum addition. The mixing or blending characteristics of SA additions accounted for the better improvement in performance.

By adding a lubricant, the sintered density distribution in Ti compacts was improved by controlling the pore morphology with respect to their size, aspect ratio and orientation. But 1wt.% SA created many pores ranging in size from 50-100μm, both in the top and bottom regions, and this led to very bad ductility. The consistency in mechanical properties of a sintered Ti Φ40 mm compact was significantly improved by adding 0.6wt.% SA. Such improvement was achieved because of a lower sintering mismatch initiated from a more homogenously distributed green density, both in the horizontal and transverse directions. MgSt was not recommended because of higher oxygen pick-up.

Rare earth elements (RE) were added to Ti metal and alloy for the purpose of scavenging oxygen and to promote better microstructural control. Three additive forms were studied. Er and LaB_6 additions were added to Ti and Ti6Al4V alloys directly. The Ti(Ti6Al4V)-Y alloy was made by mechanical milling (MM). But direct Er additions caused a segregated microstructure and processing involving the MM of Ti(Ti6Al4V)-Y leaded to oxygen pick-up. These methods are therefore not recommended. Direct LaB_6 additions achieved excellent results. The reinforcement was uniformly distributed with various orientations and the microstructure was refined. The TiB reinforcement gave excellent strength and good ductility. The acicular TiB phase seemed to be the only problem, because while it significantly improved the strength it decreased the ductility.

Theoretical research was carried out on the compaction process for internally lubricated Ti powder. A modified Cooper-Eaton formula was employed to analyse the compaction behaviour of Ti powder. There was a good fit between the simulation results and the experimental data. The theoretical research indicated that cold compaction of titanium powder could be separated into two stages: a particle rearrangement (PR) stage, which occurred in a compacting pressure range of 0-200MPa, followed by a plastic deformation (PD) initiated (PR) stage from 200-1000MPa. The existence of stage II was due to the low plastic deformability of titanium and the low density achieved at the end of stage I. Ti particles needed to be plastically deformed or even cracked into fragments to fill the gaps in-between Ti particles. At pressures between 200-600MPa, the use of an internal lubricant improved consolidation, leading to better densification because a lubricant facilitates particle motion. On the basis of this discussion, the approaches for modifying the cold compaction behaviour of Ti powder were studied.

List of Publications

Journal papers:

1. **J. Lou**, Y.M. Li, H. He, and L.J. Li, "Effect of atomisation medium on sintering properties of austenitic stainless steel by eliminating influence of particle shape and particle size." *Powder Metallurgy*, 53.2 (2010): 112-117.
2. Y.H. Hu, Y.M. Li, H. He, **J. Lou** and X. Tang. "Preparation and Mechanical Properties of Inconel718 Alloy by Metal Injection Molding." *Rare Metal Materials and Engineering*, 39.5 (2010): 775-780.
3. **J. Lou**, B. Gabbitas and D.L. Zhang, "Improving the uniformity in mechanical properties of a sintered Ti compact using a trace amount of internal lubricant", submitted to *Journal of Materials Processing Technology*, 24.9 (2014): 1798–1805
4. **J. Lou**, B. Gabbitas, and D.L. Zhang, "Effects of Initial Powder Compact Thickness, Lubrication and Particle Morphology on the Cold Compaction Behaviour of Ti Powder", submitted to *Metallurgical and Materials Transaction A*, in revision.
5. **J. Lou**, B. Gabbitas, S.Raynova, and F.Yang, "A sintering and open die forging process for a P/M Ti alloy with additions of a trace amount of erbium", submitted to *Powder Metallurgy*, in revision.

Conference Papers:

1. **J. Lou**, B. Gabbitas, and D.L. Zhang. "Effects of lubrication on the powder metallurgy processing of titanium.", *Key Engineering Materials* 520 (2012): 133-138.
2. **J. Lou**, B. Gabbitas, and D.L. Zhang. "The Effects of Lubrication on the Density Gradient of Titanium Powder Compacts.", *Key Engineering Materials* 551 (2013): 86-91.

Other conference presentations:

1. **J. Lou**, B. Gabbitas, and D.L. Zhang. "Theoretical Calculation for Internally Lubricated Ti Powder Compaction", International Titanium Powder Processing, Consolidation and Metallurgy Conference, Hamilton, New Zealand, 2013.
2. **J. Lou**, B. Gabbitas, and D.L. Zhang. "TEM observation of a Ti alloy with Yttrium additions fabricated by Mechanical Milling, Cold Compaction & Sintering.", 26th New Zealand Conference on Microscopy, Christchurch, New

Zealand, 2013.

3. **J. Lou** and B. Gabbitas. “Sintering & OPF process of P/M Ti alloy with a trace amount of Er addition”, NZ conference of Chemical and Materials Engineering 2013, Auckland, New Zealand, 2013.
4. **J. Lou** and B. Gabbitas. “Effects of LaB6 Addition on the Microstructure and Mechanical Properties of P/M Ti Alloy”, The 11th Asia-Pacific Conference on Materials Processing, Auckland, New Zealand, 2014.

Acknowledgements

First and foremost, I would like to acknowledge and extend my heartfelt gratitude to my chief supervisor—Professor Brian Gabbitas, for his vital encouragement and patient guidance, generous assistance and invaluable advice, all of which have been of inestimable worth to the completion of my thesis.

I would like to extend my appreciation to my associate supervisor Professor Deliang Zhang, Shanghai Jiao Tong University, Shanghai, China, for providing advice when I needed it.

My special thanks go to all people have helped and taught me during the three years of my study in the University of Waikato. And I would also like to thank all the classmates and friends who have given me generous support and helpful advice during the past years. They have provided much help and comprehensive supervision throughout the last four years. I have benefited a great deal from their advice and suggestions:

-Dr Fei Yang, Stella Raynova, Chris Wang, Yuanji Zhang, Brett Nichol for their technical support

-Huiyang Lu, Qian Xu, Mingtu Jia, Denshan Zhou, Paul Ewart and other group members for their full cooperation

-Dr Peng Cao, Changzhou Yu, from the University of Auckland, for their kindly help and suggestions

Also, special thanks to my parents for their patience and support during my PhD study.

Table of Contents

List of Figures

List of Tables

Abbreviations

BSE	Back Scattered Electron
CP	Commercial pure
DTA	Differential Thermal Analysis
DWL	Die wall lubrication
EDX	Energy Dispersive X-ray analysis
GA	Gas atomised
H/D	Height/radius
HDH	Hydrogenation–dehydrogenation
MgSt	Magnesium stearate
MIM	Metal injection moulding
MM	Mechanical milling
ODF	Open die forging
OM	Optical Microscopy
PD	Plastic deformation
P/M	Powder metallurgy
PPB	Prior particle boundary
PR	Particle rearrangement
PREP	Plasma rotating electrode process
PW	Paraffin wax
RE	Rare earth
SA	Stearic acid
SDT	Simultaneous DTA/TGA
SEM	Scanning electron microscopy
TEM	Transmission electron microscopy
TGA	Thermogravimetic analysis
XRD	X-Ray Diffractometry

1. Chapter 1 Introduction

1.1 Titanium and P/M processing

Strengths of up to 1380MPa, coupled with a density of 4.505 g/cm^3, give titanium and titanium alloys excellent strength to weight ratio. An adherent, protective TiO_2 film provides excellent resistance to corrosion and contamination below 535℃. Above 535℃, the oxide film breaks down and small atoms such as carbon, oxygen, nitrogen, and hydrogen embrittle the titanium [1].

Titanium alloys have many favourable properties such as high strength to weight ratio, good ductility and fracture toughness, high corrosion resistance, high melting point and good biocompatibility with human tissues, making them very important engineering materials for many applications in aerospace, chemical engineering, automotive, biomedical and other industries [2]. Fig. 1.1 and 1.2 show the development of Ti production and Ti mill product shipments during recent years [3]. In the meantime, there is a strong demand for titanium alloys, driven by the fast economic development of countries such as China and India and a strong interest in using titanium alloys for more general engineering applications. Because of the relatively high cost of titanium and titanium alloys, there is an opportunity for reducing the price of parts through more cost-effective manufacturing.

However, a main challenge confronting more widespread titanium use is its cost-affordability. The average utilization of wrought titanium is about 10-15% [4]. Titanium is very hard to machine and not easy to recycle by re-melting. It is an extremely reactive metal and readily absorbs oxygen, hydrogen and carbon, which means that melting and hot working needs to be carried out under either a vacuum or a protective atmosphere. The production of sponge Ti needs to be carried out in

argon gas at temperatures under 850-900℃. Moreover, argon gas is required at temperatures above 1600℃ during the melting of Ti sponge. Otherwise the impurity pick-up will significantly degrade the properties of the final product. In addition, further processing of titanium sponge by Vacuum Arc Remelting (VAR) to produce a titanium ingot and further processing by forging, rolling and extrusion to give milled products, which then require machining, adds further to the cost.

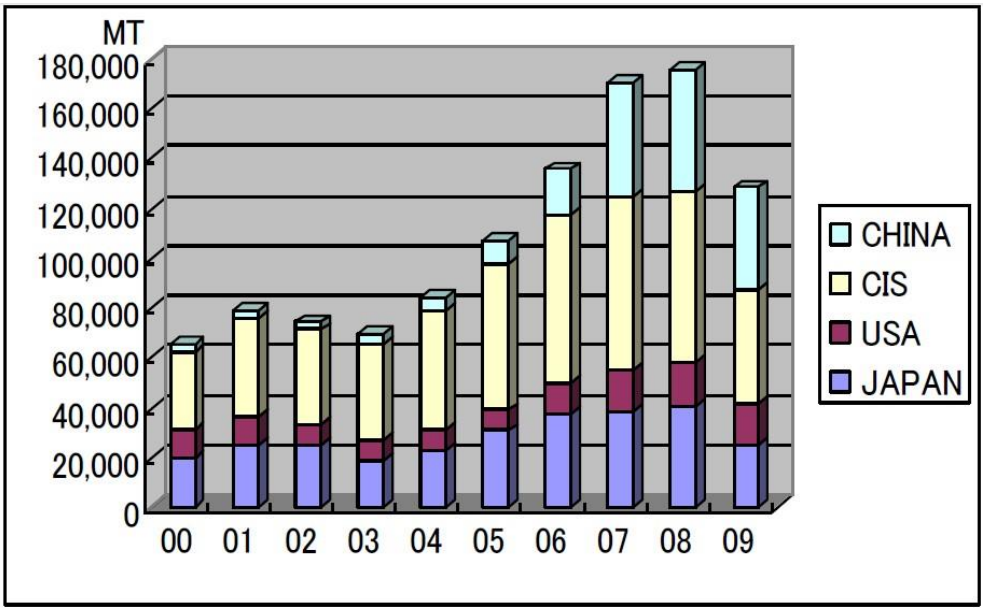

Fig. 1.1 The amount of Ti sponge produced in the main sponge making countries as a function of fiscal year: courtesy of Japan Titanium Society [3]

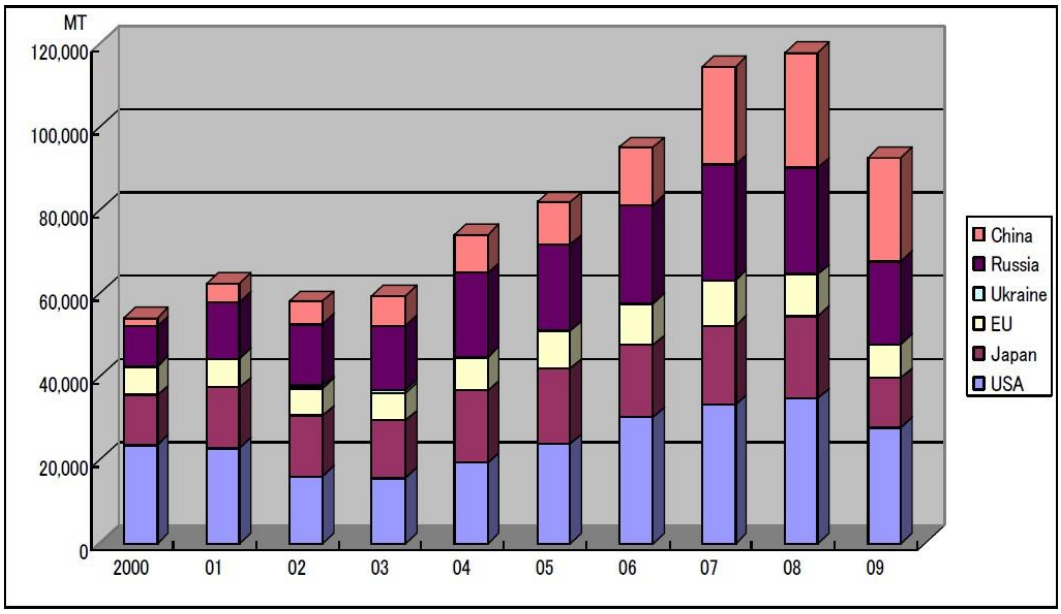

Fig. 1.2 The amount of Ti mill products in the main mill production countries as a function of fiscal year: courtesy of Japan Titanium Society [3]

As a result, the attractiveness of (Powder Metallurgy) P/M Ti is increasing. A titanium component can be fabricated through a variety of P/M techniques, such as cold compaction & sintering, hot compaction & hot working, direct hot isostatic pressing, metal injection moulding (MIM) & sintering etc. Cold compaction & sintering is the most economical and simplest approach to manufacture a Ti component with near-net-shape. A schematic picture of the P/M process is shown in Fig. 1.3.

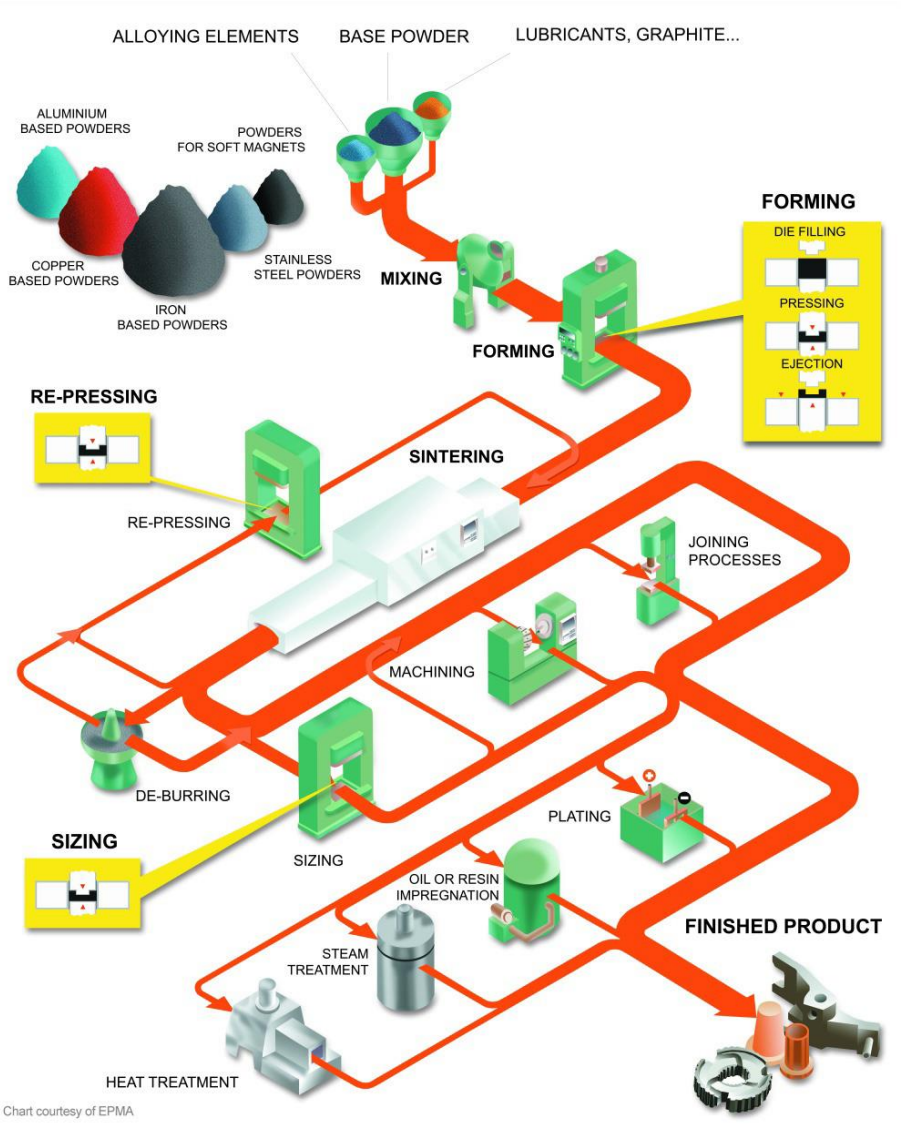

Fig. 1.3 The powder metallurgy process [5]

1.2 Compaction and its drawbacks

The compaction process plays a fundamental role in powder metallurgy and structural ceramics' manufacturing. The compaction of metal powders has the following major functions [6]:

(a) to consolidate the powder into a desired shape

(b) to impart, to as high a degree as possible, the desired final dimensions with due consideration to any dimensional changes resulting from sintering.

(c) to impart the desired level and type of porosity.

(d) to impart adequate strength for subsequent handling.

Unfortunately, conventional cold compaction and sintering has its own drawbacks. Powders with high hardness or work hardenability are quite hard to compact into shape because a very high compaction pressure is required. Compacts pressed under this process are always associated with large green density variation and such pressures may damage the die set through wear and galling. Moreover, with the development of alloying, the compositions of useful alloys have become more and more complicated. Obtaining a pre-alloyed powder can be quite expensive and some compositions are difficult or impossible to obtain. To get around this problem a blended elemental powder or a base metal plus master alloy powder can be used. The compressibility of the mixed powder and the homogeneity of this mixture are uncertain, but by mechanically milling a powder mixture to obtain a particular alloy, the homogeneity is improved. However the work hardening effect largely reduces the compressibility.

Several approaches, such as double pressing/sintering, powder forging and extrusion are used to increase the density and improve the performance of P/M components. However, the cost and limitations involved in these processes hinder the acceptance by users. Therefore, a modification of the traditional single pressing/sintering method to produce near net complex parts with a high density is still a major aim of several investigations [4].

For P/M processes for titanium and titanium alloys, several types of powders have been used, such as sponge fines, hydrogenation–dehydrogenation (HDH) powder,

gas atomised (GA) powder, hydride powder, mechanical alloyed powder and so on. Yet the good compressibility of HDH and sponge fines is associated with a very high impurity level, with HDH power having relatively high oxygen content and low green density, so that the final part is always associated with inferior density and ductility. Actually, the green density of a Ti powder compact is only about 80% of the theoretical density, which is due to the big particle size and high impurity level. On the other hand, GA powder has a relative low oxygen content and high green density, but its compressibility is too inferior and cannot be pressed by normal cold compaction. In addition, pre-alloyed titanium alloy powder is costly and only a limited selection of titanium alloy powders are pre-alloy, so that most kinds of titanium alloy powder are fabricated by Mechanical Milling (MM) or other blending methods, where the powder is hard and difficult to compact.

1.3 Lubricant and lubrication process

Lubrication is a simple and effective way to improve the performance of P/M parts [7, 8]. Lubrication is usually applied to metal powders and/or the die set prior to compaction to improve the properties of powder compacts and provide protection to the die. There are two kinds of lubrication method. The first is an internal lubrication (admixed powder lubrication) method - powder is usually blended with an amount of 0.2-2wt.% of lubricants before compaction. Sometimes a lubricant is added by using a solvent. For example, paraffin wax (PW) is always added using a PW-petrol solvent which should be allowed to evaporate completely before compaction.

Another method is die wall lubrication (external lubrication). In this process, a lubricant dissolved in a solvent is wiped onto the inner die wall. After the solvent

has completely evaporated, the inner die will become coated by the dry lubricant powder. The amount of lubricant used is about 0.05-0.1wt.% of the powder, which is much lower than that for the internal lubrication methods. The improvement in the green density under low pressure is very slight, which is of no use to the powder particles which are difficult to cold compact. But it has no effect on the bonding forces between the metal particles under high compaction pressure and consequently the density of samples, prepared by the die wall lubrication method, is higher than that for no lubrication and the internal lubrication method. In addition, the debinding process is much easier than for the internal lubrication method. Sometimes die wall lubricants must be applied, even though internal lubricants have been added, otherwise the green parts would become welded to the die wall and ejection of the green part would be quite difficult, damaging the part or even the die [6].

The principal requirements which have to be met by a suitable lubricant are summarized as follows [9]:

(a) Form a homogenous mixture with the metal powder without forming agglomerates.
(b) Have minimal influence on the flow properties of the metal powder.
(c) Produce a uniform bulk and filling density in the powder mixture.
(d) Promote excellent compressibility of the powder mixture.
(e) Have a favourable influence on the strength of the green parts.
(f) Decrease the friction between the powder and the die wall as well as the interparticle friction, even at low concentrations.
(g) Evaporate as completely as possible in the de-waxing step without leaving any residue in the sintering furnace.

1.4 De-lubrication and the subsequent sintering process

The removal of lubricants is usually carried out by thermal burn-off in the pre-sintering zone of the furnace. Titanium is a highly reactive metal with respect to most nonmetallic elements (O, H, C, N, Cl), thus the lubrication process, especially the internal lubrication process, is usually not taken into consideration for preventing contamination. The de-lubrication process is quite similar to the debinding process for MIM parts, and for which there is much published information

The brown parts, i.e. specimens which have undergone a de-lubrication or debinding process, need to be further densified by a subsequent sintering process. Lubrication inevitably causes contamination and it is necessary to de-lubricate to reduce the impurity level of the parts to be sintered [7, 8, 10, 11]. Furthermore, prior particle boundaries (PPBs) may be created by excessive lubricant additions. These problems cause deterioration in the mechanical properties of the sintered parts. Because of the high chemical activity of titanium alloy powder and the composites created in titanium alloy are very stable, the titanium sintering process needs more careful control than for ferrous alloys, stainless steels and hard alloys. In 2011 and 2012, ASTM published the standard ASTM F2885 and ASTM WK35394 for MIM Ti-6Al-4V alloy and CP Ti components for surgical implant applications respectively. A very low allowance for the major nonmetal elements in Ti and Ti alloys is set [12, 13].

1.5 Titanium with RE additions

Pure titanium is allotropic, with an HCP crystal structure (α) at low temperatures and a BCC structure (β) above 882℃. Alloying elements provide solid-solution

strengthening and change the allotropic transformation temperature. As a result, there are four categories of titanium and its alloys which can be used in industrial applications: (a) Commercially pure titanium (α); (b) Alpha Ti alloys; (c) Beta Ti alloys; (d) Alpha-Beta Ti alloys [1, 14].

Hot and cold working can be used to deform a metal part into a desired shape but at elevated temperatures metallic materials have lower yield strength and higher ductility. In addition, HCP metals such as magnesium and titanium have more active slip systems at hot-working temperatures. Moreover, there are more slip systems in the higher temperature BCC β-Ti phase making it more ductile and easier to deform than the α phase at lower temperatures.

In general, hot working of titanium ingots is carried out at temperatures below the β-transus temperature, in the α+β two phase region. The primary reason for processing in this way is to prevent very rapid grain growth occurring during heating and hot working of titanium alloys in the β phase. This yields a very coarse β grain microstructure which is not easily refined by post hot-working heat treatment. This microstructure significantly deteriorates the strength-ductility balance and fatigue properties of the alloy [15].

Contrary to titanium alloys, hot working of steel products is carried out in the pure austenitic region under very high temperature [16]. The difference is due to the fact that various alloying elements such as Al, Nb or Ti have carbides or nitrides which re-precipitate in the austenite and are effective in preventing γ or α grain growth, retardation of austenitic recrystallization and precipitation hardening. For titanium materials, the carbides and nitrides of these elements cannot be utilized because of their high solubility in both β and α phases. If finer dispersed compounds, which are able to dissolve and re-precipitate in the β-titanium phase can be found as alternatives to carbides or nitrides, β processing or β heat

treatment can be more widely used, leading to a marked improvement in mechanical properties through microstructural control in titanium materials.

Based on these factors, the oxides deriving from rare earth (RE) additions have received a lot of attention. RE elements are sometimes referred to as “Vitamins” since small additions can lead to a significant change in properties. Encouraged by their success in superalloys, RE elements were first added to Ti alloys in the 1980’s and to P/M Ti alloys in the 1990’s [17].

Another potential use for RE additions is in controlling the oxygen level in P/M Ti and Ti alloy matrices. Titanium has a strong affinity with oxygen and powders can be associated with a high oxygen level (for HDH >0.33wt.%) and the heating process can also “pick-up” oxygen. Increasing oxygen content largely embrittles the final components. Unfortunately, titanium shows a stronger affinity with oxygen than most other metal elements. Thus RE elements are taken into consideration for the purpose of scavenging oxygen in titanium. Associated heat treatment processes allow the yttrium to deprive titanium of oxygen and generated fine RE oxides (<1μm). A designed outcome is that we can receive a metal with a pure microstructure and homogenous distribution of fine oxide particles of the RE. These particles can not only clean the grains, but also provide a blocking effect on grain growth during heat treatment.

In summary, RE element alloying is expected to improve the processing ability and microstructure of the consolidated titanium alloys giving superior strength and ductility.

1.6 Object of present thesis

In New Zealand, patentable processes that can be used to produce cost competitive

titanium alloy powders from titanium oxide (TiO_2) and aluminium (Al) powders have been developed through research projects funded by the Foundation for Research, Science and Technology (FRST), Titanox Development Ltd (TDL) and WaikatoLink Ltd. Currently, TDL is in the process of constructing a pilot plant to produce titanium alloy powders in kilogram batches. Recently, FRST approved the funding for a four year research project on titanium alloy powder metallurgy (P/M) and powder coating hosted by the University of Waikato.

This PhD project is part of a larger FRST (now MBIE) contract and specifically aims to establish the effect of powder conditioning through adding micro-alloying elements and using a small fraction of binder/lubricant on the microstructure and mechanical properties of selected titanium alloys such as Ti6Al4V. The objectives of this thesis are:

(1) To establish the effect of adding a small fraction of lubricant and associated de-binding conditions on the green compact density, and the composition and microstructure of the selected titanium alloys after sintering.

(2) To establish the effect of micro additions of rare earth elements on their ability to control dissolved oxygen levels in the selected consolidated titanium alloys. The optimum amount of micro additions will also be investigated.

(3) To determine the mechanical property/microstructure (secondary phase, porosity, segregation) relationships of the selected consolidated titanium alloys produced through the powder condition.

This study is mainly based on experimental investigations. Some theoretical analysis of the scientific principles underlying the relationships among lubricant characteristics, de-lubrication conditions, micro additions, processing conditions and the microstructure and mechanical properties of consolidated materials will

also be undertaken. The experimental techniques will include (i) preparing powders of selected compositions using Ti and Ti alloy powders with different volume fractions of lubricant, (ii) characterising green powder compacts produced by using die-pressing under different conditions (iii) investigating the effects of de-binding conditions, sintering conditions, post-sintering processing routes and conditions and heat treatment on the microstructure and properties of the selected alloys with different level of micro-alloying elements. Characterisation techniques including optical microscopy, x-ray diffractometry (XRD), scanning electron microscopy (SEM) and transmission electron microscopy (TEM) will be used.

2. Chapter 2 Literature Review

2.1 Introduction

Considering that the scope of this research covers two topics for investigation, where it can be argued that there is a small connection between them, it would be clearer if the literature review is separated into two parts: the lubrication process and the effect of RE additives. An important point is that they are two different research areas and there is no obvious relationship between them.

For the lubrication part, the mechanisms of compaction, friction during processing and the properties of a compact are introduced in detail in the first section. Although compaction and lubrication are a general topic, they provide a basic understanding of the lubrication and compaction process and subsequent de-lubrication and sintering. The lubricant and lubrication section is given later. This section refers to the influence of lubrication methods, composition and concentration on the compressibility, density gradient and other properties of a powder compact. The de-lubrication and sintering process comes last. Because lubrication processes for titanium have not been investigated systematically, this review mainly focuses on the lubrication of P/M iron and a review of the research in P/M Ti processing will be given in the end of each section.

The review of RE additive processes in Ti and Ti alloys not only lists appropriate literature but also includes cast and wrought alloys. As discussed before, the main contribution of RE additions is to control the grain size and scavenge oxygen from in the matrix. The first influence is discussed in more detailed in the context of conventional cast and wrought alloys. A review of papers in alloys not processed using a P/M route helps us to understand the effect of RE additions and their oxides on the performance of Ti metal and its alloys. A second contribution will describe the properties of Ti and Ti alloy with RE additives.

2.2 Mechanism of compaction

2.2.1 Three stages of compaction

During powder compaction the porosity decrease and the contact area between metal particles increases. In cold compaction we are concerned with the densification of powder by powder particle motion and powder particle deformation. [7, 18-24]

The loose powder in a die set shows very low green density, for iron powder it is 2-3g/cm^3 and for HDH Ti powder is 1.6-2g/cm^3. Many pores are generated by the very loose packing. When a compaction pressure is applied, powder particles are forced to fill the pores and a significant rearrangement of powder particles happens. This mechanism is known as powder rearrangement. A schematic diagram of the different types of mechanism is shown in Fig. 2.1.

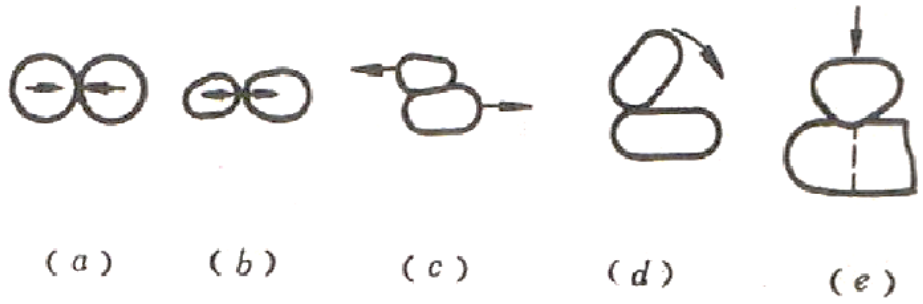

Fig. 2.1 A schematic diagram of the powder rearrangement mechanism: (a) powder particle contact, (b) particle separation, (c) particle sliding, (b) particle rotation and (e) particle motion due to the fragmentation of another particle [7]

Under high pressure, powder particles are deformed. The contact between particles changes from point-to-point and plane-to-plane. There are three types of deformation: elastic deformation, plastic deformation, and fragmentation. Elastic deformation is released after the pressure is released. Fragmentation is a common situation for brittle powder, but not very notable in iron or titanium powder.

Plastic deformation is another important mechanism for the densification process during powder compaction. This mechanism happens when the pressure reaches the in-situ elastic limit of the particles and cannot be recovered. The higher the ductility of the powder particles the more the degree of plastic deformation. During this initial stage, the pores formed between the contacting particles are surrounded by a zone of plastically deforming material. A schematic picture for this mechanism is shown in Fig. 2.2.

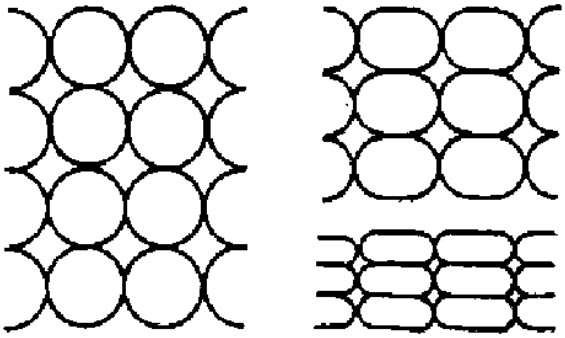

Fig. 2.2 Plastic deformation of powder particles [7]

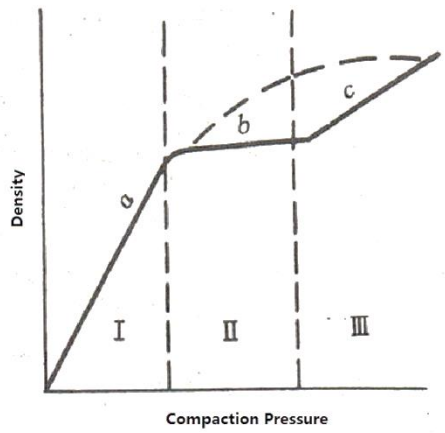

Fig. 2.3 Three stages of a compaction process [7]

The density of a compact regularly changes with increasing compaction pressure. [7, 25]. Generally, this change is separated into three stages, as shown in Fig. 2.3:

Stage I. During this stage, powder particles move and fill the gaps between other particles. The porosity of the whole compact reduces rapidly. A very small pressure (<200MPa) is able to significantly increase the green density. Powder rearrangement is the predominant mechanism in this stage. Stage I is referred to as the slide stage.

Stage II. After stage I, the density remains stable with increasing compaction pressure. This stage is always present in hard and brittle powders such as ceramics. For metal powder with excellent ductility, this stage is not obvious and most of the time is ignored.

Stage III. After stage II, the density increases again with increasing compaction pressure, but the rate of increase is lower than Stage I. During this stage, there is a large amount of plastic deformation in the powder particles. Particles are trapped and the motion of the particles is limited. Both the motion of powder particles and the plastic deformation mechanism contribute to the densification of a powder compact, with plastic deformation having the larger influence on densification. For metal powder compaction, this stage is referred to as Stage II.

2.2.2 Major model function for compaction

During compaction, the relative density of a compact increases from 0.4 to 0.8 or even 0.9, which means that the original volume occupied by the uncompacted powder particles reduces twofold. A good model for the compaction process is critical for analysing densification behaviour of a powder body and for predicting the properties of a compact. Theoretical research on the compaction behaviour of powder has received much attention. An aim of this research is to build a relationship between density (or the relative volume, porosity, relative density,

volume of porosity, reduction ratio of powder volume) and the compaction pressure. Many empirical functions and theoretical functions have been developed and some of the major functions are shown in Table 2.1 [7, 26, 27].

There is experimental evidence which shows good agreement with these functions for specific ranges of the various parameters. Some equations treat the powder compact as an elastic body, i.e. work hardening is ignored. Some equations completely ignore the friction force. The use of these equations will be further discussed in Chapter 8.

Table 2.1 Major Functions of compaction [7, 26, 27]

No.	Year	Researchers	Function	Comments
1	1923	Walker	$\beta = k_1 - k_2 \log P$	k1, k2: constant P: compaction pressure β: relative volume
2	1930	Athy	$\theta = \theta_0 e^{-\beta P}$	θ:porosity under pressure P θ:porosity under no pressure β:compaction factor
3	1938	БаЛЬЩИН	$\log P = \log P_{max} - L(\beta - 1)$	P_{max}: theoretical pressure when a compact can be pressed into full density L: compaction factor β: relative volume
4	1956	Kawakita	$C = \frac{abP}{(1 + bP)}$	C: reduction ratio of volume a, b: constant
5	1964-1980	Huang Peiyun	$m\lg\ln\frac{(\rho_m - \rho_0)\rho}{(\rho_m - \rho)\rho_0} = \lg P - \lg M$	ρ_m: theoretical density of alloy ρ_0: the apparent packing density ρ: the green density m: hardening exponent. M:compaction modulus.

2.2.3 Friction and stress during the compaction process

During a compaction process, the compacting pressures on a powder compact are separated into two parts [7, 28]. The first part is to force the powder particles to

move, deform and overcome the internal friction between them. This is referred to as real-pressure. The increasing of real pressure leads to higher green density and green strength of a compact. Another part is used to overcome the friction between powder particles and the die wall, which is the pressure-loss. The pressure-loss damages the surface of the compact and reduces the die life, which should be avoided. The stresses formed in a compact in a compacting mold are shown in Fig. 2.4.

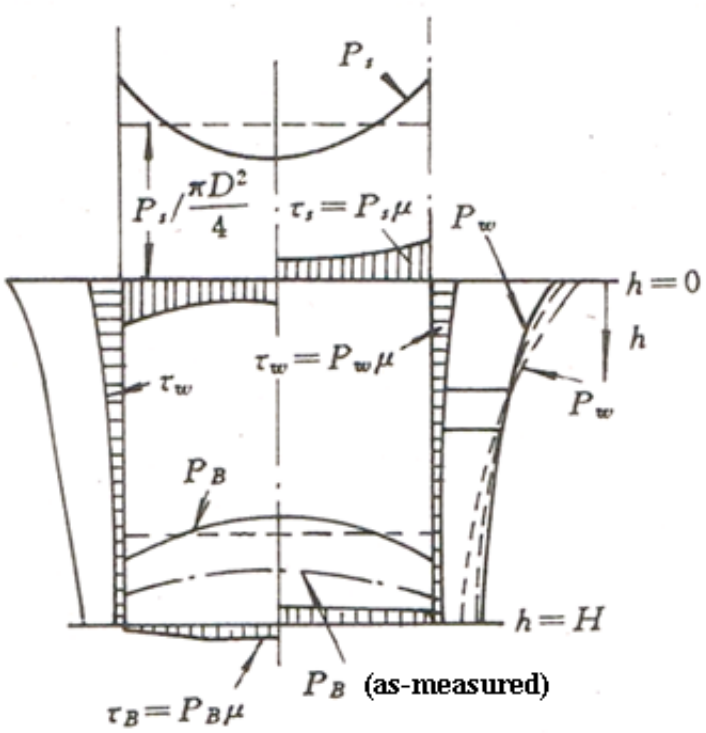

Fig. 2.4 Stress profiles of a powder compact [7]

The level of frictional force depends upon the properties of the powder, the aspect ratio of a powder compact and the surface condition of the die wall. To analyse the stress distribution and predict the properties of a compact, the friction force (or the friction coefficient), especially the die wall friction, should be tested accurately. Some instrumented dies have been developed for experimental investigation of friction in powder compaction. Such measurements enable a direct calculation of the friction coefficient at the die wall as a function of the applied pressure at each

stage of compaction/ejection without arbitrarily selected parameters for the calculation of the friction coefficient [29-31]. A typical instrument die set is shown in Fig. 2.5.

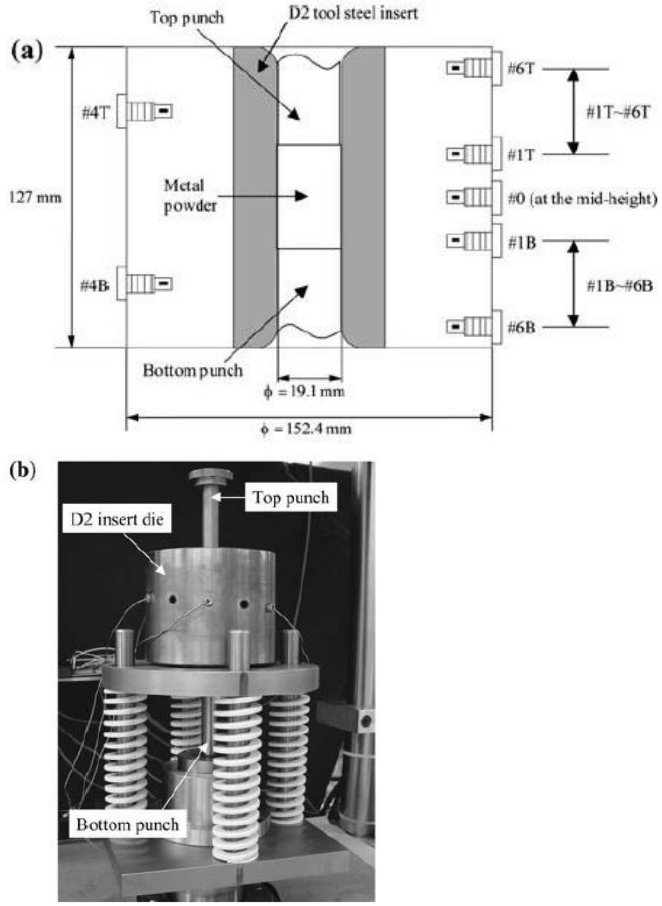

Fig. 2.5 A schematic of an enhanced instrumented die: (a) cross-sectional side view and (b) experimental set-up to simulate double-action pressing [29]

The variation of die wall coefficient of friction with increasing pressure is shown in Fig. 2.6. This is perhaps not as expected, the die wall friction coefficient is not stable nor does it increase with the green density or compaction pressure. In fact, it decreases with increasing density and pressure [25, 29-31]. Associated with the powder compaction mechanism, the friction coefficient versus pressure curves can be separated into three stages. During stage I when the particle rearrangement mechanism dominates, the coefficient of friction is high, because every single

particle is forced to climb up and down over other particles at a very low normal load. At stage II, the friction is from the elastic deformation of the particles in contact with the wall. It decreases dramatically because plastic deformation has taken place. During stage III, material spreads to the cavities and a solid surface with a high density is created close to the contact surface. The friction coefficient remains stable at this stage.

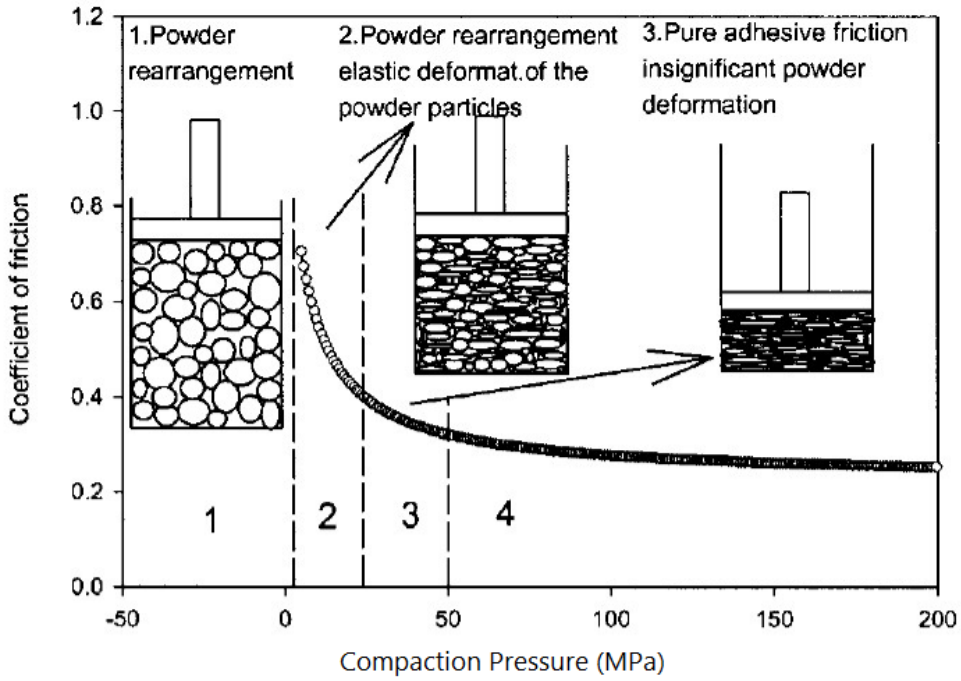

Fig. 2.6 Die wall friction coefficient for compacted powder [25]

Research on interparticle friction is very limited, since there is not a reliable approach for testing this type of friction. Sometimes the flowability of powder particles is used to represent the interparticle friction. It is proved that this friction is very dependent on the surface chemistry and powder particle size. Moreover, the resistance to flow is also sensitive to atmosphere, humidity, temperature and length of time during which particles are in contact. K. E. Amin reported that the internal friction of a coated powder monolayer depends on lubricant film thickness [32].

2.2.4 Density gradients in a compact

The creation of an inhomogeneous green density within a compact is an inherent problem in die-pressing techniques, especially in conventional single-acting compaction. Making measurements for ascertaining the density distribution for every section in a compact is quite difficult. A long time and a complicated procedure are needed for such measurements and the results are not reliable or comprehensive in most situations. A simple way to test the density gradient is to cut the sample into different layers, then test the density gradient from the top to the bottom. But this approach cannot reflect the complicated green density distribution in a layer.

To get an overall result, the density distributions in powder compacts may be measured by a number of techniques [28]. These techniques include: (1) forming identifiable layers of powder in the die; (2) the incorporation of materials opaque to X-rays whose migration during compaction may be followed by radiography, such as lead grids and fine lead balls; (3) radiography including both X-rays and gamma-rays; and (4) hardness measurements.

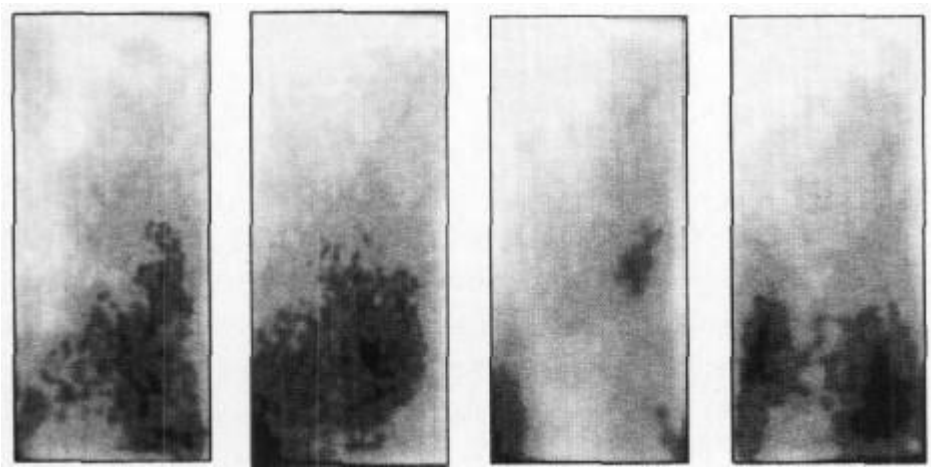

Fig. 2.7 CT images of bronze compacts (the grey and dark area show the existence of pores) [33]

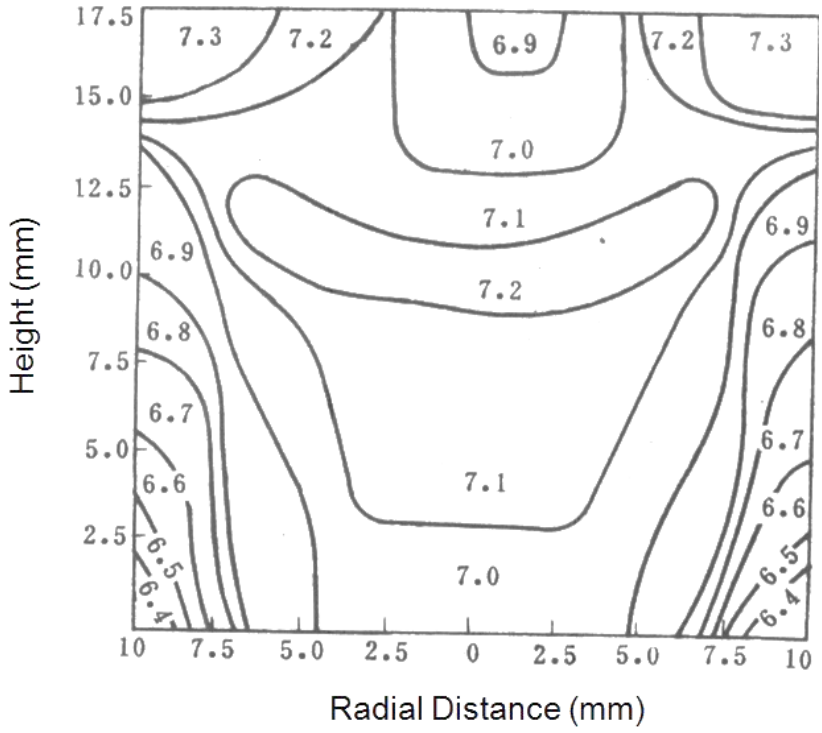

Fig. 2.8 Density profile of a nickel compact [7]

An X-ray image of a bronze compact is shown in Fig. 2.7[33]. The density variation is mainly due to the uneven distribution of pores, i.e. the gaps between powder particles, as shown in the lower dark region. A measured density profile of a nickel powder compact is shown in Fig. 2.8 [7]. In fact, the real density variation is very complicated. The top corners show the highest green density and the bottom corner shows the smallest. It is of great interest that the density decreases toward the centre at the top of the compact and increases towards the centre at the bottom of the compact. The second lowest value may be located in the centre of the compact or near the bottom centre.

Simulation is a simple way to predict the density profile. R. Rossi used the Finite Element Modelling (FEM) method to predict the density gradient and found that the numerical results for different layers in a cylindrical compact are somewhat in accordance with the experimental results [34, 35]. But the corner effect cannot be predicted accurately and in the compaction of a flange, there was a large difference

between theoretical prediction and experimental data (Fig. 2.9).

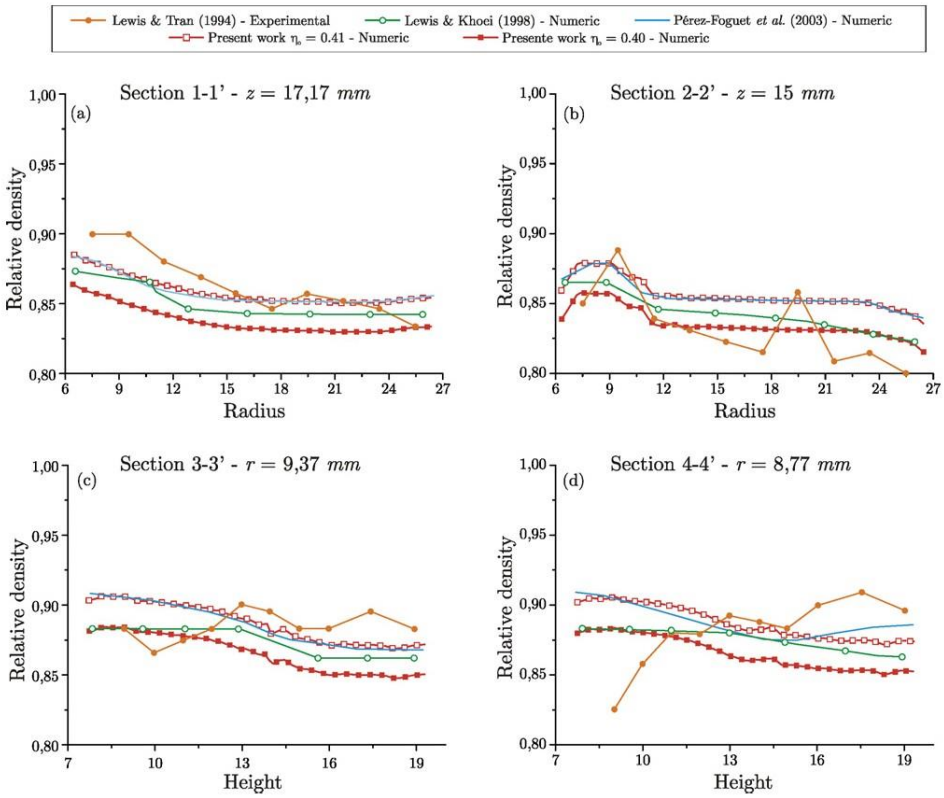

Fig. 2.9 Relative density profiles at the section lines of a flange compact [34]

2.2.5 Properties of a powder compact

Powder compacts cannot be simply treated as a bulk fully-dense material for subsequent use. To understand the influence of lubricants on the compaction behaviour, some properties of a compact and the testing methods for obtaining them need to be introduced [36]. These properties are the parameters that will be tested in this thesis and include:

(1) Compactibility and Green Strength

Compactibility, in other words shape retention, is the ability of a compact to keep its shape. It is reflected in the mass loss during severe shaking or the crushing

strength. The latter is more commonly used. The compact needs sufficient green strength to ensure that it can be handled and transferred to a sintering furnace. Moreover, the green strength must be high enough to resist the stresses introduced by the ejection forces. For a specific powder, the compactibility mainly depends on the green density of a compact and the lubrication conditions.

(2) Ejection behaviour

The maximum ejection force and the energy expended during the ejection process needs to be recorded. A mechanical tester is always employed to record this information.

(3) Other properties

Other properties are investigated for some specific purposes. For example the porosity level is always determined in order to describe the green density or green density variation in a compact. Other physical properties, such as electrical conductivity can be measured.

2.3 Lubricant and lubrication

In the literature there is a lot of information from research carried out on lubricants and lubrication processes for P/M materials. Due to the great difference in lubrication mechanism between internal lubrication and die wall lubrication, the research objects and methodologies for these two areas need to be introduced individually. For the former, the most important job is to determine the best internal lubricant composition and best additive content. Generally, the degree of compressibility is a major factor of concern for engineers and researchers. This is because it is the most direct and easily obtained function which reflects the

efficiency of lubricant on a powder. Then there is the ease of lubricant removal, or the de-lubrication ability. A lubricant which can burn off completely and quickly is recommended. Although it is widely acknowledged that an internal lubrication method provides a smaller density gradient in a compact, research to investigate the influence of such a process on density distribution only focuses on the density gradient in all layers from top to bottom. For die wall lubrication, the most important job is to know the reduction in die wall friction coefficient as a result of coating a lubricant on the die wall. The de-lubrication process for die wall lubrication is always ignored. The ejection behaviour is a very good indicator for assessing the advantage of applying a lubricant. Many comparisons have been done on the influence of these two lubrication methods.

2.3.1 Effect of internal lubrication on the compressibility of a powder compact

It is well known that consolidation mechanisms for cold compaction include powder rearrangement, plastic deformation and fragmentation (for brittle solids). For randomly packed metal powders, particle rearrangement and localized plastic deformation occur concurrently. Although at the early stage of consolidation rearrangement dominates, but as the density increases plastic deformation flattens the particle surfaces and increasingly inhibits particle motion. Consequently, with increasing compaction pressure and the resulting density increase, plastic deformation of the ductile particles becomes the dominant mechanism of consolidation. Therefore, there is a mechanism transition from the rearrangement of individual particles to plastic deformation of particles. This transition typically occurs when the pressure exceeds the bulk yield stress of the material [8, 30, 37].

The use of lubricants under cold or warm compaction does not provide any additional densification mechanism. At low pressures, below the bulk yield stress of the material, the internal friction is the major factor determining the compaction behaviour of the powder. An internal lubricant significantly reduces this friction. It is easier to force particles to slide against the die wall and against each other to fill the cavities. An enhanced particle rearrangement mechanism significantly enhances the green density. Moreover an internal lubricant can be treated as a binder, especially wax or rubber-based organics, which exhibit a strong ability to combine the metal particles together. This method is always used to aid powder compaction for powders which are hard to press or for complex shaped components.

Yet under high pressure, both the green density and the strength of the metallic part are lower than for those where no internal lubricant is used. This is due to the fact that the lubricant particles create a barrier to bonding between the metal particles, therefore the density of the powder with a lubricant is lower than that of the powder alone. Moreover, pore closure is impeded by the presence of lubricants and the degree of plastic deformation is reduced by internal lubrication. In fact, in most iron compaction, a proportion of over ~0.8wt.% of lubricants leads to reduced powder compressibility.

The influence of internal lubricants on different types of powder, friction coefficient, pressure transmission, ejection behaviour and other properties has been investigated by many researchers [37-42].

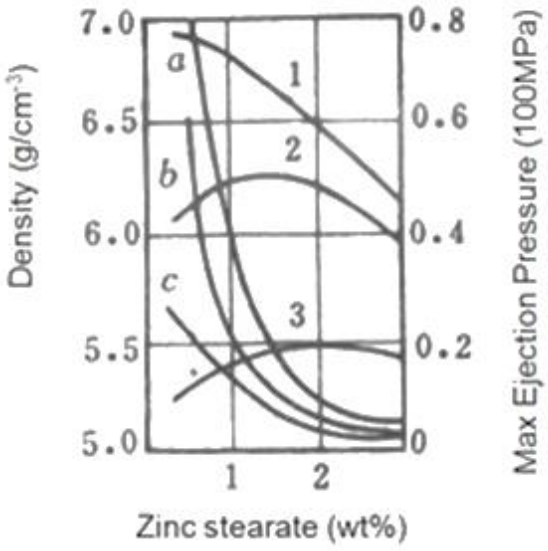

Fig. 2.10 The effects of Zinc stearate on the compaction behaviour of iron powder: 1,2,3: Green densities of samples compacted at 840MPa, 420MPa and 210MPa respectively; a,b,c: Maximum ejection pressures of corresponding samples [7]

Fig. 2.10 shows the effect of ZnSt on the compaction behaviour of iron powder [7]. When pressing at a compaction pressure of 210MPa, the green density improves with increasing ZnSt additions to 2wt.%. But for a pressure of 420MPa, the best ZnSt content is 1.4wt.%. At a pressure of 840MPa when an green density of 90% is achieved, the density decreases from a maximum at a 0.2wt.% ZnSt content. It is found that an optimum internal lubricant concentration depends on the compaction pressure or the green density.

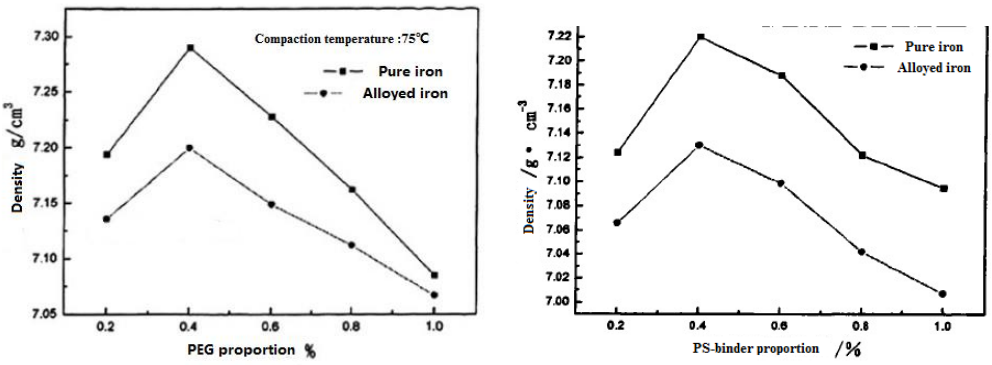

Fig. 2.11 Relationship between PEG and PS based lubricant content and the green density of warm compacted pure iron powder (water atomized) [43]

M. Yang investigated the relationship between the PEG and PS based lubricant content s and the green density of warm compacted pure iron powder and low alloy iron powder (water atomized, 600MPa). Fig. 2.11 shows that highest density >7g.cm^{-3}occurs at 0.4wt.% of lubricant addition [43].

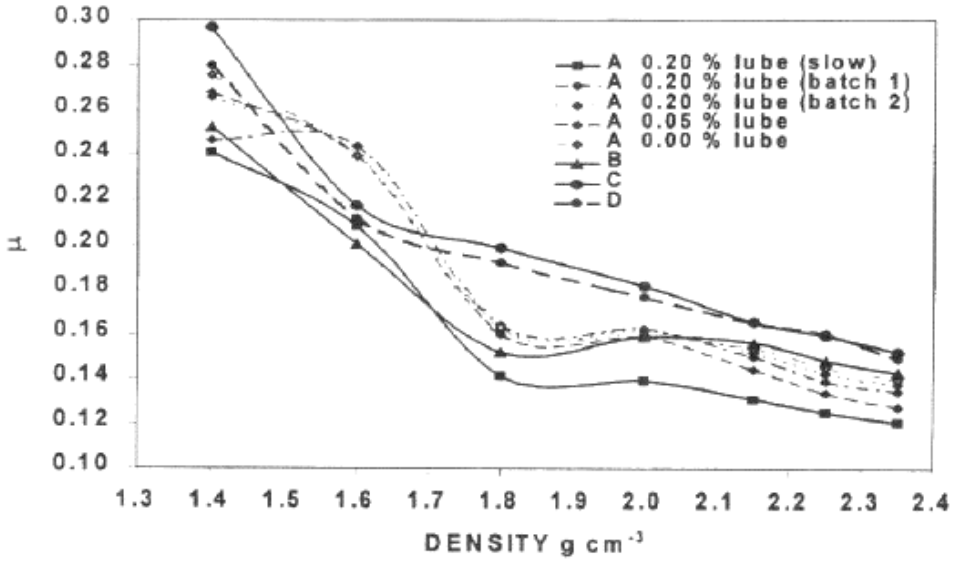

Fig. 2.12 Friction coefficient for various alumina powders and lubricant additions [44]

D. Guyoncourt has investigated the effect of lubricant additions on the die wall friction coefficient for alumina powder [44]. He concluded that a small amount of

internal lubricant gives a reduction in friction coefficient, with larger additions leading to further reductions. (Fig. 2.12)

M. Gagne investigated the lubricant distribution in powder metal parts [45]. He pointed out that the compaction temperature and pressure do not strongly affect the amount of lubricant expelled on the die walls. Indeed, most of the lubricant (>93%) remains in the bulk samples after compaction. Thus an internal lubrication process does not offer much of a lubrication effect on the die wall.

Sometimes wet mixing is employed, because some lubricants such as wax and rubber are quite big solids. Dry mixing them with small metal particles is impossible, thus a solvent is employed. Limited research has been done to compare these two mixing methods. Some researchers believe that dry mixing should be better [7].

2.3.2 The effect of die wall lubrication on the compressibility of a powder compact

A comparison of internal lubrication and die wall lubrication on the compressibility of powder compacts has been investigated by many researchers [8, 11, 44, 46-49]. For die wall lubrication, the powder particles are not lubricated so the interparticle friction does not change. For internal lubrication, there is no chance for a lubricant to build a film on the die wall during the initial stage of compaction, so the effectiveness of internal lubrication on the die wall is debatable. Through internal lubrication, a film coated on the die wall is only generated under very high pressures and is always discontinuous.

Internal lubrication is popular in industrial applications because the process of adding a lubricant is quite simple and no cleaning or re-lubrication is required for

each compaction. Although external lubrication of the die walls should significantly increase the green density of P/M compacts and reduce the environmental and the other disadvantages of internal lubricants, there remains the difficulty of getting the lubrication onto the die wall efficiently [8]. The die set needs to be cleaned and recoated with dry lubricants prior to each compaction. Thus, die wall lubrication is, for the moment, a less practical option in the context of high production rates, of the order of 15 parts pressed per minute [50, 51]. A spray method based on tribo-static charging of dry lubricant particles in a gun has been developed, which improves the re-coating rate of die wall lubrication and hence improves the production rate [40].

A. Simchi has investigated the properties of green iron powder compacts [8]. At relatively low compaction pressures (<450MPa), powder lubrication promotes better densification compared with die wall lubrication. While at higher pressures, die wall lubrication gives better densification because it does not prevent the plastic deformation of powder particles (Fig.2.13).

M. Siddiqui compared fractographs of broken green compacts of iron powder with different lubrication methods (Fig. 2.14). This work indicated that higher green density and green strength for an externally lubricated compact is due to more particle interlocking and cold welding during pressing [52].

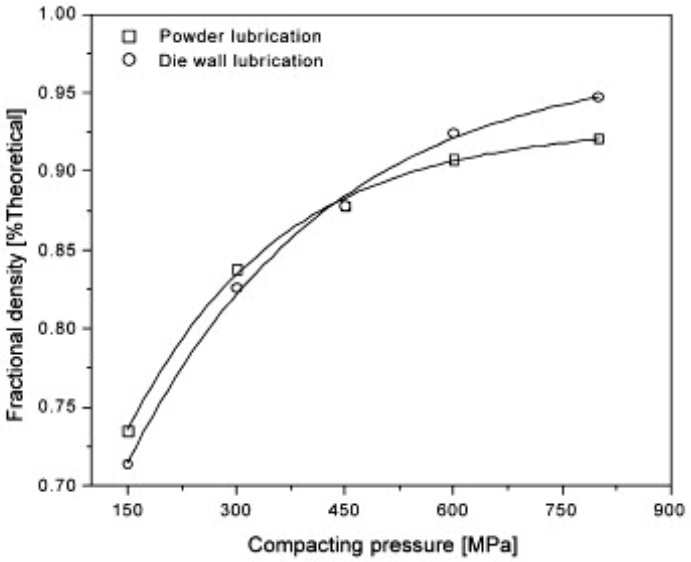

Fig. 2.13 Properties of green iron powder compact [8]

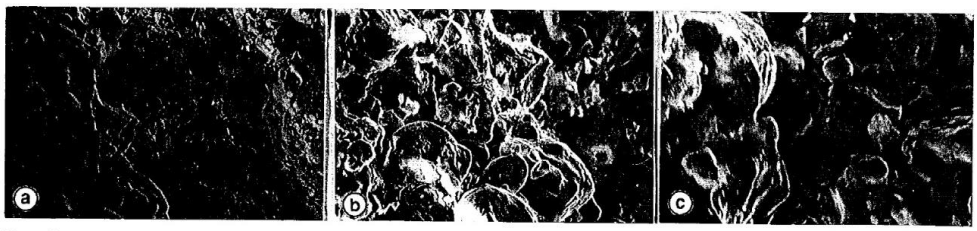

Fig. 4 Scanning electron fractographs of PASC30 green compact without lubricant. Compaction pressure: 690 MPa, Magnification: a) 370 x, b) 535 x, c) 760 x.

Fig. 5 Scanning electron fractograph of PASC30 green compact with lubricant (0,8 % graphite admixed). Compaction pressure: 690 MPa, Magnification: a) 370 x, b) 535 x, c) 760 x.

Fig. 2.14 Fractographs of broken green compacts of iron powder with different lubrication methods [52]

2.3.3 Effect of lubrication on the density gradient

A uniform density in a powder compact is known to be sensitive to the die wall friction co-efficient, because friction forces create high stress gradients during

compaction. Interparticle friction also affects the density in a compact, both its uniformity and distribution, when packing powder into a die cavity. Die wall lubrication (DWL) and internal lubrication reduce the die wall friction, and the internal lubrication reduces interparticle friction, These are effective ways to improve the green density homogeneity of a compact [53, 54].

The great contribution of lubricants in improving homogeneity of density in a compact has been acknowledged by researchers and industry. But the degree of this improvement cannot be evaluated in detail. A major barrier impeding the pursuit of this goal is that there are no rapid, reliable methods for quantifying internal density variations [33, 55].

N. Özkan has investigated the density profiles of alumina powder compacts with die wall lubrication [28]. A coloured layer method was employed in his experiments, in which alumina powder was mixed with a colour so that a compact became separated into identifiable layers. The density of powder from a layer or section could be calculated. The results (Fig. 2.15) showed that die wall lubrication provides a smaller range of green density, not only in the layers but also in the sections. Moreover, he also predicted that the maximum and minimum values of green density may be changed by the lubrication process. A hardness test was done to provide a reference for the colour layer method, and the results from the hardness measurements were in good agreement with results from the colour layer method.

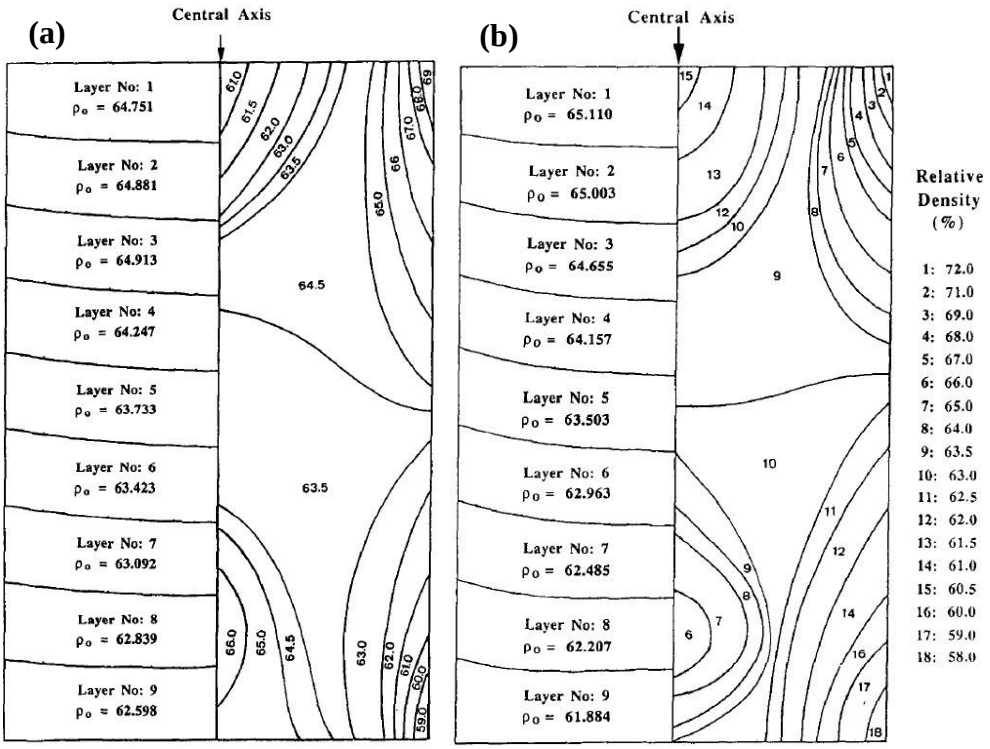

Fig. 2.15 Density profiles of alumina powder compacts with (a) die wall lubrication (b) unlubricated [28]

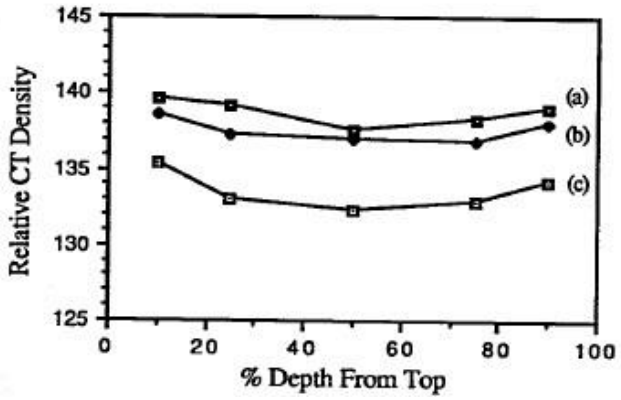

Fig. 2.16 Effects of lubricants on CT density profile: (a) 0.5wt.% of lubricant, (b) 1.5wt.% lubricant, and (c) without lubricant [56]

M. P. Wang used an X-Ray computed tomography approach to investigate the density gradient in powder compacts [56]. Fig. 2.16 gives data from this method, which shows that more uniformity is obtained from the top layer to the bottom. A

lubricant addition of 0.5wt.% showed significant improvement, but the improvement from a 1.5wt.% lubricant addition was small.

The green density inhomogeneity in internally lubricated compacts is less obvious than that in those made using DWL. Y. Taniguchi compared the effect of DWL and internal lubrication on the homogeneity of a compact and concluded that DWL becomes an effective way of increasing the pressure transmission ratio (ratio of force on the lower punch and upper punch. But internal lubrication provides a near-linear decrease in density gradient. Internal lubrication shows higher performance in improving the green density homogeneity compared with the DWL. He recommended a combination of zinc stearate as internal lubricant and paraffin wax as wall lubricant [54].

2.3.4 The effects of lubrication on other properties

The ejection force is also increased by die wall friction and a high ejection force eventually shortens the die life through die wear and galling. S.T. Hong reported that the maximum axial ejection force is controlled by the frictional coefficient and residual radial stress on the die wall. Thus a reduction in the radial stress and/or frictional coefficient is desirable. Such a goal can be achieved by lubricating the powder and die wall [50]. There is no doubt that DWL is better for reducing the ejection force and ejection energy (Fig. 2.17)

For a compact, the only disadvantage of internal lubrication is the inferior compactibility. The interparticle bonding is weakened by the internal lubricant. T. Ye reported that the microhardness of iron compacts with internal lubricant was reduced by about 10% [26]. A. Simchi compared the green strength of die wall lubrication and powder lubrication [8]. The transverse rupture tests (Fig. 2.18)

show that the green strength of powder lubricated compacts is lower than unlubricated specimens, especially at higher compacting pressures. A compact with bad compactibility means lower green strength and hardness [52]. The larger the amount of lubricant the worse the compactibility of a compact.

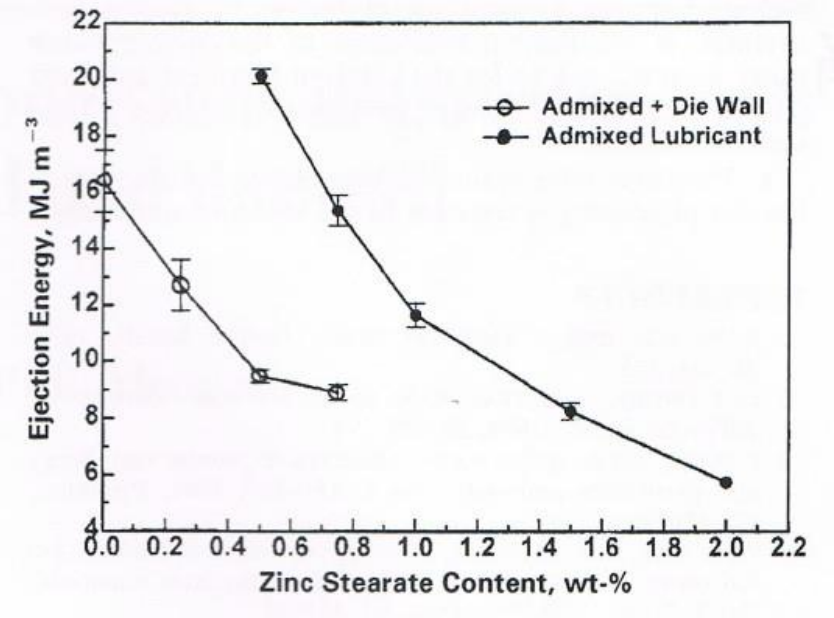

Fig. 2.17 Experimental results showing a decrease in ejection energy with an increase in ZnSt content and die wall lubrication [50]

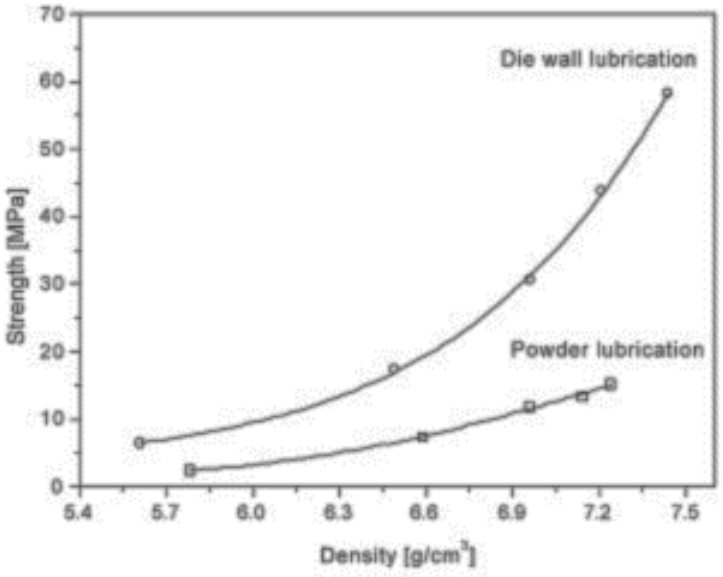

Fig. 2.18 Green tensile strength of compacts with different lubrication methods [8]

2.3.5 The effect of Lubricant composition

Various comparisons between different lubricants have been published [9, 57]. Predominant in this work is the use of stearate salt, due to the better overall results produced. But the salt shows the unpleasant property of evaporating incompletely during the de-lubrication step and leaves residues of oxides or reduced metallic elements in the sintering furnace. Therefore, the development has progressed to lubricants having a pure organic base, in most cases brittle diamides of long chain fatty acids, the so-called amid waxes. However, using amid waxes does not give an optimum reduction of the frictional forces which often results in ejection problems [9].

A. I. Lawrence has compared the green density, green strength and ejection pressures of different lubricants. The lubricants evaluated included two grades of ethylene bisstearamide (EBS 1 and EBS 2), stearic acid (HSt), zinc and lithium stearates (ZnSt and LiSt, respectively) and three composite lubricants (Comp 1, Comp 2, and Comp 3). The composite lubricants were EBS based with additions of metal stearates and other lubricating substances. Comp 1 and Comp 2 contained zinc stearate and lithium stearate is present in Comp 3 [57]. The results shown in Fig. 2.19 show that compacts with SA and metallic stearates have better compressibility than EBS wax. But metallic stearates give inferior green strength and ejection behaviour. Composite lubricants, with superior or equivalent properties for the powder, a green compact and in the sintered condition were recommended, rather than the industry standard ethylene bisstearamide lubricant. Most notably, composite lubricants are capable of reducing the force required to eject the compact from the die.

U. Klemm has compared the effects of lubricant composition in the filling density, efflux time, force transmission coefficient, wall friction coefficient, powder friction coefficient, ejection force and green density [9]. The lubricants evaluated included ZnSt, commercially used SA, melt SA, micronised SA and other organic acid and wax. He concluded that a smaller particle size contributes to the green density, but coarse lubricants reduce the ejection force required.

Y. Taniguchi compared the performance of different lubricants for giving improvements in density uniformity in iron powder compaction. ZnSt and PW were applied as internal lubricants or die wall lubricants. PW shows better performance as a die wall lubricant compared with ZnSt, and a remarkable increase in the lubrication effect is observed for a combination of ZnSt as an internal lubricant and PW as a wall lubricant [54].

(a)

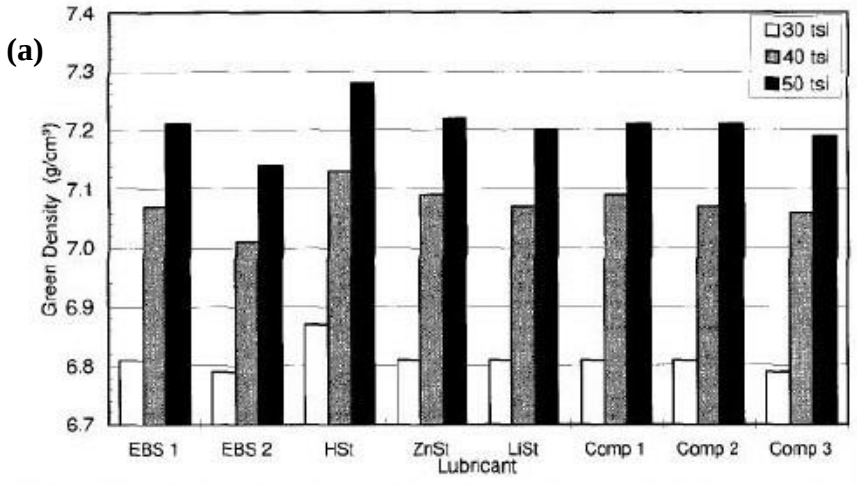

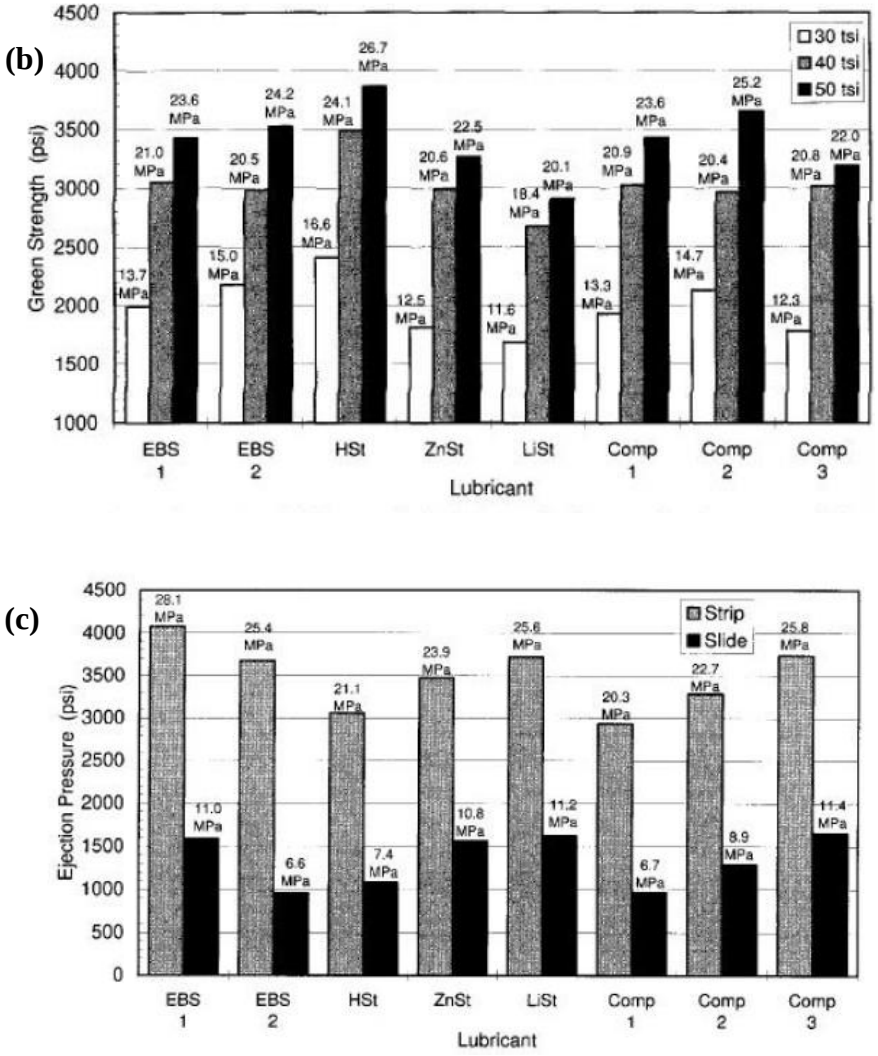

Fig. 2.19 Properties of iron powder compacts with different kinds of lubricants: (a) green density; (b)green strength; (c) ejection pressure of 50tsi (30tsi=415MPa, 40=550MPa, 50tsi=690MPa) [57]

Y. C. Lin compared the most popular lubricants used in the P/M industry, i.e., Acrawax, ZnSt and Kenolube (a mixture of the former two components). Results show that Kenolube gives the lowest ejection force; Acrawax gives the highest green strength and ZnSt yields the highest green density. For improving green density and maintaining a high level of green strength, 0.3wt.% is the best, but a further addition of up to 0.6-0.8wt.% is required. Moreover, a higher level of lubricant addition is recommended for powder with poor compressibility. Above

all, the selection of lubricant and its concentration depends on the requirement of the green compacts [58].

2.3.6 Lubrication process for P/M titanium alloys

The purpose of applying lubricants to P/M titanium processing is to provide cheap and simple direct press and sinter techniques. Encouraged by the great success achieved in the application of lubricants in iron, copper, alumina and ceramics powders, the lubrication of titanium powder is now receiving attention.

H. Takamiya reported a "Super Lubrication Approach". Lithium Stearate shows a surprisingly "super lubrication effect" restricted to a maximum temperature of around 150℃ and a higher compaction pressure ranging from 600 to 2,000MPa. This lubricant resulted in enhanced mechanical properties, comparable to those found in wrought products, with near zero shrinkage and yielding in the as-sintered condition close to that in wrought materials [59].

S.T. Hong compared the die stress profiles during compaction of commercially pure titanium and commercially lubricated iron powders, which were investigated experimentally using an instrumented die [29]. The die was designed to simulate double-action pressing with a recorded stress history. The radial stress profile at the maximum axial stress is shown in Fig. 2.20. For both the stress profile at the maximum axial stress and the residual stress profile, the unlubricated Ti powder produced a much higher radial stress at the centre of the compact, with a steep pressure gradient at both the top and bottom of the compact, while the lubricated Fe powder produced a more uniform radial stress distribution along the height of the compact. Moreover, unlubricated Ti powder has a much higher coefficient of friction at the powder-die wall and a higher ejection force. His experiments

indicated a great potential for improving the compaction behaviour via the lubrication of Ti powder.

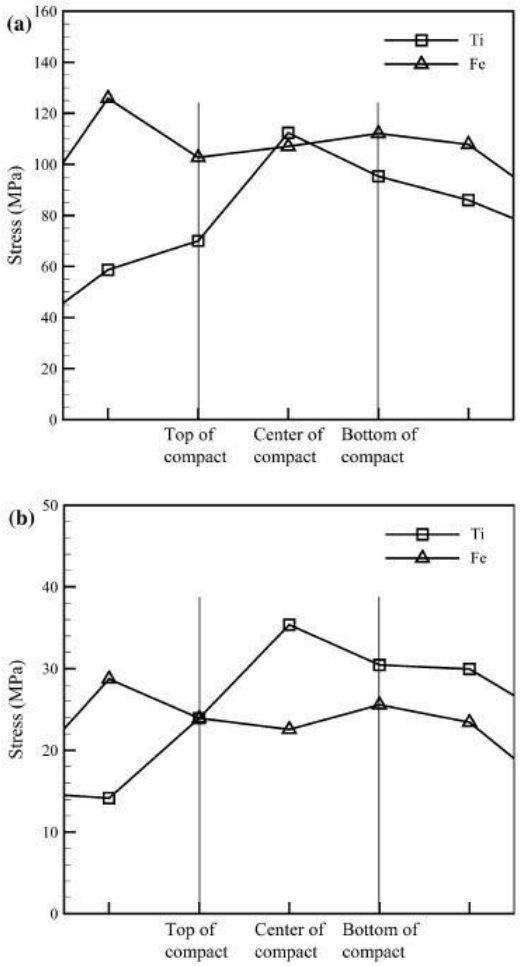

Fig. 2.20 (a) Typical profiles of the radial stress at the maximum axial stress for unlubricated Ti and lubricated Fe powders; (b) Typical profiles of the residual radial stress for unlubricated Ti and lubricated Fe powders [29]

However, internal lubrication is not widely used and has not been carefully investigated for titanium P/M. The first reason is that titanium powder causes minimal seizing and galling in steel dies when it is compacted, which is not like the compaction of aluminium powder. The second and more important reason is to avoid internal interference with the subsequent sintering process as well as contamination [4]. As a result, a uniform density is hard to obtain.

Y. Hovanski compared the effect of different kinds of lubricants on the green density and sintered density in the compaction processing of titanium powder produced as Hunter fines (via sodium reduction of titanium tetrachloraide) [60]. An SA lubricant dissolved in camphor was recommended (Fig. 2.21). The effect of lubricant concentration on the maximum die wall friction coefficient and green density is shown in Fig. 2.22. The die wall friction coefficient is largely reduced by lubricant additions. A 100:1 powder to lubricant ratio showed the best improvement in green density and the ejection force was also significantly reduced by a lubricant addition (Table 2.2).

Z. Hongqiang investigated warm pressing with DWL and internal lubrication for titanium alloy powder. $MoSi_2$ was used as die wall lubricant. 0.06-0.2wt.% of LiSt or HDPE was applied as internal lubricant. The highest sintered density was obtained at 0.06wt.% LiSt [61].

Improving the green properties of Ti metal and alloy powders has attracted much attention [62-68]. However, the use of lubrication in titanium powder metallurgy is still a new research field [69]. The effect of lubrication on different types of powders, the best lubrication process, the most suitable lubricant composition and optimised proportions of lubricant and powder need to be determined. The mechanism leading to improvement in performance also needs to be studied.

Table 2.2 Pressing characteristics of lubricated and unlubricated titanium powders [60]

Lubrication Scheme	Ejection Force (KN)
CP-Ti (no lube)	28.0
100:1 powder to lube	27.1
50:1 powder to lube	9.6
10:1 powder to lube	2.1

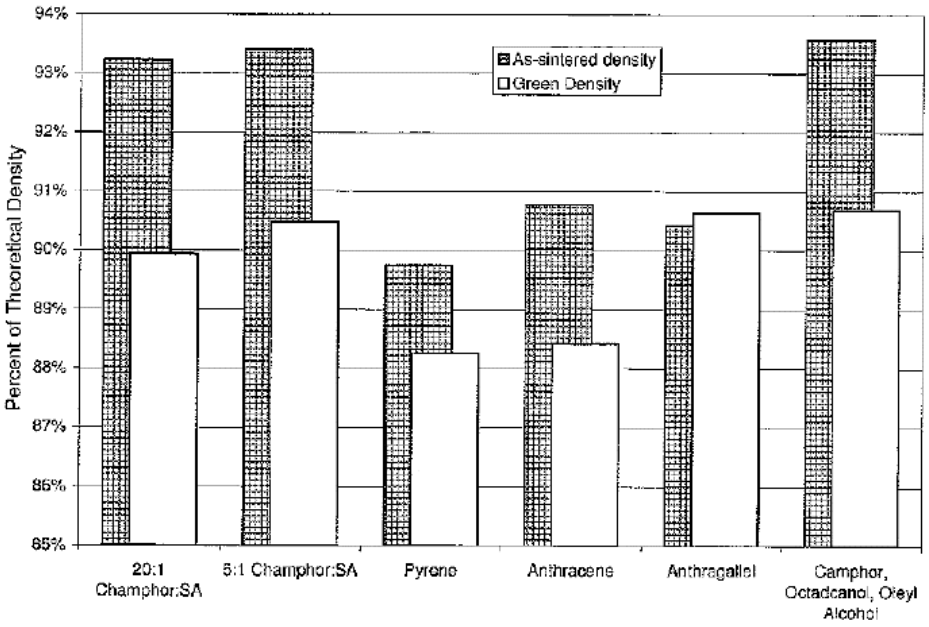

Fig. 2.21 Density effects of various lubrication schemes mixed at 50:1 with titanium [60]

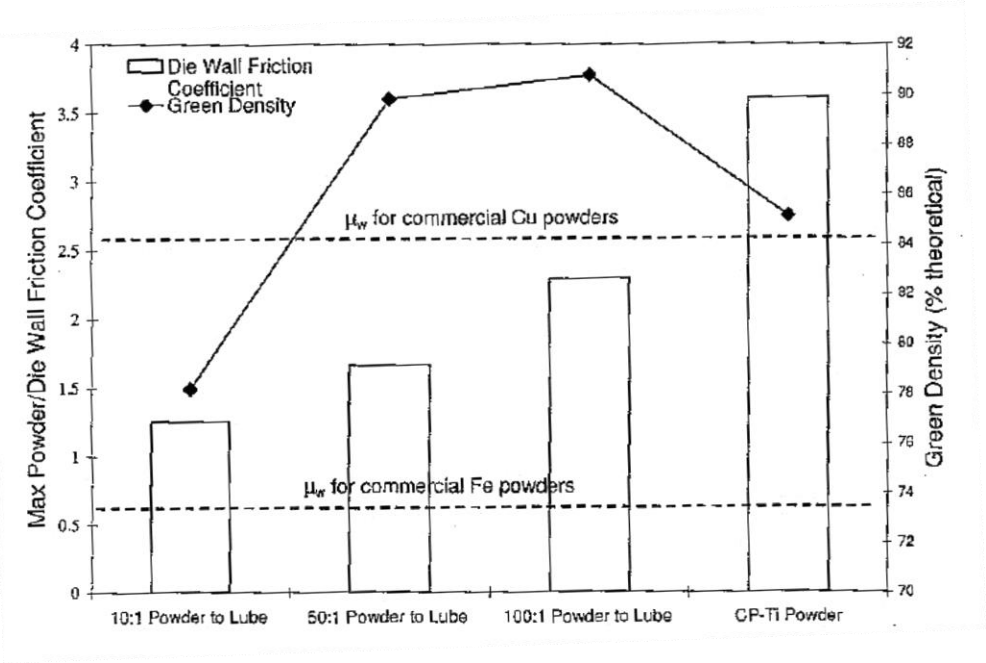

Fig. 2.22 A chart demonstrating the effect of powder to lubricant ratios in a titanium powder lubricant made from a mixture of 20:1 camphor to stearic acid [60]

2.4 De-lubrication and subsequent sintering processes

2.4.1 Objectives and methodology for the de-lubrication process

The removal of an internal lubricant is quite similar to the debinding process of metal injection moulded parts. Organic compounds need to be removed without any residue in the matrix and a subsequent sintering process is needed to further improve the density [70]. As a result, the purpose of these two processes and the mechanism for binder removal process is quite similar. The same methods can be used for studying them and optimizing the process parameters. The lubricant removal process has been investigated in the following fields:

(1) Mass loss of the lubricant. This is the most direct and simple way to predict the de-lubrication level.
(2) Residual nonmetal element content test. The most useful parameter is the carbon content.
(3) Thermo-Gravimetric Analysis (TGA). TGA indicates a lubricant decomposition mechanism and identifies residue compounds.

The process parameters and factors which influence the removal of both lubricant and binder are also quite similar. These parameters are the organic compound composition and content, powder particle types, sample geometry, heating temperature, holding time, heating rates, atmospheres, dew point and so on. However, there are still some differences between the two processes:

(1) Smaller amount of lubricant. The amount of lubricant in a powder compact (1-10vol.%) is much lower than that in MIM (30-40vol.%). A solvent removal process is not recommended and much shorter de-lubrication time is needed. For powders with lower residual nonmetal elements and a lower requirement for a protective atmosphere, a combined de-lubrication and sintering procedure

is available.

(2) Fewer composition choices. Only 1-2 compositions are used in a lubricant, which is less than that for a delicately designed MIM binder (more than 4 compositions). As a result, the de-lubrication process is quite simple, with only one heating and one holding procedure.

(3) High green strength. Generally, worries about distortion and collapse caused by the de-lubrication process are not necessary. A pre-sintering zone (>500℃) at a higher temperature and longer time is unnecessary for a compact with a lubricant. Whereas in MIM, pre-sintering should be carried out above the initial temperature for sintering, otherwise the brown parts are too brittle to be handled or transferred.

(4) Metallic salt organic compound. The binder for a MIM process consists of C, H and O (N), which can be decomposed into a gas below 800℃ in an ideal situation. But the metallic salt organic compound used in lubricants leads to residual metallic oxides which are very stable at the sintering temperature.

(5) Higher green density. The gaps between powder particles, as a potential corridor for the de-gassing of a lubricant, are closed to a larger degree after compaction. Thus the green density is an important parameter for the de-lubrication process.

The aim of de-lubrication is to get a brown part without any residue and few residual nonmetal elements. For consideration of cost affordability, the consumption of heat energy and protective gas should be taken into account.

2.4.2 Effects of process parameters on the de-lubrication of powder compacts

Several studies have been conducted to improve our understanding of effects of the different de-lubrication parameters on the process.

K.S. Hwang investigated lubricant removal in metal powder compacts [10]. His results are shown in Table 2.3. He concluded that lubricant removal is more complete when debinding is performed at low heating rates, a high hydrogen content in the atmosphere and high debinding temperature. At 90% of green density there were no barriers to the removal of lubricants. The residual composition and content of metallic stearates is also shown.

J. McGraw examined the effect of heating and green density on the completeness of lubricant burn-off [71]. It was found that high heating rates improved the de-lubrication rate, which is contrary to the results of Hwang. The effect of green density was less conclusive. High green densities promoted de-lubrication in bronze and iron compacts, but impeded de-lubrication in 316L stainless steel compacts.

There is some debate on the effect of the dew point. M. Renowden reported that water vapour had a negative effect on lubricant removal [72], whereas others recommended a high dew point [73].

In summary, controlling the de-lubrication process is similar to that for MIM green parts. The effects of some parameters such as heating rate and dew point are still not quite clear. The main difference between the de-lubrication process and debinding process of MIM is that the green density needs to be taken into consideration. But results show that only for those compacts with very high relative density (>90%) should the value of green density be taken into account [10].

Table 2.3 De-lubrication results obtained from Hwang's results [10]

TABLE III. Weight Loss (%) After Debinding at 550° C

	PASC45		PASC45+0.8w/o Zn Stearate		PASC45+0.8w/o Li Stearate		PASC45+0.8w/o Acrawax		PASC45+0.8w/o Kenolube P11	
Density, g/cm³	6.1	7.1	6.1	7.1	6.1	7.1	6.1	7.1	6.1	7.1
N_2 (-56°C)*	0.03	0.03	0.65	0.64	0.70	0.74	0.79	0.80	0.75	0.72
$N_2 + 3H_2$ (-51°C)	0.03	0.04	0.71	0.73	0.72	0.77	0.82	0.81	0.79	0.78
$N_2 + H_2O$ (+24°C)	-0.87	-0.23	-0.18	0.26	-0.30	0.26	0.06	0.32	-0.26	0.33
$N_2 + 3H_2 + H_2O$ (+35°C)	-0.06	0.00	0.54	0.60	0.65	0.68	0.72	0.74	0.66	0.73

*Dew Points in parentheses.

TABLE IV. Carbon Content (w/o) After Debinding at 550° C

	PASC45		PASC45+0.8w/o Zn Stearate		PASC45+0.8w/o Li Stearate		PASC45+0.8w/o Acrawax		PASC45+0.8w/o Kenolube P11	
Density, g/cm³	6.1	7.1	6.1	7.1	6.1	7.1	6.1	7.1	6.1	7.1
N_2 (-56°C)*	0.033	0.030	0.039	0.042	0.065	0.058	0.054	0.047	0.049	0.047
$N_2 + 3H_2$ (-51°C)	0.031	0.033	0.063	0.034	0.068	0.048	0.038	0.033	0.042	0.037
$N_2 + H_2O$ (+24°C)	0.029	0.026	0.030	0.031	0.037	0.042	0.040	0.036	0.035	0.034
$N_2 + 3H_2 + H_2O$ (+35°C)	0.026	0.025	0.025	0.024	0.040	0.030	0.029	0.028	0.028	0.028

*Dew Points in parentheses.

TABLE V. Free Lubricant Residue After Heating

		Zn Stearate	Li Stearate	Acrawax	Kenolube P11
N_2*	550°C	ZnO, 15.4%	$Li_2CO_3$3, 13.8%	0.4%	ZnO, 5.6%
	1150°C	0.3%	Li_2O, 5.3%	< 0.1%	0.2%
$N_2 3H_2$**	550°C	ZnO, 15.6%	Li_2CO_3, 14.1%	0.1%	ZnO, 5.6%
	1150°C	< 0.1%	Li_2O, 4.3%	< 0.1%	< 0.1%

*Dew Point = −56°C
**Dew Point = −51°C

2.4.3 The effect of residues on the properties of sintered compacts

Any residues can decrease the physical, mechanical or magnetic properties of sintered compacts. Their effect is always assessed from the level of these properties and the microstructures. Y. Wu has investigated the effects of residual carbon content on sintering shrinkage, micro structure and mechanical properties of injection moulded 17-4PH stainless steel [74]. Incomplete debinding gives more residual carbon. More δ-ferrite forms during sintering and hence there are changes in the shrinkage behaviour. Residual carbon led to higher strength and inferior elongation. (Fig. 2.23)

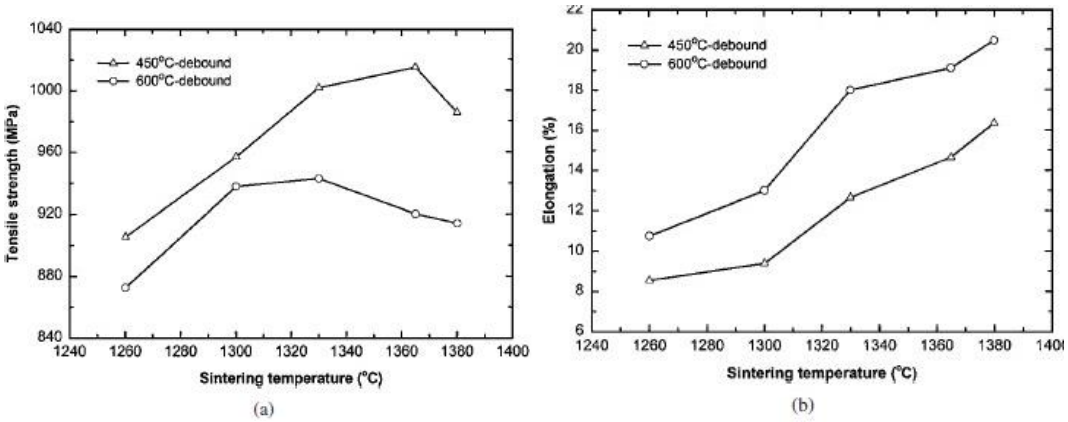

Fig. 2.23 Effect of debinding degree on the final properties of 17-4PH Stainless steel [74]

A. Simchi compared the impact energy and conductivity of compacts internally lubricated and externally lubricated after being heated at 400-1200℃. The results are shown in Table 2.4 [8]. The removal of lubricant in the internally lubricated samples significantly reduces the difference in conductivity between the specimens made using different lubrication methods. A small difference still exists in the sintered samples. And the internally lubricated samples are always associated with inferior impact resistance and elongation.

Y. Liu compared the microstructure of sintered internally lubricated and DWL iron powder compacts. Inferior bonding was found in the internally lubricated specimens, especially in the prior particle boundary regions (Fig. 2.24 (a)). Such a structure was not found is the DWL specimens (Fig. 2.24(b)). The PPB positions were occupied by the internal lubricants before sintering and a porous structure was generated after the lubricants had been removed (Fig. 2.24(c)) [11].

Table 2.4 Properties of iron powder compacted at 600MPa and sintered in hydrogen for 60min [8]

Temperature (°C)	Lubrication procedure	Density (g cm^{-3})	Impact energy (J cm^{-2})	True fracture strength (MPa)	Elongation (%)	Conductivity (Ω cm^{-1})×10^4
400	Admixed	7.11	0.4	–	–	0.1
	Die wall	7.23	0.5	–	–	15.8
600	Admixed	7.13	0.4	–	–	14.3
	Die wall	7.22	1.2	–	–	67.1
800	Admixed	7.17	20.1	175	7.3	75.8
	Die wall	7.24	29.7	228	12.2	79.4
1000	Admixed	7.17	48.8	216	12.2	75.8
	Die wall	7.22	67.4	256	18.2	78.7
1200	Admixed	7.19	67.4	262	18.6	73.5
	Die wall	7.24	76.5	294	20.3	75.2

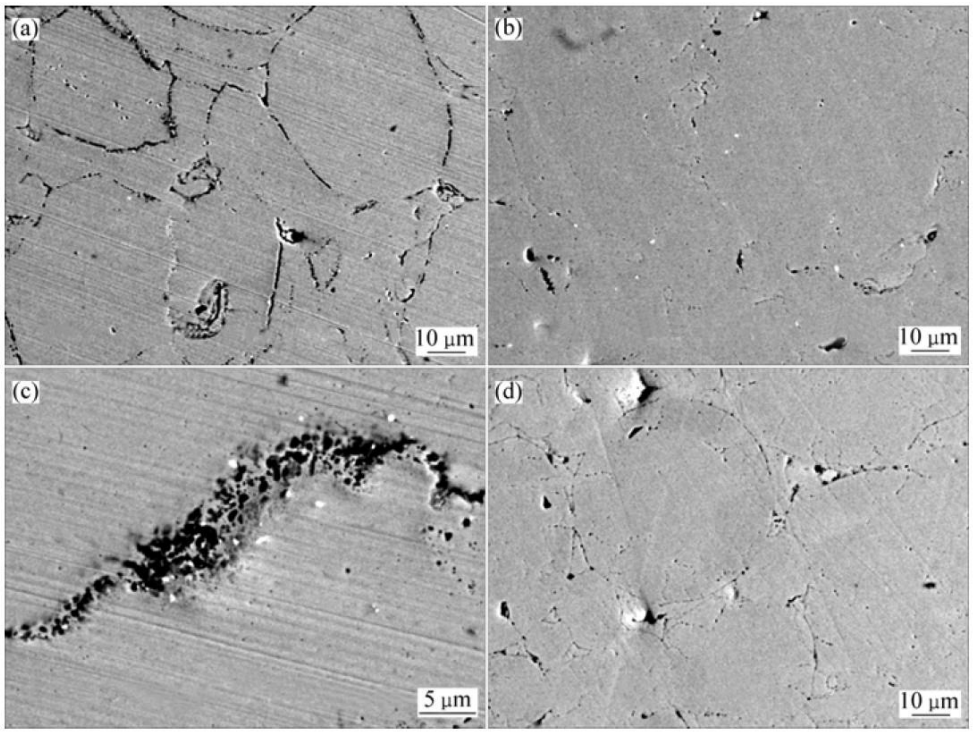

Fig. 2.24 Microstructures of sintered iron samples: (a) internally lubricated, (b) die wall lubricated, (c) PPB texture in internal lubricated samples and (d) heat treated alloy [11]

2.4.4 Sintering of P/M titanium metal and alloys

Titanium reacts with most materials at high sintering temperatures. For P/M titanium, the “pick-up” of impurities and corresponding contamination upon

processing is inevitable because of the high affinity of titanium for carbon, oxygen and nitrogen [75-77]. Lubricant additions and subsequent de-lubrication inevitably brings these elements to the titanium alloy. The effect of carbon content on the mechanical properties of CP-Ti is shown in Fig. 2.25. A carbon concentration of 0-0.1wt.% slightly decreases the elongation of the metal but a dramatic decrease begins at 0.1-0.3wt.% [78]. In the ASTM WK35394 standard, the maximum carbon limit for MIM CP titanium is only 0.08wt.% [79].

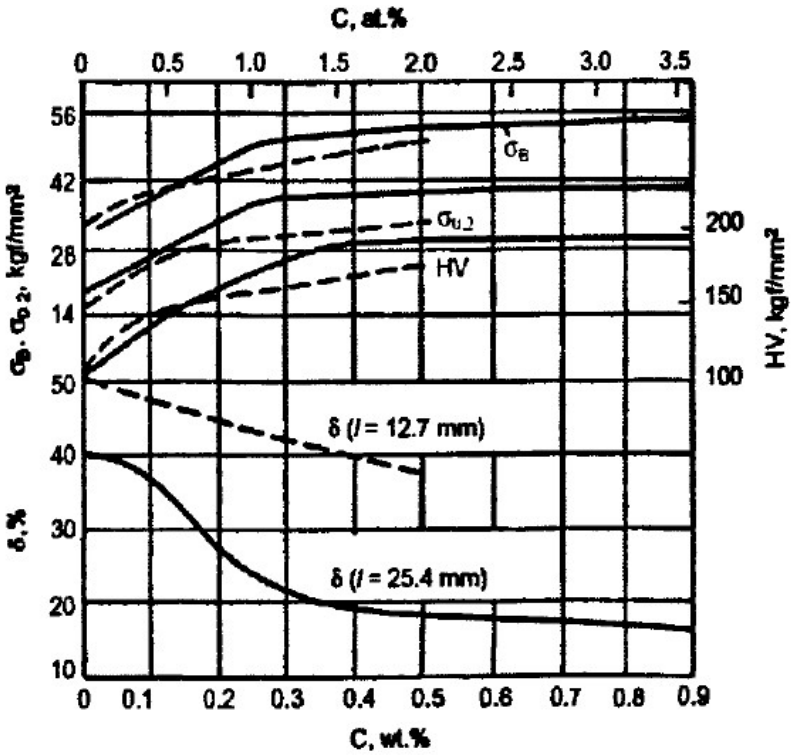

Fig. 2.25 Effect of Carbon content on the properties of CP-Ti [78]

Titanium sintering is usually carried out under high vacuum. However, a high vacuum can only prevent the further oxidation of titanium to a certain extent and is of no use for reducing interstitial oxygen level in the titanium matrix [80].

Although titanium sintering is a very complex process due to its high reactivity, oxidation, phase transformation and so on, low amounts of impurity in titanium will not change the microstructure nor will they influence the sintering kinetics of

titanium [81-89].

No specific research has been done on the de-lubrication & sintering process of titanium and titanium alloys. However, studies on the sintering of as-debound MIM parts are abundant. The mechanical properties of cold-compacted-and-sintered titanium and its alloys are determined by the sintered density, microstructural uniformity, grain size, and impurity levels. Some reports are shown in Table 2.5 [4].

Table 2.5 Representative properties of press-and sintered CP Ti and Ti alloys [4]

TABLE VI. REPRESENTATIVE PROPERTIES OF PRESS-AND-SINTER CP Ti AND Ti ALLOYS*

Description	Density (% PFD)	Oxygen (ppm)	Yield Strength (MPa)	UTS (MPa)	Elongation (%, 25.4 mm)	Reduction in Area (%)
CP Ti	95	415	224	305	24.5	23
CP Ti	98	700	283	383	37.1	30
CP Ti	94	1,200	338	427	15.0	23
CP Ti	98	3,000	483	611	11.0	10
Ti-3Al-2.5V	-	1,200	564	650	11.5	14
Ti-6Al-6V-2Fe	-	1,200	845	963	6.0	3.8
Ti-5Al-5V-5Mo-3Cr	97.3	-	966	1,067	10.1	16.9
Ti-5Al-5V-5Mo-3Cr	97.8	-	933	1,031	11.3	14.9
Ti-10V-2Fe-3Al	96	-	944	1,033	8.0	13.5
Ti-10V-2Fe-3Al	97.2	-	939	1,033	12.0	19.5

2.5 RE alloying for titanium and titanium alloys

When RE additions are made to titanium metal or titanium alloys, it is expected that the RE will be present as a RE oxide (in most situation RE_2O_3) or other composite, through combination with a non-metal element, not the RE metal. The generation of rare earth oxides leads to cleansing of the titanium metal or alloys and the presence of them is also of significance for controlling grain growth. The most important features of RE_2O_3 particles are their high chemical stability, crystal structure and dimension whether in the annealed, quenched or long-term thermally exposed condition.

The presence of uncombined RE metal must be avoided. This minimizes the

advantage of RE additions, which are very expensive. Moreover, there are no benefit from the RE metal and this may even reduce the properties of Ti metal or alloys.

There are different ways of making RE additions to titanium metal or alloys which need to be studied. The RE addition methods of RE are introduced first and then the microstructure and properties are discussed separately.

2.5.1 Addition methods for RE and the presence of RE in titanium

For adding RE elements to titanium or titanium alloys a RE element or RE oxides can be added using the following methods [90-93]:

(1) Traditional casting methods. Pure elemental RE can be added to liquid titanium. RE oxide is formed by solid-liquid diffusion and reaction processes. But the distribution homogeneity and size of RE oxides is hard to control.
(2) A rapid solidification method. This process initially produces a supersaturated solid solution of a rare earth element in Ti. Uniformly distributed RE oxides with a fine-grain size are produced after subsequent heat treatment.
(3) Powder Metallurgy methods. Ti or Ti alloy powder is mixed with RE powder or RE composite powder. Such composites contain REH_2, REB_6, intermetallics such as REAl. Some researchers prefer to use composite powders because the RE element powder is expensive and reacts with oxygen even at room temperature. Moreover, RE powder is much larger (~40mesh) than Ti powder, which creates a barrier to homogenization. Mechanical milling helps to solve this problem but may bring new problems such as unsatisfied sinterability and control of oxygen levels.

The form of RE in titanium and its alloys depends on its composition, the amount added, the Ti alloy composition and solidification speed. There are three major ways in which RE elements are present in titanium and its alloys:

(1) RE element dissolved in the titanium alloy. The room-temperature solid solubility of all RE in titanium is very low. The solubility in α-titanium is near zero in room temperature. The conventionally used RE metals, such as Y and Er, act as slight beta-phase stabilizers for Ti metal and alloys [94]. They have a higher solubility in the β-titanium region at temperatures above 900℃. However, even at 1350℃, the highest solubility of yttrium in β-titanium is only 3.7wt.% (Fig. 2.26). As a result, the amounts of RE additions to titanium are very low and usually in amounts of less than 1-2at.%.

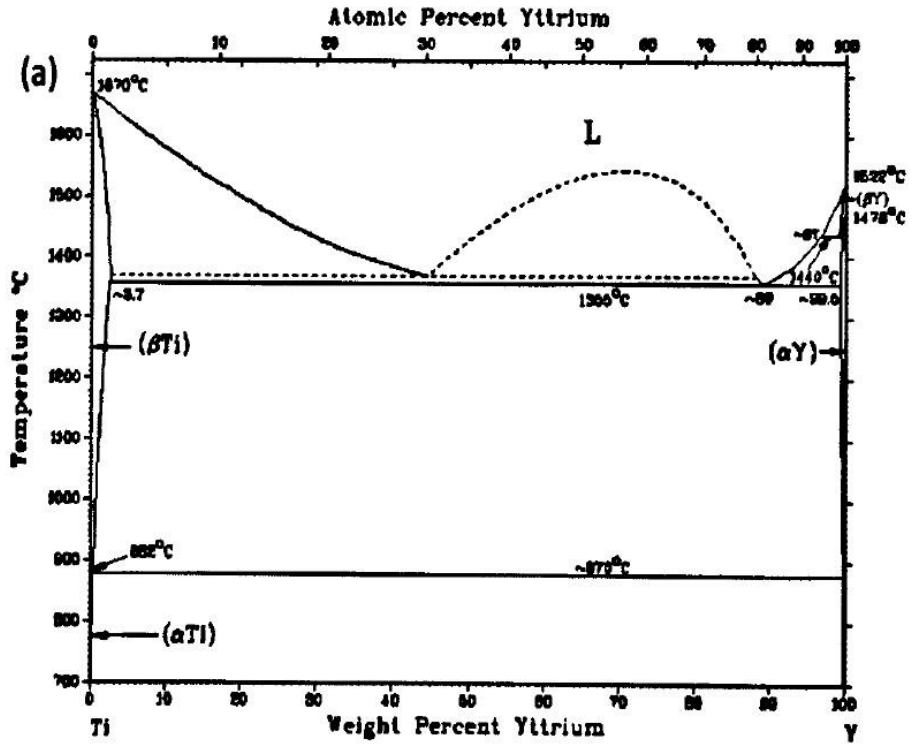

Fig. 2.26 Ti-Y binary phase diagram [95]

(2) RE oxides precipitated in the titanium matrix. The commonly used RE oxides contain Y_2O_3 and Er_2O_3. However, in the ingot making process, a refined and

uniform distribution of Y_2O_3 or Er_2O_3 is hard to achieve because either the rare earth elements or corresponding oxides have only a very small solubility in the matrix [15, 90]. In a normal casting process, the coarse precipitation of rare-earth elements or coarse oxide particles are not useful for improving the properties of titanium alloys.

(3) Complicated composite. Sometimes a complicated texture is obtained. TiAl alloy with yttrium additions shows many [Al,Y,O] based compounds [96]. For example, $Al_5Y_3O_{12}$ is obtained in a TiAl alloy oxidized at 800℃ [97]. Y Al_2 intermetallic was found by Y. Chen in a Ti-43Al-9V-0.3Y alloy [98]. $(AlTiNb)_2Er_3$ was reported by Yubin Ke in Ti-16Al-27Nb with Er additives [99].

2. 5.2 Microstructure of Ti-RE alloy

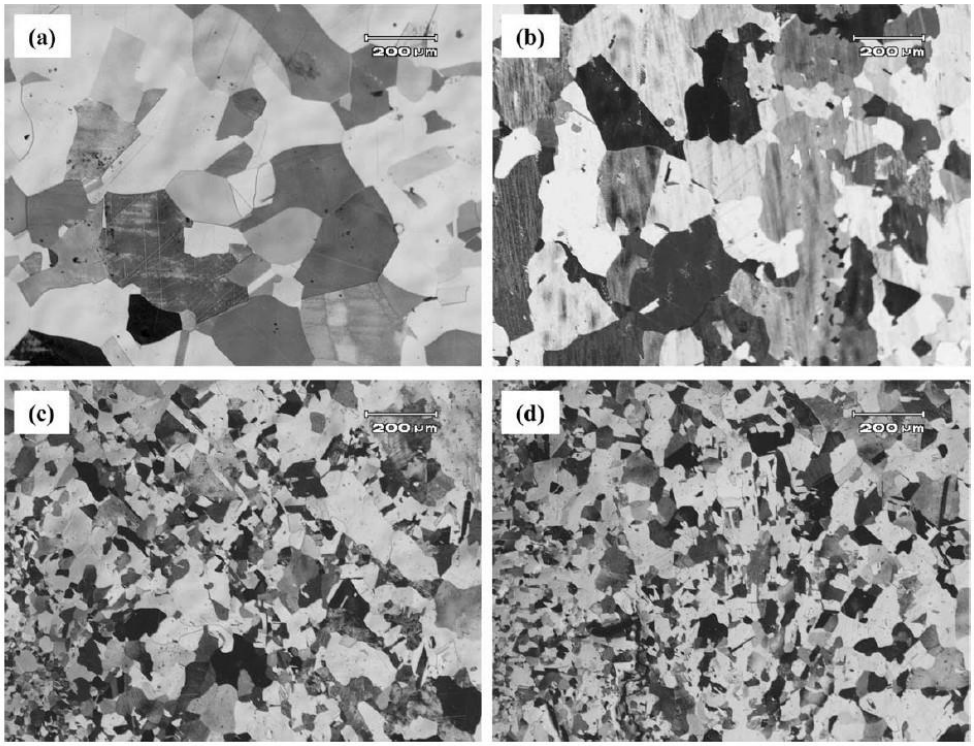

Fig. 2.27 Optical micrographs of solution treated (1400℃/1h/AC) γ-TiAl alloy with (a) Y-free, (b) 0.1at.%Y, (c) 0.6at.% Y, and (d) 1.0at.%Y [97]

For ingot titanium, RE elements improve the grain nucleation ability of titanium, thus a more refined microstructure is achieved. For hot working or recrystallization of Ti-alloys, RE oxides precipitate at the grain boundaries and reduce the grain growth in low temperature β-phase. High temperature (>1100℃) leads to the dissolution of RE oxides in a β-matrix, thus rapid grain growth begins [16]. This temperature is higher than the temperature for carbides. The effect of carbon additions is minimal at temperatures above 850℃.

RE oxides markedly refined the β grain size of Ti and Ti alloys, thus a much more refined microstructure is obtained. Y. Wu proved that the grain size gradually decreased from about 250 to 50μm with increasing Y content from 0 to 1.0at.% (Fig. 2.27). Similar results have been found by other researchers working on different Ti alloys.(Table 2.6).

Also, the lamellar thickness is refined by RE additions. Y. Chen reported that adding yttrium can refine the α_2/γ/B2 internal spacing of a Ti-43Al-9V alloy from 1.9μm to 1.1μm and promote the formation of α_2/γ lamellae [98]. Y. Wu reported that both the thickness of α_2 and γ lamellae is reduced by a 0.33at.% Y addition [100].

Table 2.6 Effects of RE or RE oxides addition on grain size of Ti alloy

Ti-alloy	Phase	RE or RE oxide	Grain size at RE-free addition	RE addition	Grain size after RE adding	Literature
IMI829	β	Gd	500μm	0.2at.%	100μm	[101]
SP-700	α+β	Y	500μm	0.07at.%	34μm	[16]
Ti-43Al-9V	Near α	Y	170μm	0.3at.%	80μm	[98]
CP-Ti	α	Y_2O_3	41μm	0.28at.%	8μm	[102]
				0.42at.%	8.5μm	
				0.66at.%	2μm	
Ti-1100	α+β	Y	980μm (prior β)	0.1at.%	250μm (prior β)	[103]

An ideal dispersion of RE oxides in Ti and its alloys is reported by V. De Castro [102]. TEM images of the Y_2O_3 dispersion in as-cast and recystallised samples are shown in Fig. 2.28. Although Y_2O_3 particles with sizes $\geqq$ 100nm were occasionally found, the particle sizes were generally less than 60nm. The particles were clearly spherical and homogeneously distributed in the inner regions of the grains, when their diameters were less than ~10nm. A SAD pattern shown in Fig. 2.29 confirms the presence of yttria. The average value for the lattice parameter of

Y_2O_3 was $\alpha=(1.15\pm0.07)$ nm and reasonable agreement with reported values for cubic Y_2O_3 (α= 1.06 nm).

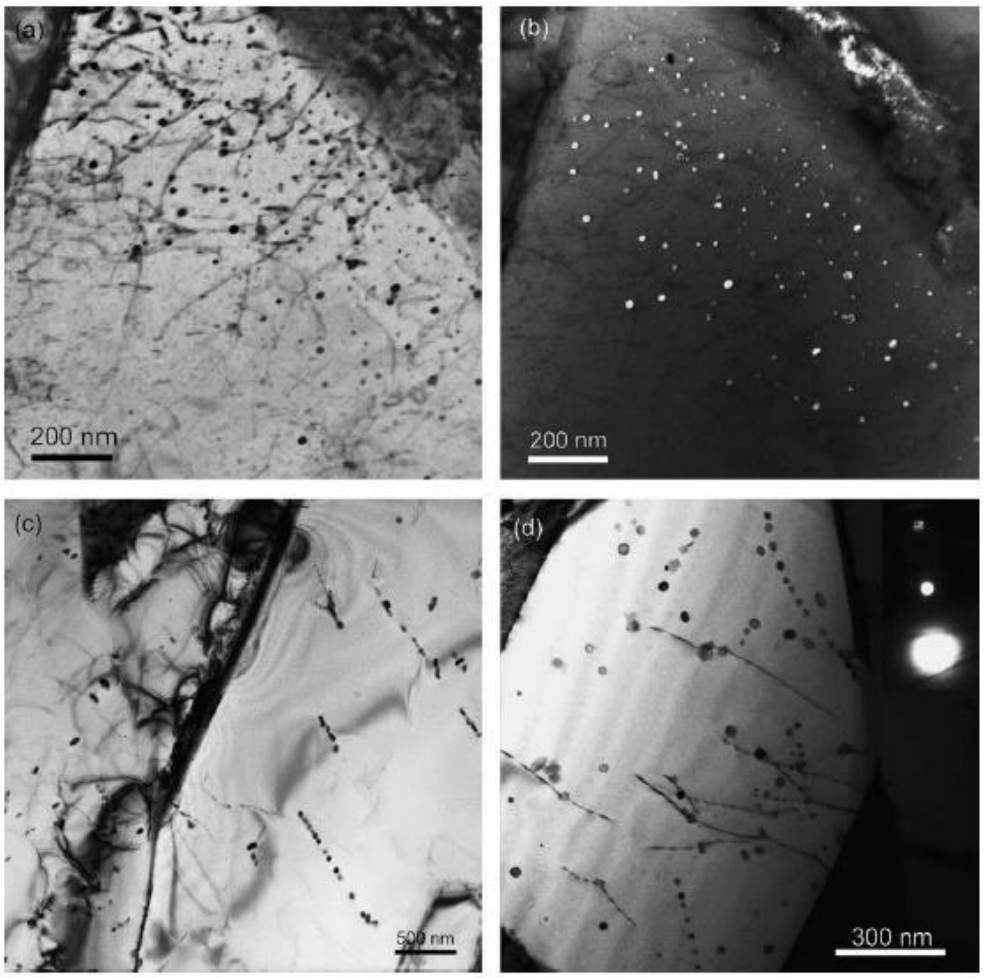

Fig. 2.28 TEM images of as-cast and recrystallized Ti-Y_2O_3 alloys: (a) bright field and (b) dark field images of recrystallized Ti-0.42wt.% Y_2O_3 alloy; (c) as-cast Ti-0.42wt.% Y_2O_3 alloy and (d) recrystallized Ti-0.66wt.% Y_2O_3 alloy [102]

W. Lu investigated the microstructural characterization of in situ synthesized Y_2O_3 in titanium matrix composites. It was found that Y_2O_3 tended to grow in a dendritic shape and becomes coarse, whereas secondary Y_2O_3 is mostly spherical and small in size [104].

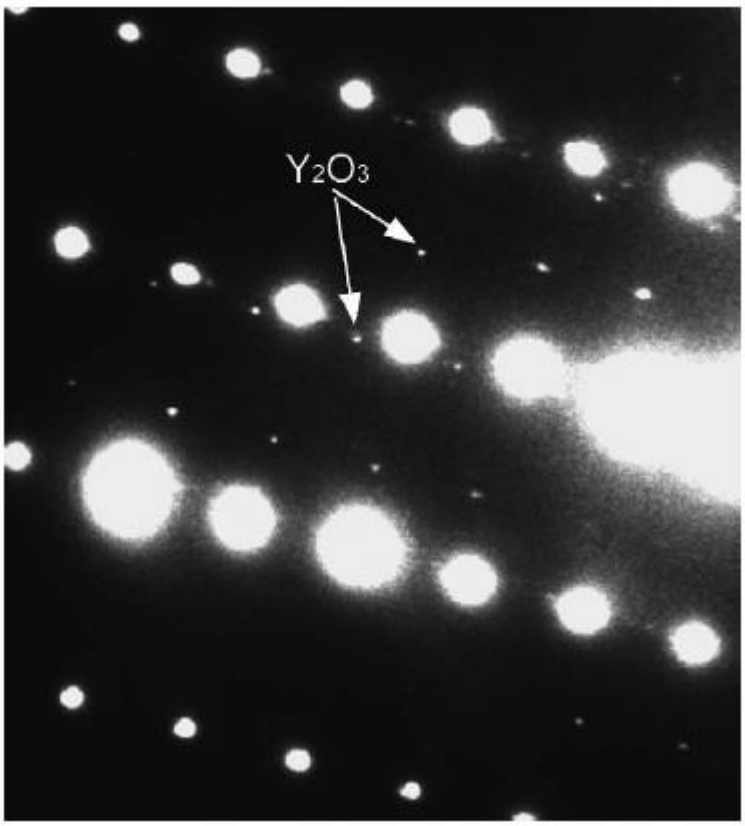

Fig. 2.29 Selected area diffraction for Ti-0.42wt.% Y_2O_3 alloy showing spots from the matrix and Y_2O_3 particles [102]

There is also a favoured orientation relationship between the yttria precipitates and the titanium matrix. A relationship of $[105]_{Oxide}//(0\ 0\ 0\ 1)_{Ti}$ and $<1\ 1\ 1>_{Oxide}//<1\ 1\bar{2}0>_{Ti}$ with the oxide particles being stoichiometric is easier to be generated in the alloy with high oxygen level. Whereas the relationship of $[106]_{Oxide}//(0\ 0\ 0\ 1)_{Ti}$ and $<1\ 1\ 1>_{Oxide}//<1\ 1\ 2\ 0>_{Ti}$ appear to be associated with oxygen deficient particles which are less stable against coarsening than stoichiometric ones. The stability of the oxide particles and their orientation relationship with the titanium matrix appears to be dependent on the oxygen content in the matrix [90, 107-115]. V. De Castro reported a differed crystallographic relationship of $[105]_{Y2O3}//(0\ 0\ 0\ 1)_{Ti}$ and $<1\ 2\ 0>_{Y2O3}//[1\ 1\bar{2}0]_{Ti}$ in the Ti-Y_2O_3 alloy [102].

2.5.3 Properties of Ti-RE alloys

The improvement in mechanical properties from RE or RE oxide additions to Ti and Ti alloys is quite notable. Firstly, they lead to a more refined and stabilized microstructure (both in the grain size and lamella structure), which significantly increases the strength and ductility. Secondly, a dispersed RE_2O_3 distribution gives an improvement in strength due to the Ostwald ripening mechanism. Lastly, the oxygen level in alloys is controlled by RE additions. For pure RE additions, the strengthening effect of an oxide dispersion is evident in titanium above room temperature. But it was not apparent at low temperatures because the solid-solution hardening is reduced due to the oxygen scavenging of the elemental metal addition. Thus a RE-free titanium may be harder than the RE-added alloy, but the ductility is certainly inferior [107]. Some researchers use multiple-reinforced composites containing RE_2O_3 for Titanium alloys. In such a process, in-situ RE_2O_3 oxides are synthesized from the reaction between many compounds. A higher strength and plasticity is obtained [116, 117].

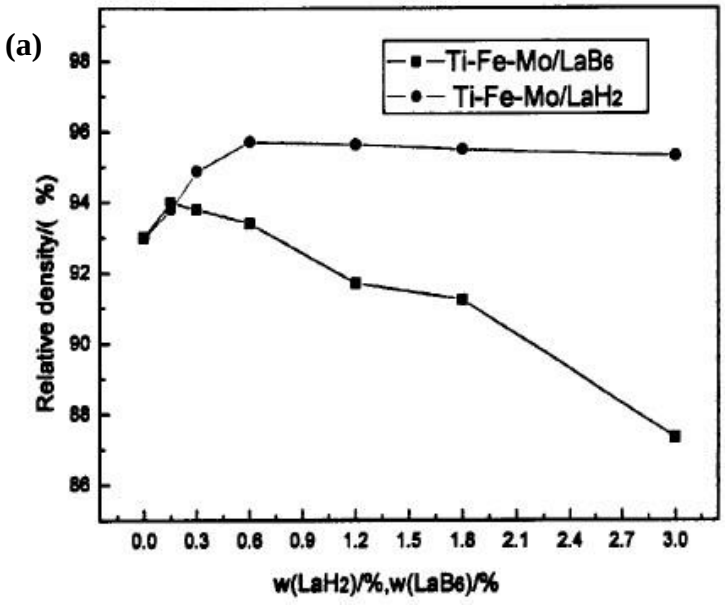

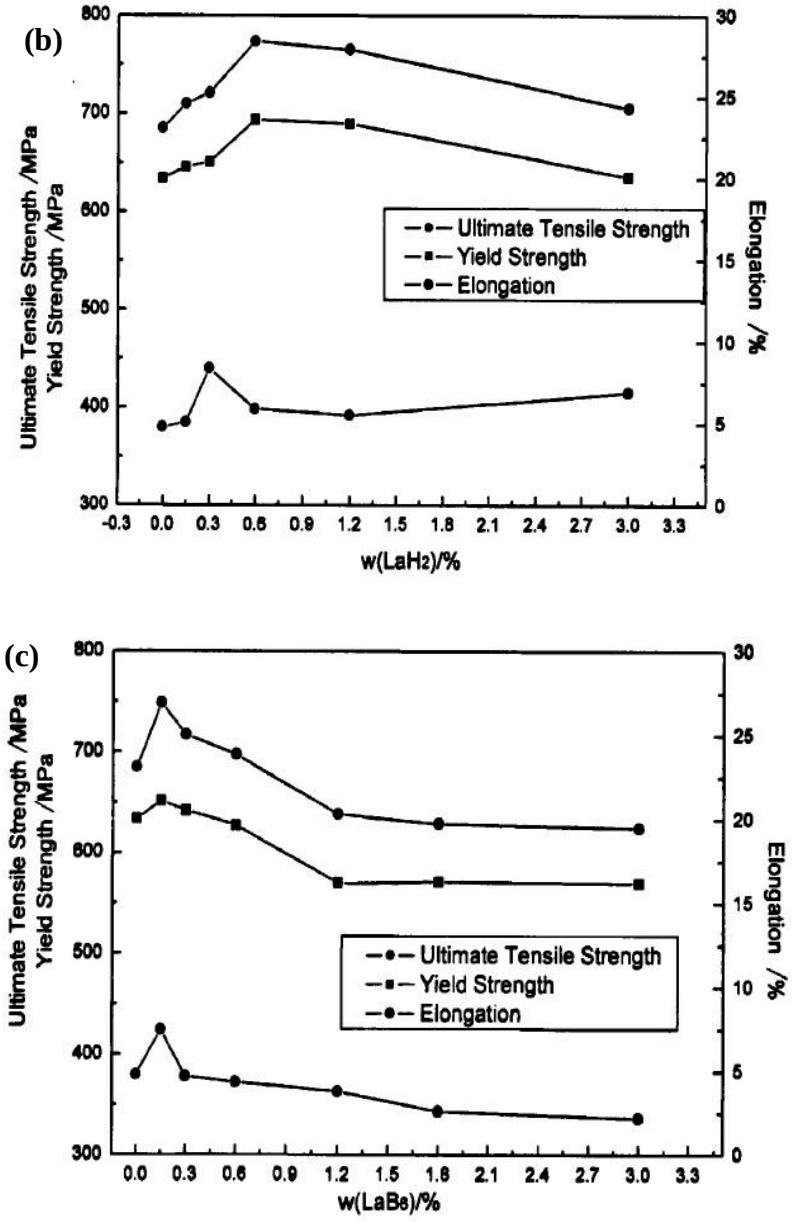

Fig. 2.30 Effect of RE composite additions on the properties of a Ti-Fe-Mo alloy: (a)Density; (b) Effect of LaH_2 and (c) Effect of LaB_6 [17]

Y. Liu reported the effect of LaH_2 and LaB_6 on the properties of Ti-Fe-Mo alloys. A small amount of LaH_2 is able to increases the sintered density by 2-3%, yet LaB_6 does not have this trend. (Fig. 2.30(a)) The strength and ductility of sintered parts is improved by a small addition, but higher additions will decrease the properties. (Fig. 2.30(b) and (c)) A forging process can further improve the mechanical properties [17].

Y. Ke reported that a 0.7at.% Y addition can improve the elongation of Ti-16Al-27Nb-0.7Y alloy from 38% to 43%, and 0.6at.% Er can improve elongation to more than 95%.. The fracture toughness is also improved by Y and Er addition [99]. H. He has investigated the effect of neodymium on the microstructure and mechanical properties of titanium prepared by metal injection moulding (MIM) [80]. It is found that the density and elongation increase and then decrease with increasing Nd content.

Y. Wu and other researchers reported that Y gives moderate improvement to the room temperature ductility because it can scavenge oxygen and promote the activity of 1/2<110] type ordinary dislocations in TiAl based intermetallics [118-122].

For high temperature properties, Y. Wu compared the mechanical properties of TiAl-base alloy with 0-0.66at.% Y from room temperature to 1000℃. From 0-800℃, Y additions give rise to better strength and elongation. A 0.33at.% addition shows the best improvement. But after 800℃, Y does not improve strength but the improvement in elongation was still notable [74]. Y. Chen reported that adding Y can increase the recrystallisation capability of Ti-43Al-9V to create plenty of smaller and uniform recrystallized grains formed in the Ti-43Al-9V-0.3Y alloy. Thus alloys with Y additions showed much lower peak stress, flow stress and superior deformability at 1200℃ [98].

There are some reports on the effects of RE elements on the oxidation resistance of P/M Ti alloys. Considering that most RE-containing Ti alloys are used for high temperature applications, the oxidation resistance is critical. Fig. 2.31 shows the results obtained by Y. Wu [74, 100, 123]. RE are thought to improve the oxidation resistance at very high temperatures, but are not helpful at room temperature. The reason is due the formation of four different oxide phases:TiO_2, α-Al_2O_3, Y_2O_3

and $Al_5Y_3O_{12}$. The Y_2O_3 and $Al_5Y_3O_{12}$ prevent the ingress of oxygen better than TiO_2, α-Al_2O_3.

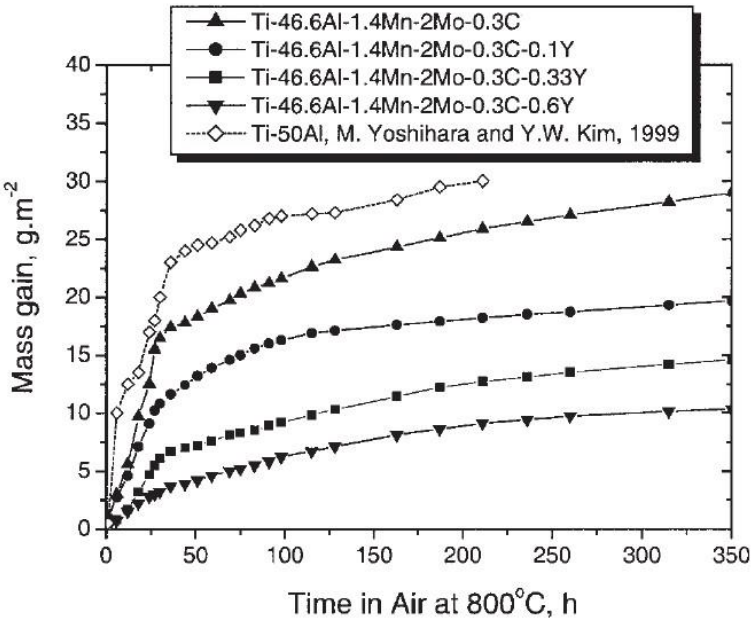

Fig. 2.31 Effect of Y on the oxidation kinetics of EPM Ti-46.6Al-1.4Mn-2Mo-0.3C-xY alloys at 800℃ [74]

2.6 Contribution and hypotheses of present thesis

Systematic research, which has been carried out for the compaction of iron/aluminium and ceramic powders with lubricant addition, is required for the compaction of titanium powder with a lubricant. This thesis will study the compaction process for lubricated Ti powder from a study of different compaction properties, such as compressibility, ejection behaviour and shape retention. The density profiles, which cannot be obtained directly from a Ti compact, will be measured experimentally using the coloured layer method.

There is no research on the relationship between the inhomogeneous green density and corresponding inhomogeneity of sintered mechanical properties. This thesis

attempts to investigate the variation in sintered mechanical properties using test-pieces taken from different regions in a compact. Such work will prove that powder lubrication is a way to produce sintered Ti parts with more homogenous mechanical properties.

Although there are many methods for adding and compositional forms of introducing RE additives to P/M Ti metal and alloys, a comprehensive comparison between these methods and forms is required. The advantages and disadvantages of these methods and forms will be discussed in this thesis. The best approaches will be recommended.

Although there is some literature which talks about the compaction mechanism of Ti powder, the reasons accounting for the drawbacks of Ti powder compaction (such as inferior compressibility and significant green density inhomogeneity) has not been studied. On the basis of the literature, theoretical research will be carried out for the purpose of explaining the differences in the compaction process for titanium and iron/aluminium. Also the influence of adding an internal lubricant to titanium powder to aid the compaction process will be studied, from the aspect of the compaction mechanism.

3. Chapter 3 Experimental Procedures

3.1 Introduction

This chapter describes the experimental methodologies, equipment and materials used in this research work. In particular, a description is provided for the lubrication procedure, compaction behaviour and tests for the powder compacts, the debinding and sintering procedure and sample characterization.

3.2 Metal powders and its conditioning

3.2.1 Metal powder and lubricants powders

Table 3.1 Particle sizes of Ti alloy particles and lubricant particles

Powder	HDH Ti	HDH Ti64	SA	MgSt	Y, Er	LaB_6	PREP Ti
Particle size	-200 mesh	-200 mesh	<50um	<5um	-40 mesh	<10um	-100-200 mesh

All powder compaction experiments were carried out using hydride-dehydride (HDH) CP-Ti and Ti-6Al-4V powder. The particle size distribution of HDH Ti powder is: D_{10}=20.84μm, D_{50}=47.69μm, D_{90}=91.03μm; of Plasma rotating electrode process (PREP) Ti powder is: D_{10}=107.24μm, D_{50}=153.48μm, D_{90}=218.67μm. The apparent densities of HDH and PREP Ti powder are 1.42g/cm^3 (31.51% relative density) and 2.74g/cm^3 (60.83%) respectively. The tap densities of HDH and PREP Ti powder are 2.08g/cm^3 (46.26%) and 2.95g/cm^3 (65.48%). Two commercial lubricants were used in this study: stearic acid (SA) and magnesium stearate (MgSt). Y, Er, LaB_6 powders are 99.9% in purity, provided by the SIGMA-ALDRICH. The morphologies of the titanium alloy powders are shown in Fig. 3.1. The particle sizes of the powder are shown in Table 3.1. Among them, the Er powder shows quite a different feature: it is

cotton-like, with a length of more than 500μm, about 500μm in width and 50-100μm thick.

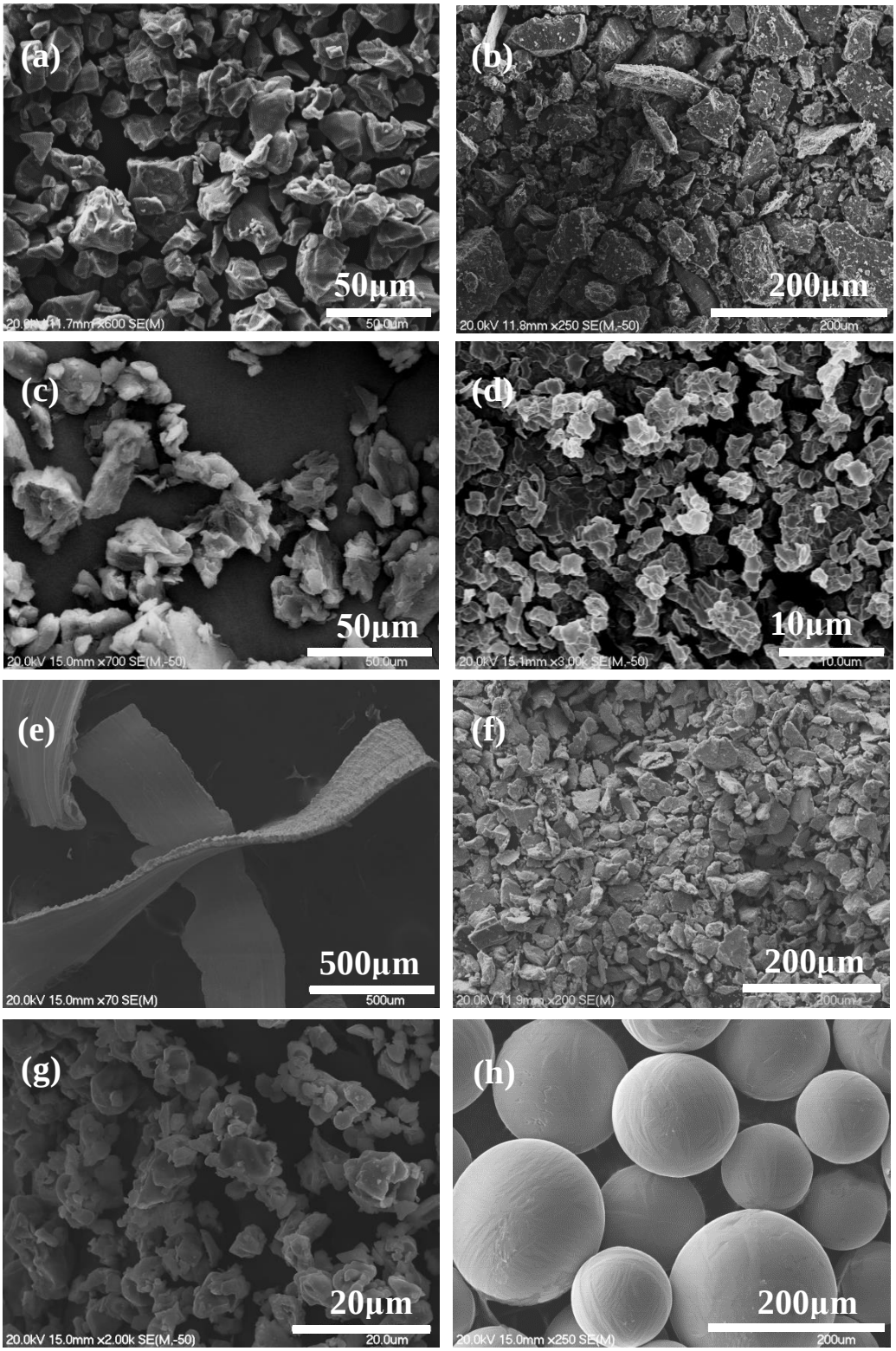

Fig. 3.1 SEM micrographs of Ti alloy powder particles and lubricant particles: (a) HDH CP Ti; (b) HDH Ti-6Al-4V; (c) SA; (d) MgSt; (e) Er ;(f) Y; (g) LaB_6 and (h) PREP CP Ti

3.2.2 Lubrication

For laboratory use, about 80 grams of powder and lubricant mixture were put in a plastic bottle to be mixed, with 3-5 small steel balls (radius =1.5mm) to assist powder blending. Eight bottles filled with mixtures containing different concentrations of lubricant were put together in a metal bottle and then blended on a roller mixer at 30Hz for 12h. This mixing condition made sure that the mixing condition for different types of mixture was the same. For comparison, an industrial mixing condition, in which 500 grams of powder mass and bigger mixing balls (radius=5mm) was used.

For wet blending, 0.6wt % of SA was dissolved into a small amount of ethanol. The SA-ethanol solvent was mixed with the Ti powder by hand. During the mixing, a heater was used to accelerate the removal speed of the ethanol. The hand mixing did not stop until most of the ethanol was removed. The mixture needed to be held for 1-2 days to remove the residual ethanol before compaction.

For die wall lubrication (DW), a saturated SA-ethanol solvent was used. Solvent was wiped onto the inner wall of the die and onto the surface of the plungers. They were then dried in air. After the solvent had completely evaporated, the inner die became coated by the dry SA powder and the die set was then ready for the compaction work.

3.2.3 Mechanical milling

The Ti alloy powder and Y elemental powder particles were mechanically milled in a high energy planetary ball mill (Retsch, Germany) under argon atmosphere. 140g powder mixture was used in each batch. Steel balls with radius= 12.5mm were used in this thesis. The Ball/powder weight ratio is 4:1. No process control

agent was used in this work. The mixture was mixed at 100rpm for 6h and then at 200rpm for 6h. The milling machine is shown in Fig. 3.2.

Fig. 3.2 Mechanical milling machine

3.3 Compaction and tests for powder compacts

3.3.1 Compaction

The powder and lubricant mixtures were compacted in different dies and presses. A φ11mm cylindrical die was used for most compression work. A 10 tonne oil press and a 50kN INSTRON tensile tester were employed to do the compaction work. A specific die was designed for making the tensile test samples. This was a dog-bone shape with a width of 8mm and a gauge length of 24mm. A 35tonne press was used for this work. A φ40mm cylindrical die was used for the compaction of very big samples and in this case a 100 tonne press was used. Images of different dies and press are shown in Fig. 3.3 and Fig. 3.4 respectively.

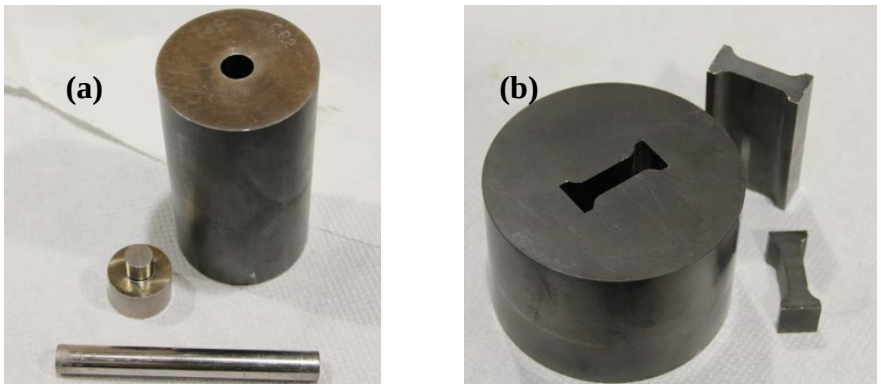

Fig. 3.3 Die sets for compaction: (a) φ11mm, and (b) tensile specimen die

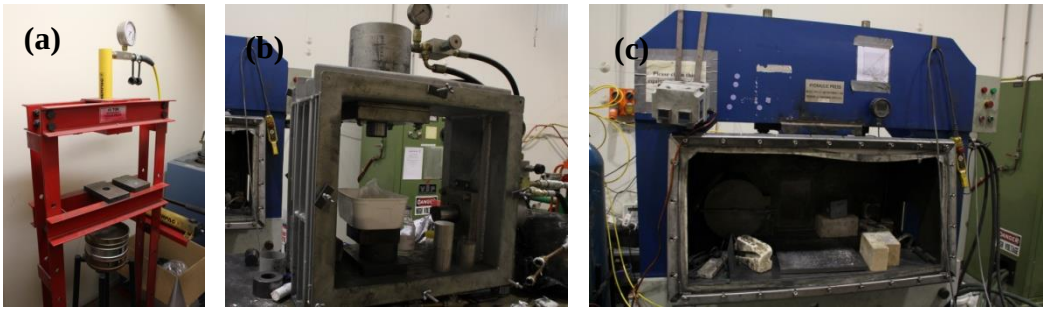

Fig. 3.4 Presses for compaction: (a) 10t, (b) 35t, and (d) 100t

3.3.2 Test for powder compacts and ejection behaviour

The relative density of powder compacts was calculated by dividing their mass by volume. Please note that this mass contains the mass of lubricant, thus the pure metal density is lower than the calculated one. The fracture strength of the green compacts was estimated using a diametrical compression test, which is based on the state of stress developed when a cylindrical specimen is compressed between two diametrically opposite stress generators on its surface. For an ideal in-line-loading case, the maximum tensile stresses, which act across the plane containing the loading axis, have a constant magnitude which may be approximated by:

$$\sigma_m = \frac{2P}{\pi D l} \qquad (3.1)$$

where:

σ_m is the maximum tensile stress,

P is the applied load at fracture,

D is the diameter of the sample l is the specimen length.

The load /displacement curves for powder compacts were recorded using an Instron tensile testing machine. This data was then used to deduce the density /pressure curves to evaluate the compressibility. The load/displacement curves for the ejection process were also recorded using an Instron tensile testing machine. The density gradient measurement will be introduced in more detail in Chapter 5.

3.4 De-lubrication, sintering and heat treatment

Compact de-lubrication was carried out in a tube furnace with a continuous argon flow. The sintering work was carried out using a ZSJ 20X20X30 vacuum furnace provided by the Advanced Corporation for Materials and Equipment (ACME). The sintering condition was plotted in each chapter. Heat treatment was carried out in a muffle furnace without protective atmosphere. A BN coating was used to coat a protective layer on specimens to avoid oxidation. An image of the vacuum furnace is shown in Fig. 3.5.

Fig. 3.5 Vacuum furnace for sintering

3.5 Mechanical tests of the final parts

3.5.1 Tensile testing

The samples for tensile testing were cut using an EDM wire cutter. The standard tensile test samples used in this work were dog-bone shaped specimens with a rectangular cross section of 2mm*2mm and a gauge length of 20mm. An INSTRON 4204 tensile testing machine was used for testing the samples using a cross head speed of 0.05mm/mim.

3.5.2 Hardness testing

To investigate the hardness profiles of the powder compacts, hardness testing was carried out on the mid-cross sections of powder compacts by using a LCR-500 hardness tester. At least 3 samples were tested at one condition to insure that the results used were typical and repeatable.

3.6 Microstructure characterization

3.6.1 Sample preparation

Samples to be prepared were cut to an appropriated shape using a wire cutter, or a diamond blade or they were selected directly for subsequent mounting. The powder, powder compacts and sintered samples were embedded in epoxy resin and hardened for 24 hours. The mounted specimens were ground using 160, 320, 600, 1000/1200, 2000 and 4000 grit SiC papers, followed by polishing using an alumina suspension (0.3μm agglomerated alumina)

3.6.2 Optical microscopy (OM) and Etching

Samples for characterization were studied using optical microscopy (Olympus BX60). To observed the microstructures, samples were etched using Krolls reagent mixed from 92ml distilled water, 6ml of HNO_3 and 2ml of HF. A typical etching time was 10-15 seconds.

3.6.3 Scanning electron microscopy (SEM) and Energy dispersive x-ray analysis (EDX)

Microstructural characterisation of powder particles, mounted samples and the fracture surfaces of tensile test samples were carried out using an Hitachi S-4000 scanning electron microscope, at an operating voltage of 20KV. Energy Dispersive X-ray analysis (EDX) was carried out using a Kevex microanalyser attachment.

3.6.4 X-Ray diffractometry (XRD)

X-ray diffraction analysis (XRD) was performed to determine the phase constituents in both powder and coating samples using an X'pert diffractometer (Philips, the Netherlands) with Cu Kα radiation. The XRD patterns were obtained

using a 0.02° step size averaging 5 seconds per increment, with a voltage of 40KV and a current of 40mA.

3.6.5 Thermogravimetic analysis (TGA) and differential thermal analysis (DTA)

Thermogravimetic analysis (TGA) and differential thermal analysis (DTA) were used to evaluate both the de-binding progress of Ti alloy powders with lubricant, and the sintering processing of milled Ti-RE element, by using a simultaneous SDT 2960 analyser under flowing argon at a rate of 150 ml/sec. The heating rate was at 10℃/min from room temperature to a selected temperature. For debinding test, 30mg of powder mixture was used and the maximum temperature was 600℃.

3.6.6 Transmission electron microscopy (TEM)

Specimens for TEM were prepared by cutting 3mm disks from the bulk material and thinning the samples down to ~ 100μm. Final jet polishing was done using a mixture of 65% methanol and 35% sulphuric acid using a polishing temperature of about -40℃.The TEM work was done using a Philips CM30 microscope.…

3.6.7 Chemical composition test

Testing for carbon and oxygen content was done at the Materials Analysis and Testing Centre, Northwest Institute for Non-ferrous Metal Research, China.

4. Chapter 4 Compaction Behaviour of Lubricated Titanium Alloy Powders

4.1 Introduction

Compaction studies in Powder Metallurgy (P/M) have received a lot of attentions and in particular the role which lubricants play in the compaction process has been studied in detail for P/M ferrous and aluminium. Research done by other scientists has shown that the influence of lubricants is different for low pressure and high pressure conditions, the boundary being the bulk yield strength of the sample [4, 8, 28, 69]. Thus if we want to investigate the effects of lubrication on the compaction behaviour of P/M titanium alloys, we should investigate the whole compaction process and split this into two regions: a low pressure region from no pressure to 400MPa, which is near to the bulk yield strength of CP Ti, and a high pressure region higher than 400MPa. Moreover, lubrication also changes the ejection behaviour and the green strength. Lubrication causes the ejection pressure to decrease sharply, which is another attractive reason for applying lubricants. However, there is one point of concern and that is that lubrication severely decreases the green strength (shape retention) of powder compacts. In order to investigate the effects of lubricants on the compaction behaviour of Ti alloy compacts, the densification behaviour, ejection forces and green strength should be considered overall.

In this research, separate investigations were carried out on the compressibility of powders in two pressure regions by analyzing the density/pressure curves (load/displacement curves) for Ti alloy powder compacts. The density and microstructure of the lubricated Ti alloy powder compacts were analysed to provide

more specific and detailed information. The ejection behaviour, shape retention and green strength of the compacts are also studied. The purpose of the present work is to compare the influence of different lubricants, their concentration and blending methods, from which optimized processing parameters can be deduced.

4.2 Experimental details

Load/displacement curves were used to assess the compaction behaviour of powders. HDH Commercial Pure (CP) Ti or HDH Ti64 powder was dry mixed with 0.3, 0.6, 1 or 2wt.% of SA or MgSt to obtain the mixture for compacting. For comparison purposes, HDH CP Ti powder with 0.6wt.% of SA was wet blended. The starting density of each compaction condition was determined by the mass/height data of the powder body. A relative density/pressure curve is deduced from the load/displacement curves. Compacts were pushed out of the die and reweighed, then the thickness and diameter were measured to obtain a green density. The procedure is similar, in principle, to that described by Gerdemann and Jablonski's work [124].

A height/radius (H/D) ratio of 1 was used for most compaction work. At this condition, 3.2 grams of Ti alloy powder and lubricant mixture was used to fill the die. In the cases where H/D=1.5, 4.8 grams of mixture was used. The mass deviation was controlled to within ±0.5wt.%

4.3 Results

4.3.1 Compaction behaviour of lubricated Ti powder under low pressure conditions

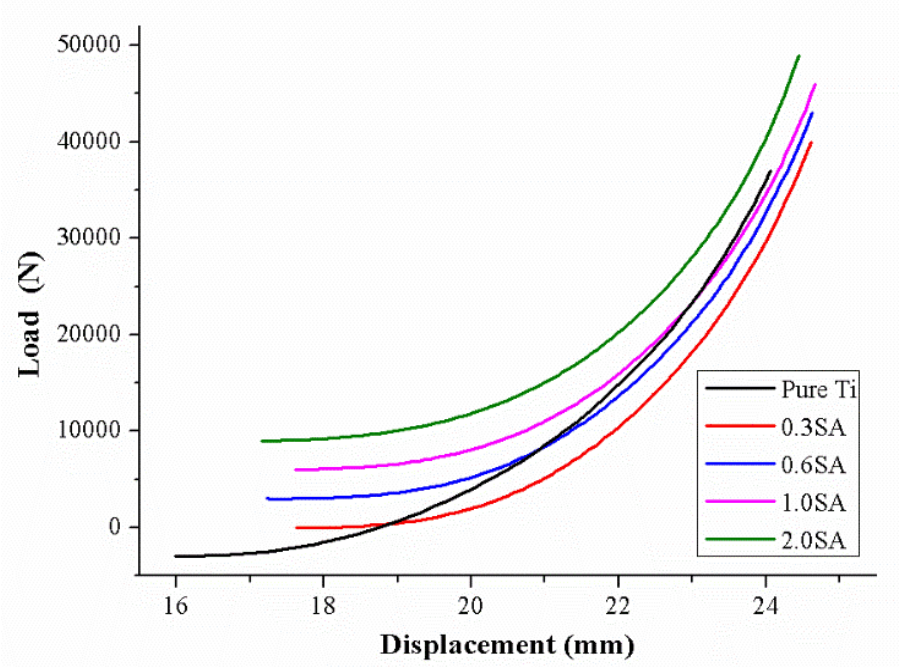

Fig. 4.1 Load/displacement curve of Ti powder compacts with different concentration of lubricants

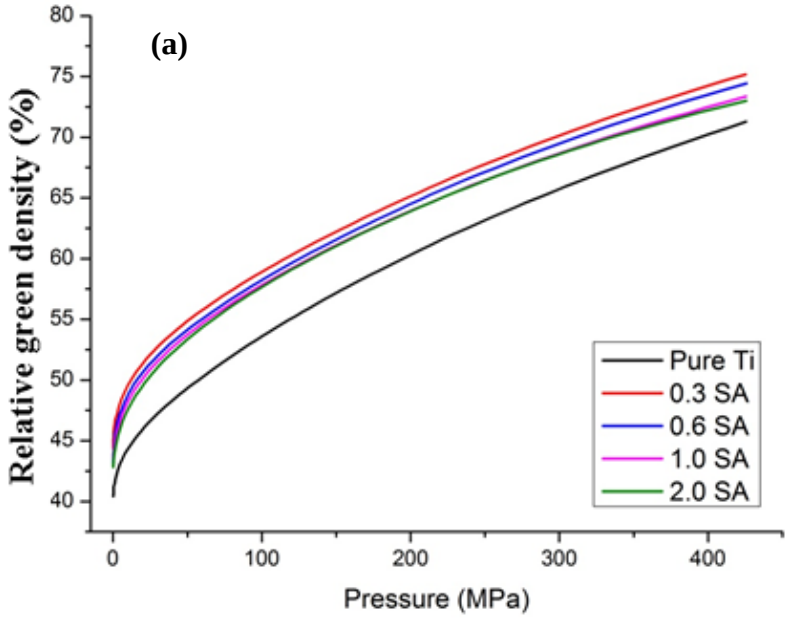

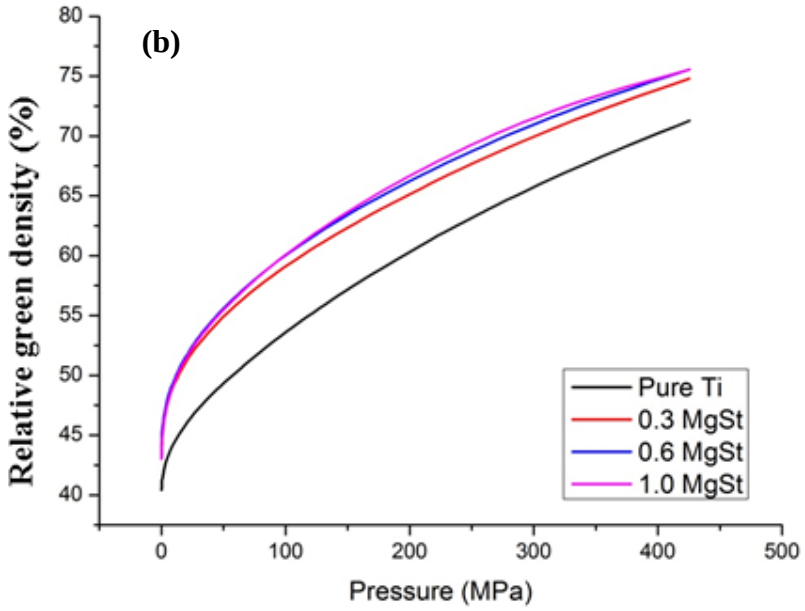

Fig. 4.2 Relative green density/pressure curve of Ti powder compacts with different concentration of lubricants: (a) SA and (b) MgSt

The load/displacement curves of the compaction processes are shown in Fig. 4.1. To avoid overlapping, a 3kN load has been added to the curves for each successive lubricant addition. The highest load for all compacts is 40kN, which gives a compaction pressure of 452MPa. Experiments have identified that the influence of variations in powder packing and stain rate are negligible.

To get a better understanding of the compaction behaviour, the green density vs. pressure curve was deduced from the original load/displacement curves. The curves for Ti-xSA and Ti-xMgSt are shown in Fig. 4.2(a) and (b) respectively. The lubricant additions improve the packing density of Ti powder. An improvement of 10-15% relative density is observed in Ti-0.3SA or Ti-0.3MgSt. But more than 0.3wt.% SA slightly decreases the green density. MgSt improves the packing density to 0.6wt.%. Beginning from 250-300MPa, the densification rate of lubricated compacts are slower than lubricant-free compact, especially in those with more than 1wt.% of lubricants.

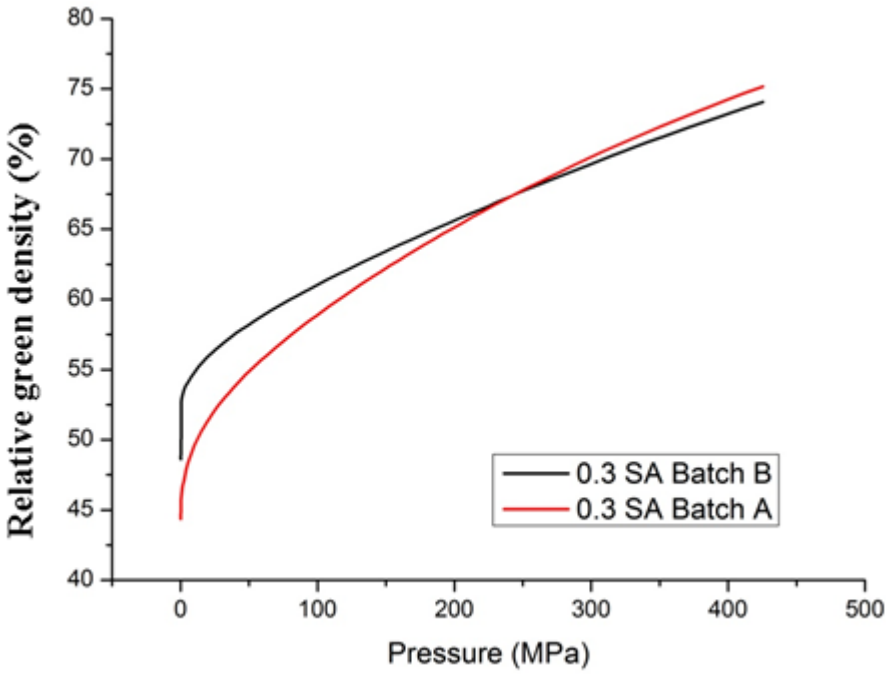

Fig. 4.3 Relative green density/pressure curve for compacts made using different batches of Ti powder

The effect of batches of powder is shown in Fig. 4.3. Batch A is fabricated by a simple milling condition for laboratory use, in which less than 200g powder mixture is packed in one bottle for mixing. Batch B is closer to an industrial condition in which 500g of powder mixture is put into a bigger container with additional milling balls for the purpose of assisting blending. The severe blending leads to a higher packing density but the densification rate of Batch A accelerates above that of Batch B immediately and will surpasses Batch B at about 250MPa.

The effects of lubricant type (SA or MgSt) and their concentration are shown in Fig. 4.4. For 0.3wt.% addition, the densification behaviours of the two compositions are equivalent. But for 1wt.%, MgSt exhibits much greater improvement in relative green density versus pressure compared with SA.

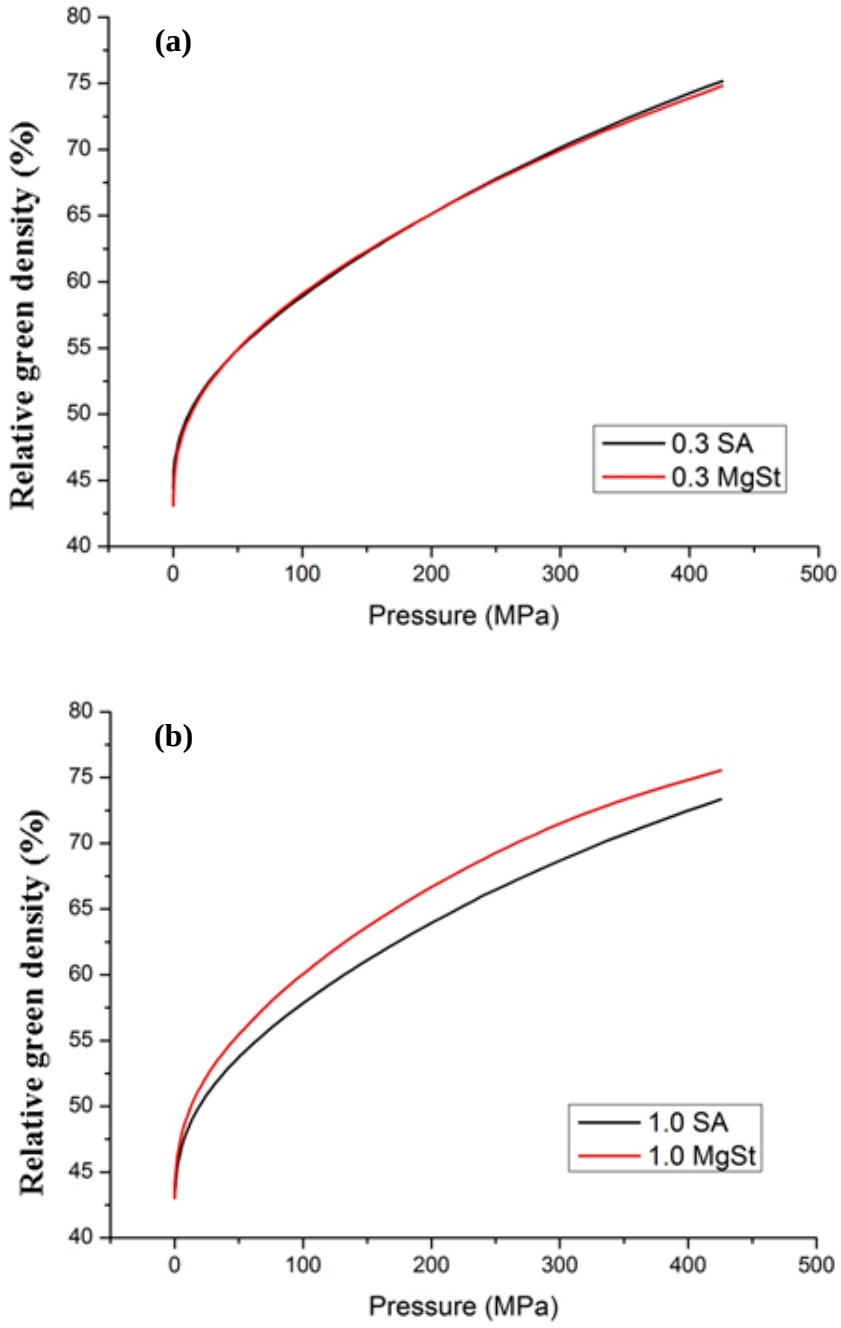

Fig. 4.4 Relative green density/pressure curve of Ti powder compacts with different composition: (a) 0.3wt.% and (b) 1wt.%

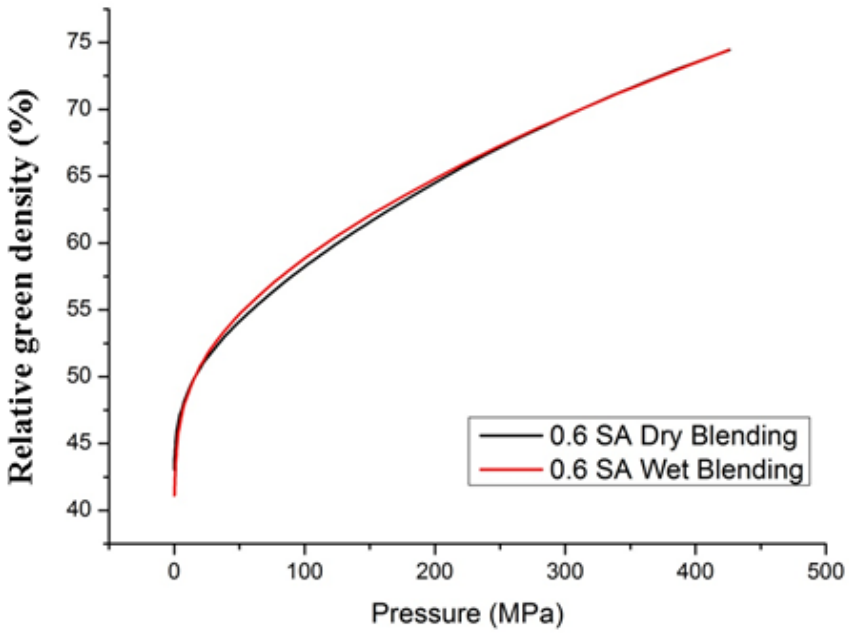

Fig. 4.5 Relative green density/pressure curve of Ti powder compacts prepared by different blending methods

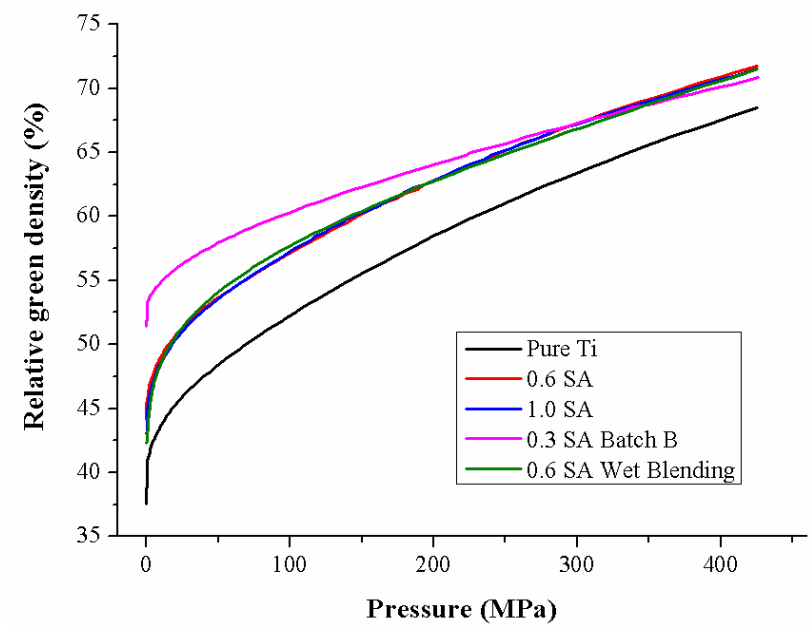

Fig. 4.6 Relative green density/pressure curve of high Height/Diameter Ti powder compacts

The effect of blending methods is shown in Fig. 4.5. Wet blending slightly improved the density to 250MPa. A comparison of different concentrations of lubricant and blending conditions for higher Height/Diameter (H/D) ratio condition

is shown in Fig. 4.6. By increasing the H/D ratio from 1 to 1.5, the density of the powder compact decreases but the degree of improvement from lubricant additions is notable. Moreover, compacts with various SA additions exhibit almost similar compaction behaviour. Batch B exhibits a higher packing density but a slower densification rate. Wet blending slightly improves the density to 250MPa. All phenomenon are similar to those found in the H/D=1 condition.

4.3.2 Density/pressure curves for the compaction behaviour of a lubricated Ti alloy powder under high pressure conditions

For powder compaction above 500MPa, the ejection pressure increases dramatically, so both die wall lubrication and internal lubrication must be applied for each condition. The curves for Ti-xSA and Ti-xMgSt compaction are shown in Fig. 4.7 and 4.8 respectively. In Fig. 4.7, Ti-0.3SA exhibits the highest density, this is due to the combination of internal lubrication and die wall lubrication. After that the compact density decreases. It is also notable that after 300MPa, a compact with more than 0.6wt.% of SA exhibits a slower rate of density increase, which indicates that too much lubricant retards densification rate. In Fig. 4.8, Ti-0.6MgSt exhibits the highest density. The compaction behaviours of Ti-0.3MgSt and Ti-1MgSt are similar. The detrimental effect of using a high SA lubricant concentration for pressures above 300MPa is not observed in MgSt addition.

A comparison between the compaction behaviour of compacts with 0.6wt.% each of SA, MgSt and SA wet blending is shown in Fig. 4.9. MgSt provides the best lubrication effect, SA wet blending is the second best, with an approximately 2% lower relative density. SA provides the worst lubrication effect an approximately 5% lower relative density than SA wet blending, with the difference in values increasing at higher pressures.

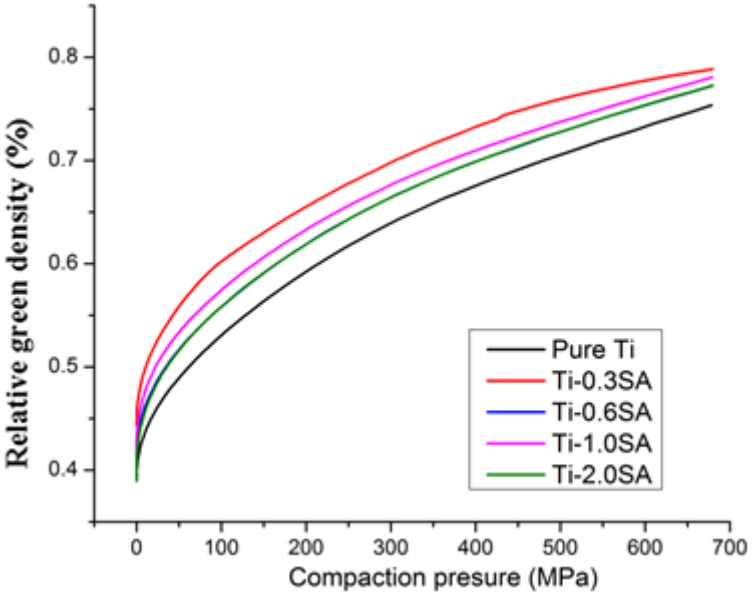

Fig. 4.7 Relative green density/pressure curves for Ti powder compacts with different SA concentrations under high pressures

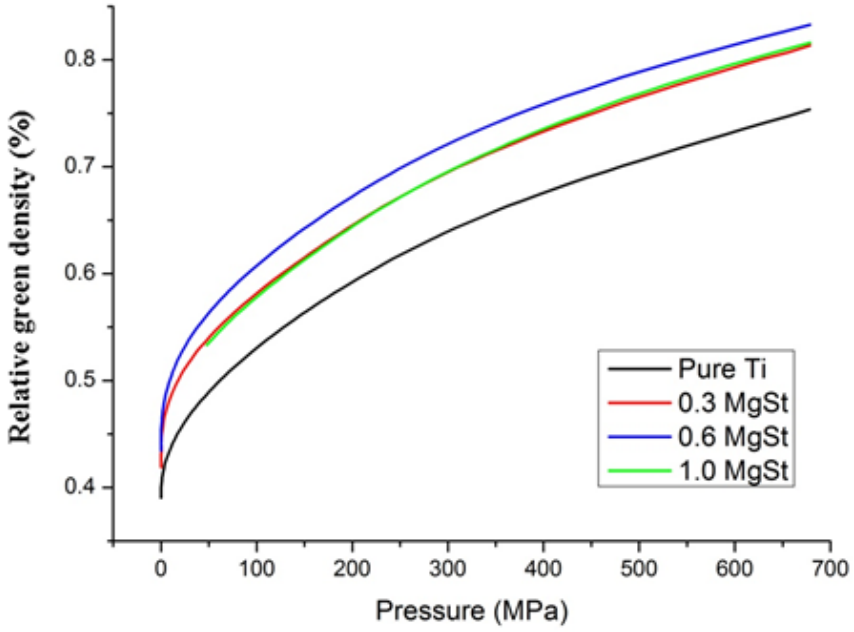

Fig. 4.8 Relative green density/pressure curves for Ti powder compacts with different MgSt concentrations under high pressures

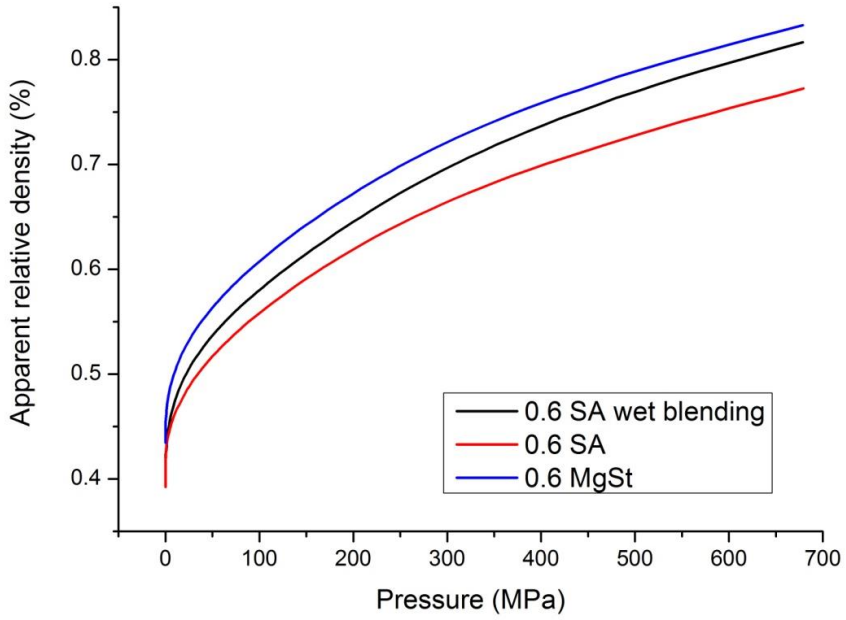

Fig. 4.9 Relative green density/pressure curve for Ti powder compacts with different lubrication condition under high pressures

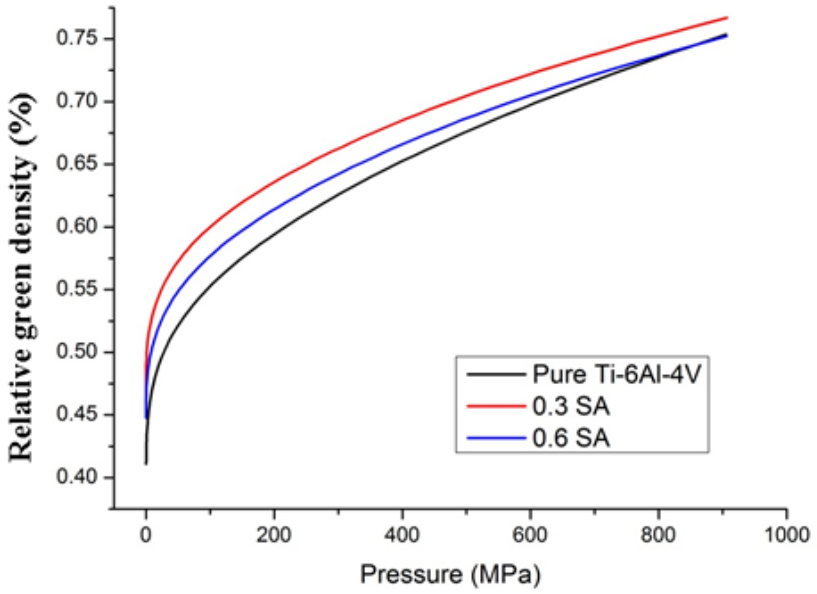

Fig. 4.10 Relative green density/pressure curve forTi64 powder compacts with different SA concentrations under high pressures

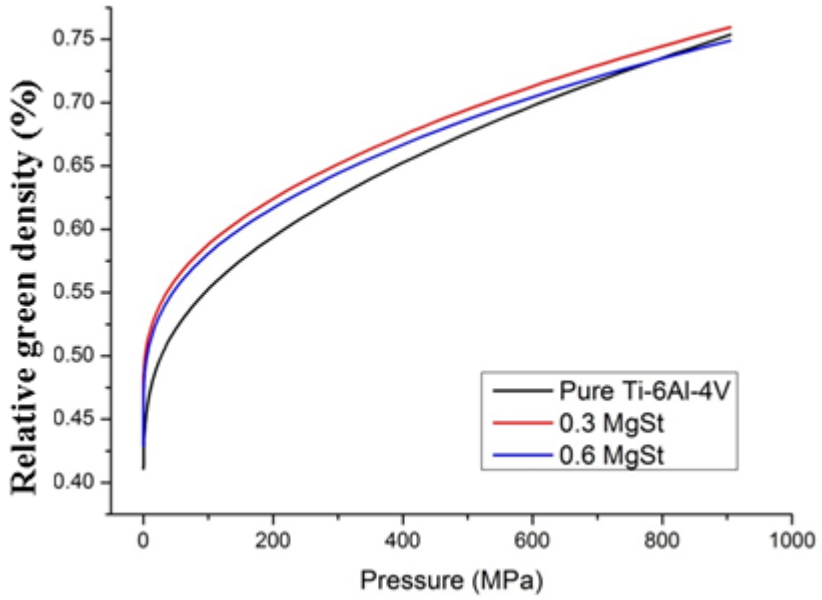

Fig. 4.11 Relative green density/pressure curve for Ti64 powder compacts with different MgSt concentrations under high pressures

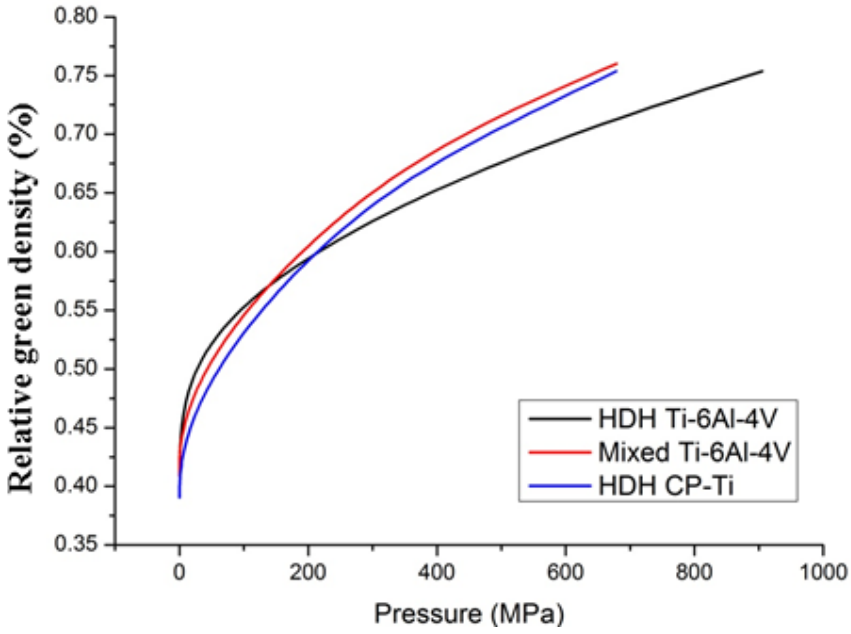

Fig. 4.12 A comparison of the compaction behaviours of HDH Ti64 powder, HDH Ti mixed with 60Al-40V master powder and HDH CP-Ti powder (without lubricant)

The relative density versus compaction pressure curves for HDH Ti64 powder compacts with SA and MgSt additions are shown in Fig. 4.10 and Fig. 4.11 respectively. Because HDH Ti64 powder is much harder and exhibits inferior

compressibility and compactibility than HDH CP Ti, a higher compaction pressure to 1000MPa was applied. Lubricants improve the density of Ti64 powder compacts, with 0.3wt.% of lubricant giving the highest density. At 0.3wt.% addition, SA exhibits a slightly better lubrication effect than MgSt. Above 500MPa pressures, any improvement in the green density significantly decreases, but the relative density of pure Ti64 does not reach the level achievable with 0.3wt.% of lubricant. 0.6wt.% SA addition decreases the green density than 0.3wt.% SA for whole pressure range. The reduction in density from a 0.6wt.% MgSt addition is smaller than that for 0.3wt.% SA. A critical effect is that the density achievable in pure Ti64 reaches that obtainable with 0.6wt.% of lubricant when the pressure exceeds 800MPa.

A comparison of the compaction behaviours among HDH Ti64, HDH Ti and HDH Ti blended with 10wt.% of 60Al-40V master powder is shown in Fig. 4.12. HDH Ti64 reaches 75% of theoretical density at 1000MPa and the densification rate is very slow after 55% of theoretical density. HDH Ti exhibits better compressibility, it reaches 75% of theoretical density at about 600MPa. The mixed powder exhibits the best compressibility, due to the bimodal particles mixture.

4.3.3 Density and microstructure of lubricated Ti alloy powder compacts

The previous section investigated the compaction behaviour of titanium and titanium alloy powders using density/pressure data recorded by a mechanical tester. This data gives information about the densification process taking place in Ti alloy powder compacts under different lubrication conditions. However these data cannot directly reflect the green density received. In fact, the spring back effect has not been taken into account. This section investigates the green density

and microstructures of cross-sections of Ti alloy powder compacts pressed using selective pressures.

The green density values of powder compacts using different lubrication conditions and pressures ranging from 300-500MPa are shown in Fig. 4.13. From Fig. 4.13(a), the green density of powder compact increases with the SA concentration, although the improvement from 0.6-2wt.% is very slight. But at compaction pressures of 400MPa and 500MPa, Ti-0.3SA exhibits great higher green density than SA-free compacts, but Ti-0.6SA exhibits no further improvement. Further SA addition decreases the green density. A double acting compaction procedure, which simultaneously presses the powder on two surfaces, was used twice at a pressure of 300MPa, and the results were compared with single action compaction. This process is designated 300MPa*2. The density values obtained from the 300MPa*2 condition are higher than those obtained at 400MPa, but lower than 500MPa. The trend in the green density vs. SA concentration is similar to that when using a compaction pressure of 500MPa. For die wall lubrication, compacts exhibit an inferior improvement to the internal lubricated sample. As shown in Fig. 4.13 (b), compacts with MgSt addition exhibits higher green density than those with SA additions, but the improvement from more than 0.6wt.% addition is very slight. The green density values obtained from the actual compaction process are in good agreement with data obtained from the load/displacement curves.

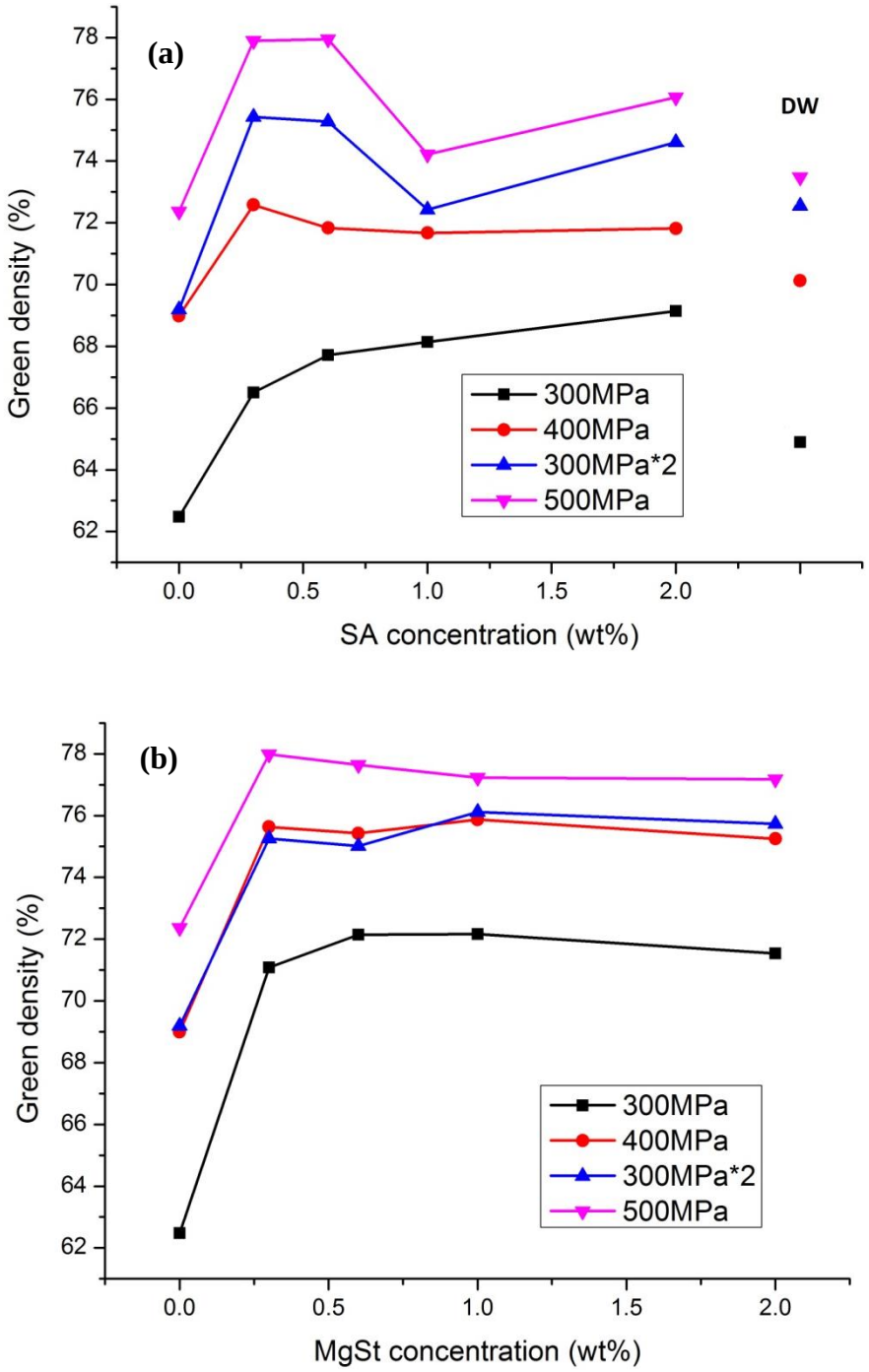

Fig. 4.13 Effects of lubricant concentration on green density of powder compacts: (a) Effect of SA and (b) Effect of MgSt

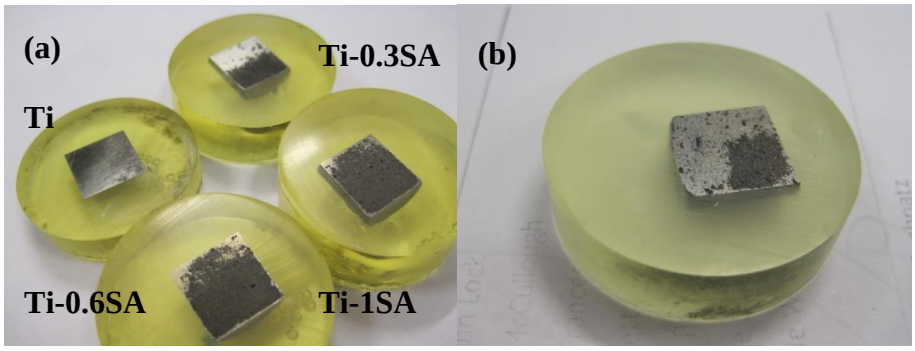

Fig. 4.14 Cross sections of powder compacts prepared from powder with different SA concentration: (a) Dry blended and (b) 0.6SA wet blended

Images of powder compact cross-sections are shown in Fig. 4.14. All powder compacts pressed using compaction pressures under 400MPa were ground using 120mesh grinding paper to get the mid-cross section. Obvious differences can be seen in the images. A lubricant-free compact displays a very bright surface with metallic luster. With a 0.3wt.% SA addition there is a two-phase structure with the half closest to the upper plunger, i.e. near to the surface in contact with the applied pressure, displays a similar bright and smooth surface to the pure Ti compact, whereas the half closest to the lower plunger displays a dark and porous structure. A compact with more than 0.6wt.% SA also displays a two-phase structure, but the area giving a bright appearance is much smaller and can only be found in the top corner and edge of a compact. A compact with 0.6wt.% of SA, mixed by wet blending, or MgSt displays a structure as shown in Fig. 4.14 (b). They also exhibit a two-phase structure, but the bright area is very porous.

Fig. 4.15 shows SEM micrographs of the cross-sections shown in Fig. 4.14. From Fig. 4.15(a), it is very clear that powder particles in lubricant-free compact and the bright region in Ti-0.3SA compact have been severely pressed. The bonding force of particle to particle is strong and deformed particles could not be ground off from the surface. But Fig. 4.15(b) shows there is a very clear boundary between the bright region and dark region. Fig. 4.15(c) proves that the dark region consists of a lot of

power particles which have not been well compacted and the feature of interparticle locking is limited. Fig. 4.15 (d) shows the dense region in Ti-0.6SA. Powder particles have been compacted together, which results in a large amount of particle interlocking. But this interlocking is not strong enough to keep particles stable during grinding. Fig. 4.15 (e) shows the dense region of a compact with 0.6wt.% of SA prepared by a wet blending method. The powder particles have been completely deformed but the bonding force from particle to particle seems to be very weak. Surface particles appear to have been ground off, leading to a very porous bright surface. Fig. 4.15 (f) shows the darker region the same compact. A visual observation suggests that the powder particles have been compacted to a more severe degree which is much more obvious than Fig. 4.15 (c). But the grinding-off effect is also notable. The characteristics of powder compacts with MgSt is similar to those with 0.6wt.% SA prepared by wet blending.

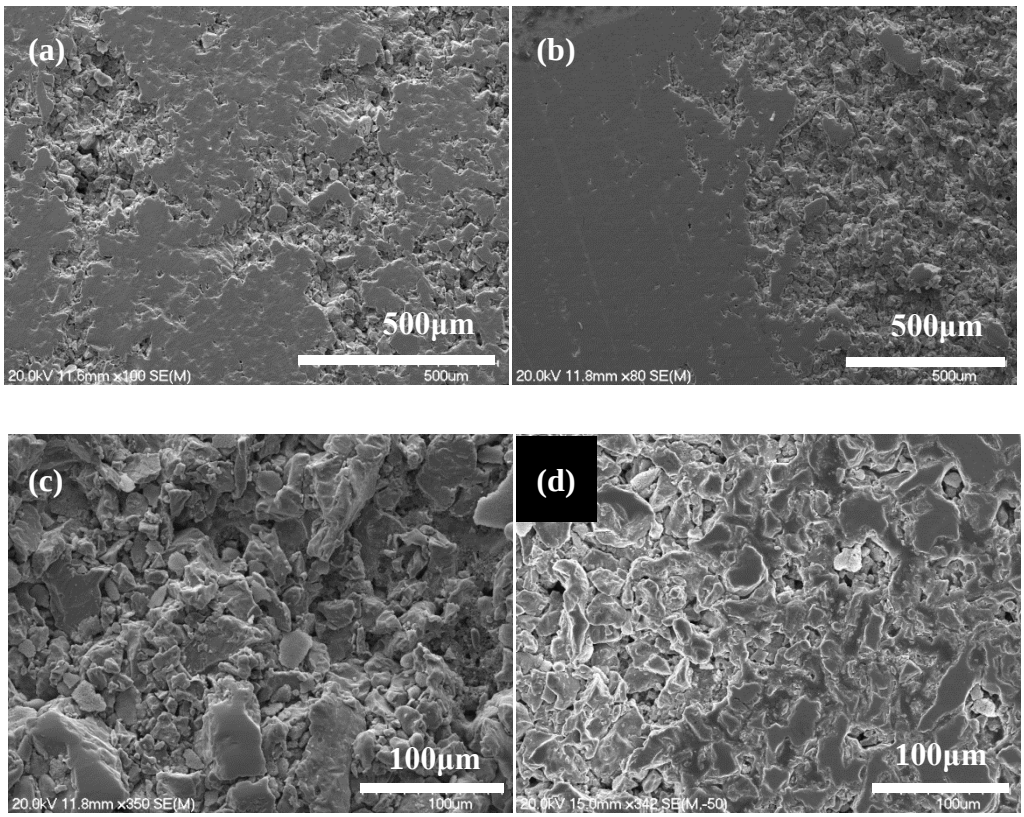

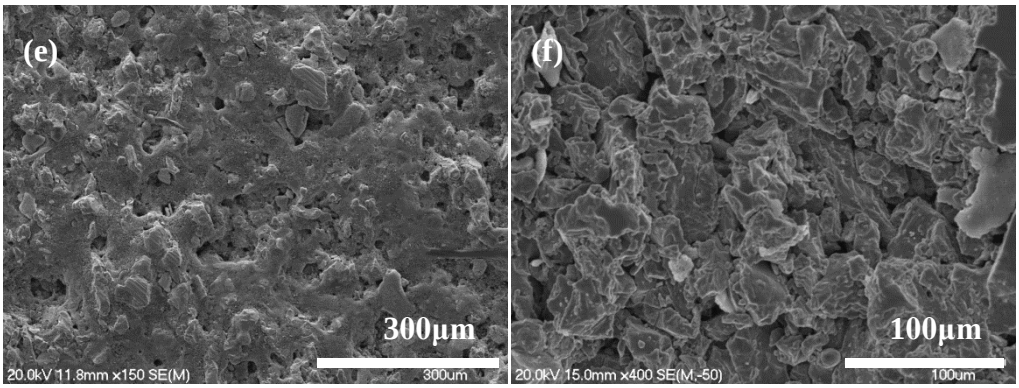

Fig. 4.15 SEM micrographs of cross sections of Ti powder compacts: (a) white region in Ti-0.3SA; (b) boundary region in Ti-0.3SA; (c) black region in Ti-0.3SA; (d) white region in Ti-1SA; (e) white region with 0.6wt.% SA wet blended and (f) black region with 0.6wt.%SA wet blended

4.3.4 Shape retention and green strength of lubricated Ti alloy powder compacts

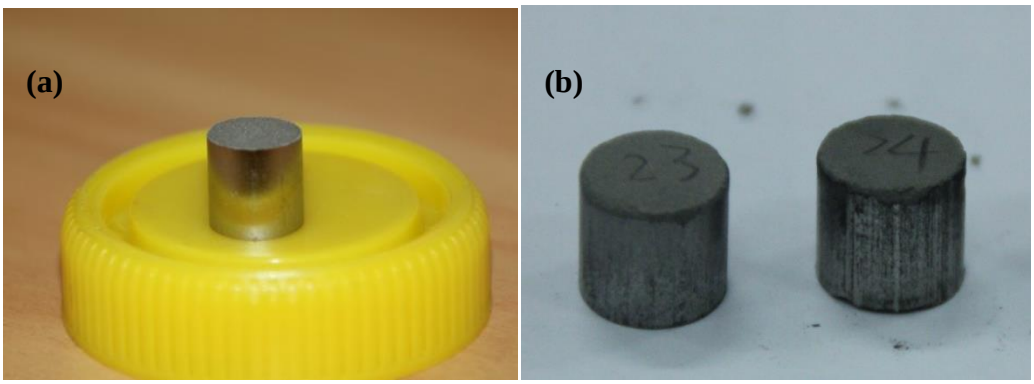

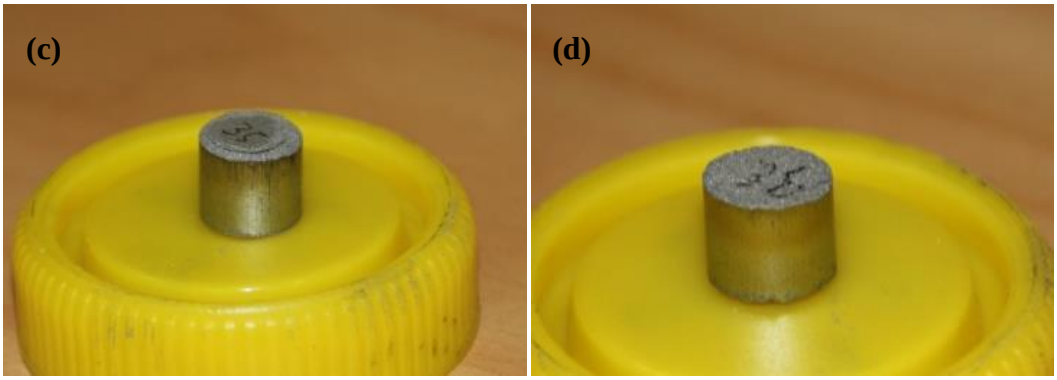

Fig. 4.16 Four kinds of surfaces of powder compacts: (a) Complete (n≈100%); (b) Nearly complete (n>99%); (c) Edge damaged (97<n<99%) and (d) Top damaged (n<95%)

In the meantime of increasing the compressibility of metal powder, it significantly decreases the shape retention of a powder compact. The evaluation of shape retention can be reflected in the weight loss before/after compaction and green strength of a compact. After being ejected from the die, a powder compact loses some of the more loosely bonded surface powders due to the weaker bonding force and excess ejection force. In order to characterize the powder compact surface after ejection from the die, four descriptors for surfaces of powder compacts have been used in this study, as shown in Fig. 4.16. The formula for the weight loss of a powder compact is listed below:

$$n = \frac{m_p - m_c}{m_p} \tag{4.1}$$

Where:

n is the function of shape retention,

m_p is the mass of powder used for compaction,

m_c is the received mass of powder compact.

Table 4.1 Surface types of powder compacts with different SA concentration

Pressure	0SA	0.3SA	0.6SA	1SA	2SA	DW
300MPa	◎	●	●	◎	◎	◎
400MPa	○	◎	◎	◎	◎	○
500MPa	×	◎	◎	◎	◎	×
300MPa*2	○	○	○	○	○	○

○：Complete; ◎: Near complete; ●: Edge damaged; ×: Top damaged; 300MPa*2: two direction compaction

Table 4.2 Surface types of powder compacts with different MgSt concentration

Pressure	0.3MgSt	0.6MgSt	1MgSt	2MgSt
300MPa	◎	●	●	◎
400MPa	●	●	●	●
500MPa	●	×	×	●
300MPa NE	●	●	●	●
400MPa NE	●	●	●	●
300MPa*2	○	○	○	○

NE: In this condition, the compact is ejected from the surface on which the compaction pressure is applied

The surface types of all powder compacts with SA and MgSt additions are listed in Table 4.1 and 4.2 respectively. The *n* values of powder compacts with SA and MgSt additions are listed in Table 4.3 and 4.4 respectively. From Table 4.1 to 4.4, we can conclude that in the lower pressure regions, lubricant additions are detrimental to shape retention, with MgSt exhibiting the more apparent effect. A notable decrease in *n* can be seen at lubricant concentrations of 0.3 to 0.6wt.% SA and 0.3 to 1wt.% MgSt, but after that the shape retention is stable or even improved. But for compactions made at 500MPa pressure, the shape retention is

improved by lubrication. Compacts pressed using pressures under 400MPa exhibit the best shape retention, but compaction at a pressure of 500MPa is not recommend for the ejection process. A double acting compaction process using a compaction pressure of 300MPa increases the overall strength of the powder compact, leading to an undamaged and complete powder compact shape.

Table 4.3 Values of *n* for powder compacts fabricated with different concentrations of SA concentration

Pressure	0SA	0.3SA	0.6SA	1SA	2SA	DW
300MPa	-	99.2	99	-	-	-
400MPa	-	-	99.4	-	-	-
500MPa	87.3	99	99.1	-	-	93.4
300MPa*2	-	-	-	-	-	-

-:>99.5% (at this time, the *n* value is of no meaning)

Table 4.4 Values of *n* for powder compacts fabricated with different concentrations MgSt concentration

Pressure	0.3MgSt	0.6MgSt	1MgSt	2MgSt
300MPa	99.4	97.2	97.7	-
400MPa	98.9	98.2	97.9	98.7
500MPa	96.5	87.8	87.5	98.5
300MPa NE	97.8	97.6	97.6	98.1
400MPa NE	96.6	97.6	97.1	97.7
300MPa*2	-	-	-	-

To further investigate the shape retention of powder compacts, the green compaction strength was investigated. Powder compacts produced using different lubrication conditions were pressed using a 400MPa compression pressure followed by a second pressure of 300MPa to completely retain the compact shape. The green

crushing strength of the powder compacts is shown in Fig. 4.17. lubricant-free powder compact exhibits the highest strength. The strength decreases 60% by adding 0.3wt.%SA and continues to slightly decrease with further additions. Compacts with a MgSt lubricant have a slightly lower green strength.

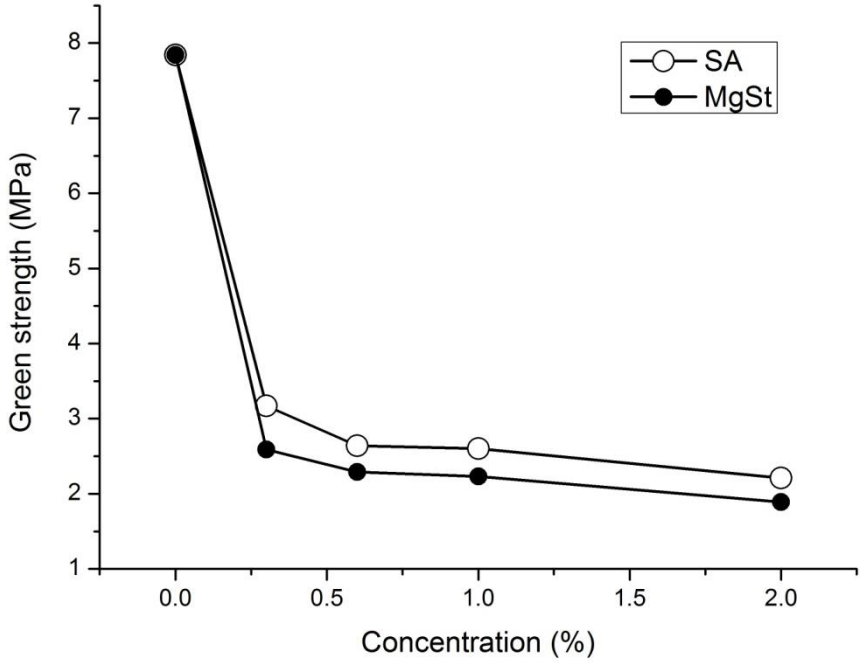

Fig. 4.17 Effects of lubricant on the green compacting strength of powder compacts

4.3.5 Ejection behaviour of lubricated Ti alloy powder compacts

The ejection pressure can be reduced and the ejection process made easier by the addition of lubricants, which will benefit the shape retention of a powder compact as well as prolonging die life. In this work, the ejection process was recorded from a load/displacement curve for the ejection process. The original curve obtained from the mechanical testing equipment is shown in Fig. 4.18. The ejection process can be separated into three stages. At first, the load increases sharply to a very high pressure (>100MPa), then it decreases rapidly to 0.5-0.7 of the maximum pressure. This is the stage I, where the compact starts moving out of the die and

the ejection process begins. The start pressure, i.e. the maximum pressure during the ejection process, is the pressure required to start the ejection. After that, the ejection pressure remains stable. During this time, the whole compact is moving in the die. This is stage II. The area of stage I and II is the ejection energy for the ejection process. In the final stage (stage III), the ejection pressure decreases rapidly, which means that the powder compact has been extruded from the die.

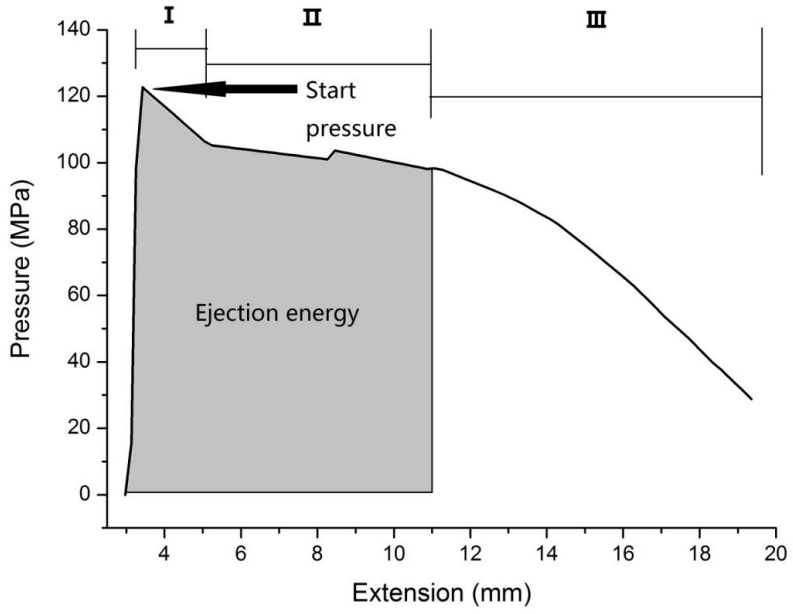

Fig. 4.18 Load/displacement curve of the ejection process obtained from a mechanical testing machine

The start pressure values for compacts with SA and MgSt are shown in Fig. 4.19. The starting load reduces with an increase in lubricant concentration. The highest reduction occurs at Ti-1SA and further addition to 2wt.% does not lead to further reduction. MgSt exhibits smaller reduction in ejection start pressure compared with SA.

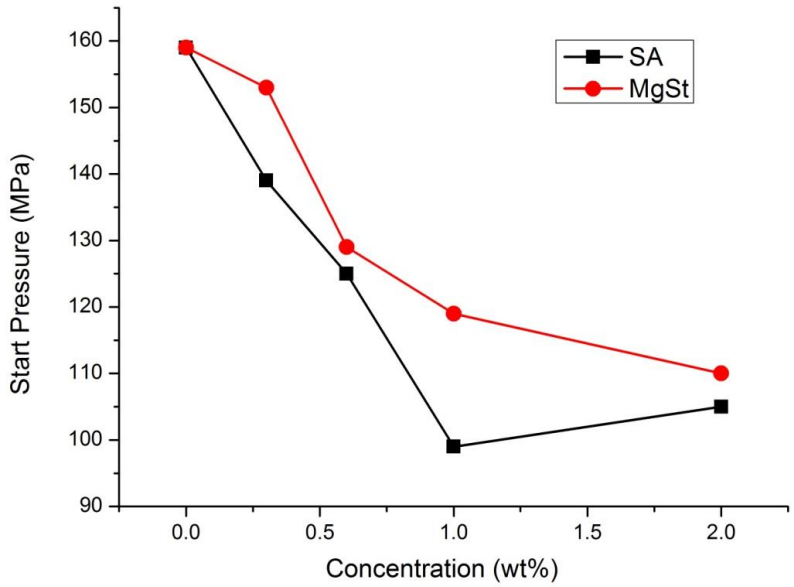

Fig. 4.19 Start load of powder compacts with different lubrication conditions

Fig. 4.20 shows values for the ejection energy with increasing concentration of lubricant. For single acting compaction, 0.3 to 0.6wt.% of SA does not reduce the ejection energy. In fact, the energy increases about 20J. More than 1wt.% of lubricant is needed. The reason is because the friction is increased by the ground off particles from the compact which are coated on the die wall. These particles are generated by the low green strength and excess ejection force. A double acting process at an ejection pressure of 300MPa improves the strength of the lower surface and hence eliminates the problem, as shown in Fig. 4.20.

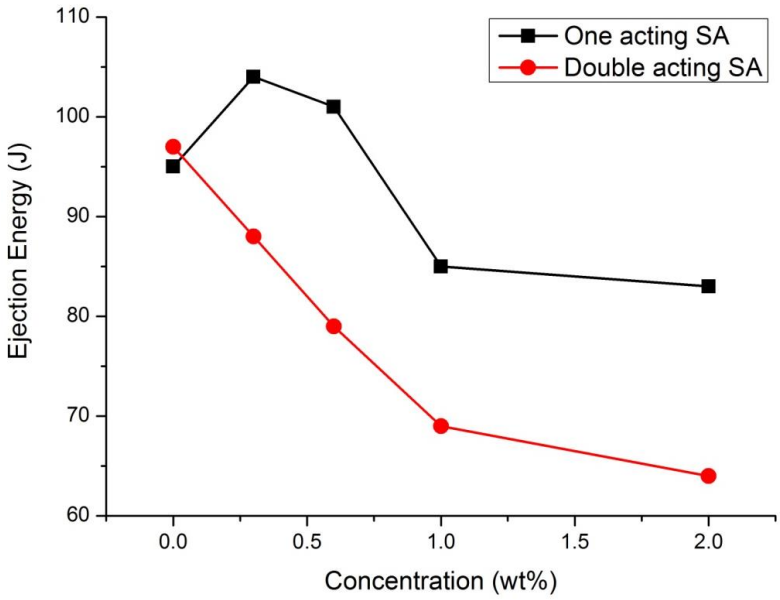

Fig. 4.20 Ejection Energy of compacts with different lubrication conditions and compacting methods

A comparison of the pressure/extension curves gives us information about the influence of lubrication on the ejection process. The curves of 0-2wt.% of SA are shown in Fig. 4.21. Lubricant-free compact exhibits a very high start pressure. The pressure reduces to about 125MPa for Ti-0.6SA and approximately 100MPa at 1-2wt.% SA. But after that, we can see a clear difference. For lubricant-free compact, the pressure decreases dramatically from 158 to 120MPa in a very short extension range, and then continues to decrease to 80-90MPa at stage II. During the whole ejection process, the curve is very smooth. For a compact with 0.3 to 0.6wt.% of SA, the pressure decreases after the ejection begins, but the rate is much slower than that for the pure Ti, and at stage II the pressure keeps at about 110MPa, which is much higher than that for pure Ti. Thus higher ejection energy is obtained. For samples with 1 to 2wt.% of SA, the pressure decreases to 80MPa at stage II, which is lower than that for pure Ti and thus the ejection energy is lower. For samples with SA additions, the curve is not very stable.

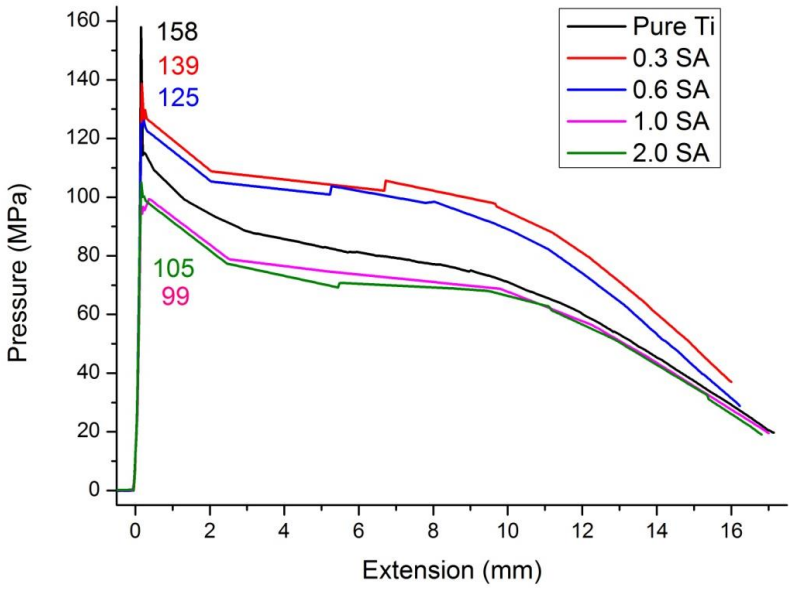

Fig. 4.21 Pressure/Extension curves of powder compacts with different SA concentrations

A comparison of single acting and double acting compact ejection with 0.6wt.% SA is shown in Fig. 4.22. Double acting ejection slightly improves the start load, but then it decreases rapidly and the curve is very stable.

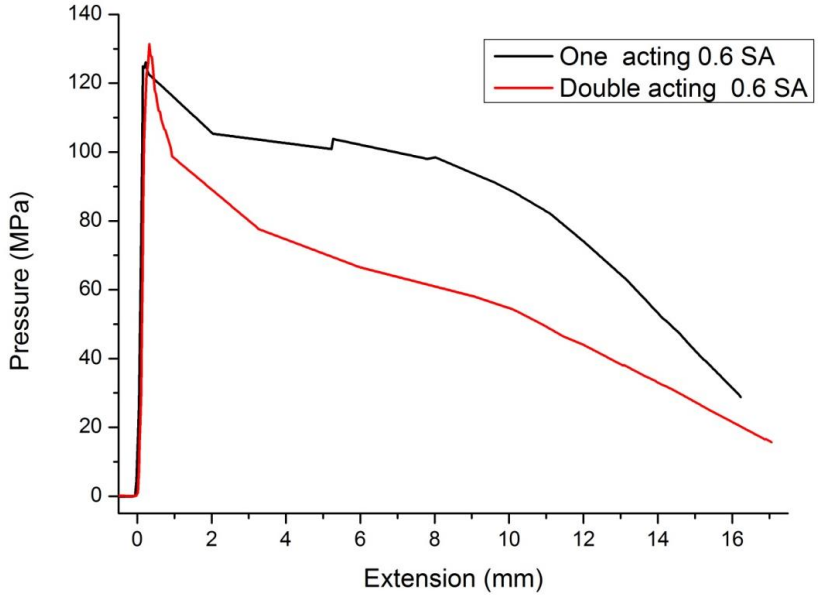

Fig. 4.22 Pressure/Extension curves of powder compacts with 0.6wt.% of SA pressed by different compacting method

4.4 Discussion

4.4.1 Mixing effect

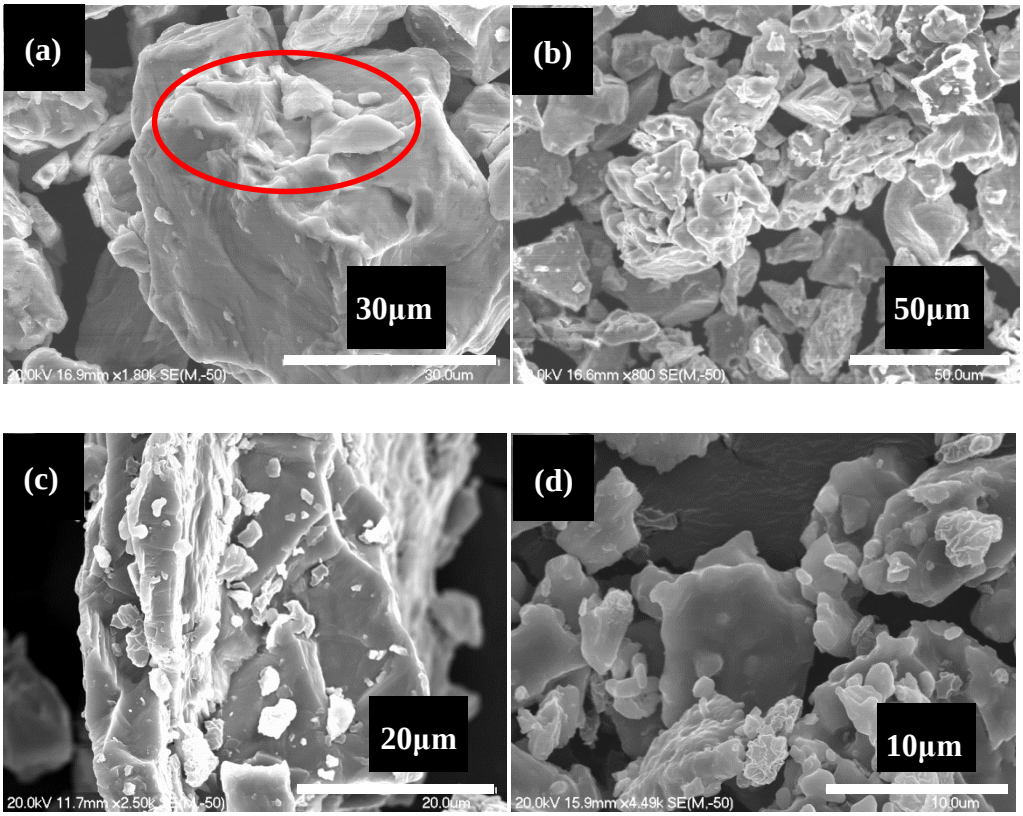

Fig. 4.23 SEM micrographs of Ti powder particles mixed with different lubricant concentrations: (a) 0.6SA; (b) 2SA; (c) 0.6MgSt and (d) 2MgSt

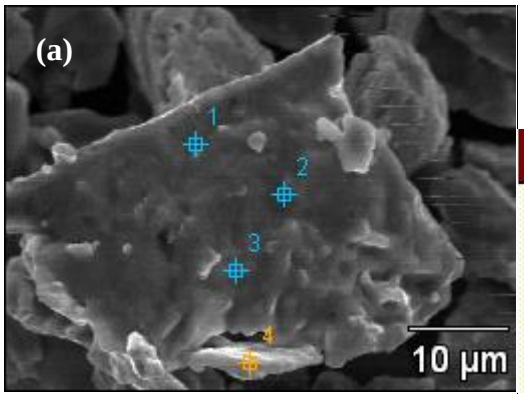

(b)	C-K	O-K	Ti-K
1			100.00
2	1.99	0.00	98.01
3	1.00	0.00	99.00
4	2.19	0.00	97.81

Fig. 4.24 EDS results of Ti-0.6SA: (a) SEM picture and (b) EDS results of points in Fig. 4.24(a)

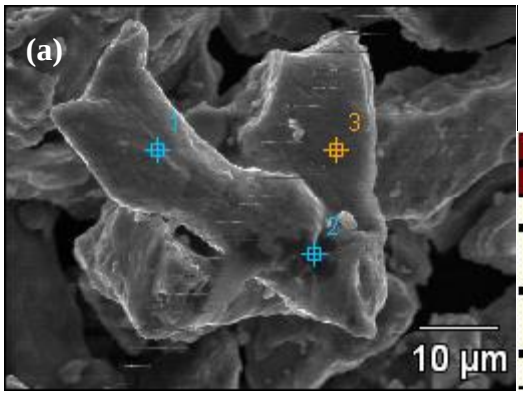

(b)	C-K	O-K	Ti-K
1	1.58	0.00	98.42
2	33.47	2.68	63.85
3	0.52	0.00	99.48

Fig. 4.25 EDS results of Ti-2SA: (a) SEM picture and (b) EDS results of points in Fig. 4.24(a)

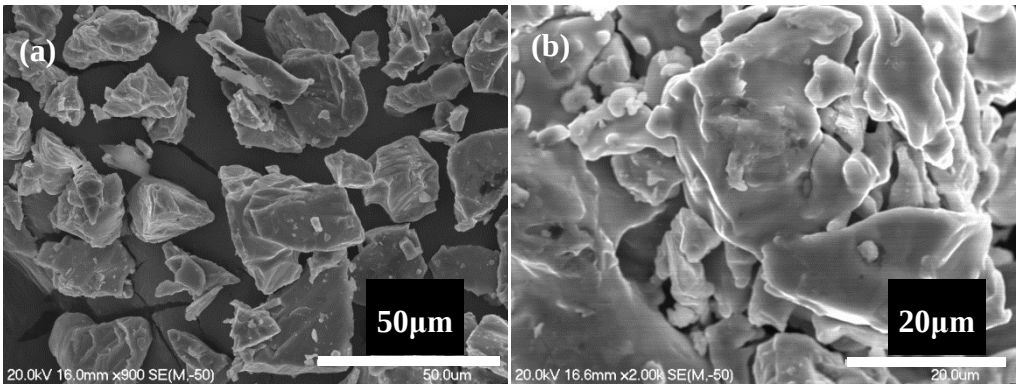

Fig. 4.26 SEM pictures of powder particles: (a) wet blended 0.6SA and (b) 0.3 Batch B

The compressibility and green strength of a powder compact are influenced by the mixing ability of a lubricant. The SEM micrographs of Ti powder particles mixed with different concentrations of SA and MgSt are shown in Fig. 4.23. For SA addition, most huge SA particles have been crushed into a very thin layer and coated on the Ti powder particles. But some retained SA agglomerates can be found in the corner of the particles, as shown in Fig. 4.23 (a). A higher SA concentration leads to more SA agglomerates, as shown in Fig. 4.23 (b). The EDS result as shown in Fig. 4.24 reflects that 0.6wt.% of SA leads to a very thin coating on the Ti particles, the carbon content is very low and oxygen content is negligible. At some region, such as point 1, there is a lack of SA. But in compacts with 2wt.% SA, as shown in

Fig. 4.25, we find that whole particles have been coated by the SA and agglomerates of SA, which have very high carbon content and visible oxygen content can also be observed. The compositional structure of SA is $C_{18}H_{36}O_2$, the weight ratio of C to O is about 27:4, which is very similar to point 2. For the MgSt lubricant, there are many small MgSt particles coated on the titanium particles. For the wet blended 0.6wt.% SA condition, agglomerates were hardly to be seen as shown in Fig. 4.26 (a). For Batch B, the lubricant seems to be crushed into the layer coated on the particles without any agglomerates, but the surface of the particles is somewhat damaged by the severe blending, as shown in Fig. 4.26 (b). Thus we can come to the conclusion that the coating homogeneity is controlled by the lubricant composition, lubricant concentration and blending method.

For an ideal coating situation, all the powder particles have been coated by an equally thick lubricant layer. Assuming that the powder particles are spherically shaped, the theoretical layer thickness can be calculated by the following equation:

$$h = \left(\sqrt[3]{1 + \frac{W \times \rho_m}{(1-W)\rho_l}} - 1 \right) R_p \qquad (4.2)$$

where: h is the theoretical layer thickness

W is the mass fraction

ρ_m is the density of bulk metal

ρ_l is the density of bulk lubricant

R_p is the average powder particles radius.

The Rp is about 37.5μm. Calculated results of the theoretical layer thickness are shown in Table 4.5. It is very hard to homogenously coat the powder particles with a 1μm lubricant layer. Thus it is commonly found that the powder particles are

coated with a discontinuous SA layer and some agglomerates. More agglomerates should be generated with higher SA additions.

Table 4.5 Theoretical layer thickness of lubricant layer

Composition	Weight fraction (%)	Volume fraction (%)	Theoretical layer thickness (μm)
SA	0.3	1.42	0.18
	0.6	2.79	0.36
	1.0	4.57	0.59
	2.0	8.74	1.16
MgSt	0.3	1.25	0.16
	0.6	2.46	0.31
	1.0	4.04	0.52
	2.0	7.77	1.02

4.4.2 Compaction

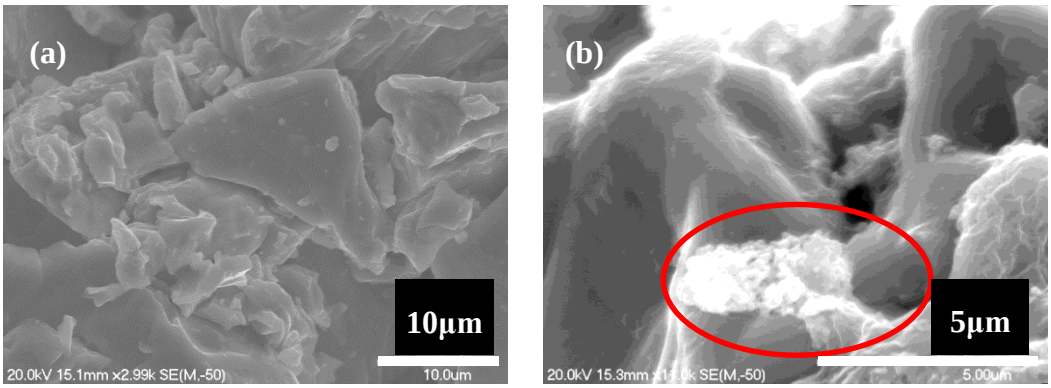

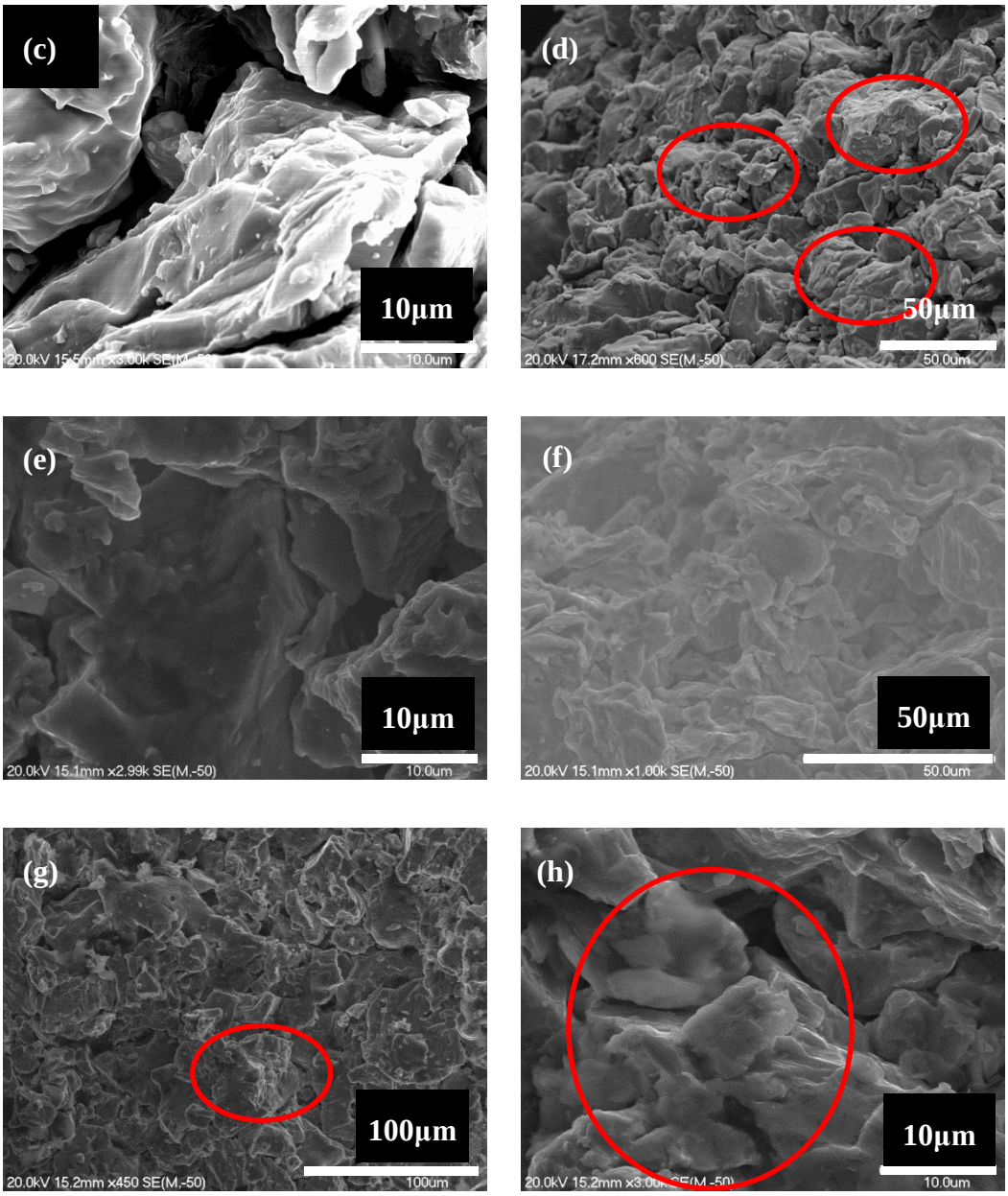

Fig. 4.27 SEM micrographs of powder compacts: (a) centre in Ti-0.3SA; (b) agglomerates in Ti-0.3SA; (c) centre in Ti-2SA; (d) edge in Ti-2SA; (e) centre in Ti-0.3MgSt; (f) edge in Ti-0.3MgSt; (g) centre in Ti-1MgSt and (h) edge in Ti-1MgSt

The different mixing effects of lubricants lead to different compaction effects. The distribution of lubricant after compaction is shown in Fig.4.27. In compacts with 0.3 to 0.6wt.% SA, SA can only be found in some of the gaps between particles. No obvious agglomerates of SA can be observed, as shown in Fig. 4.27(b). But in compacts with 1 to 2wt.% SA, many larger agglomerates can be seen near the edge.

Even in the centre region of the power compact, we can find the evidence of agglomerates, as shown in Fig. 4.27(c). These agglomerates inevitably prevent the plastic deformation of metal power particles and particles which will be hardly compacted together. This phenomenon is also observed in the compacts with MgSt additions, as shown in Fig. 4.27(h). The excess lubricant in compacts with 1 or 2wt.% MgSt fills the gap between particles. After the whole compact reaches a high density (above 75%), lubricant in the gaps between particles will be extruded from the gap and then transmitted onto the surface of the powder compact. This transmission leads to higher amounts of lubricant on the surface region of the compact which coats the die wall, even though there was no original die wall lubricant. But this transmission will decrease the bonding between the particles which have already been compacted. Thus the green strength decreases as well as the green density.

4.4.3 Analysis of compaction

The results presented here agree with those reported by other researchers working on ferrous alloys [8, 28]. The consolidation mechanisms of cold compaction include powder rearrangement and plastic deformation. Under low compacting pressures, when powder rearrangement dominates, the density increases with the internal lubricant because it reduces interparticle friction. A higher green density is easily achieved. But then plastic deformation becomes the dominant mechanism of consolidation, the lubricant inhibits any further densification because it occupies the pores thus limiting the maximum obtainable density. This transition occurs at a time when the applied pressure exceeds the bulk yield stress of the material; for titanium this is about 300-400MPa.

But a very notable difference with ferrous alloys is that in the compaction of Ti

alloys it is very hard to get a green density higher than 80%. Thus the effect of whether lubricants will retard the further densification is debatable, because the volume fraction used in the present work is no more than 10%. The distribution effect should be taken into account when explaining most of the characteristics in the lubrication and compaction processing of Ti powder.

It is impossible for SA, which has a similar particles size to the titanium particle, to breaks into a very thin layer or very fine particle coated on the metal particle. As discussed in the previous section, it always breaks into a discontinuous thin layer with agglomerates located inside the corner of the powder particles. A discontinuous thin layer cannot fully lubricate the surface of the metal particles and further additions do not improve the compressibility. Agglomerates prevent the in-situ densification process by occupying the gap between particles. Hence more than 0.6wt.% of SA does not give any further improvement in the green density.

For MgSt, a small particles size leads to a homogenous distribution on the metal particles. During compaction, these fine particles will be compacted into thin layers and then lubricate the powder during the powder rearrangement process. A higher concentration leads to a greater lubricated area, so that the compressibility is improved by a further increase in lubricant to 0.6wt.%. But for increases in lubricant to1 or 2wt.% MgSt, the high volume fraction prevents in-situ densification behaviour.

A further discussion will be given in later chapters which combines these results with the theoretical research.

4.4.4 Shape retention and ejection

As discussed in the last section, lubricants decrease the particle to particle bonding

surface area and retard the plastic deformation of Ti powder particles. So the green strength of a lubricant-free compact is superior to that with a lubricant. Fig.4.17 shows that powder compact with lubricants have only 1/4 to 1/3 of the green strength of those without a lubricant. This lower strength leads to edge cracking during ejection, as shown in Fig. 4.28.

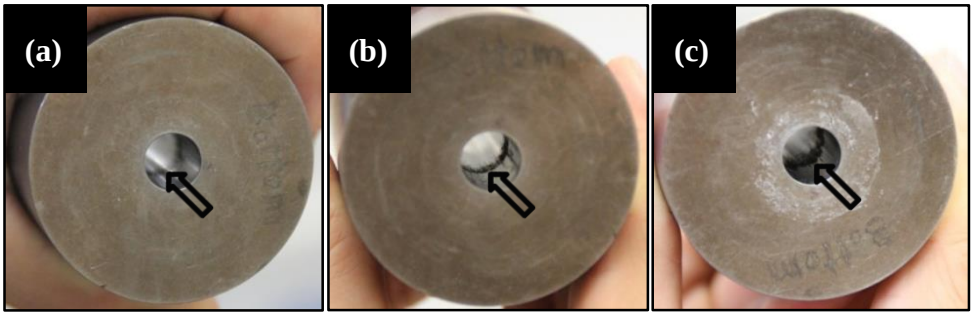

Fig. 4.28 Residual powder particles on the inner die wall: (a) Pure Ti; (b) SA addition and (c) MgSt addition

The retained particles coated on the inner die wall have a detrimental effect on the ejection process. Although the start pressure is reduced by lubricant additions, the retained particles increase the moving pressure during stage II. The higher ejection energy is the result of these particles. To decrease the energy, fewer retained particles are required and an effective way of doing this is to use a double acting ejection process which increases the density of the ejection surface.

4.5 Conclusion

(1) A small amount of lubricant improves the compressibility of Ti powder compacts, especially in the low pressure region (<400MPa).At higher compaction pressures, compacts containing more than 1wt.% of lubricant exhibit inferior green density. The compaction behaviour Ti64 alloy is also improved by lubricant

additions.

(2) Up to about 0.3wt.% SA additions improve the green density. MgSt exhibits a better lubrication effect and up to 0.6wt.% additions improve the compact density.

(3) The degree of mixing of the lubricant with the titanium powder accounts for the different lubrication effects. A homogenous mixing of lubricant leads to increased lubricated area and the effectiveness of lubrication. Agglomerates and excess lubricant, which occupy the inter-particle gaps, prevent in-situ densification.

(4) Lubricants have strong influence on shape retention in green compacts and the green strength. Increased lubrication reduces the ejection start pressure. But retained particles increase the ejection energy. This problem can be overcome by increasing the density of the lower surface of a compact.

(5) The best improvement in compressibility is achieved from a 0.6wt.% MgSt addition. For SA additions, 0.3wt.% is the best.

5. Chapter 5 Density Distributions of Lubricated Ti Alloy Powder Compacts

5.1 Introduction

The existence of density gradients in metal compacts has been recognized for over 50 years. In the P/M industry efforts to achieve a uniform density distribution have been routinely achieved by controlling such factors as applied pressure, compaction mode, part geometry, particle size and lubrication [4, 28, 69, 125]. However, previous attempts to quantify these gradients were limited by the techniques used and the ambiguity of the results. For compacts with lubricants, because the internal pores between metal particles are filled by organic lubricant, the commonly used methods for testing the density gradient such as x-ray scanning are not available, because the internal pores between metal particles are filled by organic lubricant [33, 56]. Thus, a more suitable method for testing the density distribution of lubricated Ti alloy powder compacts is needed.

This research describes a coloured layer method from which the in-situ density data for a compact can be obtained experimentally. The existence of lubricants in the powder compact has a negligible effect on the measurement and by evaluating the data, the influence of lubricants on density distribution is obtained. The hardness profiles of the powder compact can also be tested and this provides an indicator of the density distribution. The hardness profile and the measured densities in a cut sample provide comparative evidence for the coloured layer method. From an analysis of the density gradients, the effect of lubricants on the density variation in Ti-powder compacts was established. Because there is a lot of raw data for the density or hardness gradients the key results showing profiles of the density are tabulated in this thesis. The raw data can be found in the appendix.

5.2 Experimental details.

The density gradient was measured using a coloured layer technique in combination with hardness measurements. For the coloured layer technique, Ti powder and lubricant mixtures with different colours were produced by mixing the components with commercial inks. The ink used is shown in Fig. 5.1. The ink was dissolved in ethanol and then mixed with powder to produce coloured powder after the ethanol had been completely evaporated. The pictures of the original uncoloured powder and coloured powder are shown in Fig. 5.2.

Fig. 5.1 Commercial ink used for mixing

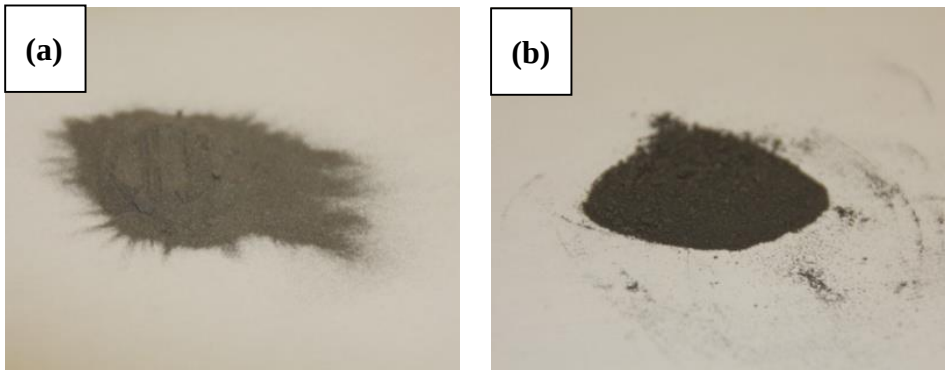

Fig. 5.2 Pictures of uncoloured powder and coloured powder: (a) uncoloured and (b) coloured

Compaction tests showed that a small volume of ink does not influence the compressibility of the Ti power. In order to form the coloured layers with

different heights, uncoloured powder and lubricant mixtures with a known mass (m_1= 0.8, 1.6, 2.4g) were poured into the die and pressed with a pressure of 10MPa in order to make the powder's surface flat. Then coloured mixture with a relative mass (m_2= 3.2g – m_1 = 2.4, 1.6, 0.8g) was poured in and then pressed using the ultimate compaction pressure. As a result, three mass ratios of uncoloured powder mixture to coloured mixture were used in this work: 3:1, 1:1 and 1:3. The compaction pressures used were 400MPa or 500MPa and using a double acting compaction arrangement a second pressure of 300MPa was applied to improve the density of the lower surface. The mid-cross-sections of the compacts were accessed by grinding with a grinding machine. The thicknesses of the exposed layers, as a function of the radius, were measured using an optical microscope. The compaction process is shown in Fig. 5.3.

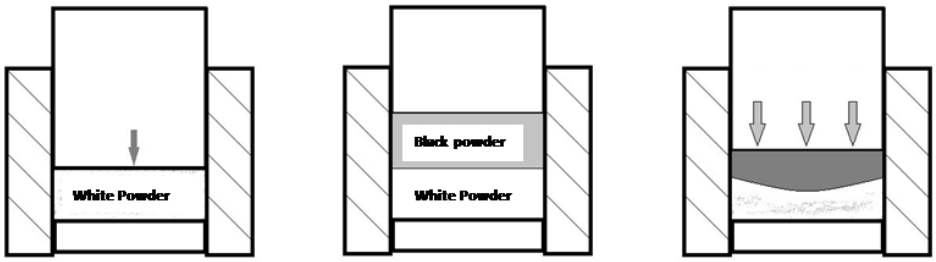

Fig. 5.3 Compaction steps for the colour layer method

For the hardness tests, the ϕ11 powder compact was mounted in a resin base and then ground using abrasive paper (to No. 600) to get the cross section. The cross - section was cut by a small knife to get a 5*5 mesh structure. Brinell hardness measurements were carried out on 25 spots of the mid-cross sections of the powder compacts, as shown in Fig. 5.4(a). Each condition was tested at least 3 times to get a typical result. For ϕ40 powder compacts, half of a compact was placed on a wooden base used to support the compact and then hardness tests were carried out as shown in Fig. 5.4(b). In this case 7 ×7 spots were tested.

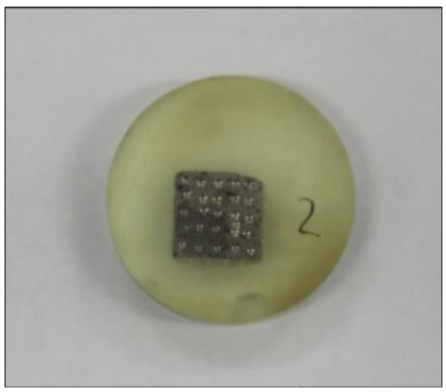

Fig. 5.4 Brinell hardness test for powder ϕ11mm compacts

5.3 Results

5.3.1 Pictures of the mid-cross section of lubricated Ti powder compacts fabricated by incorporating the colouring method

Cross sections of lubricated Ti powder compacts along a plane parallel to the pressing direction and fabricated by incorporating a colouring method are shown in Fig. 5.5. The interface between black and white surfaces is very clear. Before the powder mixtures are compacted, the interface between the black powder and the original powder is horizontal. After compaction, we find that these interfaces have been bent around an axis normal to the pressing direction of the compact and the two end points are above the central position of the interface. A visible comparison tells us that the curvature of the interface obtained from the compact without lubricant is larger than that from a Ti-0.3SA compact. The lower end point of the interface is caused by the friction between the die wall and the powder particles and the nature of the friction transmission process which causes the interface to bend.

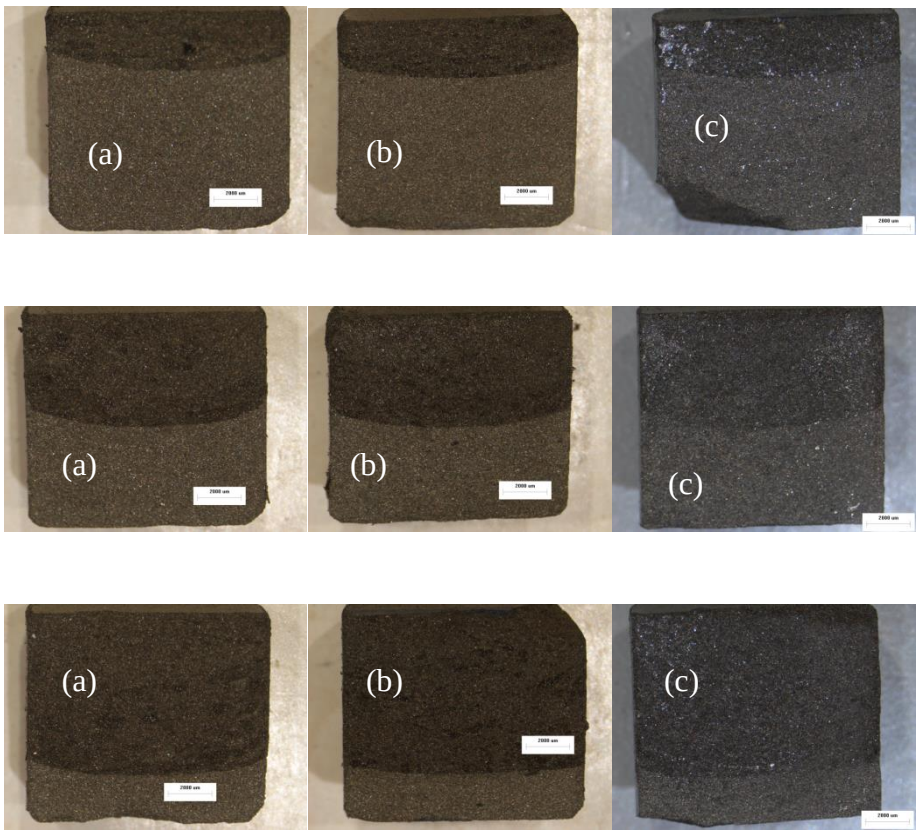

Fig. 5.5 Cross section of lubricated Ti powder compact fabricated using a colouring method: (a) Pure Ti (b) Ti-0.3 SA (c) Ti-0.6 SA

The height of the interface to the top surface of a compact was recorded using Photoshop software and the volume of each layer can be calculated from these data. The masses of the powders with different colours are known, so the densities of each layer can be calculated approximately. By fitting a fifth-order polynomial curve to the measured height values, a function *f(r)* was obtained. The volumes of the layer were then calculated using the following equation [28]:

$$V = 2\pi \int_0^r rf(r)dr \tag{5.1}$$

where:

r is the radius of the compact,

f(r) is a function of the radius.

From the data, we can build up the density layers of the Ti-powder compact. But for the exact density profile, we need density values from different points or sections in a compact. The volume from different sections of the layers, with radii ranging between r_1 and r_2, may also be calculated as:

$$V = 2\pi \int_{r_2}^{r_1} rf(r)dr \qquad (5.2)$$

Where:

r_1 is distance from the starting point of a section to the trunk axis,

r_2 is distance from the end point of a section to the trunk axis.

Assuming that the powder mass from of each section is equivalent, the density values of all sections can be calculated. In this case, each layer was divided into 5 sections and data from each of them were used to draw the density profiles.

5.3.2 Density values of different layers obtained from a colour layer method

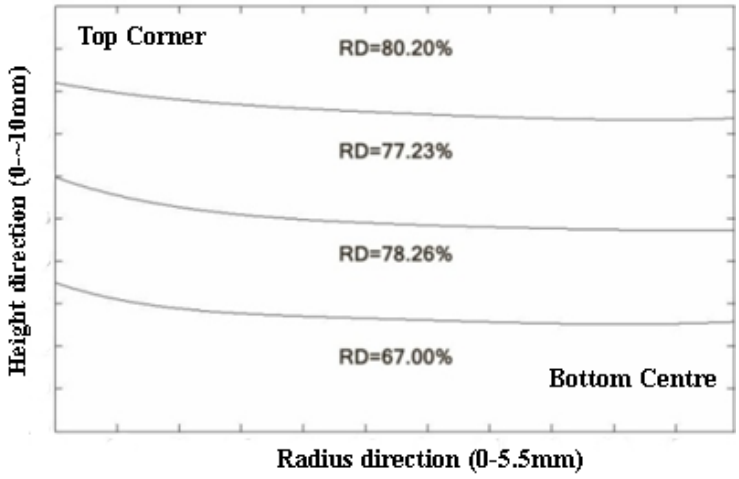

Fig. 5.6 Density values of different layers of half a pure Ti compact obtained from a colour layer method

Table 5.1 Density values of different layers obtained from a coloured layer method (pressed under 400MPa)

layer / Compact	1	2	3	4
Pure Ti	**80.20%**	77.23%	78.26%	**67.00%**
Ti-0.3SA	74.76%	**77.94%**	77.44%	**73.90%**
Ti-0.6SA	78.15%	**73.15%**	**78.75%**	77.16%
Ti-1SA	77.89%	75.43%	**78.57%**	**74.69%**
Ti-0.3MgSt	**78.36%**	78.71%	78.26%	**70.67%**
Ti-0.6MgSt	**80.09%**	75.54%	77.39%	**71.15%**
Ti-1MgSt	**81.06%**	75.42%	76.84%	**72.57%**
Ti-0.6SA(wet)	**78.60%**	76.36%	77.52%	**72.42%**

The density values of different layers from one half of a pure Ti compact are shown in Fig. 5.6. As expected, the top layer, subjected to the highest pressure, shows the highest value. The bottom layer on which a double acting pressure is applied shows the lowest value. The layers between them have intermediate values but not in a successive sequence. The difference between the biggest value and the lowest is 13.2%.

The densities of different layers from powder compacts pressed under pressures of 400MPa and 500MPa respectively are given in Table 5.1 and 5.2. The highest values from all compacts are in bold and the lowest values are in bold and underlined. Under a compaction pressure of 400MPa with SA additions, the differences between the highest values and the lowest ones decrease significantly. But the locations of the highest and lowest values are shifted, in other words, the density distribution seems to be independent of the pressure transmission. For compacts with MgSt and SA under wet blending conditions, this variation in density does not exist, the values are in good agreement with the pressure transmission. The improvement in the density distribution is indicated by the reduced difference between the highest and the lowest values, which decrease to about 8% for all MgSt concentrations and 6.18% for SA blending.

Table 5.2 Density values of different layers obtained from coloured layer method (pressed under 500MPa)

layer / lubricant	1	2	3	4
Pure Ti	**82.28%**	79.13%	77.48%	**72.03%**
Ti-0.3SA	**79.46%**	78.94%	75.44%	**72.90%**
Ti-0.6SA	**80.15%**	76.24%	78.25%	**73.30%**
Ti-1SA	79.19%	**79.83%**	77.14%	**74.65%**
Ti-0.3MgSt	**80.52%**	79.31%	75.46%	**72.31%**
Ti-0.6MgSt	**81.61%**	78.17%	76.29%	**71.75%**
Ti-1MgSt	**81.24%**	77.40%	78.83%	**74.61%**
Ti-0.6SA(wet)	**80.83%**	77.64%	76.18%	**72.77%**

With a 500MPa compaction pressure, the density values of all layers have increased. The difference between the highest and lowest values is 10.25%. For the compacts with SA additions, the distribution shows a similar trend to that when using a 400MPa compaction pressure, where a 5-7% range is observed. This

is better than the 7-10% found in compacts with MgSt additions and SA wet blending.

5.3.2 Density profiles for lubricated Ti powder compacts

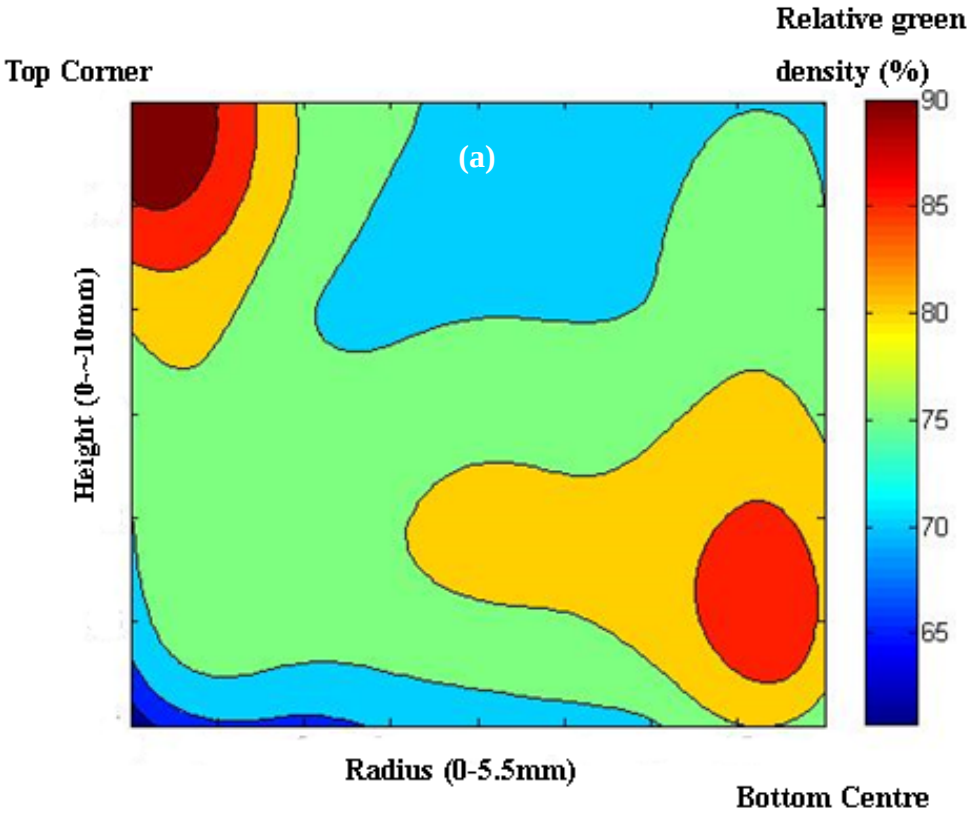

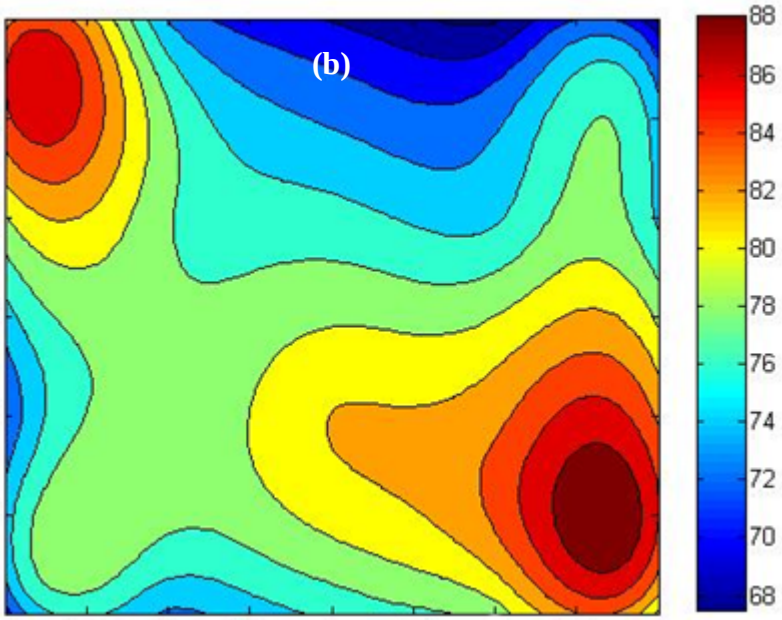

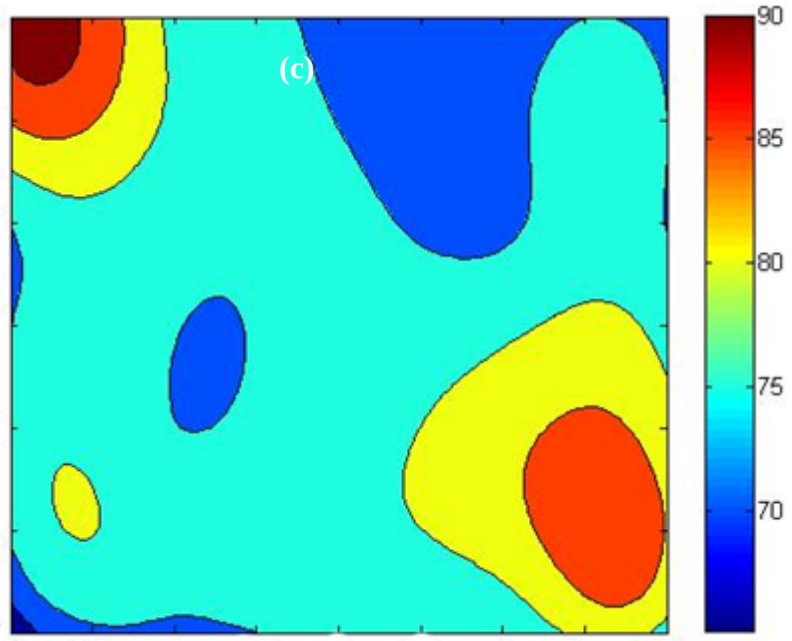

Fig. 5.7 Density profiles for one half of a compact pressed under a compaction pressure of 400MPa: (a) Pure Ti, (b) Ti-0.3SA, and (c) Ti-0.3MgSt

Thecalculated density distributions for sections of half-compacts are illustrated in Fig. 5.7. Fig 5.7(a) shows the density profile of pure Ti. The highest density is located in the top corner of the compact, which is 91.08%. The density decreases along the vertical and horizontal axis. The bottom corner shows the lowest density of 60.77% and near the top centre shows the second lowest of 69.36%. However, the density then increases towards the bottom centre. A second highest value of 82.45% is obtained near the bottom centre. In Fig. 5.7(b) for a compact with a small amount of SA, the top left hand corner has a density of 82.64%, which is not the highest value. In fact, the highest value of 83.60% is located at the bottom in the centre of the compact. The lowest value of 67.44% is located at the top of the compact near the centre, which is lower than the value at the bottom corner of 70.76%. Fig. 5.7(c) shows a similar trend to the Fig. 5.7(a), the highest value is located at the top left hand corner and the lowest value is located in the bottom left hand corner, whereas the centre areas show the second highest values. The

range is much lower than the latter. Profiles for other lubrication conditions, associated with their relevant colour layer pictures, are shown in the appendix.

To evaluate the density profiles, the density values at the top and bottom corners, the top and bottom centre positions (the max values from the top corner and the bottom centre regions, the min values from the bottom corner and the top centre regions) are given in Table. 5.3. When compacted under a pressure of 400MPa with a SA addition, the maximum and minimum density distributions are not located in the top and bottom corners. However for compacts with MgSt, SA with wet blending and SA under a 500MPa compaction pressure, the locations of maximum and minimum density are similar to those observed in pure Ti.

Table 5.3 Relative density values of different sections obtained from colour layer method

	Top corner	Top centre	Bottom corner	Bottom centre
Pure Ti	**91.08%**	69.36**%**	**60.77%**	82.45**%**
Ti-0.3SA	82.64**%**	**67.44%**	70.76**%**	**83.60%**
Ti-0.6SA	**86.64%**	**69.70%**	70.93**%**	85.93**%**
Ti-1SA	**85.34%**	**68.99%**	71.23**%**	83.36**%**
Ti-0.3MgSt	**89.55%**	68.15**%**	**65.10%**	84.14**%**
Ti-0.6MgSt	**90.35%**	70.85**%**	**65.18%**	83.21**%**
Ti-1MgSt	**90.16%**	69.31**%**	**66.32%**	84.37**%**
Ti-0.6SA (wet)	**89.62%**	68.46**%**	**68.43%**	83.38**%**
Ti-0.6SA(500MPa)	**91.34%**	72.63**%**	**68.40%**	84.52**%**

5.3.3 Evaluation of density profiles

The density profiles and the density values for four corners have been presented and analysed in the last section. However, they cannot directly reflect the density

distribution in a powder compact. We need something to tell us whether or not the density distribution in a Ti-0.3SA is more uniform than that in a pure Ti compact. Therefore a function was used to evaluate the density variation within the density distribution. The density values were obtained from the calculated density taken from 20 sections. The standard density deviation was calculated using the following equation:

$$\sigma = \sqrt{\frac{1}{n}\sum_{i=1}^{N}\rho\left(D_n - D_a\right)^2} \tag{5.1}$$

Where,

σ is the standard density deviation;

N is the number of sections to be calculated, which in this case is equal to 20;

ρ is the repetition factor, which is attributed to the distance from a section to the central axis of the compact;

D_n is the relative density of this section;

D_a is the average relative density.

The change in standard density deviation in a powder compact with increasing amounts of lubricant additions is shown in Fig. 5.8. This experiment has been repeated twice to verify the trend and obtain the deviation.

The data in Fig. 5.8 shows that a powder compact without any lubricant has the highest σ values of 6.71%. The green density of related Ti compacts is only 72%, thus 6% is a significant density variation. With lubricant additions this variation is reduced to around 5%. The improvement from 0.3-1.0wt.% seems to be very stable,

i.e. it fails to prove that higher lubricant concentration leads to a better green density inhomogeneity. The deviation is more than ±0.5% for most lubrication conditions. The σ values of compacts with SA addition seem to be lower than those with an equivalent MgSt addition.

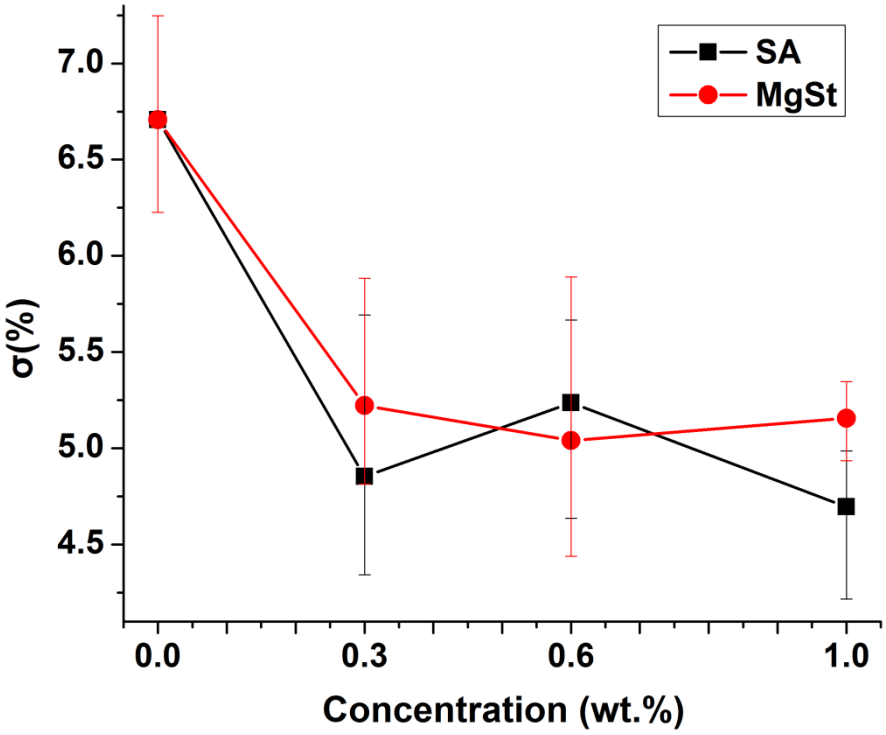

Fig. 5.8 Standard density variation in powder compacts pressed under 400MPa

5.3.4 Density profile in a larger 40 mm diameter compact

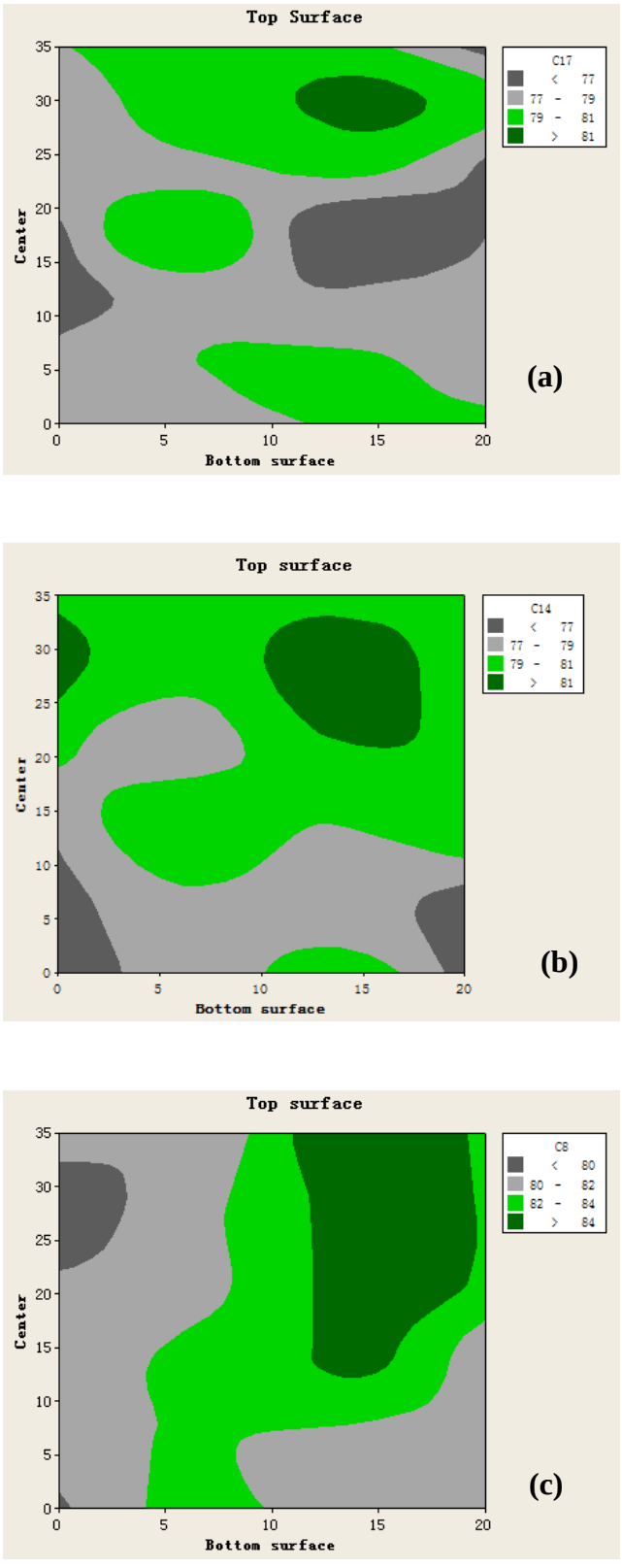

Fig. 5.9 Density Profiles of ϕ40mm powder compact: (a) Pure Ti, (b) Ti-0.3SA, and (c) Ti-0.6SA

Fig. 5.9 shows the density profiles of a φ40 mm powder compact. The density values of all the sections shown in Fig. 5.9 were obtained from parts cut from a powder compact. This method takes longer to do than the coloured layer method and the measurement used for testing the density is not accurate, because the parts to be measured are very small and porous. In fact, a compact with more than 1wt.% of SA is very hard to cut using the wire cutting method.

From the density profile, we find that the top right hand corner shows the highest density. But the location of the lowest value is not clear, and it is very hard to find a second highest and lowest value in the compact. The transition in the density values is improved by adding a small amount of lubricant. In those compacts without a lubricant, more light green and deep grey regions are observed.

5.3.5 Hardness profiles

5.3.5.a An ϕ11mm powder compact

Table 5.4 Hardness distribution of ϕ11 powder compact

(a) Pure Ti

105.82	**87.58**	**85.34**	**85.18**	**95.25**
94.28	**86.34**	**81.56**	**84.1**	**85.18**
81.38	**75.59**	**73.89**	**77.8**	**72.87**
75.39	**72.82**	**72.08**	**73.39**	**71.46**
70.59	**74.39**	**67.29**	**68.71**	**64.36**

(b) Ti-0.3SA

53.71	43.92	41.91	42.45	48.53
42.81	39.70	37.97	38.67	41.85
35.98	32.87	29.94	31.74	34.83
28.13	27.88	26.37	27.39	27.65
24.14	24.99	27.96	26.50	26.27

(c) Ti-0.6SA

49.77	42.28	37.87	40.02	40.78
36.56	38.01	36.67	36.12	38.52
31.64	32.46	32.54	32.09	33.48
24.89	25.88	26.49	26.26	28.6
24.98	22.59	24.16	23.59	25.62

(d) Ti-1SA

44.54	36.55	35.52	33.66	37.31
34.47	31.21	31.5	30.46	34.33
27.66	26.07	26.16	22.73	27.69
21.22	21.09	21.41	20.43	22.3
21.93	20.86	22.85	21.83	22.41

(e) Ti-2SA

46.83	36.07	35.05	34.47	39.69
33.2	31.21	30.96	30.85	31.71
28.91	29.83	26.65	28.89	31.71
24.84	23.21	24.19	23.38	23.71
23.83	22.76	25.07	23.33	21.7

Table 5.5 Evaluation of hardness distribution in compacts with different SA addition

SA (wt.%)	0	0.3	0.6	1	2
Max.(HBS)	105.82	53.71	49.77	44.54	46.83
Min.(HBS)	64.36	24.14	22.59	20.43	21.7
Average (HBS)	79.31	34.57	32.47	27.85	29.28
Range (HBS)	41.46	29.57	27.18	24.11	25.13

The hardness values from different regions in a powder compact are shown in Table 5.4. At least 3 samples were tested to verify the trend. Unlike the density profiles, the hardness profiles are for a whole compact. An evaluation of theses profiles is summarised in Table 5.5. The hardness values decrease significantly by adding 0.3wt.% of SA. The highest hardness value is reduced by a half from 105.82HB to 53.71HB with a 0.3wt.% SA-addition, and further decreases to 49.77 with 0.6wt.% SA and to about 45% with 1-2wt.% SA. The lowest hardness value is also significantly reduced from 64.36HB to about 20HB with SA additions. The location of the highest value is always at the top corner. The lowest value is located in the region near the bottom corner. The top centre shows a lower density than the top corner. The bottom centre usually shows a higher density than the bottom corner.

Because a double acting pressing technique is not applied to the bottom surface, the bottom layer does not show the second highest density, but the hardness distribution results are in general agreement with those obtained from the coloured layer technique.

5.3.5.b Half of a ϕ40 powder compact

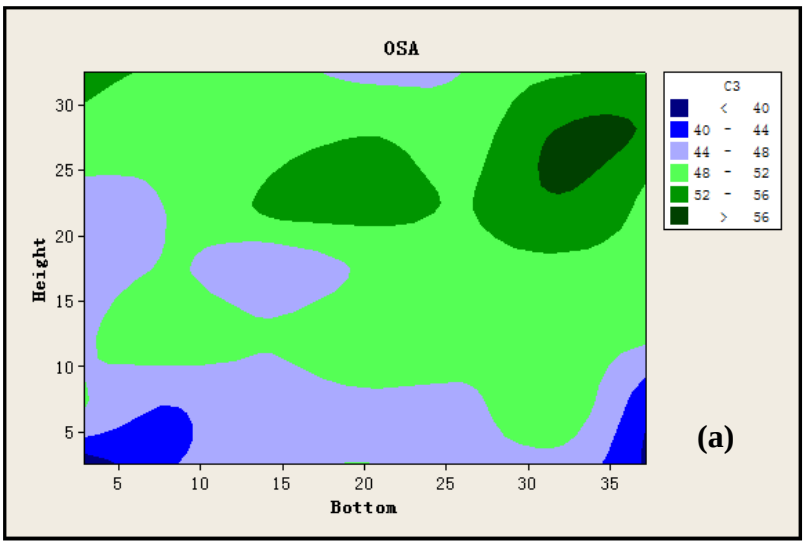
0SA
C3
< 40
40 - 44
44 - 48
48 - 52
52 - 56
> 56
Height
Bottom
(a)

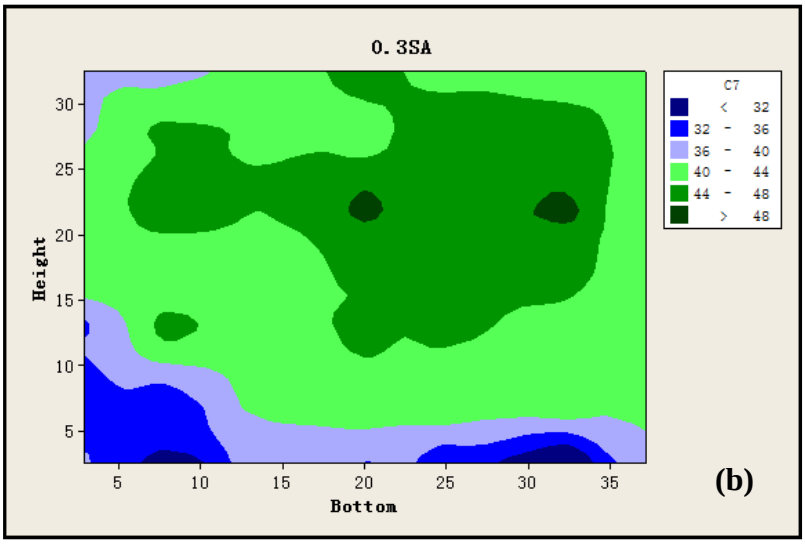
0.3SA
C7
< 32
32 - 36
36 - 40
40 - 44
44 - 48
> 48
Height
Bottom
(b)

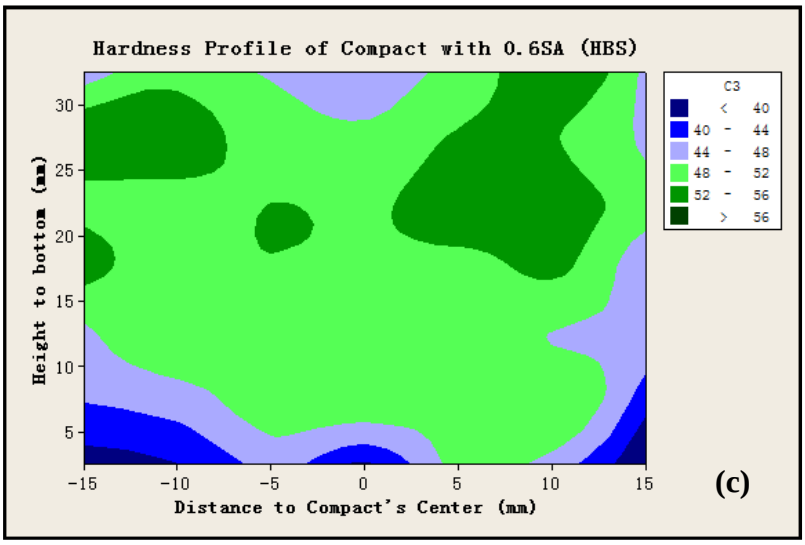
Hardness Profile of Compact with 0.6SA (HBS)
C3
< 40
40 - 44
44 - 48
48 - 52
52 - 56
> 56
Height to bottom (mm)
Distance to Compact's Center (mm)
(c)

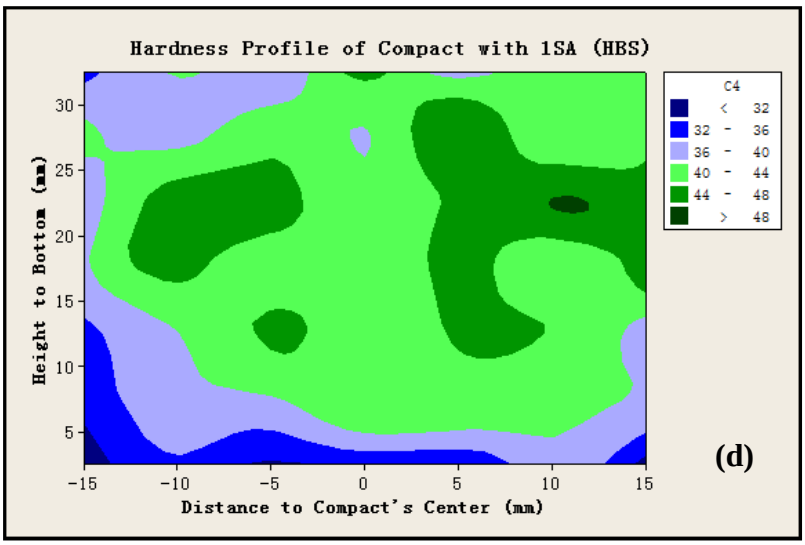

Fig. 5.10 Hardness Profiles of compact with different SA addition

The hardness values from different regions from φ40 mm powder compacts are shown in Fig. 5.10. The results are in agreement with those obtained from the coloured layer technique.

5.4 Discussion

Both SA and MgSt can improve the density distribution in Ti powder through its lubrication effect. There is a clear difference in the density distribution between powder compacts mixed with SA and MgSt. In fact, 0.6wt.% of SA mixed by wet blending shows a similar effect to that obtained from MgSt, so the lubrication ability alone is not the main reason accounting for the difference. Another possible reason is the mixing effect.

As discussed in the last chapter, the difference in the distribution of lubricants leads to different compaction behaviour. Under high pressure, the powder particles contact each other, and are either plastically deformed or broken into fragments leading to more closely combined particles with improved

densification. For SA, the lubricant agglomerates into the hollow space between powder particles and these are not compacted under low pressure. Lubricant particles tend to become compacted after the surrounding metal particles have been tightly pushed together to a very high in-situ density. At this stage, for the regions with very high green density (>85%), the flowability of the lubricant is very limited because many potential 'corridors' for movement have been closed. The retained lubricant prevents the in-situ densification of these regions with a more highly compacted density. On the other hand, the density of regions with lower compacted density is improved by the lubrication effect. With the exception of the much smaller sized MgSt, or wet blended SA, these agglomerates are hard to observe. At lower pressure the lubricant particles are more easily compacted into a thin coating on a powder particle. This is very useful in accelerating the densification rate. Thus SA provides a more even density distribution in the powder compact. The addition of more lubricant creates more lubricated areas on the powder particle surface and provides more agglomerates in the powder compact. In fact, in the compact with 1wt.% of MgSt, some agglomerates can also be found at the compact edges, as discussed in last chapter.

Additions of SA are more effective in improving densification than MgSt additions. The de-lubrication process for removing MgSt creates some retained MgO in Ti alloys, therefore SA, at lower concentrations, is a better choice for the internal lubrication process. Although present work fails to prove that a 0.6wt.% of SA provides a better improvement than 0.3wt.%, for the consideration of stability, a higher concentration of 0.6wt.% SA is recommended.

The density values of parts cut from a ϕ40 mm compact give some justification of the effectiveness of the coloured layer method. The density profiles of bigger compacts are in general agreement with those obtained from smaller compacts using the coloured layer method. The reason for discrepancies in density values is

because the density value of a section is not from a point or a small area, but from a wider area with different degrees of densification. Testing the density values of different sections is not an effective way to get the density profiles since it consumes almost the same time and effort to get data as the coloured layer method. Moreover, the accuracy of the water replacement method for testing the real density of a small porous part is doubtful. So a better approach is to cut the sample into 4-5 layers and then test the green density of these layers. But this method cannot test the density of all the sections in one layer.

Determining the hardness profile is an easier and simpler way to understand the density distribution. The hardness profiles are in agreement with those obtained from the coloured layer technique. For a part without lubricant, the hardness profile can tell us the real density indirectly, because a relationship between hardness and in-situ density can be established. But for a part with lubricant, such a relationship is impossible to be established, because a lubricant decreases the hardness of a compacted part and the more lubricant used the lower the hardness. All we are able to say in is that in a given part, section A has a higher density than section B, since it has a higher hardness. But we cannot say that a particular section is 16% higher in green density than section B. So this method is better when used for a pure alloy without lubricant additions.

5.5 Conclusion

(1) The coloured layer method is a very useful technique for measuring the density distribution in a powder compact. The deviation value can be used to quantitatively evaluate the overall density distribution of a powder compact.

(2) The green density decreases towards the top centre of the compact and increases towards the bottom centre.

(3) The density distribution in HDH Ti powder compacts can be improved by adding a small amount of lubricant. SA gives better results than MgSt, with 0.6wt.% of SA considered to be the optimum addition.

(4) The difference in the lubrication effect between SA and MgSt is due to their mixing or blending characteristics. SA agglomerates fill in the hollow space between powder particles in the compact and prevent the in-situ densification in highly compacted regions.

(5) Density and hardness profiles obtained from parts cut from a larger compact are in general agreement with the results obtained from a coloured layer method, but they are not quite suitable for assessing density distribution in compacts with lubricant additions.

6. Chapter 6 De-lubrication and Sintering of Lubricated Ti Alloy Powder Compacts

6.1 Introduction

Cold compaction & sintering is a particularly attractive manufacturing process for manufacturing titanium components as it decreases the cost of parts by reducing the buy-to-use ratio and eliminates costly forming and machining steps [4, 124, 126]. However for big or complex shapes, the uniformity in mechanical properties of the final parts is often not guaranteed: quite different mechanical performance is exhibited by different regions of a part [4, 29]. This problem is initiated by uneven stress transmission during compaction which affects the green density distribution in a Ti powder compact [4, 28, 29, 33, 53, 56, 60, 125]. Although the expected overall green density of hydride-dehydride (HDH) Ti metal and alloy powder compacts is 70-80%, variations from this green density are noticeable. Internal stress occurs by uneven shrinkage during sintering and in turn leads to geometrical distortion or defects in the sintered parts, resulting in reduced mechanical properties in local zones and unreliable overall properties. As a result, although the data obtained from laboratory conditions is good, the real yield of P/M Ti metal and alloys is limited.

Some advanced compaction methods such as cold isostatic pressing, double acting compaction and instrumented dies have been developed in an attempt to mitigate the green density inhomogeneity, yet these methods have too many specific requirements for parts and excessive input. On the other hand, powder lubrication is a simple and cost-saving approach for conferring on powder a better rheology [8, 30, 69]. Chapter 5 has shown the benefits of adding internal lubrication as a way of improving the green density distribution of small Ti compacts. However, using an organic based lubricant in the P/M processing of Ti metal and alloys is

quite challenging [4, 10] and there are serious concerns about the effect on properties of residual contaminants. The amount of lubricant which can be accepted by a P/M Ti or Ti alloy compaction needs to be carefully studied.

This work follows on from previous chapters, which has shown that when making Ti powder compacts, powder lubrication is a way to produce sintered Ti parts with more homogenous mechanical properties [69, 125]. It also focuses on an investigation of factors affecting the uniformity of density in a powder compact and the mechanical properties of the corresponding sintered part.

6.2 Experimental details

Green Ti powder compacts with a height/diameter ratio of approximately 1:1 were made by pressing 160 grams per batch of Ti/lubricant powder mixture in a 40 mm cylindrical steel die under a uniaxial single action pressure of 400MPa, The de-lubrication of the powder compacts was carried out in a tube furnace with a continuous argon flow (150 mL/min) and at a heating rate of 5℃/min up to 500℃ over a 6h period, this processing regime was set to minimise the contaminants during the removal and decomposition of lubricants.

Sintering was conducted at 1300℃ or 1350℃ for 120 min in a vacuum furnace under a vacuum of 10^{-3} - 10^{-2} Pa and at a heating rate at 10℃/min followed by furnace cooling. The density of the sintered samples was measured using Archimedes method. For pure Ti compacts sintered at 1300℃ or 1350℃, the height and diameter of a sintered cylinder was measured to analyse the shrinkage behaviour of a green compact after sintering. Then the cylinder was cut into 8 layers, each with the same thickness to measure the density of all the layers. Flat, dog-bone shaped tensile test-pieces with dimensions of approximately 2mm×2mm

cross section and 20mm gauge length (total length: 35.6mm) were cut from the sintered samples. For the sintered pure Ti powder compact (sintered at 1300℃ or 1350℃), the test-pieces were cut from the centre of the horizontal plane of the compact. A combination of diameter, density and mechanical properties should provide data for any variation in properties of a sintered cylinder in the vertical direction.

For sintered parts made with internal lubricant, any improvement needs to be analysed not only in the vertical direction, but also in the radial direction. Thus the cutting position for tensile test specimens in the cylindrical sintered material was changed, as shown in Fig. 6.1. Six tensile test specimens were cut from one half of a cylinder and a typical tensile test specimen is also shown in Fig. 6.1. Positions 1-3, which are from the top region, are near the surface on which the compacting force is applied. The gauge region of the tensile test specimens is located approximately 10 mm from the top or bottom surfaces in the thickness direction to avoid any edge effects caused by being too close to the edge. Because of the cutting and polishing effect, the location of tensile test specimens cut from positions 3 and 6 are approximately 2-5mm from the parallel diameter of a cylinder.

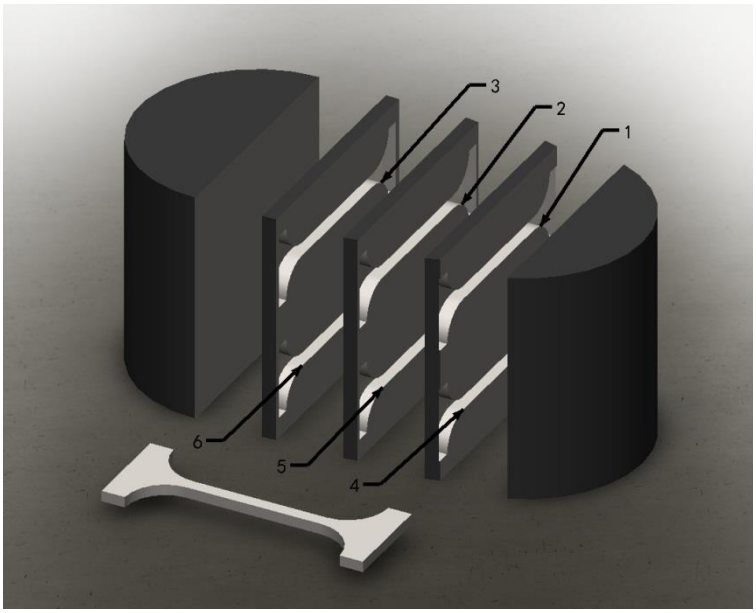

Fig. 6.1 A schematic drawing showing the shape and positions of the tensile test specimens cut from a sintered powder compact

The porosity of the various cross sections was analysed using optical microscopy and the pore size and pore aspect ratios were measured using ImageJ software. The microstructure and fracture surface of the test-pieces were analysed by SEM,. Tensile testing of the test-pieces was conducted at room temperature using an Instron universal testing machine at a strain rate of 10^{-4} s^{-1}. The strain was measured using an extensometer with a gauge length of 10mm.

6.3 Results

6.3.1 Density and porosity of sintered Ti compacts

Fig. 6.2 shows the density of green and sintered Ti powder compacts with varying lubricant concentrations. An increasing amount of lubricant addition increases the density of both green and sintered Ti powder compacts. MgSt additions give a marginally higher improvement in density. In order to achieve a higher density in a sintered pure titanium powder compact, for subsequent mechanical testing, a

higher sintering temperature of 1350℃ was used. A density of 94.2% was achieved which is comparable with that of cylindrical compacts with lubrication.

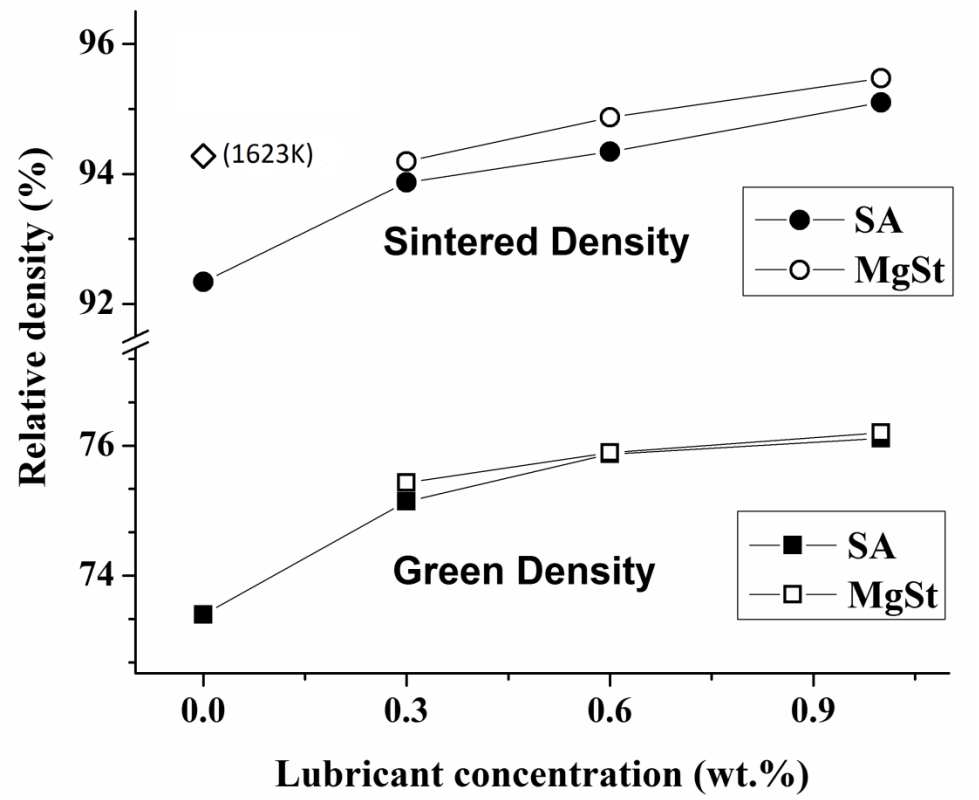

Fig. 6.2 Relationship between lubricant concentration and density of green and sintered Ti powder compacts

Fig. 6.3 shows the polished mid-cross-sections of selective zones from sintered Ti powder compacts. These micrographs are taken from regions at least 3mm from the edge to minimize the pure edge effect. Such a microstructural analysis reflects the pore morphology with respect to their size, shape and orientation. Only those micrographs from compacts with 0-1wt.% of SA are shown because they reveal typical types of pore features. Fig. 6.3a shows a very porous structure in the pure titanium including a large number of small pores. An SEM micrograph of these pores is show in Fig. 6.4(a), which shows that these small pores have a near-spherical geometry (aspect ratio < 1.5) and are less than 10μm diameter. The anisometric characteristic and preferential orientation of pores are not very

obvious. Fig.6.3(b) shows a lower overall porosity level in a Ti-0.3SA compact with most of the pores remaining very small. The top edge (TE), bottom corner (BC) and intermediate zones exhibit only small pores. However, some crack-like voids are found at the top centre (TC) and bottom edge (BE) zones, as shown in Fig. 6.4(b). The larger diameter of these kinds of pores is approximately 100-200μm and the aspect ratio is very high. Another important phenomenon is that the voids are anisometric and elongated preferentially in a radial direction. This pore feature is observed from the cross sections of a pure Ti compact sintered at 1350℃ and Ti-0.3SA and Ti-0.3MgSt compacts sintered at 1300℃. Fig. 6.3c shows that a Ti-0.6SA compact exhibits a very low porosity level. All zones had fine pores with near-spherical shapes. Ti-0.6MgSt and Ti-1MgSt compacts also exhibited similar pores. For the Ti-1SA compact, although its density is higher than that in Ti-0.3SA and Ti-0.6SA compacts, large pores with diameters ranging from 50-100μm appear again in the top and bottom regions, whereas the intermediate regions are free of these pores, as shown in Fig. 6.3(d). The pore shape is irregular and the orientation is random, as shown in Fig. 6.4(c).

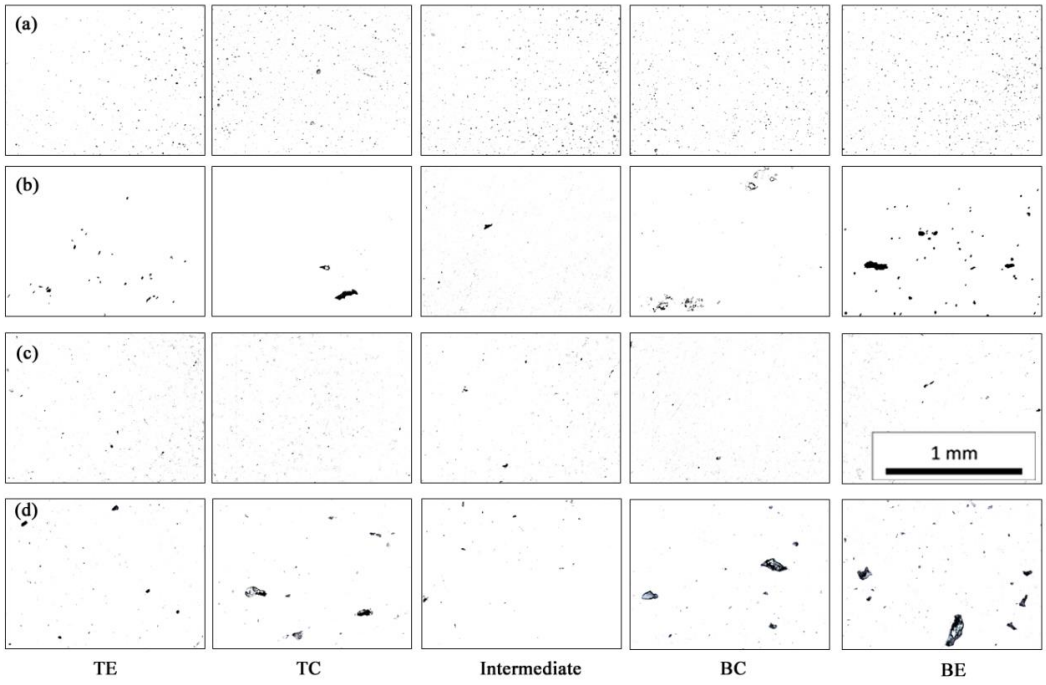

Fig. 6.3 Optical micrographs of selective zones from the mid cross sections of as-sintered compacts: (a) pure Ti sintered at 1300℃; (b) Ti-0.3SA; (c) Ti-0.6SA; (d) Ti-1SA (TE: Top Edge; TC: Top Centre; BC: Bottom Centre; BE: Bottom Edge)

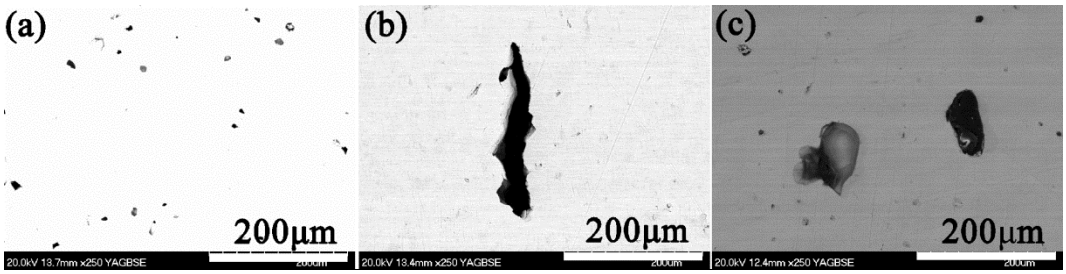

Fig. 6.4 SEM micrographs of sintered pores: (a) small pores in a pure Ti compact sintered at1300℃; (b) crack like voids in a Ti-0.3SA compact; (c) larger pores in a Ti-1SA compact

6.3.2 Shrinkage and mechanical properties of sintered pure Ti compacts

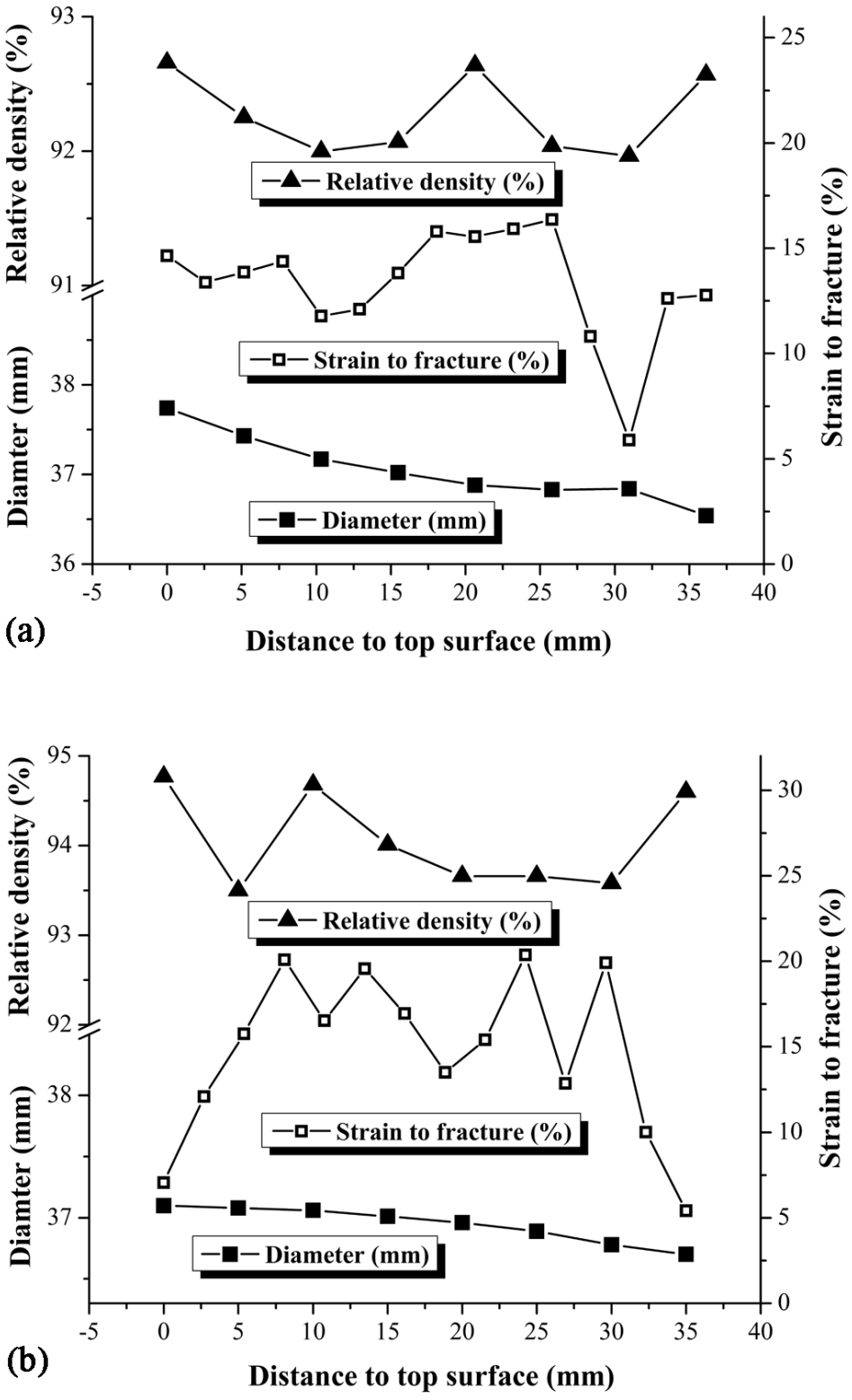

Fig. 6.5 Relative density, diameter and strain to fracture of sintered pure Ti compacts as a function of the distance to the top surface: (a) sintered at 1300℃ and (b) sintered at 1350℃

Fig. 6.5 shows the relative density, diameter and strain to fracture of pure Ti compacts sintered at 1300℃ and 1350℃, respectively as a function of the distance from the top surface. Minimum shrinkage takes place on the top layer and an ordered sequence is observed from the top to the bottom layers. The density of the top and bottom layers is a bit higher than that found in intermediate layers. The maximum difference is approximately 0.7% and 1.3% for sintering temperatures of 1300℃ and 1350℃ respectively.

For compacts sintered at 1300℃ the results from tensile testing showed a range in tensile strength varying from 524 to 567MPa with an average value of 535MPa. The ductility measured as percentage strain to fracture is reasonably stable with respect to position in the compact. For compacts sintered at 1350℃ the tensile strength varied from 560 to 613MPa, with an average value of 576MPa and better average ductility at intermediate positions. However the ductility of test pieces cut from locations at the top and bottom of this compact was very low. This lower level of ductility was recorded only once in the bottom layer of a compact sintered at 1300℃. Even in the intermediate layers of a compact sintered at 1350℃, the consistency of ductility is not as good as in a compact sintered at 1300℃.

6.3.3 Mechanical properties of test-pieces cut from positions 1-6

Table 6.1 lists the tensile properties of test-pieces cut from positions 1-6 in sintered compacts with different lubricant concentrations. To obtain a comparable density between the compacts with and without addition of a lubricant, a pure Ti compact was sintered at a higher temperature (1350℃) whereas the compacts, with a lubricant, were sintered at 1300℃. All test-pieces, except those cut from the centre of the compacts, have poor ductility. Only in Ti-0.6SA is the average ductility just

a bit lower than that of the tensile test specimens cut from the centre of a compact and with an equivalent distance to the top surface.

As shown in Table 6.1, those test-pieces numbered 1-3 exhibit higher tensile strength and ductility than test-pieces 4-6. In fact, pieces with inferior strength (<600MPa) and strain to fracture (<2%) are mainly located at the bottom of all compacts. The highest tensile strength seems to be independent of the position from which the test-pieces were taken in a compact, but the highest strain to fracture (shown in bold in Table 1) is always located in position 1 with the exception of Ti-1MgSt, also shown in bold in Table 6.1. For nearly all conditions, position 3 has lower ductility compared with positions 1 and 2, indicating that specimens from the TE always have better properties than those from the TC position. The lowest stain to fracture and associated tensile strength for all compacts (inclined and underlined in Table 6.1) were from positions 4, 5 and 6 without any preference, only in a Ti-1SA compact is the lowest value from position 3.

Fig. 6.6 shows the variations of the tensile strength and strain to fracture in Ti powder compacts with different levels of lubricant are contained within elliptically shaped envelopes. A pure Ti compact has the ellipse with the largest variation, followed by Ti-0.3SA and Ti-0.3MgSt compacts. An addition of 0.3wt.% SA makes the ellipse move a little to the right but 0.3wt.% MgSt causes a larger shift. A Ti-0.6SA compact has a much smaller ellipse and the ellipse moves to upper right of that for a Ti-0.3SA compact, which indicates that both the overall strength and ductility are improved for this amount of lubricant. The ellipse for Ti-0.6MgSt compact is located below that for a Ti-0.6SA compact and its area is larger than that for a Ti-0.6SA compact. A Ti-1MgSt compact shows a smaller ellipse than that of Ti-0.6MgSt (the low value position 6 of this compact is left out from the graph because it is too far from the other values), but the overall strength is much higher. Although a Ti-1SA compact has the smallest ellipse area, this composition has poor

ductility. This information leads to the conclusion that a Ti-0.6SA compact has the best overall tensile strength and strain to fracture and uniformity of properties across the whole powder compact.

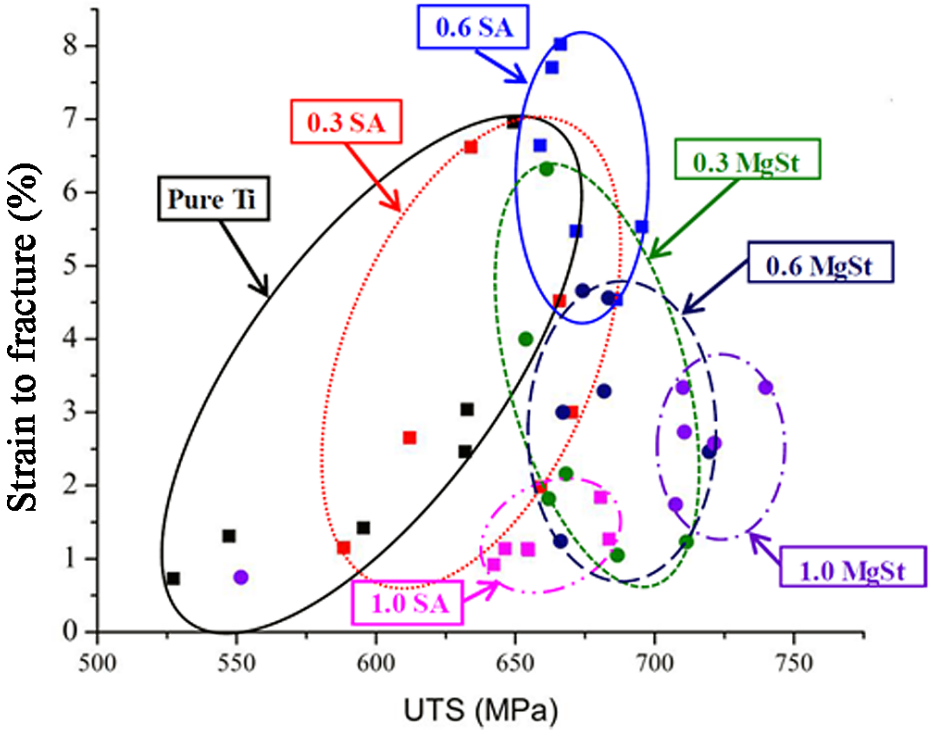

Fig. 6.6 Variations of tensile strength and strain to fracture of Ti powder compacts with different amounts of lubricant

Table 6.1 Tensile properties of test-pieces cut form different powder compacts

(see next page)

Table 6.1 Tensile properties of test-pieces cut from Ti compacts

Compact	Mechanical properties	Position of test-pieces						Average
		1.	2.	3.	4.	5.	6.	
Pure Ti	Tensile Strength (MPa)	**649.35**	632.00	595.48	547.22	*527.18*	632.76	597.30
	Strain to fracture (%)	**6.96**	2.46	1.42	1.31	*0.73*	3.04	2.65
Ti-0.3SA	Tensile Strength (MPa)	**634.1**	665.79	670.20	612.06	*588.46*	659.14	638.29
	Strain to fracture (%)	**6.62**	4.52	3.00	2.65	*1.15*	1.98	3.32
Ti-0.6SA	Tensile Strength (MPa)	**666.14**	695.34	663.14	*686.24*	671.86	658.93	673.61
	Strain to fracture (%)	**8.02**	5.53	7.71	*4.54*	5.47	6.64	6.32
Ti-1SA	Tensile Strength (MPa)	**680.66**	683.68	*642.29*	646.29	654.70	654.39	660.34
	Strain to fracture (%)	**1.84**	1.27	*0.92*	1.14	1.12	1.14	1.24
Ti-0.3MgSt	Tensile Strength (MPa)	**661.14**	668.14	711.33	653.77	661.89	*686.61*	673.81
	Strain to fracture (%)	**6.32**	2.16	1.23	4.00	1.82	*1.05*	2.76
Ti-0.6MgSt	Tensile Strength (MPa)	**674.17**	683.4	719.54	667.03	681.87	*666.17*	682.03
	Strain to fracture (%)	**4.66**	4.56	2.46	3.00	3.29	*1.24*	3.20
Ti-1MgSt	Tensile Strength (MPa)	710.60	**710.13**	**739.89**	721.42	707.53	*551.59*	690.19
	Strain to fracture (%)	2.73	**3.34**	**3.34**	2.58	1.74	*0.75*	2.41

6.3.4 Fracture features of test-pieces cut from positions 1-6

Fig. 6.7 shows SEM micrographs of fracture surfaces. Judging from the fracture pattern and the pore size, there are four typical fracture surface features. Fig. 6.7(a) and 6.7(b) show a crack-like void with a major length >300μm. The direction of the void length is along the radial direction, in other words, perpendicular to the thickness direction. This kind of void is associated with the origin of failure and the cause of degraded mechanical properties. Such voids can be observed in test-pieces with inferior ductility in pure Ti, Ti-0.3SA and T-0.3MgSt compacts. The facture surfaces of test-pieces with better ductility are shown in Fig. 6.7(c) and 6.7(d), they have the texture of a shear type of facture with some cleavage planes visible. This type of fracture surface is a feature in most compacts with a strain to fracture > 4%, which can be found in test-pieces from Ti-0.6SA compacts, some from pure Ti, Ti-0.3SA and Ti-0.3MgSt. Test-pieces cut from Ti-0.6MgSt and Ti-1MgSt compacts show fracture surfaces containing many small cleavage planes, as shown in Fig. 6.7(c) and 6.7(f). This indicates that there is little tendency for plastic deformation in these test-pieces. Many pores of size 50-100μm were on the facture surfaces of Ti-1SA test-pieces, as shown in Fig. 6.7(g) and 6.7(h). These pores are most likely responsible for degradation in ductility.

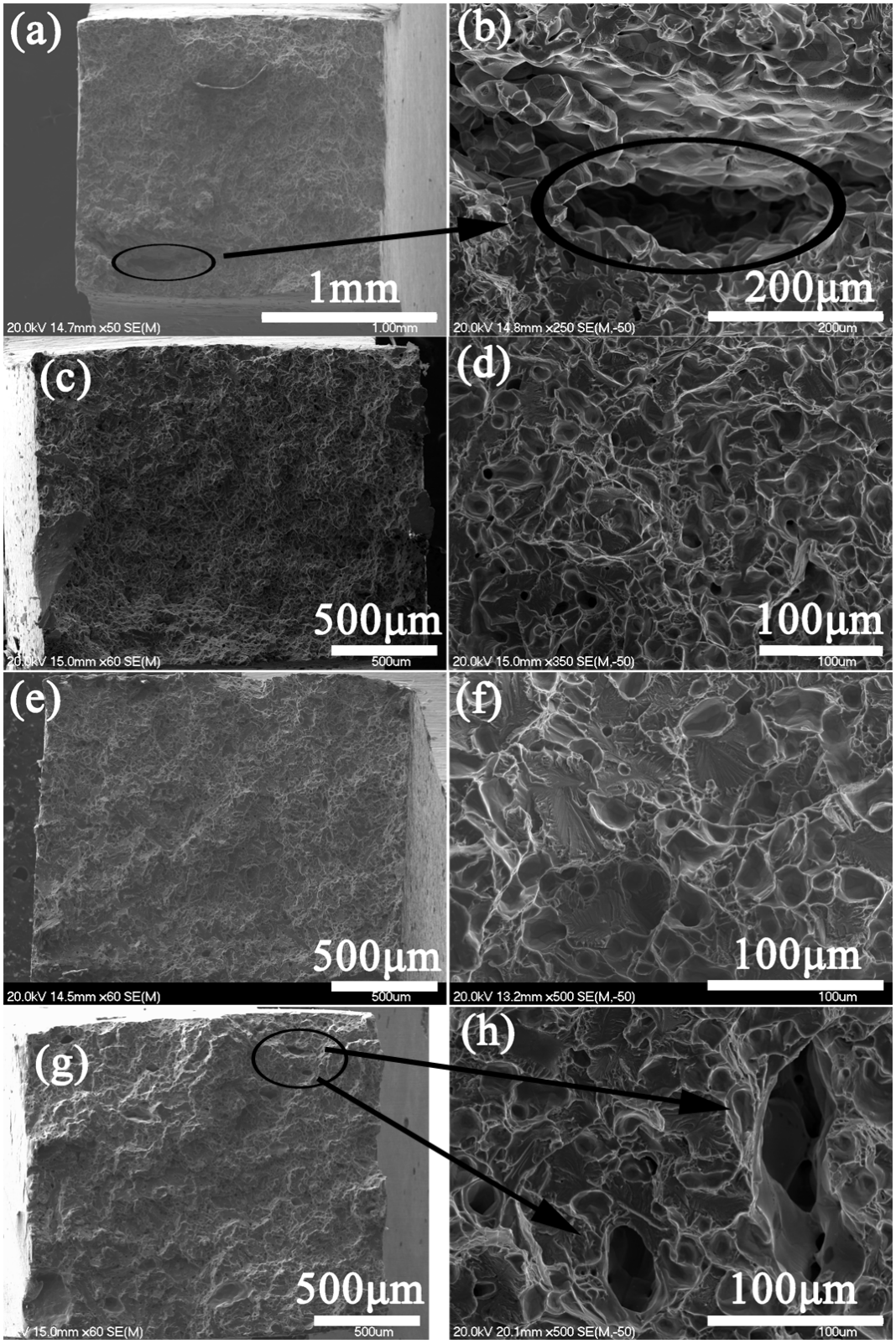

Fig. 6.7 SEM fractographs of Ti test-pieces cut from compacts with different amounts of lubricant: (a) and (b): Ti-0.3SA; (c) and (d): Ti-0.6SA; (e) and (f): Ti-1MgSt; (g) and (h): Ti-1SA

6.3.5 Effect of lubricant on oxygen and carbon pick-up

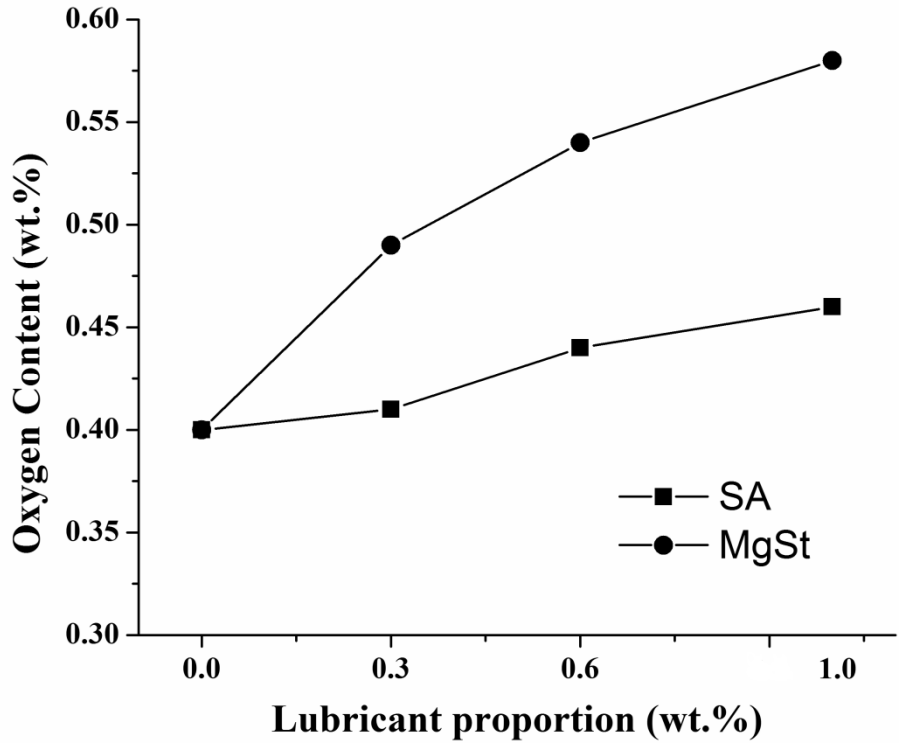

Fig. 6.8 Oxygen level of sintered compacts with different lubricants addition

Fig. 6.8 shows the oxygen levels for the sintered compacts with different amounts of lubricant. The SA additions give an oxygen pick-up of 0.06 time of its proportion and for MgSt this is about 0.18 time. MgSt additions do not cause any significant microstructural changes and there are no obvious pockets in the microstructure where MgO or Mg can be found. The carbon level in sintered compacts with different lubricant additions is about 0.04wt.%, which is much lower than the maximum requirement of 0.08wt.% [79]. Thus the effect of residual carbon on the mechanical properties of a sintered Ti alloy can be ignored.

6.4 Discussion

6.4.1 Uniformity of sintered mechanical properties

The tensile property data seems to suggest that the inferior mechanical properties of the bottom zone in a compact derive from its lower sintered density and higher level of porosity which contribute to a degradation of properties. However, the green density shows a bimodal distribution from top to bottom, i.e. the intermediate zones always show lower green density than the lower region [28, 69]. Fig. 6.5 shows that the green density difference in a vertical direction is able to be somewhat compensated for and there are indications from the literatures suggesting that gravity effects in a big compact might be the reason [127, 128].

In a powder compact, the green density variation not only exists in a vertical direction, but also in the horizontal direction. The TE position shows a higher density than the TC zone and the BC shows a higher density than the BE zone, which creates a "V" shape high density region through a cross section [69]. The density difference between the outer and inner layers near top or bottom surface is higher than that in the intermediate layers. During sintering, the lower density regions shrink more than the higher density ones. Internal stresses can arise from this differential degree of densification [129-133]. For samples with a small shape and thickness, warping may take place. For a Φ40 mm compact with a H/D ratio = 1, bending or deformation is near impossible, thus the stress only results in defects and a localised high or low sintered density. For a pure Ti compact sintered at 1300℃, the sintered density is not high enough, and small pores are distributed along the particle boundaries. This near homogeneous distribution leads to a stable ductility. When an internal lubricant or a higher isothermal temperature is applied, the density increases to about 94% and pores are combined together by a grain boundary diffusion mechanism to further densify the compact. Lou reported that lower porosity but a higher pore size may decrease the ductility of stainless steel [134]. If crack like voids are generated, the ductility will drop dramatically.

The level of stress depends on the degree of mismatch caused by shrinkage and the nature of the stress depends on the green density gradient between different zones. In the top zones, the TE shows higher density than the TC region, thus the TC is placed under a biaxial tension by the TE zones. Considering the almost free sintering in the thickness direction, shrinkage is prohibited only in a radial direction and hence the pores or voids grow in this direction. That is why pores with preferential orientation are observed in Fig. 6.4 and 6.7. The green density of the TC zones is not too bad (higher than that at the BE), only a small number of these pores can be expected. At the bottom of a compact, the situation is the opposite. The BE, which shrinks the most rapidly, is constrained by the BC with a higher density. Thus a large number of pores in the outer zones are generated. Test-pieces cut from the lower region contain such pores and these crack like voids have been observed as potential sources of brittle fracture. These aligned pores must be avoided because they are nearly impossible to eliminate by subsequent hot working [135]. In the intermediate region, the green density variation is very small, thus the shrinkage is free, leading to refined and spherical pore morphology.

The use of internal lubrication leads to an improved green density distribution. Such improvement does not only exist in the vertical layers but also in the horizontal direction [69]. An addition of 0.3wt.% of lubricant is not enough to homogenise the whole compact. A further addition to give an increased amount of 0.6wt.% leads to a better and more efficient lubrication effect. That is why 0.6wt.% SA shows the best uniformity of mechanical properties. MgSt shows a bad lubrication effect because of its smaller size compared with SA and the HDH Ti powder particles [125].

All test-pieces cut from the sintered Ti-1SA compact show quite bad ductility. The distributed pores located in the top and bottom zones, with size ranging from

50-100μm, are the cause of fracture. These pores are initiated from the compaction process. Although 1wt.% SA is not too high, the significantly larger particle size causes excess lubricant to be extruded from the centre to the surface of the compact [45, 125]. De-lubrication removes the lubricant but the pores remain. After sintering, residual pores with a random orientation remain in the same place and this causes deterioration in the ductility of all test-pieces cut from these regions. To avoid this phenomenon, when a lubricant addition ≥1wt.% is to be used, the lubricant should have a smaller particle size such as found in MgSt or added by using a solvent.

6.4.2 Oxygen content

The impurity level is a very important factor controlling the mechanical properties of sintered titanium metal and alloys [136, 137]. The oxygen level of the original powder is 0.33wt.% and a cold compaction and sintering process introduces 0.07wt.% of oxygen to a pure Ti compact. DTA/TGA curves of SA and MgSt are shown in Fig. 6.9.

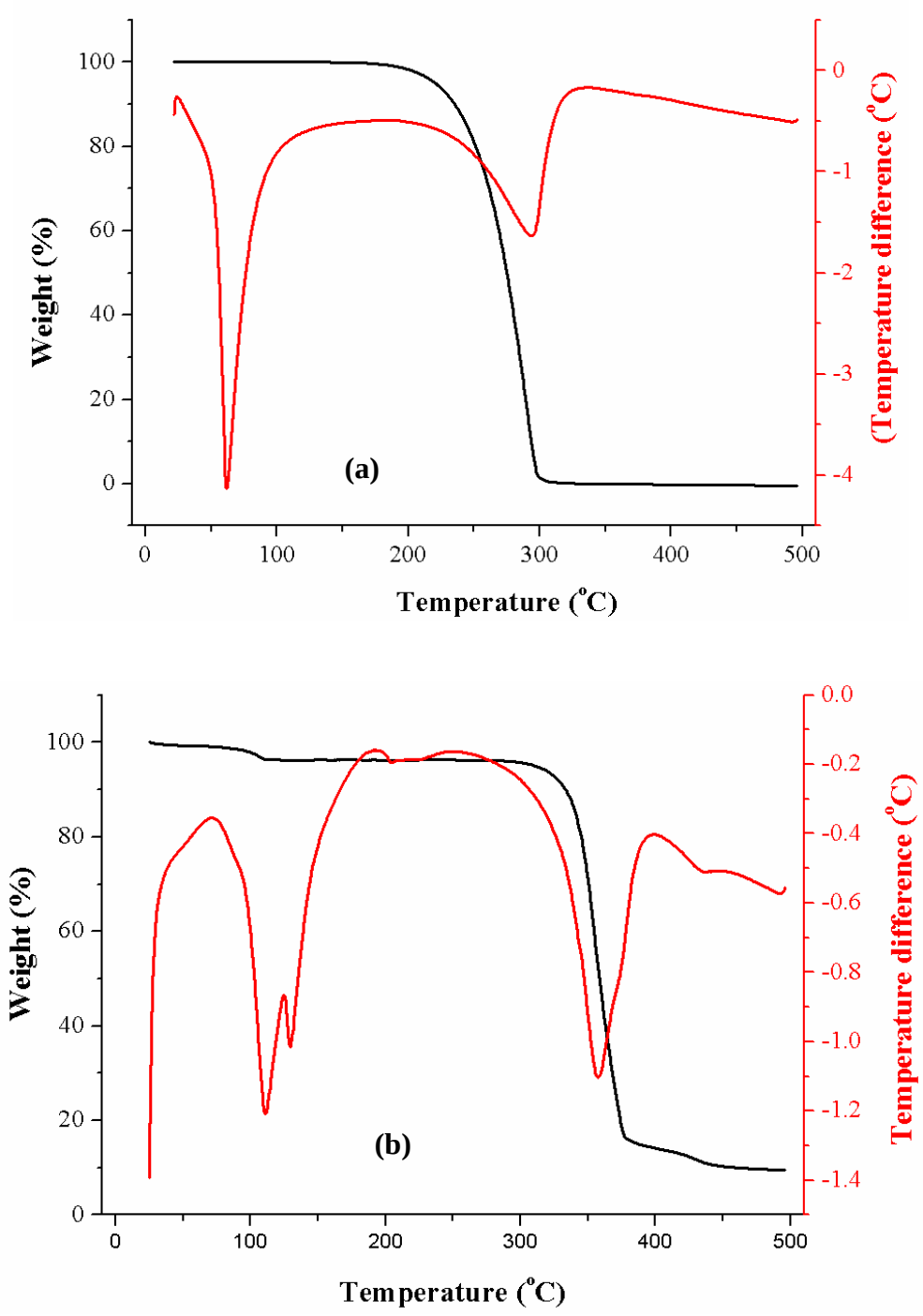

Fig. 6.9 DTA/TGA curves of (a) SA and (b) MgSt heated at 10℃/min in an argon flow atmosphere

Evaporation of SA starts at 200℃ and it is completely removed by the time the temperature reaches 300℃. MgSt exhibit the lowest starting temperature for

decomposition at about 330℃ and 9.5wt.% of the resides still exist after heating to 500℃. The reaction for the decomposition of MgSt is as follows:

$$[CH_3(CH_2)_{16}CO_2]_2Mg \xrightarrow{200℃\text{-}400℃} MgO \qquad (6.1)$$

Ideally, the decomposition of MgSt to MgO only creates 6.82% of residue as a proportion of the initial amount of MgSt. However, the real oxygen pick-up is higher than the ideal situation. Fig. 6.10 shows the DTA/TGA curves of Ti-2SA and Ti-2MgSt powder mixtures heated at 10℃/min in an argon flow atmosphere. Fig. 6.10(a) indicates that de-lubrication of Ti-2SA primarily occures at the temperature ranging from 200-350℃.At 400-450℃, the weight of mixture is almost stable, indicating that the de-lubrication process is almost completed. After 450℃, oxidation takes place. Fig. 6.10(b) indicates that de-lubrication of Ti-2MgSt occures from 220-450℃or even higher temperature. At 450℃, an drop in weight and an endothermic peak are observed. However, obvious oxidation happens immediately. Thus the de-lubrication process is not finished. Residues are sustained in the Ti-xMgSt powder mixtures and the impurity level of a sintered compact should be higher.

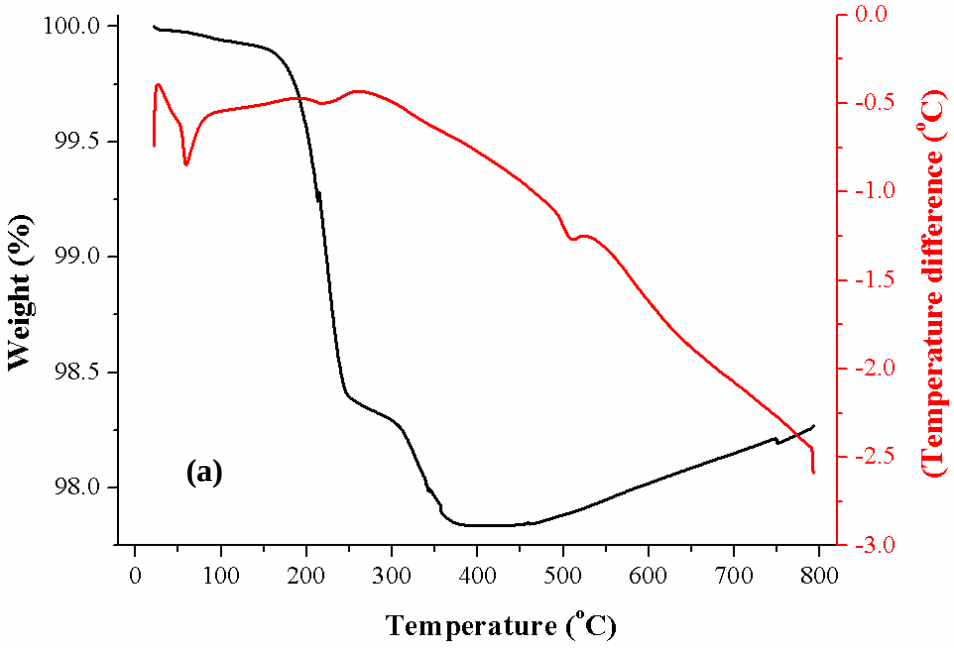

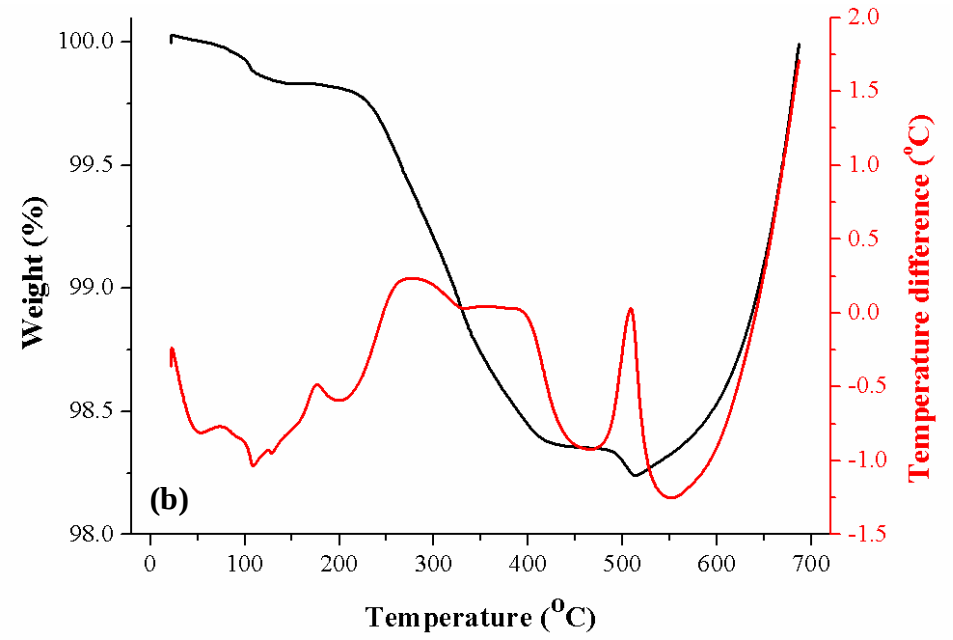

Fig. 6.10 DTA/TGA curves of (a) Ti-2SA and (b) Ti-2MgSt powder mixtures heated at 10℃ /min in an argon flow atmosphere

For the de-lubrication of big powder compacts, the degree of de-lubrication (sintered weight change divided to the lubricant's weight contained in a compact) ranged from 82-88 and 78-85wt.% for Ti-xSA and Ti-xMgSt compacts respectively. After debinding, a layer of lubricant or its decomposed compound is coated onto the surface of a compact and the inner surface of the pores. During sintering, these residual organics are released to the vacuum and make the atmosphere more oxidizing [10]. A compact therefore absorbs more oxygen and the picked-up oxygen level is higher than the results obtained from the TGA curves. A high oxygen level leads to a higher tensile strength and lower ductility [3]. Thus MgSt is not recommended as a lubricant for use in titanium powder processing in spite of its acceptable consistency of mechanical properties.

6.5 Conclusion

(1) The uniformity of ductility in the vertical direction of a Ti compact is degraded when the sintered density increases from 92.2% to about 94%. This is because pores become combined together and crack liked voids are generated. The appearance of these voids is accounted for in the inferior ductility of test-pieces cut from a Ti compact.

(2) Additions of 0.3-0.6wt.% SA and 0.3-1wt.% MgSt improve the sintered density distribution in Ti compacts by controlling the pore morphology with respect to the size, aspect ratio and orientation. But 1wt.% SA creates many pores ranging in size from 50-100μm both in the top and bottom regions and this leads to very bad ductility. The consistency in mechanical properties of a sintered Ti Φ40 mm compact with a H/D ratio =1 is significantly improved by adding 0.6wt.% SA.

(3) Variable mechanical properties in a large sintered Ti compact are initiated by a variation in green density. Such a variation in the horizontal direction in a compact creates uneven sintering stresses leading to pores with a high aspect ratio and a preferential orientation. An improvement in the consistency in mechanical properties from adding an internal lubricant is because of an improvement in green density distribution in the horizontal direction.

(4) Additions of SA lead to additional oxygen pick-up of about 6% and this is acceptable. By comparison MgSt leads to an additional three fold oxygen pick up compared with SA, thus MgSt is not recommended as an internal lubricant for use in P/M Ti alloy processing.

7. Chapter 7 Sintering of Titanium and Its Alloys with Small Amounts of Rare Earth (RE) Additions

7.1 Introduction

Very recently, adding RE to sintered titanium metal and it's alloys has attracted a lot of attention [17, 91, 138-142]. The appeal for adding RE is to assist with scavenging impurity elements, refining the microstructure and hence improving the mechanical properties of Ti metal and alloys. RE are added to the matrix in the forms of metal, intermetallic, oxides, hydrides and so on. Owing to their acute reactivity, introducing RE elements is virtually impossible [138]. The properties would not be modified until a huge mass of RE element is added [142]. The effect of introducing RE oxides on the ductility is trivial, but it can also scavenge some chlorine impurities [140, 143]. More recently attention has been given to the use of master RE alloys or RE composites [91].

This work started mid-2012, with the aim of controlling the oxygen level in titanium alloy powders and refining the sintered microstructure. Some Y and Er powders had already been purchased a few years earlier, and LaB_6 powder was purchased this year. These RE powders were mixed with Ti metal or Ti6Al4V alloy powder either by direct addition or by mechanical milling (MM).

One of the materials of interest is HDH CP Ti powder with not too high an oxygen content (0.2-0.3wt.%). Excellent mechanical properties have been obtained in parts made using this powder. Thus the Ti-Y, Ti-Er and Ti-LaB_6 were fabricated to test the mechanical properties, to see whether there are any benefits from RE addition to a Ti alloy to improve properties. Because pure Ti metal exists at room temperature as a single α phase, more microstructural analysis was carried out on a Ti6Al4V-RE alloy, which has an α/βstructure at room temperature.

However, because of the very high oxygen content of the current used HDH Ti6Al4V powder, the mechanical properties of the Ti6Al4V-Er alloy were not measured. However, for a Ti6Al4V-Y alloy, because the mechanical milling was carried out using GA Ti6Al4V powder, with lower oxygen content, the mechanical properties in this case were investigated.

This chapter investigates the effects on microstructure and properties of adding Er, Y and LaB_6 to Ti and/or Ti6Al4V alloy. The Ti(Ti6Al4V)-RE (Er, Y, LaB_6) alloy was processed as follows:

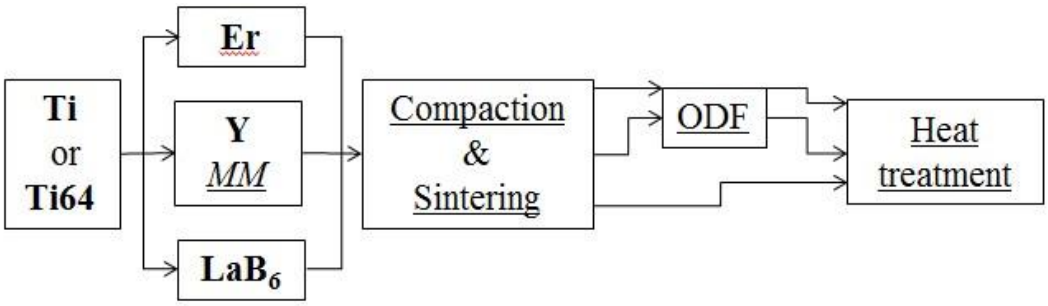

Various microstructures and quite different mechanical properties were obtained after sintering, open die forging (ODF) and heat treatment. To get a clear understanding of the process deriving from rare-earth additions, this discussion is analysed from the aspects of microstructure and mechanical properties. The influence of RE additions on microstructural refining and oxygen scavenging are discussed. This will provide preliminary knowledge about the influence of RE additions on the microstructure and mechanical properties of Ti metal and its alloys.

7.2 Experimental details

For direct Er additions, 0.4wt.% (0.115at.% for pure Ti) of Er was added to Ti and

Ti64 powder respectively. The mixing was carried out in a stainless steel container on a roller mixer for 3h at a rotational speed of 50Hz.

For the mechanical milling process using Y additions, 1wt.% of Y was added to Ti and Ti64 powder respectively. The mixture was milled at 200rpm for 6h. Only a Ti6Al4V-1Y alloy was used for microstructural and mechanical property analysis. Because compaction of MM powder is impossible, the milled powder was added with an equivalent mass of HDH Ti6Al4V powder to get a Ti64-0.5Y alloy (0.27 at %).

For an investigation of LaB_6 additions, only a Ti-0.6LaB_6 alloy was fabricated. The mass ratios of La and B in the alloy are 0.41 and 0.19wt.% respectively and so it can be regarded to be a Ti-0.4La-0.2B alloy. The atom ratios of La and B are 0.14 and 0.85at.% respectively. If all the La and B atoms are combined with O and B in the form of La_2O_3 and TiB respectively, 0.07wt.% of O and 0.84wt.% of Ti will be consumed. As a result, 0.48wt.% of La_2O_3 and 1.04wt.% of TiB are formed.

11mm diameter, 40 mm diameter and dog-bone dies were employed in present work. Cold compaction was done using a pressure of 400-700MPa and compacted samples were sintered at 1350℃ for 2.5h. An ODF process was carried out on the sintered Ti-0.4Er, Ti6Al4V-0.4Er and Ti6Al4V-0.5Y alloys. A sintered compact, made using 70 grams of powder and with a 40mm diameter, was heated under argon to 1100℃, at a heating rate of about 125℃/min, using an induction coil. The compacts were not held at the forging temperature before forging. A powder compact was open die forged (ODFed) using a 100 tonne hydraulic press, at an applied pressure of about 783MPa. The total reduction in height of the sample was about 62%. Wire cutting was used to cut the forged samples into tensile test pieces.

A heat treatment process was also carried out to optimise the microstructure and mechanical properties of sintered and forged samples. Test pieces for heat treatment

were encapsulated under vacuum in a quartz tube, which had been repeatedly evacuated and flushed with argon. Then the tubes were put into a muffle furnace at the pre-selected temperature. A commonly used heat treatment was used for the Ti6Al4V alloy: The regime is:

Solution treatment: 900℃ for 1h followed by water quenching; Aging treatment: 550℃ for 6h followed by furnace cooling.

The fabrication methods used and the intended use of the samples are listed in Table 7.1.SEM and EDS were used to analyse the microstructure of sintered, ODFed and heat treated samples. The fracture surfaces were also observed by SEM. OM was used to measure the grain size of the heat treated samples. TEM was also used to investigate the morphology of the precipitates formed as a result of RE and RE oxide additions to both Ti metal and Ti alloy.

Table 7.1 Fabrication methods and the usage of Ti(Ti64)-Re alloys

Alloy	addition method	ODF process	Heat treatment	Usage
Ti-0.4Er	Mixing	Yes	-	Mechanical properties Microstructural analysis
Ti64-0.4Er	Mixing	Yes	Traditional	Microstructural analysis
Ti-1Y	MM	-	-	Only for XRD
Ti64-0.5Y	MM	Yes	Traditional	Mechanical properties Microstructural analysis
Ti-0.6LaB_6	Mixing	-	-	Mechanical properties Microstructural analysis

7.3 Direct Er powder additions and the ODF process

7.3.1 Sintering

The green densities of Ti-0.4Er and Ti6Al4V-0.4Er are 74.99% and 70.56% respectively, which is in the normal compaction range for Ti and Ti6Al4V samples. After sintering, the densities increased to 95.56% and 91.91% respectively, which is a little higher (about 1%) than the sintered density of Er-free compacts. Two worm-like-voids were found in the sintered sample, which can be clearly seen by the naked eye, as shown in Fig. 7.1(a). Compared with the erbium powder shown in Fig. 7.1(b), the shape of the voids and their size are nearly identical to that of the Er particles.

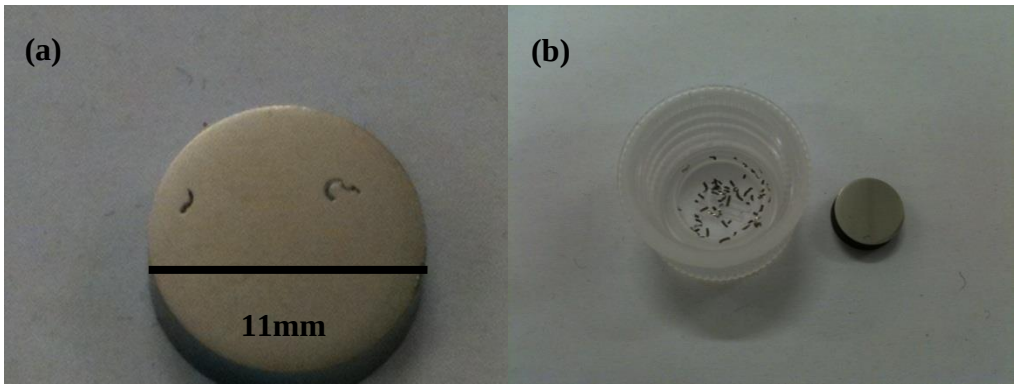

Fig. 7.1 Images of 11mm diameter Ti and Ti6Al4V sintered samples with erbium: (a) Ti-0.4Er and (b) Ti6Al4V-0.4Er with some erbium powder particles visible in the plastic container

Fig. 7.2 shows back scattered electron (BSE) images of voids present in Ti-0.4Er and Ti6Al4V-0.4Er alloys. A two phase structure with a white and grey appearance is observed. The voids are located in the centre of the phase with a white appearance. EDS results indicate that this phase is Er-rich. Columnar grains, which are a product of solidification of the liquid phase, are found on the surface of the voids. A liquid Er-rich phase has penetrated into the grey matrix and for Ti-

0.4Er, the penetration distance is about 200μm and for Ti6Al4V-0.4Er it is a little higher, with a penetration distance of 400μm. Samples cut from the sintered compacts with/without the segregation and void structure have quite different properties. Thus they cannot be used for mechanical testing.

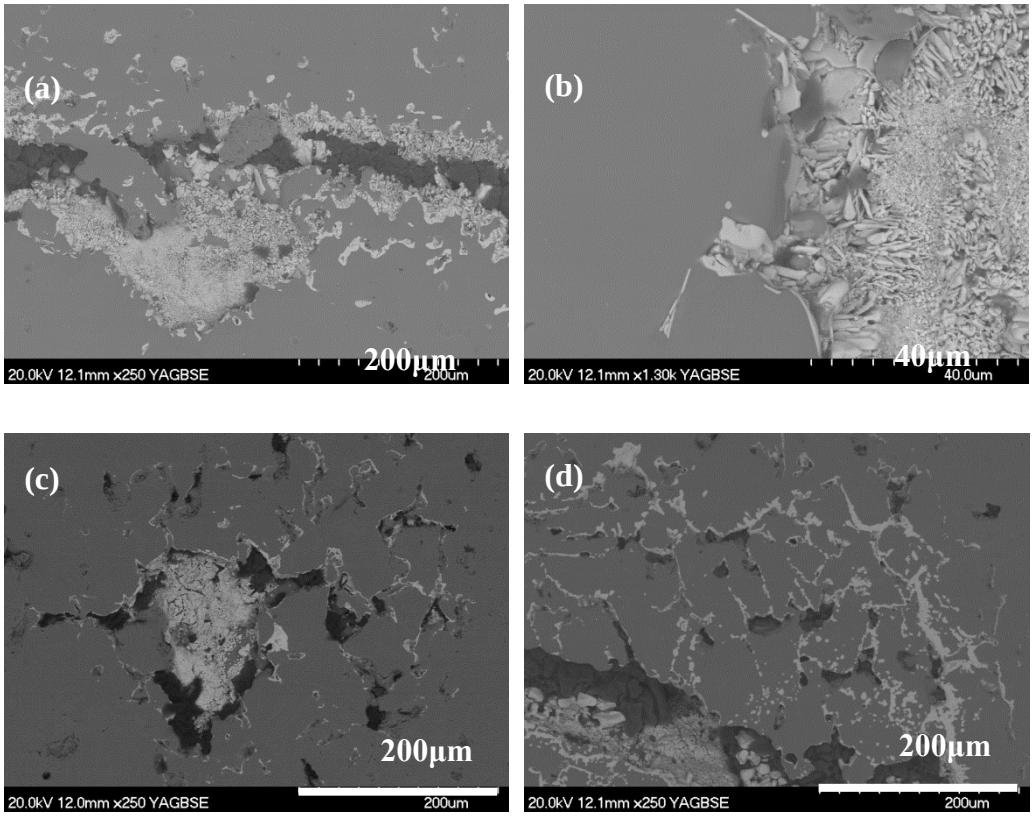

Fig. 7.2 Back Scattered Electron (BSE) images of as-sintered Ti-0.4Er and Ti6Al4V-0.4Er: (a) and (b), Ti-0.4Er; (c) and (d), Ti64-0.4Er

Fig. 7.3 shows the elemental distribution in the matrix and in the white area in a Ti6Al4V-0.4Er alloy. The matrix is almost Er-free. The liquid phase is Er based because it has Er in abundance with a very low Ti content. V content is lower than found in the matrix whereas Al, C and O contents are higher.

The formation of a liquid phase can be explained by reference to the Ti-Er binary phase diagram. As shown in Fig. 7.4, the Ti-Er system is a typical eutectic phase diagram, with liquid formed from 1300-1340℃. Therefore the liquid phase is

generated due to the higher isothermal sintering temperature of 1350℃. The formation of Er segregation and voids will be explained in the discussion section.

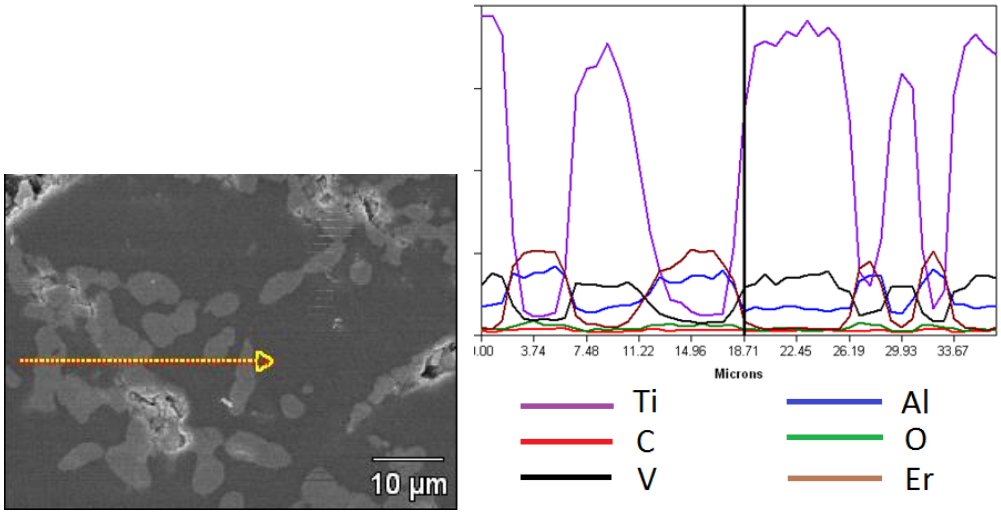

Fig. 7.3 Elemental distribution along a line in the microstructure near the voids in a Ti6Al4V-0.4Er alloy.

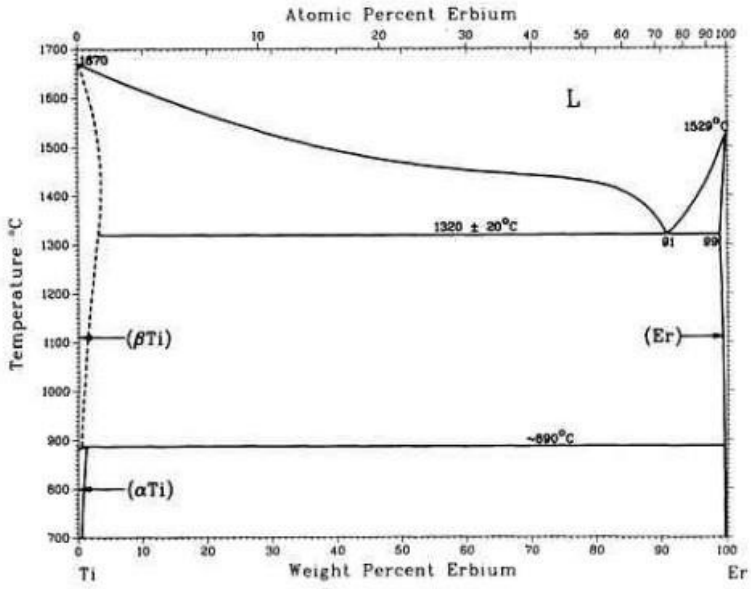

Fig. 7.4 Ti-Er binary phase diagram

7.3.2 Open die forging

Fig. 7.5 shows the Er distribution in an ODFed sample. Fig. 7.5 (a) depicts many white spots ranging in size from 1-5μm in the transverse face, which is perpendicular to the press direction. Fig. 7.5 (b), which is taken from the longitudinal face, indicates that the Er segregation has been elongated to an acicular form with an aspect ratio of 8-10. At the centre, the segregation is almost gone, but at the edge of an as-forged sample, large amounts of Er segregation still exist, as shown in Fig. 7.5(c). The diffusion distance of the Er has increased to 600-1000μm. Thus ODF leads to homogenisation of the Er distribution. Fig. 7.5(d) shows that big voids have been closed.

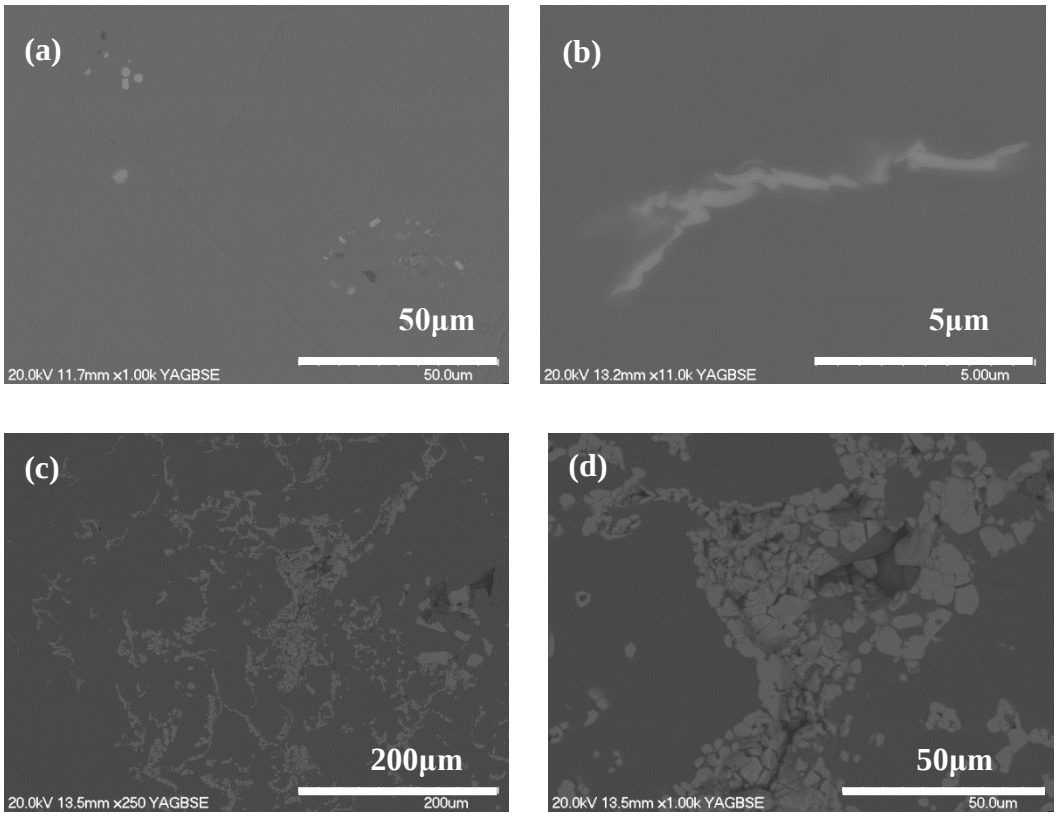

Fig. 7.5 SEM images of as-forged Ti-0.4Er samples: (a) radial direction in the centre region; (b) longitudinal direction in the centre region; (c) edge region showing the existence of Er segregation; (d) a higher magnification image of (c) showing the closure of voids

Table 7.2 gives the mechanical properties of as-forged Ti-0.4Er alloy. Test-piece no.1, which is from the top surface on which the applied pressure acts, has

excellent UTS and ductility. But test-piece no.3, which was cut from the bottom surface, has lower properties. This result is acceptable because it lies in the range of values for an as-forged pure Ti sample (700-800MPa and 6-14% strain). However, there is no obvious improvement as a result of Er additions is.

Fig. 7.6 shows the fracture surfaces of test pieces No.1 and 3. Cracks can be found in the fracture surface, which must be sites of fracture initiation. In sample No.1, shown in Fig. 7.6(a), the crack is not very clear and its length is only 300μm. Er rich segregation was found along the two sides of the crack. In sample No.3, shown in Fig. 7.6(c), T-shaped long cracks (~1mm) are found. Er segregation was also found to be associated with the crack. Thus Er segregation still exists in the test pieces which cause deterioration in mechanical properties.

Table 7.2 Mechanical properties of as-forged Ti-0.4Er samples

No.	**UTS (MPa)**	**Strain to break (%)**
1	764	10.50
2	818	7.77
3	729	1.16

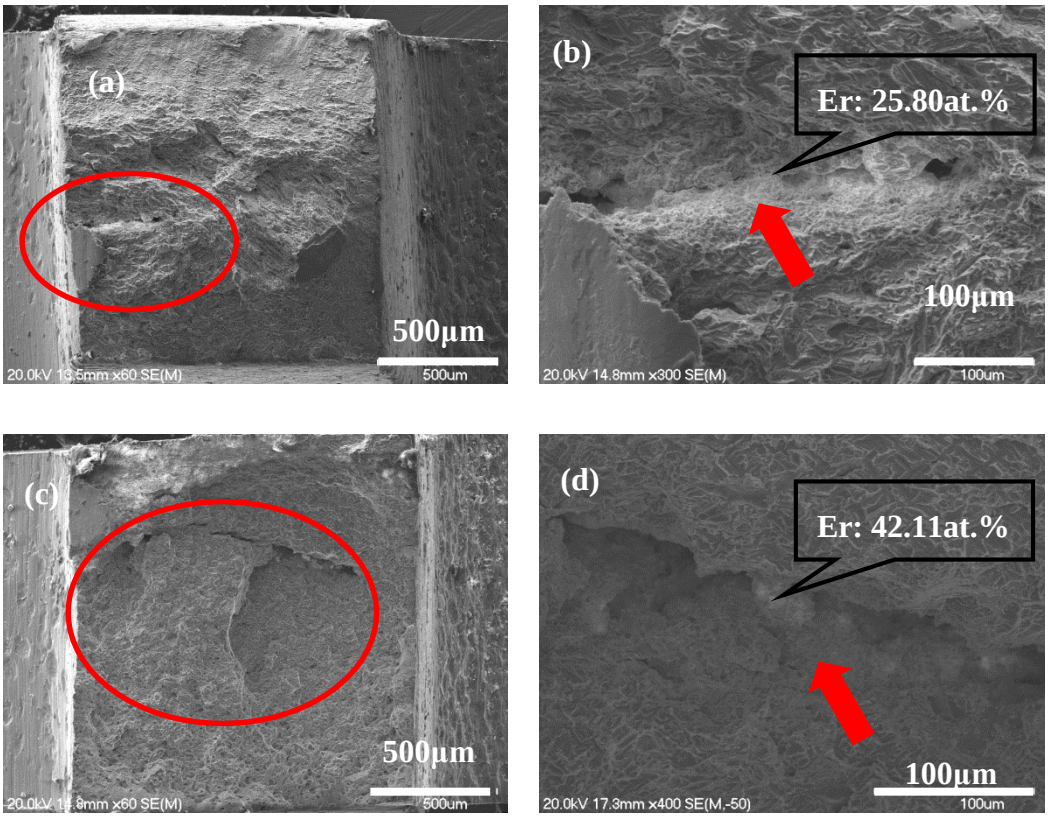

Fig. 7.6 Fracture surfaces of test pieces cut from as-forged Ti-0.4Er alloys (a) No.1; (b) the crack in Fig. 7.6 (a), indicating the existence of ER segregation. (c) No.3; (d) the crack in Fig. 7.6 (c)

Fig. 7.7 shows an Er platelet observed in a Ti6Al4V-0.4Er alloy. A near spherical plate with a white appearance is located in the matrix. The diameter of the plate is about 40µm and the thickness is at the micron level, indicating that it was forged from a bulk texture to a thin plate. The boundary between the plate and the matrix is cracked. Furthermore, the plate has many cracks. Therefore the strength of material with Er segregation is far more inferior than the Ti alloy matrix. It also depicts that the segregation is rich in Al and O but low in V.

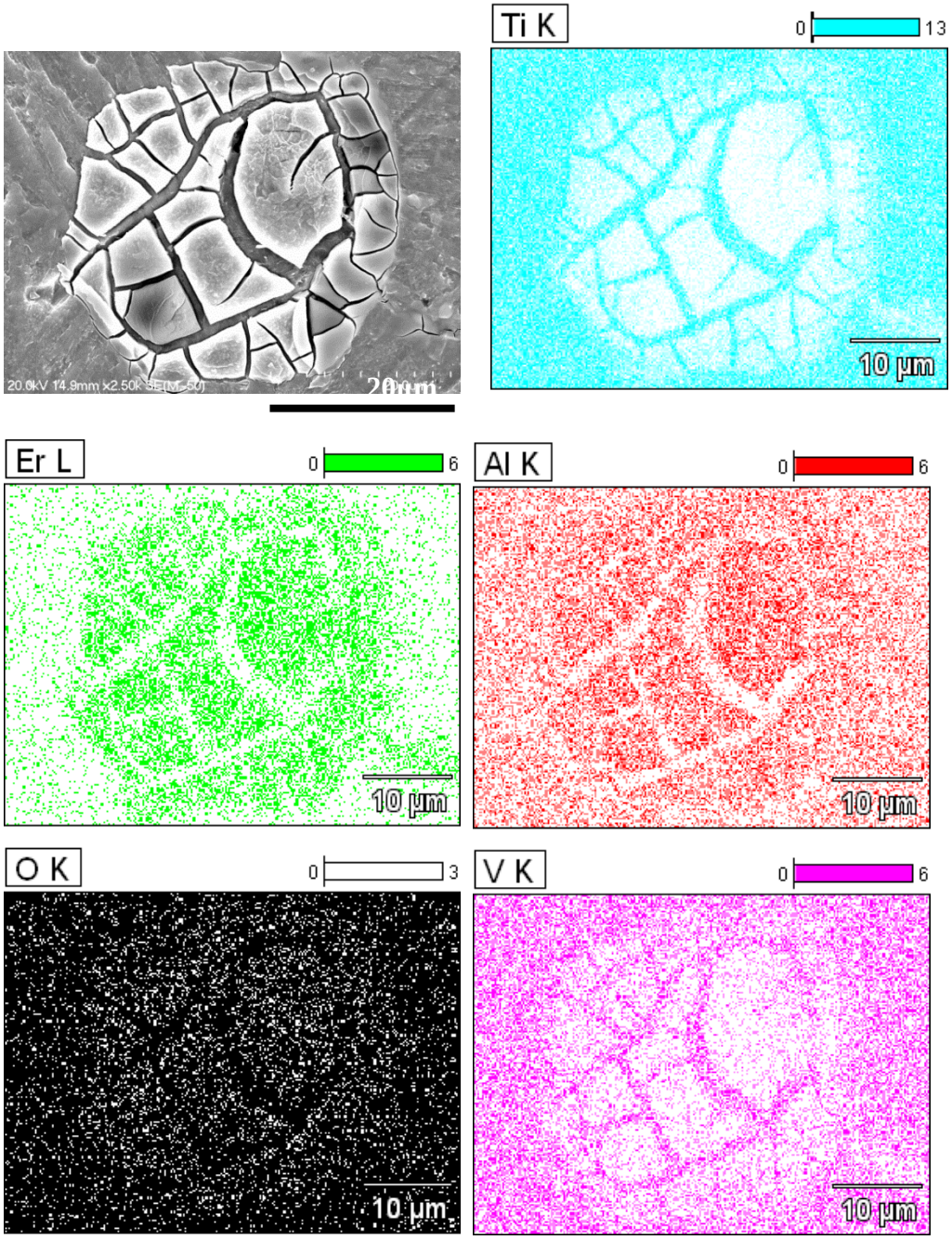

Fig. 7.7 An Er platelet in a Ti6Al4V-0.4Er alloy and associated elemental mapping

The heat treat microstructure of a Ti6Al4V-0.4Er alloy will be introduced in the next section, together with results for the heat treated Ti (Ti6Al4V)-0.5Y alloy.

7.4 Mechanical milling, compaction and sintering of a Ti alloy with Y additions

7.4.1 Mechanical milling

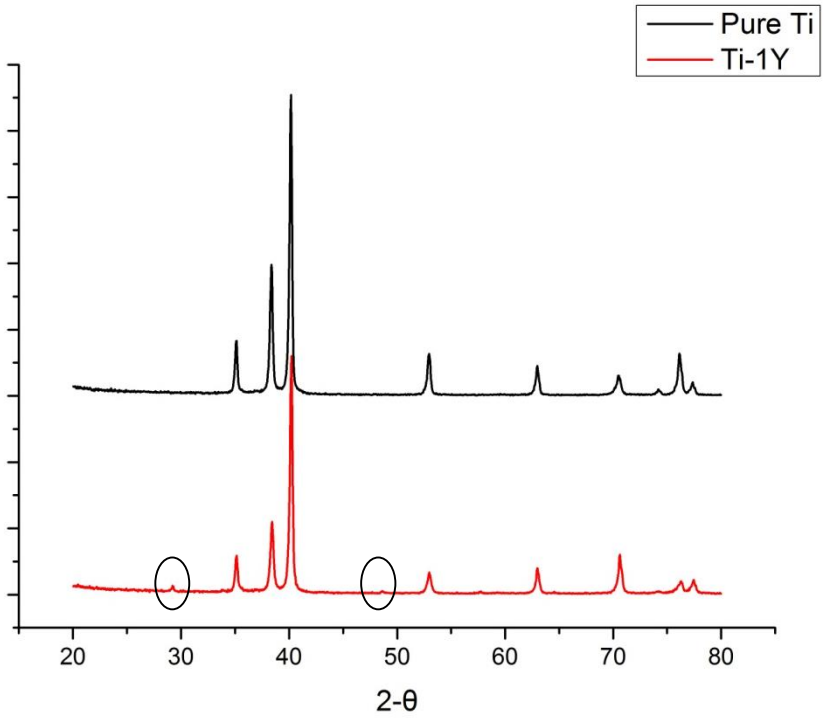

Fig. 7.8 A comparison of XRD results obtained from sintered Ti-1Y and pure Ti samples

A MM Ti-1Y alloy was fabricated to identify whether a new phase would be generated during the MM process. XRD results from the powder are shown in Fig. 7.8 along with results from pure Ti powder as a comparison. Very weak Y peaks, at values of 2θ close to 28 °and 48 °, were obtained.

7.4.2 Sintering

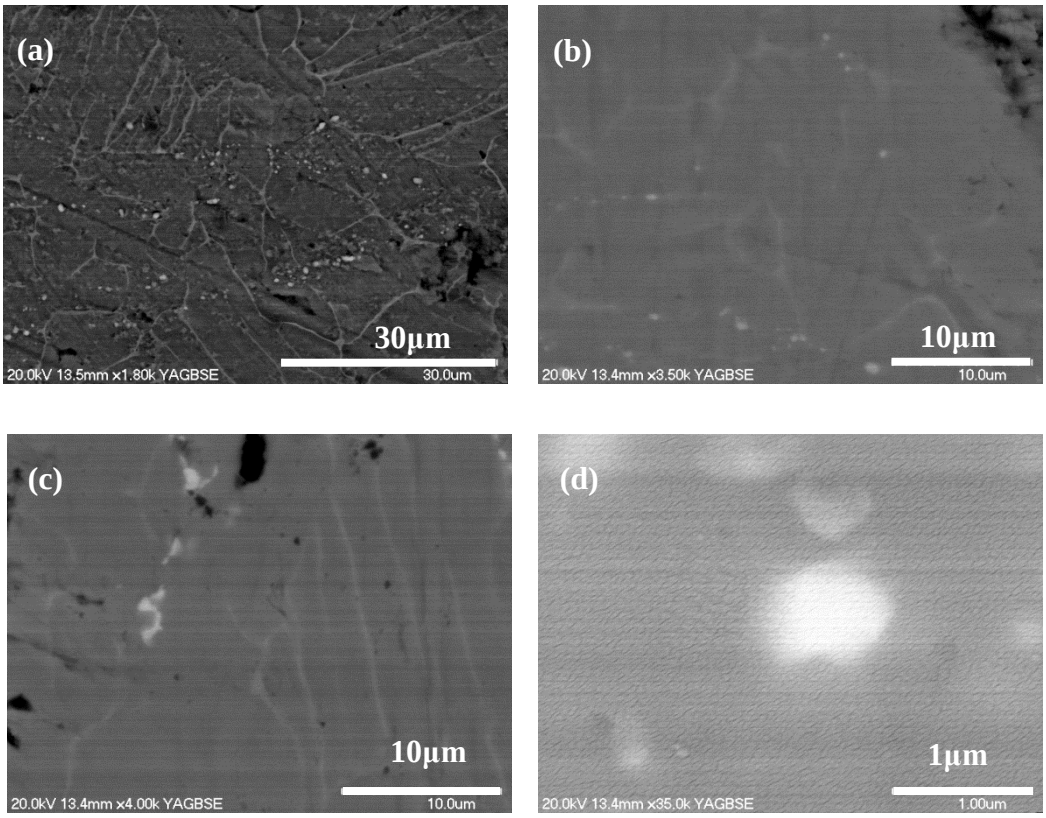

Fig. 7.9 BSE images of a sintered Ti6Al4V-0.5Y alloy

Fig. 7.9 shows the microstructure of a Ti6Al4V-0.5Y alloy. From the BSE images, the Y containing particles with a particle size of about 500nm are found in the α + β microstructure. The Y particles do not appear to have affected the formation of the α + β phase. Fig. 7.10 shows elemental mapping for Y from one of the spots with a white appearance.

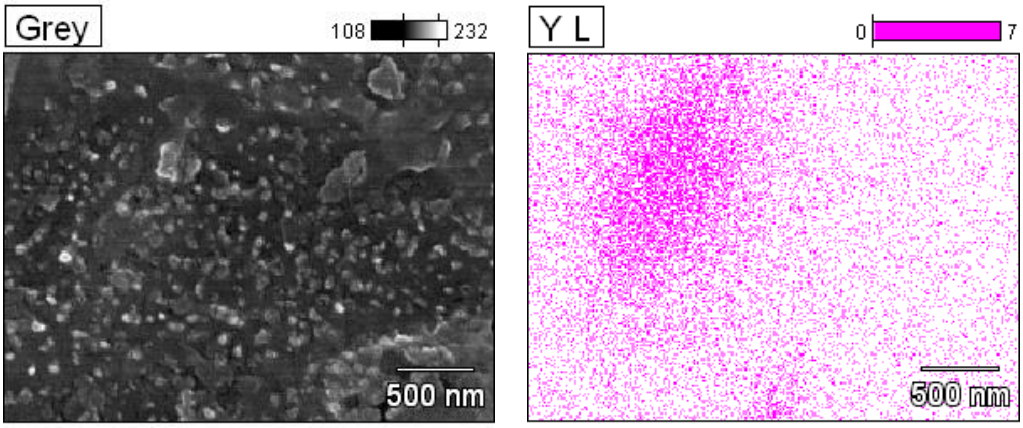

Fig. 7.10 Y elemental mapping from a white spot

7.4.3 Mechanical properties

Fig. 7.11 shows the strain stress curves for sintered and forged Ti6Al4V-0.5Y alloy test-pieces and their fracture surfaces. The UTS for forged samples is quite high, but the sintered ductility is near to zero. For the forged samples, the strain to fracture varied, one test-piece exhibited about 4% strain to fracture (about 3% elongation), whereas another test-piece exhibited negligible elongation.

Fig. 7.11(b) and (c) show evidence of powder particle surfaces, which indicates that the sintering process used in this case does not lead to strong bonding among particles. Failure initiates at the weak particle boundaries. Moreover, the matrix exhibits brittle features: many cleavage patterns are observed. Fig. 7.11(d) shows that many secondary dispersoids with size ranging from 0.5-1μm. Some of them are located in the hollow.

Fig. 7.11(e)-(g) show the fracture surface of an as-forged sample with 1.3% strain to fracture. From Fig. 7.11(e), the facture surface consists of two regions. The bottom region, as shown in Fig. 7.11(f) at higher magnification, proves that cracks initiate in and propagate along a particle boundary. Compared with the fracture surface in Fig. 7.11(c), the only difference is the absence of pores, indicating that the ODF process has created a higher density. The top region, as shown in Fig. 7.11(g), indicates some cracking. These cracks provide evidence of cracking along particle boundaries. Besides the cracks, the top region of the fracture surface contains some small dimples with particles, in the hollow spaces, as shown in Fig. 7.11(h). EDS shows that these particles are Y rich. Thus an yttria dispersoid is a potential barrier to dislocation motion in a Ti matrix, since the yttria dispersoid forms on dislocations (see Fig. 7.14(e)). A test-piece which gave 4% stain to fracture showed a larger area of small dimples.

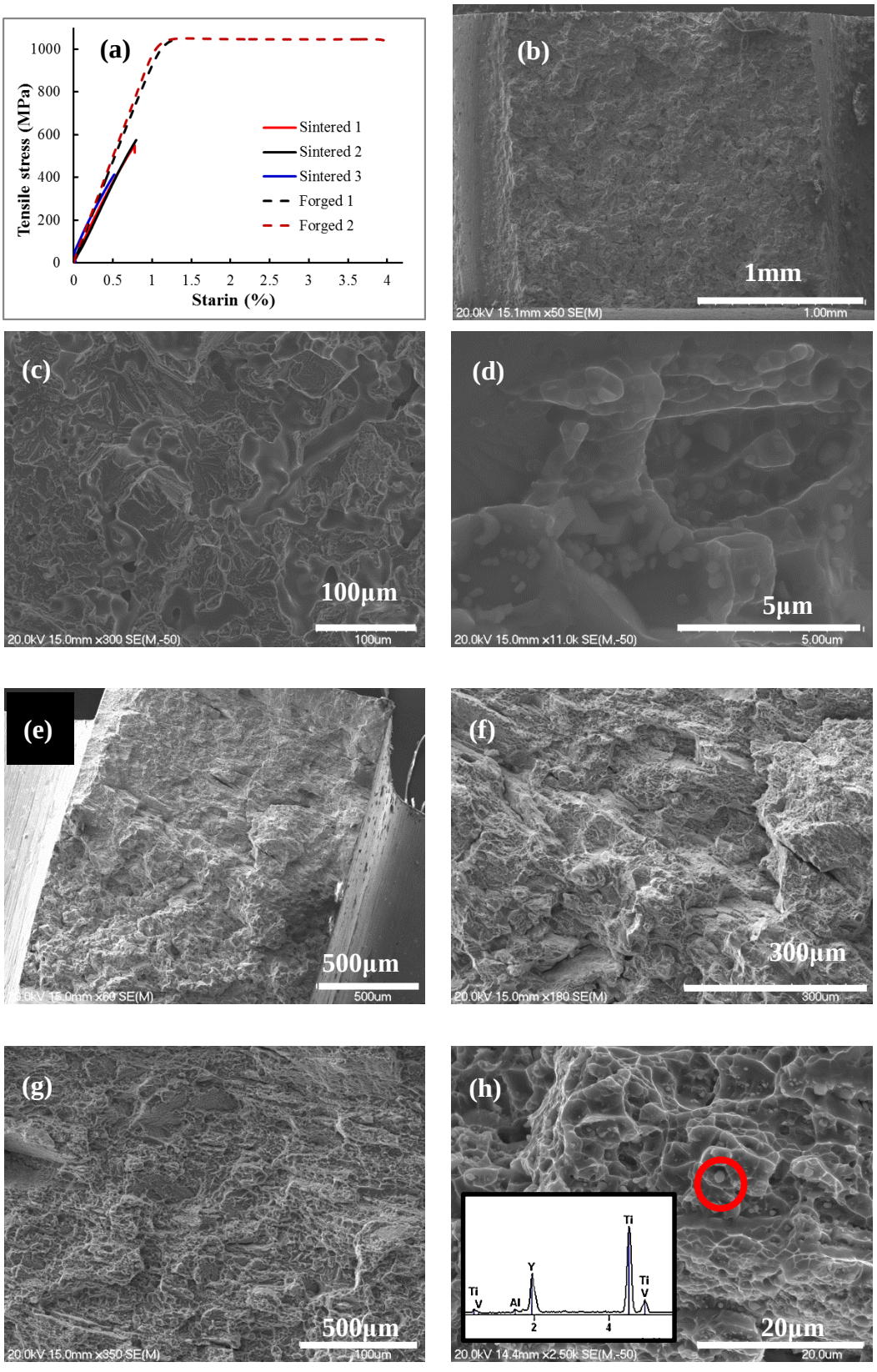

Fig. 7.11 Mechanical properties of MM Ti6Al4V-0.5Y alloy: (a) stress/strain curves; (b) fracture surface of a sintered sample; (c) higher magnification for Fig. 7.11(b); (d) Presence

of Y; (e) fracture surface of a sintered sample; (f) higher magnification for the bottom region from Fig. 7.11(e); (f) higher magnification for the top region from Fig. 7.11(e) and (h)

7.4.4 Heat treatment

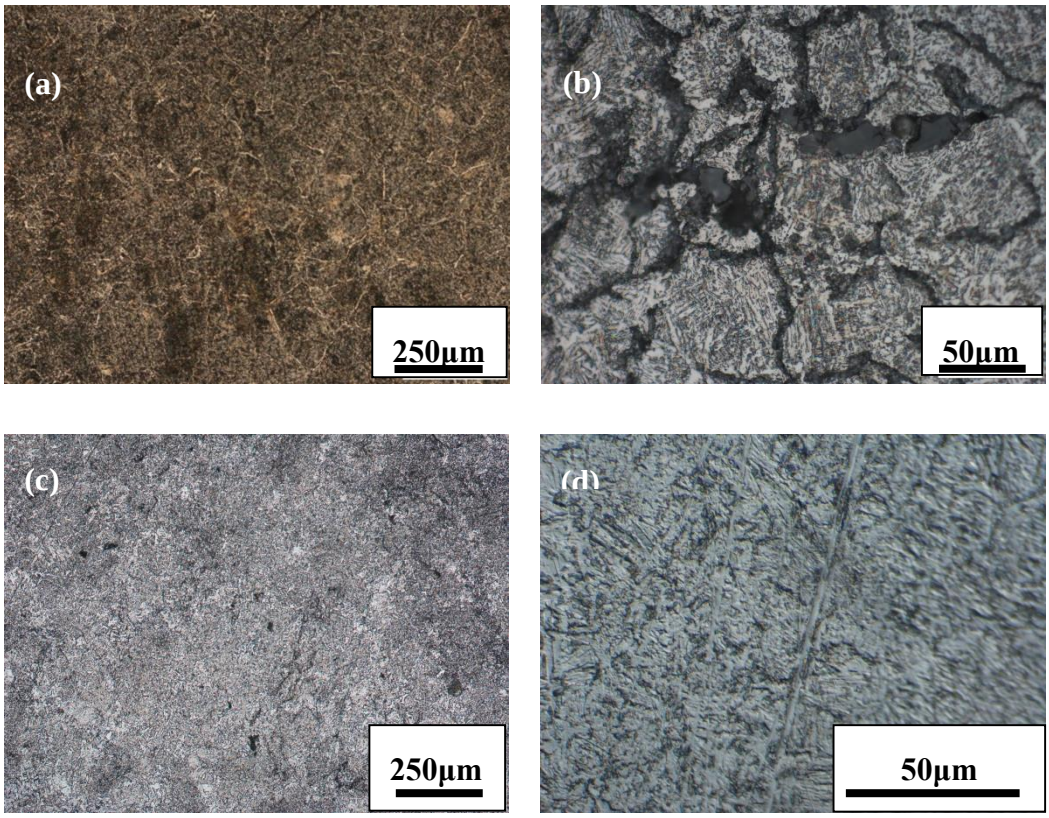

Fig. 7.12 Microstructures of ODFed & heat treated material: (a) and (b) Ti6Al4V-0.4Er; (c) and (d) Ti6Al4V-0.5Y

The microstructures of heat treated Ti6Al4V-0.4Er and Ti6Al4V-0.5Y are shown in Fig. 7.12. In these micrographs the α+β microstructure is much clearer than in the sintered microstructure. Clear prior β grain boundaries can be seen in the Ti6Al4V-0.4Er alloy, the grain size ranges from 50-250µm, the average value is 106µm. Some cracks can be seen in Fig. 7.12(b), where signs of the Er liquid, shown as the grey areas, inside the cracks. Because the volume fraction of Er is quite small, segregation must be prevented otherwise the benefit of adding Er is wasted. For a

Ti6Al4V-0.5Y alloy, as shown in Fig. 7.12(c), the prior β grain boundaries are obscure. The formation of this structure is mainly due to the mechanical milling process. The size of the β phase can be indirectly measured from the average length of the α lamella of 36μm, indicating that the microstructure of this Ti6Al4V alloy has been refined.

The SEM images of as-sintered, solution treated and aged Ti6Al4V-0.5Y samples are shown in Fig. 7.13. In Fig. 7.13(a), there are many small irregularly shaped particles, in the size range from 1-5μm. After solution treatment, the microstructure transforms into a martensitic structure and the particles are very difficult to find, as shown in Fig. 7.13(c). The diameter of the particles is about 300nm, as shown in Fig. 7.13(d). It can be concluded that a solution treated alloy is super-saturated with Y. After aging, a dispersion of particles re-appears in greater number with increased diameter to about 500nm. Thus an aging process leads to a re-precipitation of Y_2O_3 particles. TEM images of aged samples are shown in Fig. 7.14. Fig. 7.14(c) shows some big Y_2O_3 particles ranged from 2-4μm. Meanwhile, there is a dispersion of very small second phase particles with the particle size ranging from 5~25nm, as shown in Fig. 7.14(e). The dispersoids are often found to be decorating dislocations. The selected area diffraction patterns as shown in Fig. 7.14(b), (d) and (f) show the α phase and diffraction spots from the particle dispersion. The indexed diffraction patterns of Fig.7.14(d), as shown in Fig.7.14 (g), has identified that the large particle is Y_2O_3. Such pattern is similar to the results from Castro's work [143].

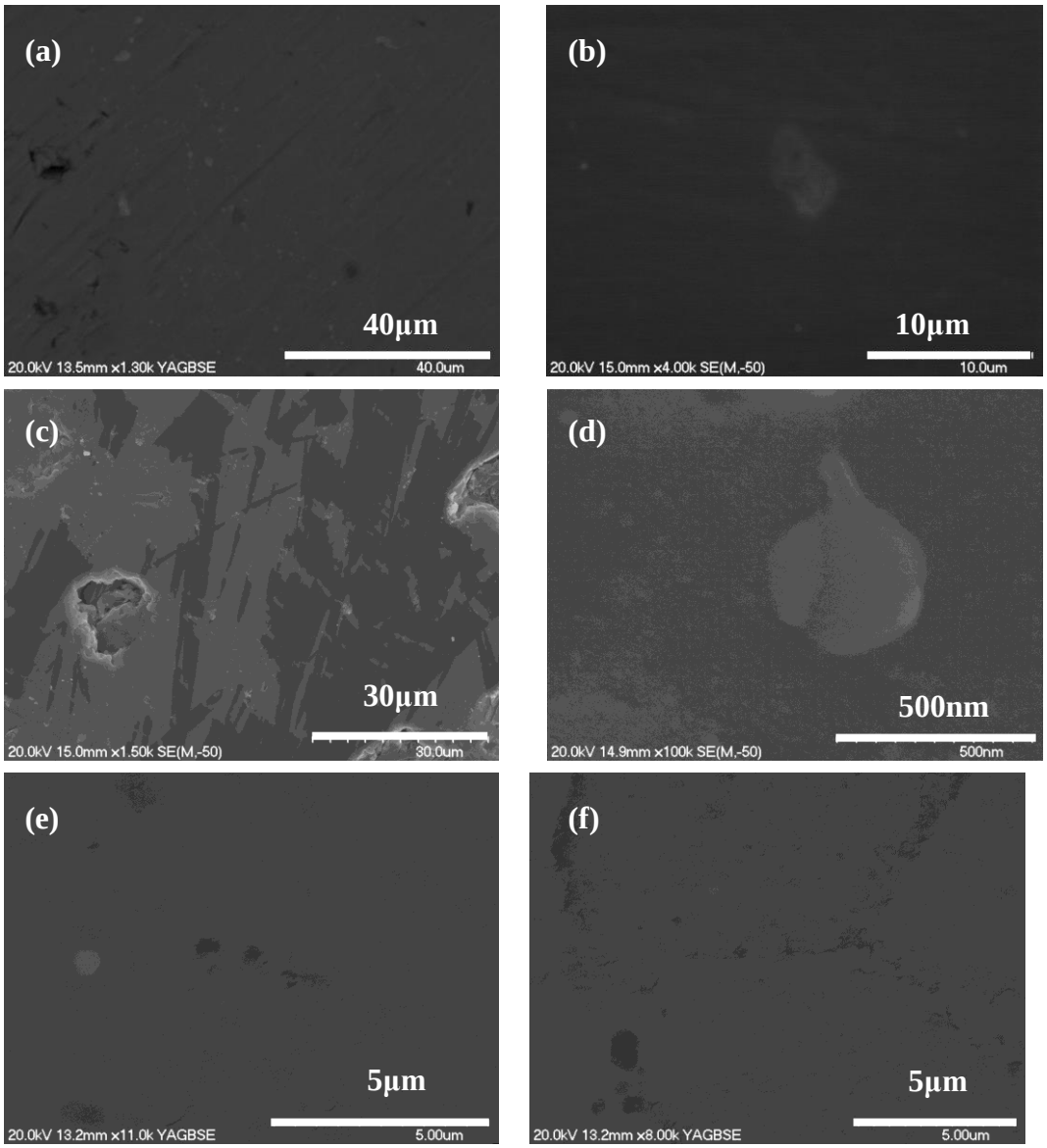

Fig. 7.13 SEM pictures proving the existence of Y during the heat treatment process: (a) and (b) sintered; (c) and (d) solution treated; (e) and (f) aged

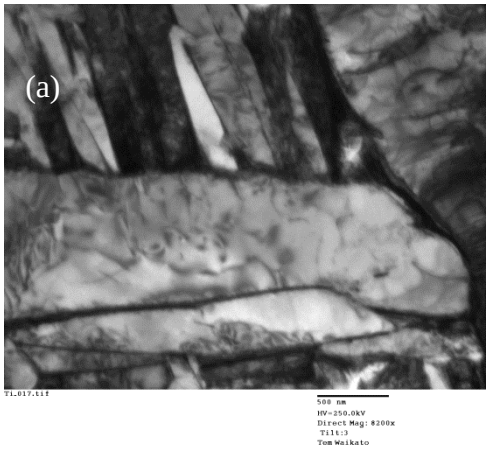
(a)
Ti_017.tif
500 nm
HV=250.0kV
Direct Mag: 8200x
Tilt:3
Tom Waikato

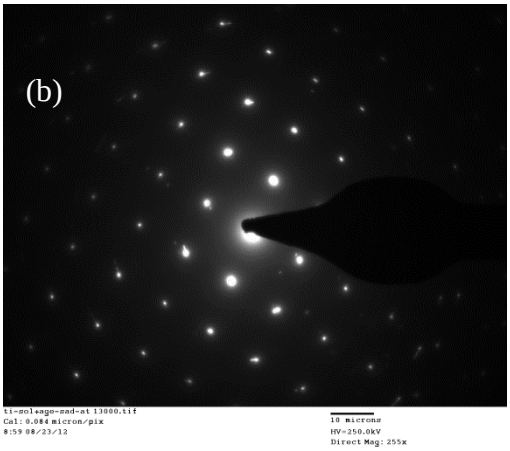
(b)
ti-solsage-znd-at 13000.tif
Cal: 0.084 micron/pix
8:59 08/23/12
10 microns
HV=250.0kV
Direct Mag: 255x

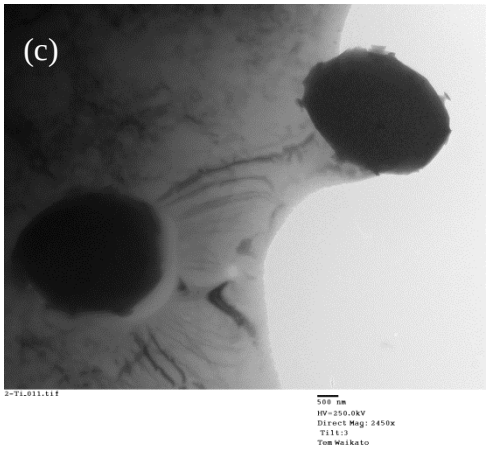
(c)
2-Ti_011.tif
500 nm
HV=250.0kV
Direct Mag: 2450x
Tilt:3
Tom Waikato

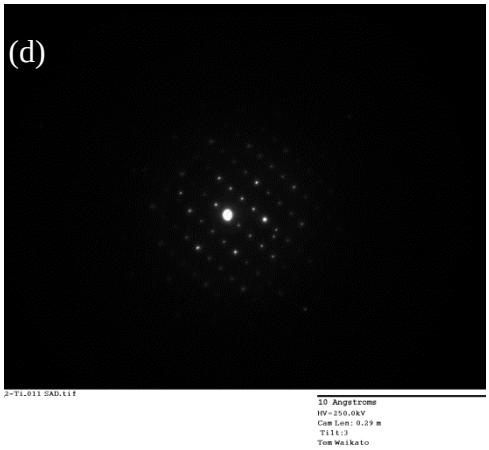
(d)
2-Ti_011 SAD.tif
10 Angstroms
HV=250.0kV
Cam Len: 0.29 m
Tilt:3
Tom Waikato

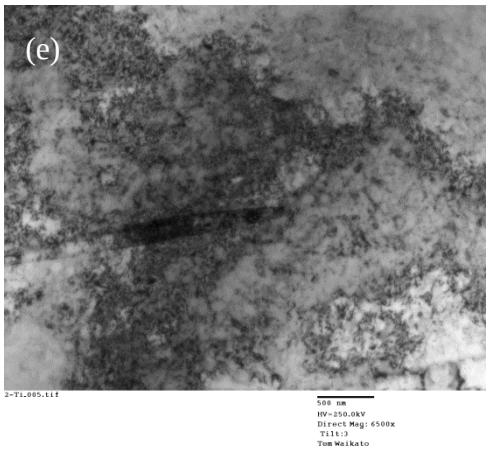
(e)
2-Ti_005.tif
500 nm
HV=250.0kV
Direct Mag: 6500x
Tilt:3
Tom Waikato

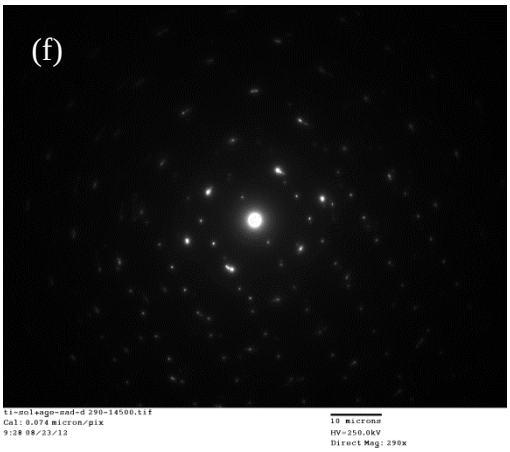
(f)
ti-solsage-znd-d 290-14500.tif
Cal: 0.074 micron/pix
9:38 08/23/12
10 microns
HV=250.0kV
Direct Mag: 290x

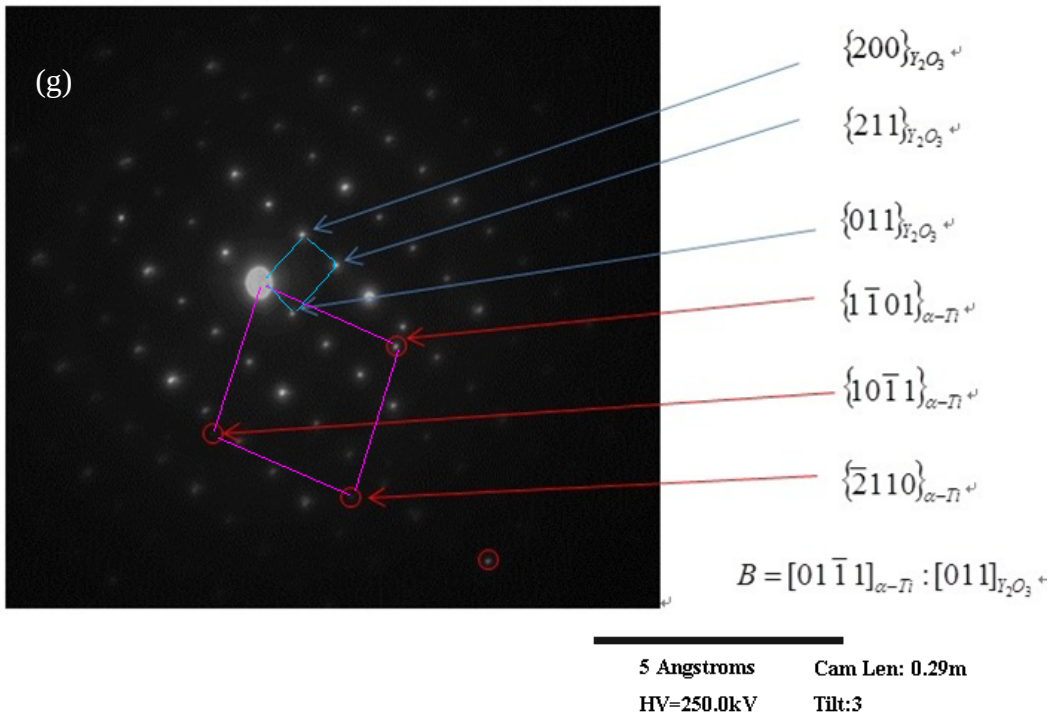

Fig. 7.14 TEM images of aged Ti6Al4V-0.5Y samples: (a) matrix; (b) SAD for the α phase; (c) Y rich spot; (d) SAD from a particle; (e) dispersoids in the matrix ; (f) SAD from the particle dispersion and (g) indexing for Fig.7.14(d)

7.5 Addition of LaB_6

7.5.1 DTA/TGA results

The DTA/TGA results for Ti-10wt.%LaB_6 and Ti6Al4V-10wt.% LaB_6 are shown in Fig. 7.15. For pure Ti, the α-β transformation starts at about 900℃. But for Ti6Al4V, the transformation temperature is a little lower, at 800℃, because V is a β-phase stabiliser for Ti (Al is an α-phase stabiliser but its effect is weaker than V). There is a small exothermic peak at about 950℃. However this is not very clear and therefore the reaction between Ti and LaB_6 can hardly be observed by DTA/TGA.

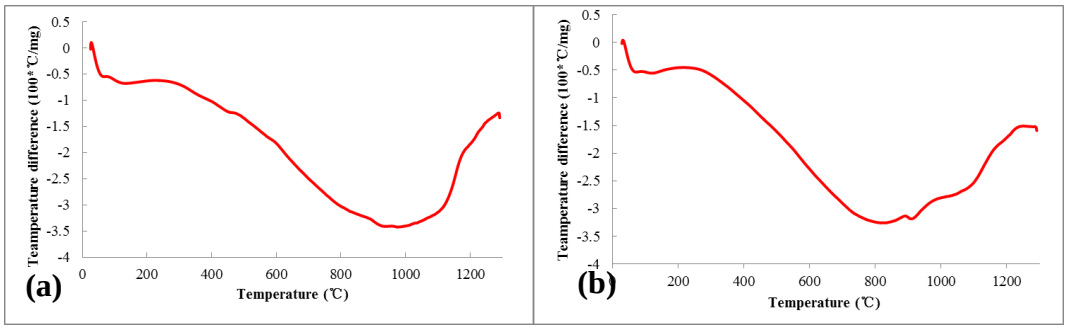

Fig. 7.15 DTA/TGA curves of (a):Ti-10wt.%LaB_6 and (b): Ti6Al4V-10wt.% LaB_6

7.5.2 Microstructure

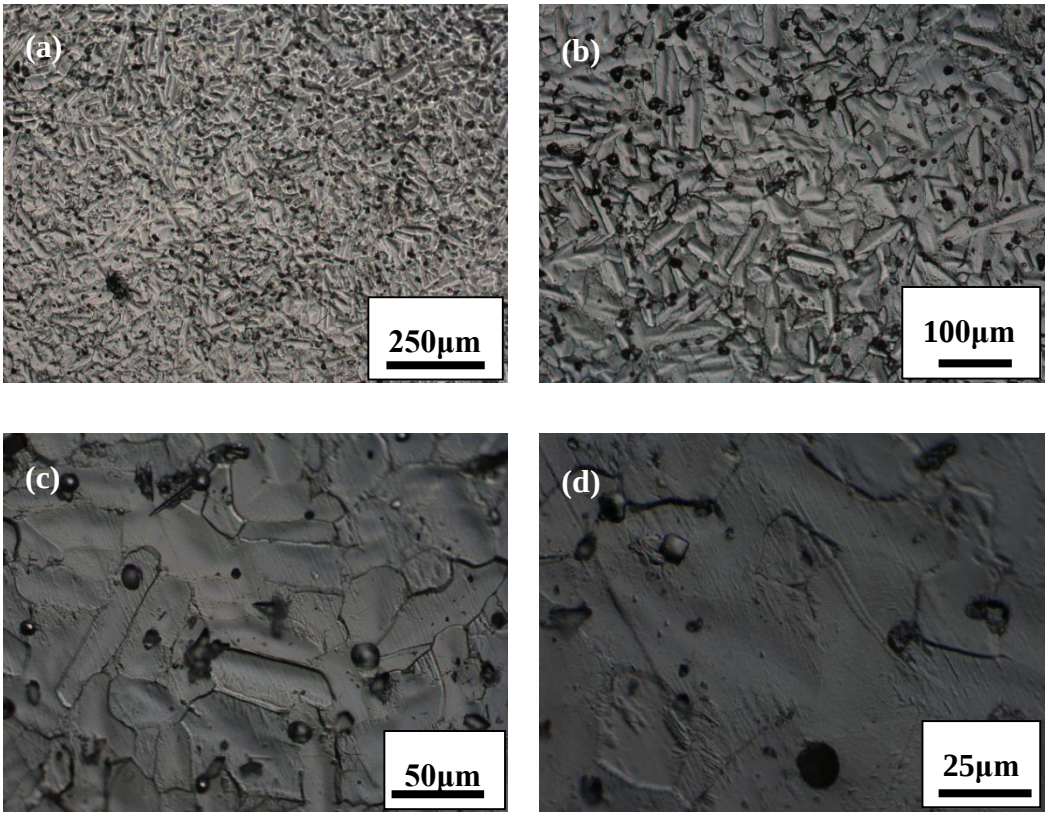

Fig. 7.16 Microstructure of an etched Ti-0.6LaB_6 sample

The green density of an 11 mm diameter sintered compact is 83.55%, the sintered density is 98.77%. No references could be found which indicates whether an addition benefits the sintering process. however it is reported that excess LaB_6

decreases the sintered density [17]. An OM image of an etched sample is shown in Fig. 7.16. It shows a quite different microstructure to that found in pure Ti. The grain shape has been changed from equiaxed to plate-like, with a random plate orientation. The average length of the plates is 75μm, with a width of about 29μm. Some laths and particles are observed in Fig. 7.16, which indicates the existence of a reinforcement phase.

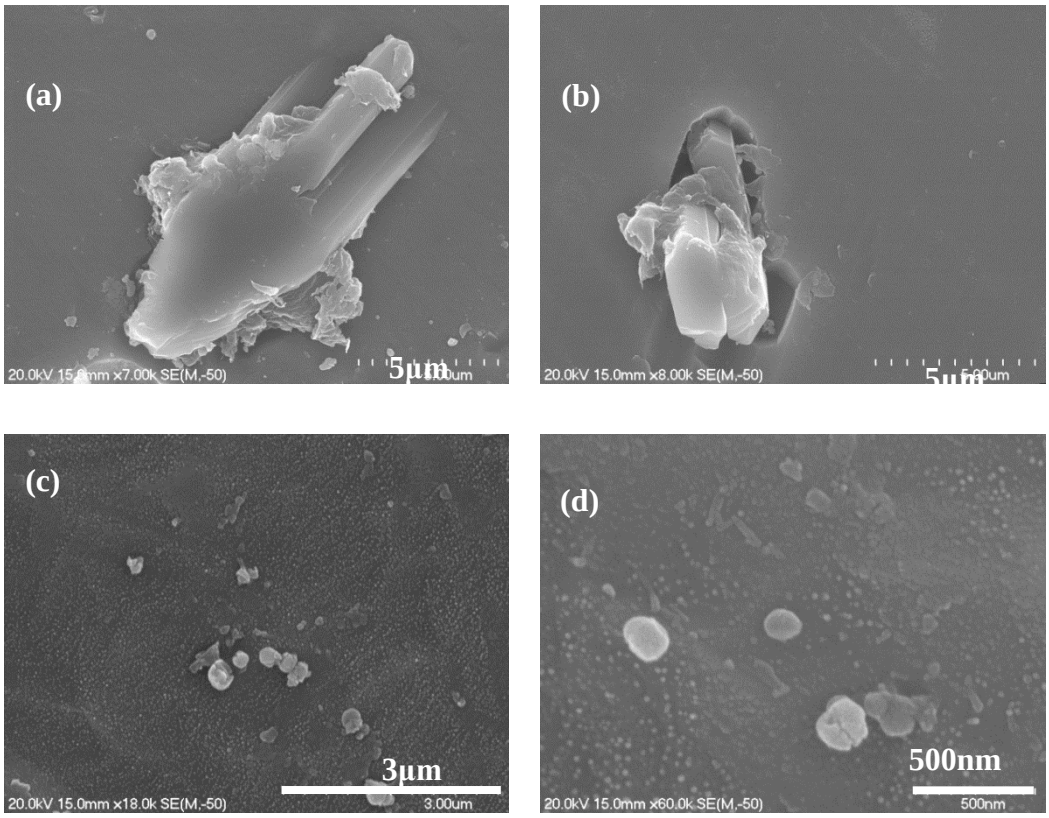

Fig. 7.17 SEM images of a sintered Ti-0.6LaB_6 sample

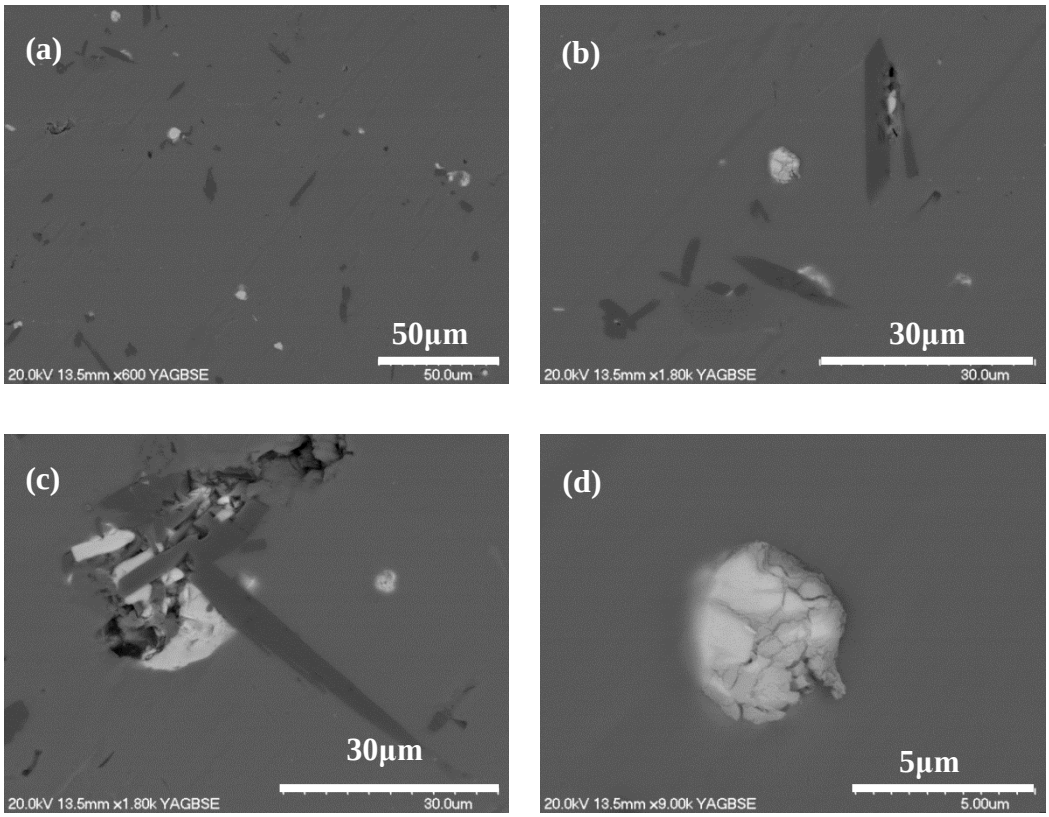

Fig. 7.18 BSE images of a sintered Ti-0.6LaB_6 sample

Observations of the reinforcement by SEM are shown in Fig. 7.17. There are two typical reinforcement textures: whiskers which are 15-20µm long and 2-3µm wide and small particles with <300nm diameter. BSE images, shown in Fig. 7.18, can help us to distinguish these two phases within the mixture. The dark whiskers are homogenously distributed in the matrix with a random orientation. The particles, with a white appearance, have a lower volume percentage compared with the whiskers and most of these particles are located near to the whiskers. The EDS results shown in Fig. 7.19 indicate that the particles with an acicular shape texture are TiB. The EDS results shown in Fig. 7.20 indicate the existence of La_2O_3. There was no evidence of any other phases. Thus it is likely that most of the LaB_6 has been transformed into TiB and La_2O_3.

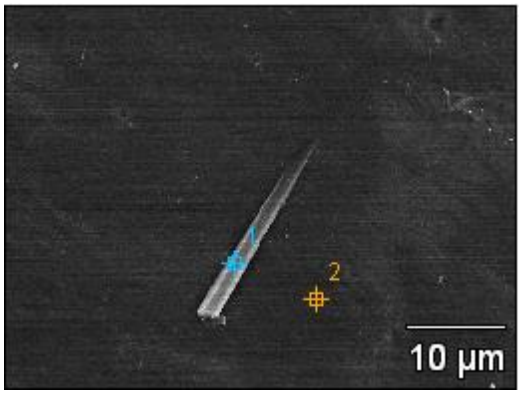

	B	Ti	V
1 wt%	29.04	70.75	0.21
2 wt%		99.48	0.52
1 at%	64.46	35.44	0.10
2 at%		99.51	0.49

Fig. 7.19 SEM image and EDS data showing the presence of TiB

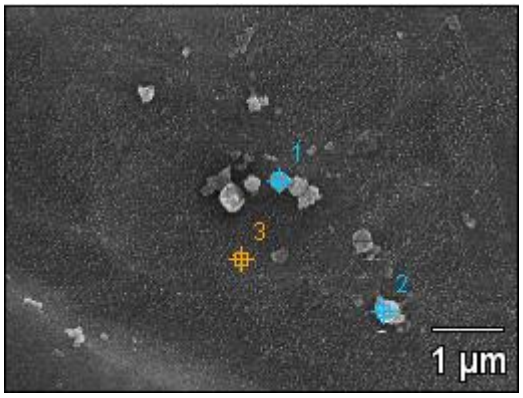

	C	Ti	V	La
1 wt%	2.40	93.48	0.03	4.09
2 wt%		99.48	0.18	0.34
3 wt%		99.45	0.55	0.00
1 at%	9.16	89.46	0.03	1.35
2 at%		99.72	0.17	0.12
3 at%		99.48	0.52	0.00

Fig. 7.20 SEM image and EDS data showing the presence of La_2O_3

7.5.3 Tensile properties

The average tensile strength of the sintered alloy is 731.1MPa (708.21-749.34) with a strain to fracture of 6.97% (3.38%-10.12%). The properties of pure Ti are 578MPa and 14% respectively. Thus the strength improves about 26.5% and the ductility decreases about 50%.

SEM images of the fracture surface are shown in Fig. 7.21. The fracture surface contains a large number of small cleavage planes. There are also some holes with a diameter of 2-5μm, indicating that those TiB whiskers which are inclined to the fracture surface have been pulled out from these holes. Some whiskers along a

transverse section are cracked. The effect of La_2O_3 on the tensile properties is not clear and its role in fracture behaviour cannot be identified by SEM. Thus the change in mechanical properties is primarily due to the TiB whiskers.

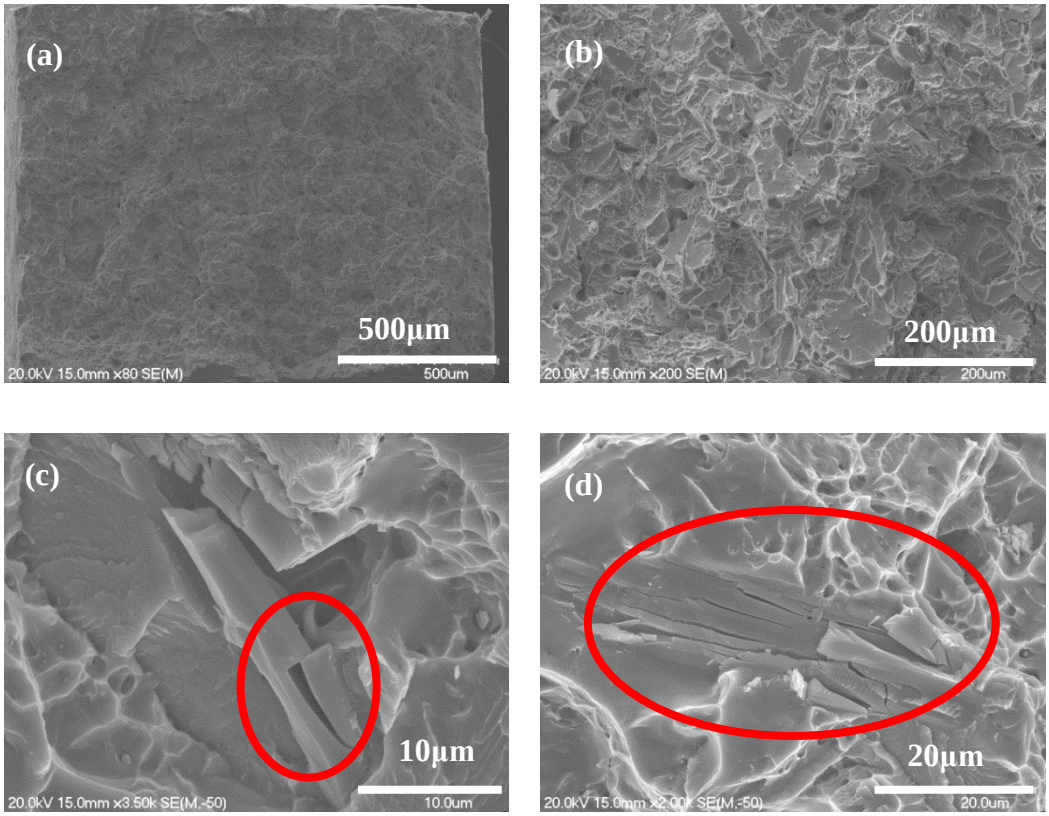

Fig. 7.21 Fracture surface of a sintered Ti-0.6LaB_6 sample

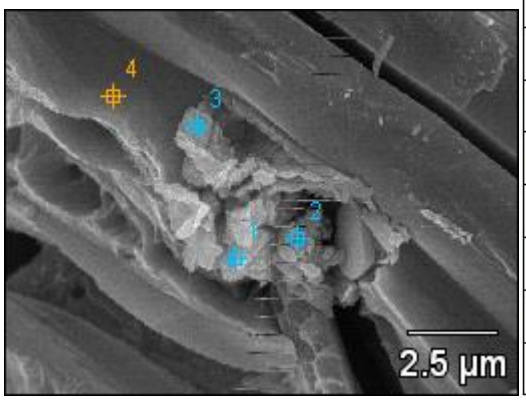

	B	C	O	Ti	La
1 wt%	5.56		11.75	44.78	37.90
2 wt%	1.33			31.95	66.72
3 wt%	7.70		20.06	61.16	10.55
4 wt%	6.97	2.58		89.78	0.00
1 at%	20.94		29.90	38.05	11.11
2 at%	9.68			52.51	37.81
3 at%	21.39		37.67	38.35	2.28
4 at%	23.46	7.83		68.24	0.00

Fig. 7.22 EDS data from La_2O_3 situated close to a TiB whisker

7.6 Discussion

From the experimental work, RE in Ti alloys exist in the form of RE metal and RE sesquioxide. In the case of LaB_6 additions, a TiB phase has been generated. This section analyses the characteristic shape of the RE containing phases and the synthesis mechanisms for them. Because there was no reaction between the blending or MM process for Ti (or Ti6Al4V) with Y, the microstructural observations begin with a sintered sample.

7.6.1 Sintered microstructure

A direct Er addition leads to large amounts of Er-segregation in the area where an Er particle was situated, and this creates worm-like voids. Segregation formation is due to a combination of liquid phase formation and the lower diffusivity of RE atoms in titanium metal and titanium alloys. The data in Table 7.3 lists the diffusion coefficient of oxygen in various phases and indicates that it is difficult for RE atoms to diffuse out of the oxide coating on their surface [139]. Furthermore, any free RE atoms are very easily trapped by the soluted O atoms in the matrix [16, 90].

Table 7.3 Diffusion coefficient of elements related to the scavenging process [139]

Diffusion event	Temperature (°C)	Diffusion coefficient ($m^2 s^{-1}$)
$[O]_{Ti}$ in α-Ti phase in CP-Ti	~882	$\sim 1 \times 10^{-13}$
$[O]_{Ti}$ in β-Ti phase in CP-Ti	~882	$\sim 1 \times 10^{-11}$
$[O]_{Ti}$ in β-Ti phase in CP-Ti	~1300	$\sim 1 \times 10^{-9}$
$[O]_{Ti}$ in β-Ti phase in Ti–6Al–4V	~1300	$\sim 1 \times 10^{-10}$
O in Y_2O_3	~1300	$\sim 1 \times 10^{-12}$
Y in Y_2O_3	~1300	$\sim 7 \times 10^{-15}$

From Fig. 7.4, The liquid phase exists from approximately Er-5Ti to Er-15Ti over the 1300-1400C temperature range. Hence Er particles will absorb Ti (or Al) atoms to form a liquid phase. As more and more Ti atoms diffuse to the liquid

phase, the liquid phase transforms to a solid phase again. Thus an Er-rich solid phase will be generated at the liquid-solid interface. A long time is required for RE atoms to diffuse into the matrix [2]. Thus Er diffusion in the solid phase is very slow. The liquid phase will diffuse along the surface of the Ti particles. The liquid phase in a Ti6Al4V alloy is able to penetrate over a longer distance, because the sintered density is lower than that of pure Ti. This motion creates more solid phase and reduces the volume of the liquid phase [144]. However, the amount of compensation from the solid phase to the liquid phase is limited. The particle rearrangement process of the surrounding particles cannot overcome the voids because the Er particle size is too big. As a result, direct additions of Er metal powder, even though the particles can join a liquid phase sintering process, fails to create a uniform distribution of Er atoms. This microstructure has a negligible effect in refining the microstructure and for oxygen pick-up. In fact, most of the RE atoms exist in the form of RE metal segregation, which is detrimental both to the strength and elongation.

An advantage of MM processing is that the larger sized Y metal powder is broken into small dispersoids, 1-5μm in diameter. The uniformly distributed Y atoms scavenge a lot of oxygen atoms in the matrix to form Y_2O_3. The dispersoids have an effect of controlling the prior β grain growth at high temperature and also control the growth of α laths. However, MM creates fresh surfaces in the Ti (Ti6Al4V) and Y particles, which inevitably absorb oxygen from the air. Moreover, the sintering ability of the powder decreases, so that a lower density and higher porosity are obtained.

The addition of LaB_6 seems to lead to a good sintered microstructure. Due to the fine particle size of the LaB_6 powder (10μm), very small La_2O_3 particles and TiB whiskers are formed. The chemical equation for this reaction is as follows:

$$12Ti + 2LaB_6 + 3[O] = 12TiB + La_2O_3 \quad (7.1)$$

Fig. 7.17 indicates the refining effect of LaB_6 on pure Ti. The only thing to be concerned about is the formation of TiB whiskers and their effect on mechanical properties.

7.6.2 ODFed microstructure

Processing using ODF is beneficial, since it helps to increase density and diminish the residual pores. For a Ti(Ti6Al4V)-0.4 Er alloy, the coarse Er segregation can be broken-up by severe hot working. But the ODF process used in this work failed to create an Er distribution in the matrix: Er segregation is inevitable and the existence of segregation wastes a large amount of expensive Er metal and creates a brittle phase. Therefore more work is required to further homogenise the microstructure.

For a MM Ti(Ti6Al4V)-0.5Y alloy, an ODF process reduces all the residual pores in a Ti6Al4V-0.5Y alloy. Thus it may be a good way for improving the sintered density of MM Ti-Re or Ti6Al4V-RE alloy.

7.6.3 Heat treated microstructure

Heat treatment is usually carried out on a Ti6Al4V alloy to optimise the microstructure and improve the mechanical properties. A solution treatment makes the α phase transform to the β phase. Water quenching produces martensite and subsequent aging leads to the re-precipitation of the β structure and an optimised α+β microstructure.

For a Ti6Al4V alloy with RE additions, pure RE metal dissolves in the β phase which has a higher RE solubility. The solid solubility of La in βphase is about 8wt.%, but it has a low solid solubility in α-Ti at room temperature [17]. Y and Er show similar behaviour in β-Ti and α-Ti phases. However, the dissolution of RE is limited by its diffusivity in Ti. We have observed that Er-segregation cannot be eliminated after heat treatment. Yet in Y containing alloys, a solution and re-precipitation process to form Y-rich dispersoids is observed. This process indicates that the remaining Y metal atoms in the dispersoids can diffuse out of the small dispersoids into the β-Ti phase. It seems as though the rapid cooling rate produced by water quenching creates a supersaturated solid solution of Y in a solution treated Ti matrix. Subsequent aging leads to the internal oxidation of Y metal, which causes the re-precipitation of yttria dispersoids.

When the RE forms a RE oxide, it is very stable during the heat treatments used in this work. S. Hotta showed that yttria dispersoids are able to control the amount of β grain growth up to 1200℃, which means that ~~about~~ the dispersoids are stable at this temperature [16]. V. Castro reported that for Ti-Y_2O_3 alloy, yttria dispersiods tend to become more spherical without significant coarsening, when recrystallised at 1100℃ after cold rolling [102].

The substantial microstructural refinement in terms of the prior-β grain size and the subsequent α-Ti lath size is attributed to the grain boundary pinning effect of the Re_2O_3 particles. The relationship between β grain size, yttria volume fraction and yttria particle size is expressed by the following equation [16]:

$$R = \beta\left(r / f_v^{\,m}\right) \tag{7.2}$$

Where R is the radius of the average β grain size, β and m are constant, f_v is the volume faction of yttria and r is the radius of the precipitates.

In a Ti6Al4V-0.4Er alloy, clear prior β grain boundaries are observed and very large α laths. But a Ti6Al4V-0.5Y alloy has a much refined microstructure. The results show that the refining effect of RE additions depends on the uniformity of their distribution.

7.6.4 Mechanical properties and oxygen pick-up effect

For a Ti alloy with RE additions, the mechanical properties primarily depend on the distribution of the RE form and the morphological features of precipitation. A pure RE metal is softer than Ti metal. It breaks easily during tensile loading and therefore large amounts of Er-segregation must be prevented.

The MM process creates a large number of yttria dispersoids, which is beneficial to the tensile strength of a Ti alloy. Some yttrium may be trapped inside the oxide layers, but a re-precipitation process caused by a solution treatment and aging process diminishes most of them. The uniformly distributed dispersoids enhance the strength but decrease the ductility[102]. However, the more pronounced influences are the lower sintered density and higher oxygen content. The former is the primary reason for the unstable strength and no ductility in a sintered sample. The latter accounts for the unstable ductility in an ODFed sample. As a result, the mechanical properties of samples produced by this approach are not satisfactory.

For LaB_6 addition, Y. Liu showed that a small amount of LaB_6 can improve the strength of a Ti-1.5Fe-2.25Mo alloy [17]. The improvement in strength is only about 10% and the ductility is stable at about 5%. He reported that it is only when the LaB_6 addition is 1.2% that an acicular boride is observed. The results of this

work disagree in part with Liu's findings. A large improvement has been achieved in strength. In fact, the strength of Ti-0.6LaB_6 is comparable with the best results achieved for Ti-1.5Fe-2.25Mo alloys with 0-1.2wt.% LaB_6, even the LaB_6-free alloy itself contains a great amount of reinforcement. Also, the ductility of the Ti-0.6LaB_6 is higher than reported in Liu's work. Such an improvement is due to the formation of an acicular TiB phase, which in addition, provides another strengthening mechanism for the Ti from the La_2O_3 particles. The only disadvantage of a LaB_6 addition is that the acicular shaped form of the TiB decreases the ductility too much.

The oxygen scavenging effect is very hard to quantify. The oxygen mass to be obtained and the oxide mass produced are calculated from the chemical equation, which is for ideal conditions. In fact, even in a MM process, the dispersoids with diameters smaller than 5μm will trap some Y metal, which is proved by the re-precipitation of Y_2O_3. Thus the influence of oxygen pick-up can only be indirectly reflected by the ductility improvement. However, the present work fails to observe a ductility improvement. The ductility of Ti metal decreases as a result of large amounts of Er segregation, oxygen pick-up from the MM process and the morphology of the TiB secondary phase for approaches using Er, Y and LaB_6 additions respectively.

7.6.5 Further consideration on RE additions

Direct Er additions, compaction, sintering, ODF & heat treatment seem to be an impractical approach. It wastes a large amount of expensive Er powder and creates Er segregation which is the main culprit of embrittlement. Smaller sized Er particles may bring some advantages for solving this problem. But such powder continues to increase the oxygen content. Using an extrusion process,

where there is a greater effect on the microstructure, may give better Er uniformity and better properties.

The MM, compaction, sintering, ODF & heat treatment process achieves interesting results resulting in uniformly distributed yttria with a small size and refined microstructure. However, its creates fresh Ti surfaces for oxygen pick-up. The exact amount of additional oxygen pick-up is variable, but never less than 0.2wt.%. This pick-up offsets the oxygen-scavenging effect of the Y. Hence only when a MM process is inevitable, is this processing addition recommended.

The direct mixing, compaction & sintering of Ti-0.6LaB_6 achieves excellent results in obtaining uniformly distributed reinforcements, a refined microstructure, and more importantly, excellent strength and good ductility. It seems to be the best way of making RE additions and calls for other RE composites to be made available. LaB_6 powder has a very fine particle size, it is inexpensive and not a problem when exposed to air. The only problem is that the acicular TiB morphology decreases the ductility.

7.7 Conclusion

(1) Direct Er additions lead to the formation of defects such as segregation and voids due to the low diffusion rate and large Er particle size. An ODF process closes the voids and partially eliminates the Er inhomogeneity. But the residual Er segregation embrittles the Ti alloy. Therefore direct RE additions are a great challenge.

(2) Mechanical milling creates many small Y dispersoids in the Ti matrix, ranging from 1-5μm. A precipitation-solutioning-re-precipitation process after a standard heat treatment process for Ti6Al4V was observed. The well distributed

dispersoids led to a refined Widmanstätten microstructure. However, the MM process itself introduces excess oxygen into the matrix and the milled powder has poor sinterability.

(3) Direct LaB_6 additions achieve excellent results. The reinforcement is uniformly distributed with various orientations and the microstructure is refined. The TiB reinforcement gives excellent strength and good ductility. The acicular TiB phase seems to be the only problem, because while it significantly improves the strength it decreases the ductility.

8. Chapter 8 Theoretical Analysis of Compaction Process and Discussion on Approaches for Modifying the Cold Compaction Behaviour of Ti Powder

8.1 Introduction

The application of an internal lubricant is able to significantly improve overall green density and green density homogeneity of a Ti alloy compact [1-3]. However, with the compaction of lubricated Ti alloy powder there are some disadvantages to be confronted, such as inferior compressibility under high pressures (only 70-80% green density), significant density variation (the green density varies from 70-88%) and a difficult lubricant removal process. Therefore a deeper understanding of the compaction mechanism of Ti alloy powder with/without a lubricant is required.

This work has investigated the cold compaction process of a lubricated Ti metal powder. The Cooper & Eaton formula, which separates the compaction behaviour into particle rearrangement (PR) and plastic deformation (PD) processes, has been applied to analyse the green density vs. pressure curves for Ti powder compaction [4]. A further discussion will be given with respect to the two mechanism types and this will help us to understand more clearly what happens to the powder body after adding an internal lubricant. On the basis of this discussion, the approaches for modifying the cold compaction behaviour of Ti powder are studied. Variations in compact thickness, the use of internal lubrication and additions of PREP powder were used and a comparison was made with the compaction behaviour of aluminium and iron powders. A discussion on these variables provides an explanation for Ti powder compaction behaviour.

8.2 Experimental details

Besides the HDH Ti powder, spherically shaped powder made by the plasma rotating electrode process (PREP) (0.09wt.% O content, -100-200mesh, supplied by Xi'an Baode Powder Metallurgy Co. Ltd., China)was employed, to blend with the HDH powder. HDH and PREP powders were blended with a mass ratio of 1:1 using a roller mixer.

For compaction experiment concerns with the height/diameter ratio, 1.8g, 2.5g, 3.2g or 4.6g powder (or powder/lubricant mixture) were weighed out and poured into the die. The mixing process has been described in Chapter 3 and 4. Such a weight insured that the height/diameter (H/D) ratio of compacts pressed at 400MPa was approximately 1:2, 1:1.5, 1:1 and 1.5:1 respectively, i.e. the thickness of the compacts was about 5.5, 8.25, 1.1 and 16.5mm respectively. A stearic acid-ethanol solvent was used as a die lubricant. Compacts were pressed under a pressure of approximately 20MPa prior to compaction experiments. Then the die was placed into the Instron Tensile Machine and compaction was carried out using a ram speed of 0.02 mm/s. The compaction process for every compact was automatically stopped when the highest pressure (~900MPa) was reached. Compacts were then ejected from the die and their density was calculated. The procedure is similar in principle to that described by in Gerdemann and Jablonski's work [124].

To produce compacts to be used for mechanical testing, the cold compaction process was done using a 100 tonne oil-press. A powder and lubricant mixture, weighing 160 grams, was compacted in a 40 mm cylindrical steel die under a uniaxial single acting pressure of 400MPa, with an H/D ratio of the green compact of approximately 1:1. Sintering was conducted at 1350℃ for 120 min in a vacuum furnace under a vacuum of 10^{-3} - 10^{-2} Pa and at a heating rate at 10K/min, followed by furnace cooling.

8.3 Theoretical analysis of compaction process

8.3.1 Theoretical basis

Several theoretical formulas have been developed and used to analyse the compaction behaviour of powder compacts. Among them, specific attention has been given to the Cooper & Eaton formula, which separates the compaction behaviour into a particle rearrangement process and a particle plastic deformation process [105]. Having considered the pore size in a powder compact, Cooper and Eaton separated the compaction process into two steps. The first step is the filling of voids of the same order of size as the original particles. This step occurs as particles slide by one another. The second is associated with the filling of voids smaller than the original particles. The same differential equations ($\mathrm{dV/dP} = \mathrm{kP^2 exp(-k/P)}$) were used to depict the densification behaviour of pores during these two steps. Ozaki assumed that the first step is due to a particle rearrangement process and the second is due to plastic deformation [145]. The detailed equation is as follows:

$$C_p = C_{1p} + C_{2p} = a \times \exp\left(-b/P\right) + A \times \exp\left(-B/P\right) \tag{8.1}$$

Where P is the compaction pressure, C_p is the ratio of powder porosity reduction under pressure P, $C_{1p}=a\times exp(-b/P)$ is the contribution of stage I to the whole compaction process, $C_{2p}=A\times exp(-B/P)$ is the contribution of stage II to the whole compaction process, a, b, A, B are constants, $B>b$

The relationship between compacting pressure and density can be established by this equation with respect to the physical properties and particle morphology of the powder. Thus it can be used to explain many phenomena in powder compaction. After a small modification to this equation, Gerdemann and Jablonski

[124] used it to analyse the compaction behaviour of Ti and Ti 6Al 4V alloy powder.

$$D_P = D_0 + A \times [1 - \exp(-a \times P)] + B \times [1 - \exp(-b \times P)] \quad (8.2)$$

Where D_p is the green density of the compact under pressure P, D_0 is the initial density. A and a are rearrangement components; B and b are work-hardening components. By separating the compaction behaviour of the Ti metal and alloy powder into two stages, he provided an interesting explanation for the influence of powder type and powder particle size. He reported that the particle rearrangement stage I ends at about 100MPa, and only makes a 14-32% contribution to the whole process, and after that the work-hardening mechanism accounts for almost all of the further densification. However, the meaning of the "work-hardening stage" is unclear and the contribution ratios of each of the stages does not agree with the results from aluminium and iron compaction [26, 146].

Ye [7] made a modification to the Cooper Eaton equation by introducing the Kawakita formula [8] to calculate the contribution of the PR mechanism. In Ye's work, the Kawakita formula replaced the C_{1p} component to avoid overlapping. The formula is as follows:

$$C_p = C_{1p} + C_{2p} = a \times P/(1 + B \times P) + c \times \exp(-d/P) \quad (8.3)$$

Where $C_{1p}=a \times P/(1+B \times P)$ is the contribution of the powder rearrangement mechanism to the whole compaction process; $C_{2p}= c \times exp(-d/P)$ is the contribution of the PD mechanism to the whole compaction process; a, b, c, and d are constants.

Fig. 8.1 shows an estimation of the results for the compaction behaviour of pure Ti powder. C_{1p} increases very fast before 100MPa and this increase almost stop at 200MPa. C_{2p} is negligible under 50MPa and increases rapidly after that. At higher

pressure, C_{2P} gives a bigger contribution than C_{1p}. The simulated curves fit the experimental result very well from 0-500MPa. After that, the experimental curve is higher than the simulated one, which indicates that the real contribution of stage II is about 2% higher than that for the simulated result. The R^2 value for all simulation work is around 0.999. Such comparisons from the lubricated compacts give similar results.

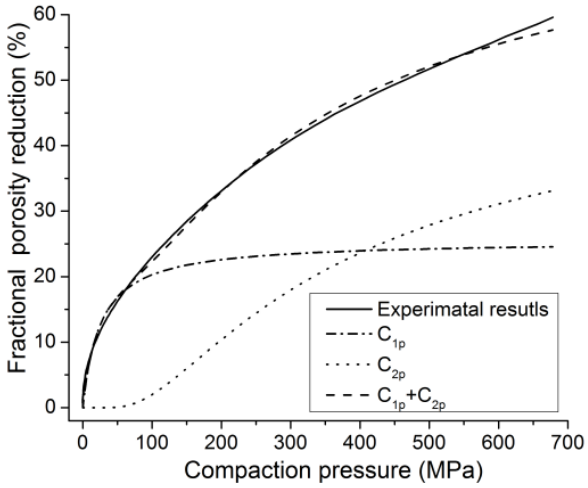

Fig. 8.1 Simulation results showing the contribution of the two stages and a comparison between experimental results and a simulated curve

There is a variation in the apparent densities of powders with different amounts of lubrication. Because a lubricant leads to closer powder particle packing, the contribution of the green density in the PR mechanism must be considered. The following modified equation is used in the present work:

$$d_p = d_0 + d_{1p} + d_{2p} = d_0 + C_{1p} \times (1 - d_0) + C_{2p} \times (1 - d_0) \qquad (8.4)$$

Where, d_p is the relative density under pressure P; d_0 is the relative packing density without pressure; $d_{1p}=C_{1p}\times(1-d_0)$ is the relative green density increase due to the PR mechanism under pressure P; thus the contribution of d_0+d_{1p} should be

considered in the powder rearrangement mechanism; $d_{2p}=C_{2p}\times(1-d_0)$ is the relative green density increase at stage II.

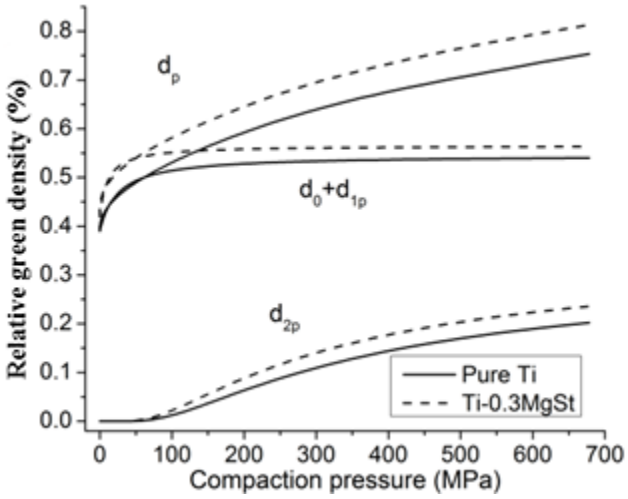

Fig. 8.2 Comparison between contributions of the two stages on the compaction behaviour of pure Ti and Ti-0.3MgSt

Fig. 8.2 shows a comparison of the simulation results for Ti and Ti-0.3MgSt compaction. A lubricant improves both the d_0+d_{1p} and d_{2p} components. For stage I, the improvement for compaction pressures under 50MPa is significant. For stage II, the improvement is notable for pressures under 300MPa and after that the rate of increase is almost equivalent to that of pure Ti.

8.3.2 Contribution of the two stages

Fig. 8.3 shows the influence of lubricant on the d_0+d_{1p} value for compaction pressures under 200MPa when the contribution from a pure PR mechanism is almost completed. A lubricant significantly improves the value. The best concentration is for additions of 0.3 and 0.6wt.% of SA and MgSt respectively. However, the highest value recorded for a compaction pressure of 200MPa is only about 58%, which is much less than values of more than 80% achievable for iron

or aluminium compaction [7, 9]. The low level of packing of Ti particles at this density indicates that particle motion still provides the biggest contribution to any further compaction.

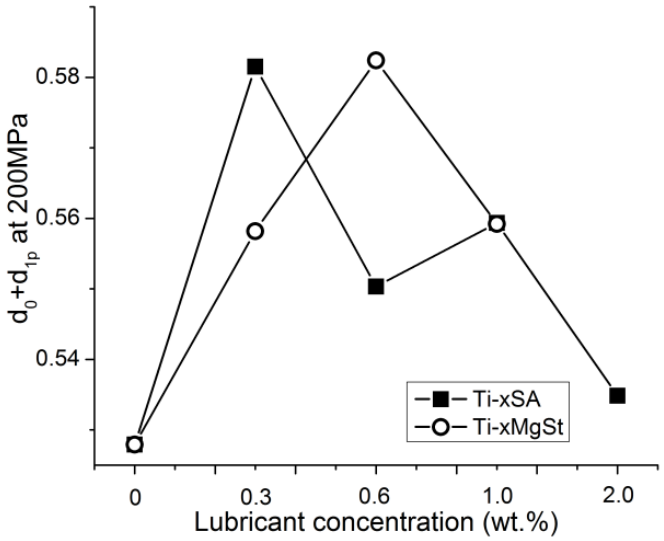

Fig. 8.3 Influence of SA and MgSt on the contribution of the PR mechanism in Ti powder

In chapter 4, Fig. 4.15 has shown the cross sectional images from powder compacts pressed under 400MPa. Among them, Fig. 4.15(d) shows the cross section from a Ti-1SA powder compact with a relative green density of 75%. The voids among the particles are still at the 10μm level and the gap between particles is very big. Particles on the right hand side show obvious characteristics of plastic deformation, whereas the ones on left hand side have un-plastic deformed features. Therefore the PR mechanism and PD are contributing at this stage.

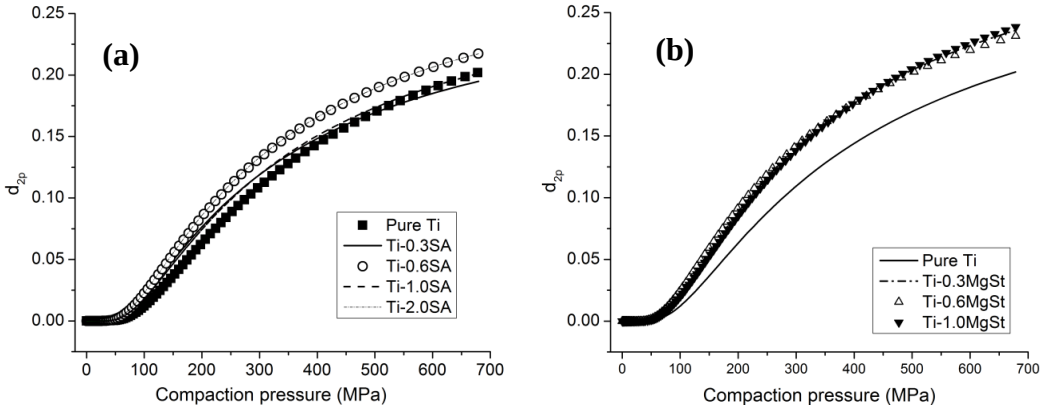

Fig. 8.4 d_{2p} vs. compaction pressure for different lubricants for Ti powder compaction: (a) SA and (b) MgSt

Fig. 8.4 shows d_{2p} vs. compaction pressures for different lubrication conditions. Compared with a pure Ti compact, when starting from a lower pressure, the compacts with lubricants show an improved increase in green density at stage II (d_{2p}) for pressures less than 200MPa. After 200MPa, SA and MgSt show different behaviour. For SA additions, as shown in Fig. 8.4(a), Ti-0.6SA and Ti-2SA have the highest d_{2p} and their curves are above that for pure Ti over the whole compaction pressure range. Whereas Ti-0.3SA and Ti-1SA have a lower d_{2p} and this is surpassed by pure Ti when the pressure is above 500MPa. It is important to notice that the d_0+d_{1p} values for Ti-0.3SA and Ti-1SA are higher than those for Ti-0.6SA and Ti-2SA. Thus the lower d_{2p} value seems to be compensating for the higher d_0+d_{1p} value. For MgSt additions, as shown in Fig. 8.4(b), the densification rates for all lubricated compacts overlap. All of them are above the Ti-xSA and pure Ti curves, indicating that the improvement at this compaction stage is more significant and stable.

8.4 Approaches for modifying the cold compaction behaviour of Ti powder

8.4.1 The effect of H/D ratio

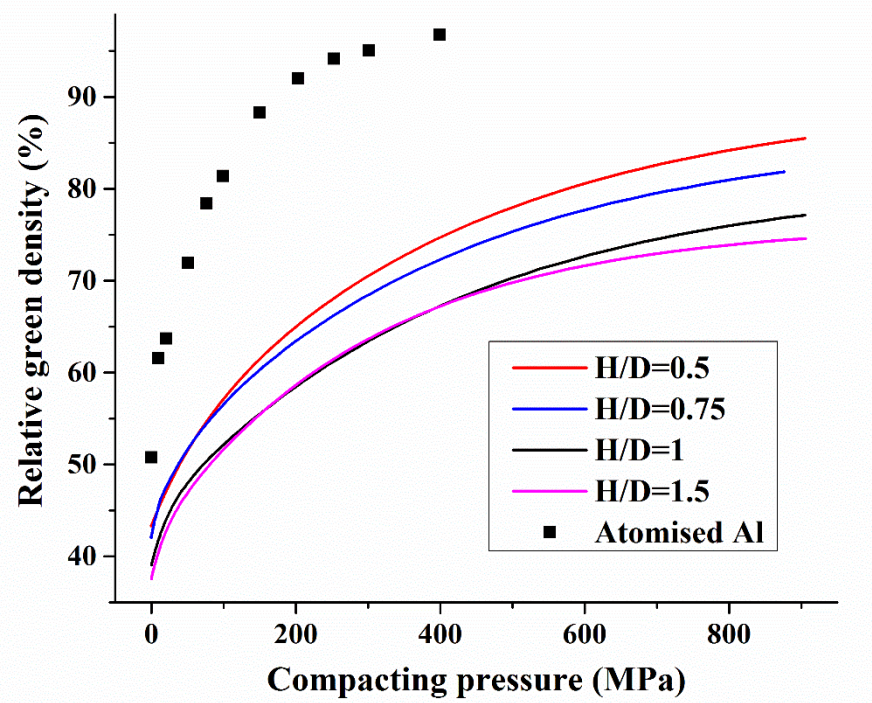

Fig. 8.5 Effect of H/D ratio on density/pressure curves for Ti powder compaction. A density/pressure curve for aluminium powder compaction is also shown for comparison [146]

Fig. 8.5 shows the influence of H/D ratio on the relative green density/compaction pressure curves f Ti powder. The packing density, D_0, decreases slightly with increasing H/D ratio and then the densification rate dramatically reduces when the thickness of a compact increases. For compacts with H/D ≧ 1, the densification rate is very slow when the pressure goes above 700MPa and the green density remained constant at a relative low density of 75% and 72% for compacts with H/D=1 and 1.5 respectively. The green density given by all the curves for Ti powder compaction is far below that for aluminium powder [146]. Aluminium compaction gives a higher packing density (D_0>0.5) and a more rapid

densification rate until 200MPa. More than 90% density can be achieved at 200MPa for aluminium powder compaction, whereas 800MPa is required for Ti powder compaction with H/D=0.5. For aluminium, the green density reached 92-95% for pressures above 300MPa. For iron powder compaction, more than 85% or even 90% green density is easy to achieve, even though the compact thickness is more than 10mm [26].

8.4.2 Combined effects of lubrication and H/D ratio

Fig. 8.6 shows the influence of lubrication on a compact with H/D=0.5 and 1. The use of internal lubrication slightly increased d_0 and more noticeably provided a higher slope in the compaction curves at low pressures. The largest increment for change in slope occurred at about 350MPa, with values increased by 8.6 and 4.0 % for compacts with H/D =0.5 and 1 respectively. It is noticeable that although the compact with H/D=1 shows that more pore volume has been filled, the improvement in degree of compaction from the internal lubrication is not as good as that in a compact with H/D = 0.5. Above 350MPa, the incremental change in compaction decreased, but for all the ranges investigated, the lubricated compact showed superior density compared with that for a lubricant free compact. The results are also quite different from those found in an investigation on iron compaction [8]. Simchi reported that the ethylene bisstearoylamide improves the green density of iron powder at very low pressures but the incremental change in green density decreases rapidly from 150MPa. A die wall lubricated compact achieved the same level of compaction as an internally lubricated compact at 400MPa and then exceeded it at higher pressures. The curve for a lubricated compact with H/D=0.5 is quite similar to that for iron.

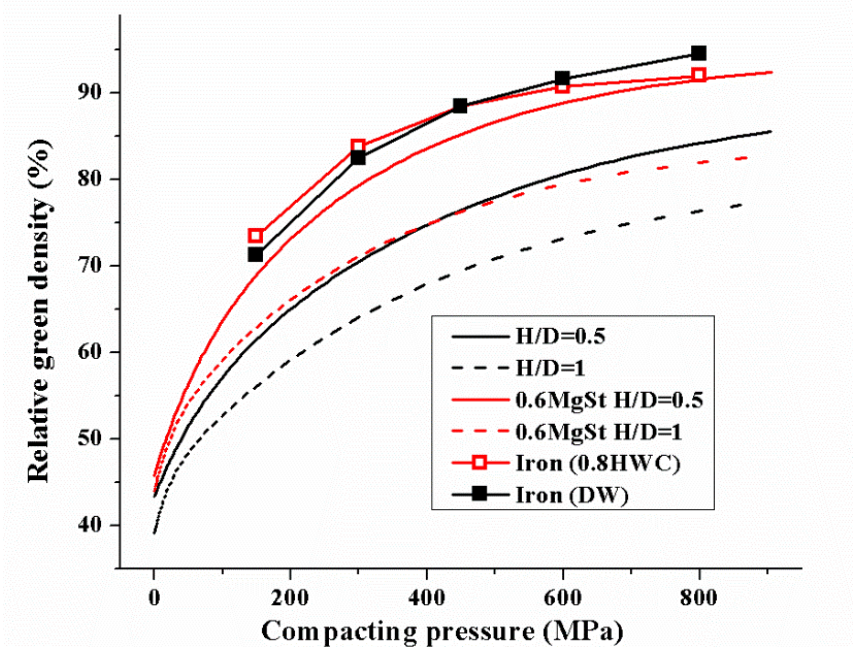

Fig. 8.6 Effect of lubrication on the density/pressure curves for Ti powder compaction with H/D ratios =0.5 and 1. The data for iron powder compaction with lubrication are also shown for comparison [8]

8.4.3 The effect of different powders

Fig. 8.7 shows the influence of powder type. The replacement of HDH powder by 50wt.% of PREP powder (H+P) leads to a much higher D_0 (56% compared with <44%) and a faster densification rate from 0-50MPa. The green density of a compact with H/D=0.5 and 1 is almost identical from 0-50MPa. After 200 MPa, the compacts fabricated from the different kinds of powder with the same H/D powder ratio show a very similar densification rate. If the curvature is ignored, the curves seem to be parallel. More than 90% density is achieved at 1000MPa for a H+P Ti powder compact with a H/D ratio=0.5. This is almost 6% higher than for pure HDH powder. For a sample with H/D ratio =1, the increment from PREP powder additions is more than 10%.

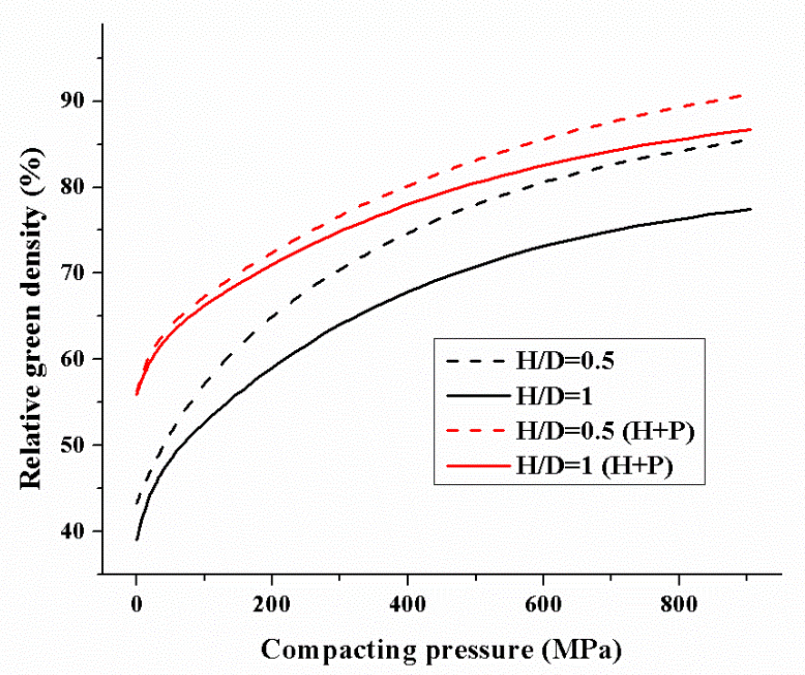

Fig. 8.7 Effect of powder type on the density/pressure curves for Ti powder compaction. The curve for a compact fabricated from HDH CP Ti powder with equivalent H/D ratio was also listed for comparison

The mid-cross-section of a H+P Ti powder compact pressed at 650MPa with H/D=1. The green density of this compact is 85.5%. Two different types of powder particles can be clearly distinguished. The existence of almost spherical particles indicates that the PREP particles hardly joined the plastic deformation process. The HDH particles, with irregular shape, filled the gaps between the PREP particles. Distortion, cracks and even many small fragments are observed. Thus it can be concluded that the PREP powder was the main reason for the higher packing density and that the HDH powder contributed more plastic deformation. A considerable volume is still occupied by the pores and the size of many pores is just a bit smaller than the HDH particles, indicating that a particle rearrangement mechanism makes a further contribution to the densification of a powder compact.

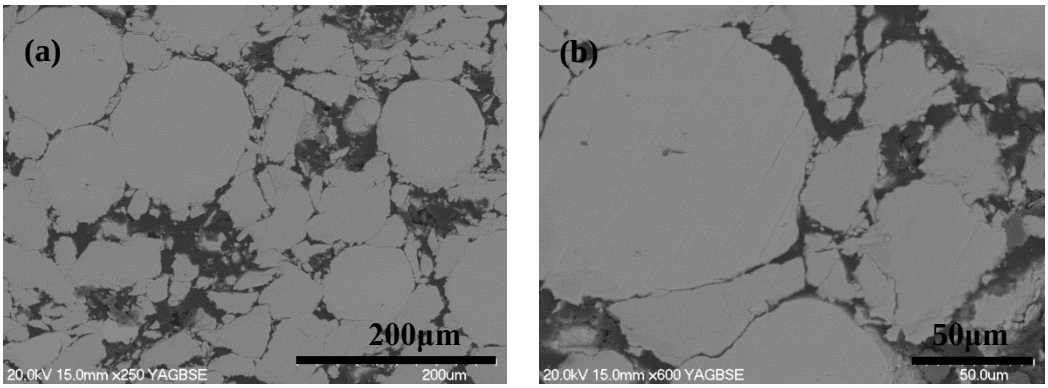

Fig. 8.8 BSE images of the mid-cross-sections of a H+P Ti powder compact pressed at 650MPa with H/D=1

8.4.4 A comparison of the mechanical properties of sintered HDH and H+P Ti powder compacts

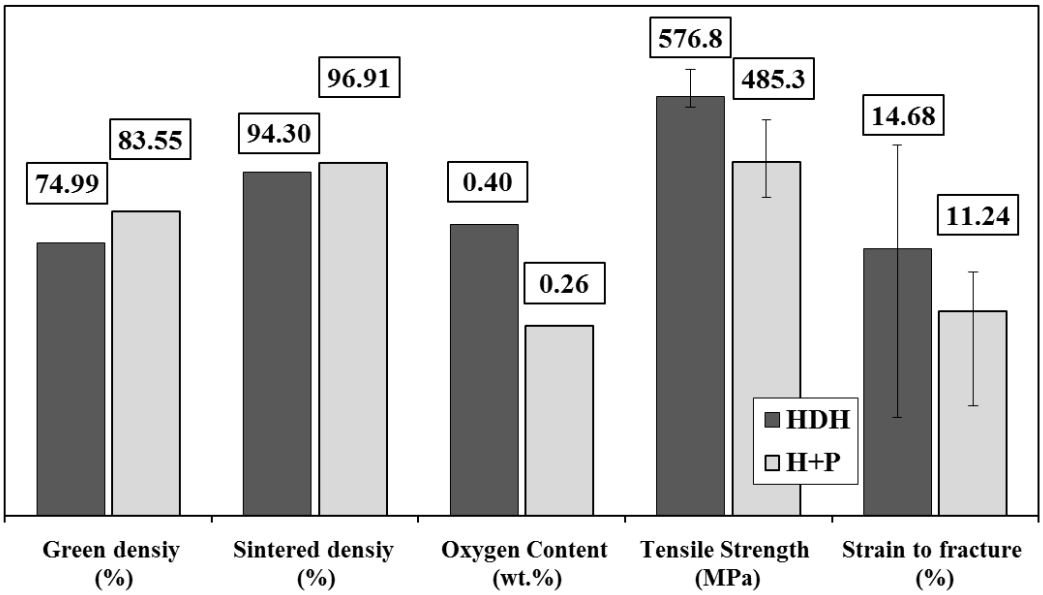

Fig. 8.9 Properties of sintered HDH and H+P Ti powder compacts (the shown data are the average value)

Fig. 8.9 gives the density, mechanical properties and oxygen content of sintered HDH Ti and H+P Ti powder compacts. The addition of PREP powder leads to a much higher green density and in turn a higher sintered density. A lower oxygen

content is also as expected. Due to the lower level of oxygen in the H+P powder, a lower tensile strength in a compact made from H+P powder is not unexpected. However, this compact has a lower ductility. An analysis of the porosity in the microstructures of the two samples is shown in Fig. 8.10. An H+P sample shows a lower porosity compared with an HDH sample, but some of the pores have irregularly shaped pores, as shown in Fig. 8.10(c). Such pores seem to be located around the spherical surface of PREP particles.

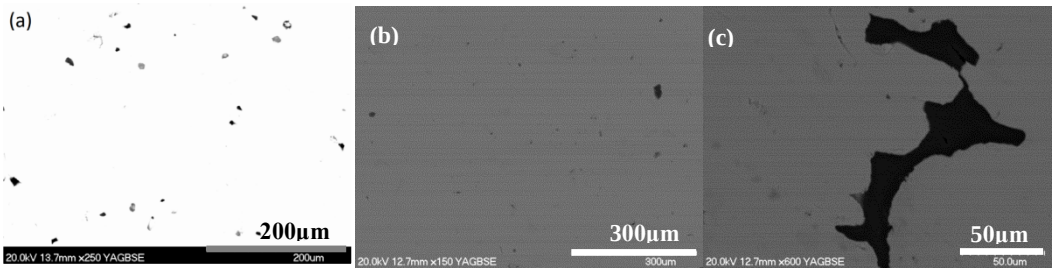

Fig. 8.10 Porosity in the sintered Ti powder compacts. (a) HDH Ti; (b) HDH+PREP Ti; (c) Detail of a large pore in H+P Ti.

Fig. 8.11 shows SEM micrographs of the fracture surfaces of test-pieces from sintered Ti powder compacts. An HDH sample shows that the failure takes place in the interparticle region rather than at the particle boundaries, as shown in Fig. 8.11(a). Yet in an H+P sample, besides the shear characteristics, there is evidence of some stepwise cracking at the surface of spherical powder particles, as shown in Fig. 8.11(d). The diameter of these particles is about 100-200um, indicating that the boundary of an original PREP particle is potentially an origin for failure.

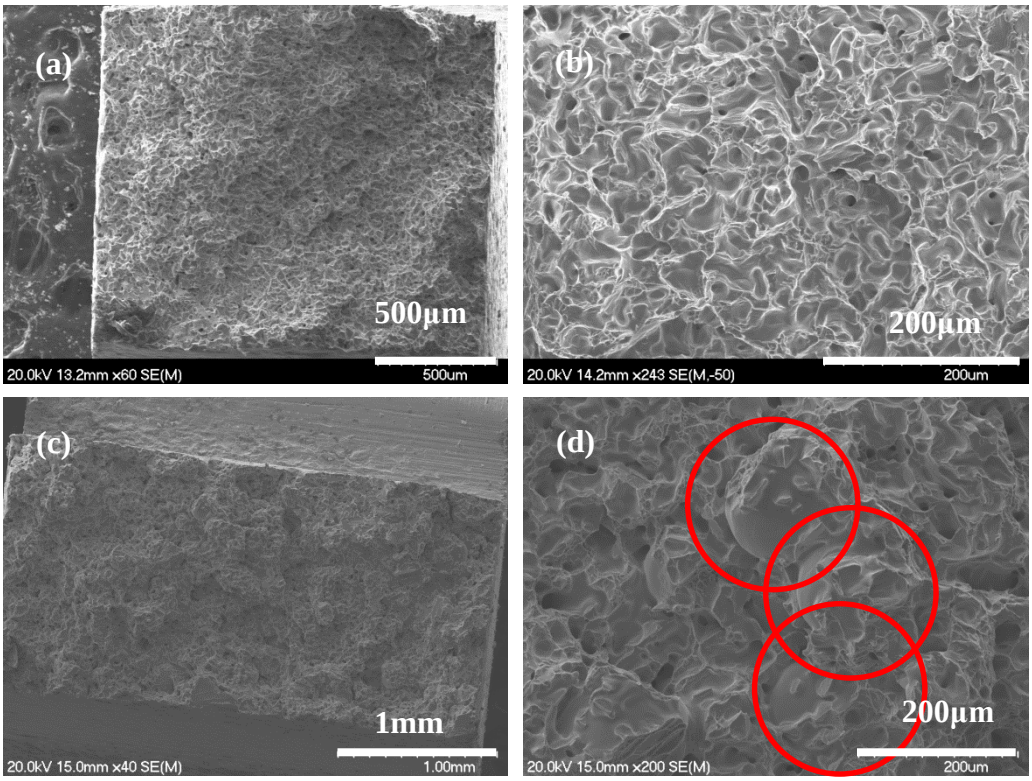

Fig. 8.11 SEM fractographs of Ti test-pieces cut from Ti compacts: (a) and (b) HDH; (c) and (d) HDH+PREP.

8.5 Discussion

If we consider the compaction of metal powder to be a combination of particle rearrangement and plastic deformation mechanisms, the ideal compaction curve should have a first stage characterised by the most rapid densification rate to almost 90%, and then a final stage with a slower densification rate to almost full density, as shown in Fig. 8.12 [7]. The condition for this assumes that all particles are monosized and spherical. In this situation, a high d_0>0.6 can be achieved (0.64 for random packing) and repacking occurs due to the shear stress between particles in stage I. The friction between particles and mechanical inter-locking at contact points resists a tendency for particle sliding and rearrangement because of the surface texture and the roughness of the particles. A shear stress is needed to

flatten a powder particle surface and release the inter-particle locking. During this stage some local plastic deformation occurs [147]. As a result, the end of stage I is a combination of particle rearrangement and plastic deformation mechanisms, but the latter mechanism only offers assistance for the former. Then stage II follows. The particle packing is almost fixed and increasing pressure only results in a hydrostatic pressure on the particles. New contact points between powder particles will not be created but the area of each contact point increases. At this stage the contribution from a particle rearrangement mechanism is negligible at all pressures.

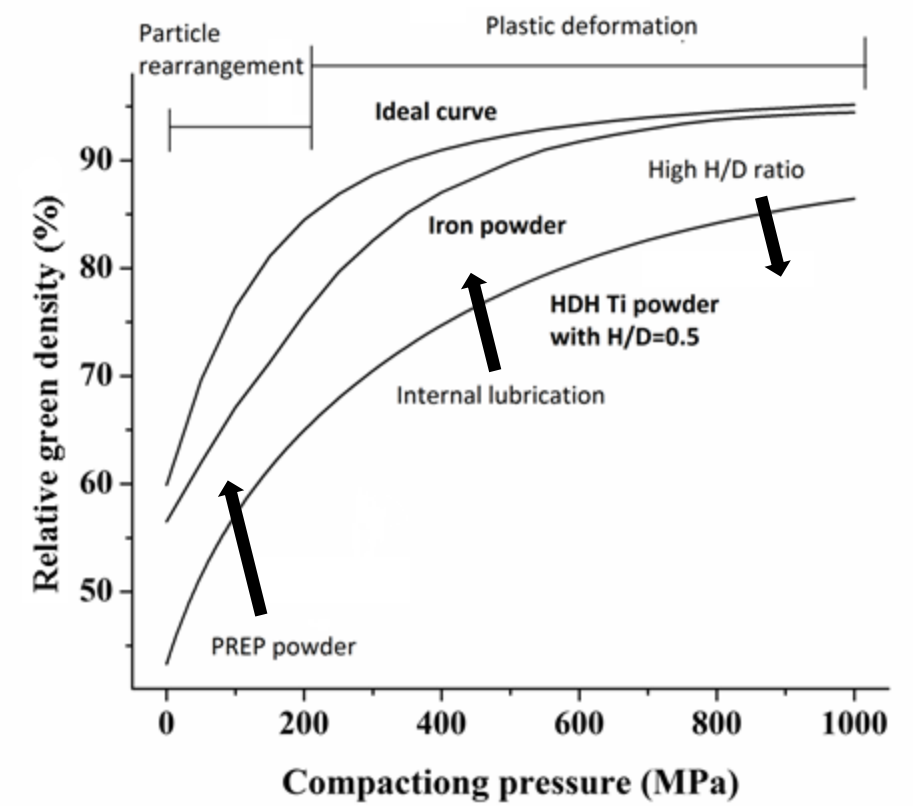

Fig. 8.12 A comparison of compaction curves for ideal compaction, iron powder [26] and HDH Ti powder with H/D ratio=0.5. The influence of an addition of PREP powder, internal lubrication and the application of a high H/D ratio are also shown

The conventional compaction process for aluminium and iron powder, with a high packing density and better ductility gives a curve with almost equivalent data to the ideal curve [26, 146]. The only difference is that the transition from stage I to stage II occupies a larger pressure range of 100-400MPa. This difference is attributed to the features of the real powder particles. These features include the ductility of the bulk metal, particle shapes, particle size distribution, particle tapping level and the thickness of a powder compact and so on. For stage I, the particle morphology is a critical factor. Particles should undergo considerable plastic deformation to flatten the surface and then enable them to repack at a higher density. This process is almost complete at a pressure of 400MPa for aluminium and iron powder particles, when a final density of more than 90% can be achieved.

The curvature of the density/pressure curves for Ti powder under different conditions is quite similar to the two stage curves: one stage with a rapid densification rate from 40 to 70 % (under a pressure range from 0 to 200MPa) and then another stage with a slower densification rate (under 200MPa). Hence some researchers have used the two stage formula to calculate the contribution of the two mechanisms [124]. However, an important point is that the final density for stage I is no more than 60 % for most compaction conditions, which is much lower than that for aluminium and iron. Furthermore, the final density for stage II ranged from 72-90% using different H/D ratios, which is also lower than for other powders. Therefore more attention should be paid to the real mechanism for stage II in titanium compaction. Rather than a plastic deformation mechanism, it is more likely that there is a longer transition between stages I and II during aluminium and iron compaction. This phenomenon is proved by a modification to the compaction behaviour. So many gaps are found between particles in the microstructures of compacts whose density ranges from 70-80%. The size of these gaps is of the same order of magnitude as the titanium powder. To overcome these

gaps, nearby Ti particles must undergo severe plastic deformation to decrease their size so that they are able to fill these pores. As the pore size decreases, the starting size of the gaps is smaller. Due to the work hardening effect, more significant plastic deformation or even internal fracture of the particles is required for further densification.

For higher powder masses of pure HDH powder, giving in turn a higher compact starting thickness, leads to higher friction between the die wall and the powder particles. Therefore pressure transmission will be more difficult and a lower density in the bottom layer is expected. Chapter 5 has indicated that a minimum density of 65% and a maximum density of almost 90% [69, 125] is obtained for a powder compact with H/D=1, when using a pressure between 400-500MPa . This "lower" density level must be considered to be just a lower level of plastic deformation or a change in the compaction mechanism. The microstructure of the compact, shown in Fig. 4.15, indicates that the particles are mainly bonded by inter-particle locking rather than by metal-to-metal contact (cold welding). In a powder lubricated compact, the bonding is not as strong as in a lubricant free compact. But because particles can be ground off using an abrasive paper, this means that the degree of cold welding is limited. Chapter 4 has indicated that the green strength of a Ti powder compact drops by 60% when 0.6% MgSt is added [69]. For a sample with H/D=1 with a lubricant, the two layer structure shown in Fig. 4.14(a) and 4.15(b) indicates that the bonding level of the top 5mm is much higher than that for the bottom 5mm. Thus in the top area, more cold welding can be seen, showing that more energy is absorbed by particles at the top and more plastic deformation has taken place here. A compacting pressure of 400MPa only leads to a higher relative density to about 5mm. For further improvement in the overall density, a higher pressure is needed. For a sample with H/D≥1, pressure transmission is very difficult, so that particles in the bottom layers undergo a

smaller amount of plastic deformation making it harder to achieve a high repacking level. The overall density increase is therefore smaller.

If stage II is considered to be a particle repacking process initiated by plastic deformation, an internal lubricant will inevitably improve the compressibility during this stage. This work indicates the existence of this type of behaviour. Improvements in compaction density can be sustained to very high pressures (>1000MPa) to achieve densities above 90%. In research on iron compaction, the improvement shown from lubricant additions, compared with titanium compaction, works until the particle rearrangement mechanism is almost completed. After that the volume of the lubricant hinders further densification [8]. An addition of 0.6wt.% MgSt only occupies 2.9vol.% of pore volume, so it is impossible to block compact densification when a compact has under 10% porosity. A smaller incremental improvement in densification in compacts where H/D=1 is likely to be due to difficulties in pressure transmission. The curve for compaction pressure versus green density, for Ti-0.6MgSt with H/D=0.5, is very similar to that for iron. Thus there is a stage III, which is a real plastic deformation stage and correlates to stage II in iron or aluminium compaction, when the compaction pressure varies from 400-1000MPa. This stage is achieved by a particle rearrangement mechanism, which is completed early on in thinner compacts.

An internal lubricant helps with particle motion. It helps the PR mechanism, either in stage I or II, which is proved by the effect of MgSt. On the other hand, the improvement to stage II from SA additions is inferior and unstable. Ti-0.3SA and Ti-1SA have higher d_0+d_{1p} values, but lower d_{2p} than Ti-0.6SA and Ti-2SA. The difference is accounted for by the influence of particle size. The size of the SA particles is similar to the HDH powder but is much bigger than MgSt. Homogenous mixing for SA and Ti powder is impossible and SA agglomerates

are easily trapped in the hollow space between Ti particles. The blocking effect of big SA agglomerates on the compaction of Ti powder has been investigated in Chapter 4 and 5. The randomly distributed SA agglomerates leads to unstable compaction behaviour for stage II.

An addition of PREP powder leads to a significant improvement in packing density and promotes more rapid densification at the very early stages of compaction. The bigger size and spherical shape of PREP powder substitutes for the pores between HDH powder particles with irregular shape. Close packing is more easily obtained [148]. A higher overall density is achieved because less repacking is required. However, the change in particle shape does not lead to better plastic deformability of the whole mixture. In fact, the ease of deformation of PREP powder particles is debatable. Fig. 8.8(d) shows that PREP powder almost keeps its spherical shape after compaction under a pressure of 650MPa. The degree of deformation in PREP powder is limited whereas it is relatively high in HDH powder. The sintered mechanical properties also provide evidence for this behaviour. Sintered H+P Ti compacts have a higher density and lower oxygen content than sintered HDH Ti compacts, thus the former compacts should have slightly lower strengths and at least 5% higher ductility than latter compacts from considerations of oxygen content [149]. However, the strength is lower but the ductility is also 3% lower. The inferior bonding between the HDH and PREP powder is most likely the reason. The inter-particle pores are easier to eliminate by the self-diffusion of Ti atoms in HDH Ti powder, which has undergone a larger degree of plastic deformation, than in the PREP powder. As a result, the bonding between the HDH Ti particles is stronger than those between HDH Ti and PREP Ti particles.

This work has focused on modifications in compaction behaviour of Ti powder as a result of changes in three variables: H/D ratio, the use and amount of internal

lubrication and a substitution of HDH irregularly shaped particles by spherically shaped powder particles. The application of these methods changed the compaction behaviour with respect to the packing density, die wall friction characteristics and inter particle friction characteristics. The inferior compressibility of HDH Ti (low green density, inferior pressure transmission and significant density variation) is mainly attributed to its large particle size, coarse grain size and lower ductility. These limitations can be overcome until the physical or even chemical properties of Ti powder have been changed (PREP powder particles hardly participate in the plastic deformation of Ti powder if a large amounts of HDH powder particles exist).

8.6 Conclusion

(1) A modified Cooper-Eaton formula was employed to analyse the compaction behaviour of Ti powder. There is a good fit between the simulation results and the experimental data.

(2) The theoretical research indicated that cold compaction of titanium powder can be separated into two stages: a PR stage which occurs in the compacting pressure range of 0-200MPa followed by a PD initiated PR stage from 200-1000MPa. The existence of stage II is due to the low plastic deformability of titanium and the low density achieved at the end of stage I. Ti particles need to be plastically deformed or even cracked into fragments to fill into the gaps between Ti particles.

(3) The use of an internal lubricant improves density at compacting pressures of 200-600MPa due to its improvement on the particle rearrangement mechanism. The compaction curve of Ti-0.6MgSt under H/D=0.5 is very similar to that for

iron powder. Because of its larger particle size, SA gives an inferior and unstable improvement compared with MgSt during stage II.

(4) A higher H/D ratio leads to lower pressure in the lower zones of a Ti compact. The bottom layer shows low density because the repacking is retarded by less plastic deformation. A high compact thickness significantly decreases the density of a Ti powder compact. When the H/D ratio is $\geqq 1$, the densification rate is almost zero when the pressure reaches 600MPa.

(5) The addition of PREP powder improves the packing density of the Ti particles, but the PREP particles do not take part in the plastic deformation during stage II. Moreover, the inferior plastic deformability of PREP particles creates weak bonding between the PREP particles and HDH particles in a sintered part.

9. Chapter 9 Conclusions and Recommendations

9.1 Conclusions

- A small amount of internal lubricant (SA or MgSt) improves the compressibility of Ti powder compacts, especially at lower pressures (<400MPa). Yet at higher pressures, lubricants hinder any further improvement. An addition of up to 0.3wt.% SA improves the green density. MgSt shows a better lubrication effect and an addition of up to 0.6wt.% improves the density. The difference in the lubrication effect between SA and MgSt is due to their mixing or blending characteristics. A homogenous mixing of lubricant and powder leads to an increased lubricated area and overall effectiveness of lubrication. Lubricants have a strong influence on shape retention, green strength and ejection behaviour of Ti powder compacts.

- A coloured layer method is a very useful technique for measuring the density distribution in a powder compact. The density distribution in HDH Ti powder compacts can be improved by adding a small amount of lubricant. SA gives better results than MgSt, with 0.6wt.% of SA considered to be the optimum addition. The mixing or blending characteristics account for the better improvement from SA additions. SA agglomerates tend to fill the hollow spaces between powder particles in a compact and prevent the in-situ densification in highly compacted regions. Density and hardness profiles obtained from parts cut from a larger compact are in general agreement with the results obtained from a coloured layer method, but they are not quite suitable for assessing the density distribution in compacts with lubricant additions.

- Additions of 0.3-0.6wt.% SA and 0.3-1wt.% MgSt improve the sintered density distribution in Ti compacts by controlling the pore morphology with respect to their size, aspect ratio and orientation. But 1wt.% SA creates many

pores ranging in size from 50-100μm, both in the top and bottom regions, and this leads to very bad ductility. The consistency in mechanical properties of a sintered Ti Φ40 mm compact with a H/D ratio =1 is significantly improved by adding 0.6wt.% SA. An improvement in the uniformity of mechanical properties, as a result of adding an internal lubricant, is because of a more uniform green density distribution both in the horizontal and transverse directions. Any sintering mismatch is therefore minimised. Additions of SA lead to additional oxygen pick-up of about 0.06wt.% and this is acceptable. By comparison, MgSt leads to an additional three fold oxygen pick up compared with SA, and therefore MgSt is not recommended as an internal lubricant for use in P/M Ti alloy processing.

- Direct Er additions lead to the formation of defects such as segregation and voids. The segregation cannot be eliminated by an ODF process. Therefore direct RE additions are a great challenge.MM of Ti(Ti6Al4V)-Y powder mixtures creates many small Y dispersoids in the sintered microstructure, ranging from 1-5μm. A precipitation-solutioning-re-precipitation process after a standard heat treatment process for Ti6Al4V was observed. The well distributed dispersoids led to a refined Widmanstätten microstructure. However, the MM process itself introduces excess oxygen into the matrix and the milled powder has poor sinterability. Direct LaB_6 additions achieve excellent results. The reinforcement is uniformly distributed with various orientations and the microstructure is refined. The TiB reinforcement gives excellent strength and good ductility. The acicular TiB phase seems to be the only problem, because while it significantly improves the strength it decreases the ductility.
- A modified Cooper-Eaton formula was employed to analyse the compaction behaviour of Ti powder. There is a good fit between the simulation results and the experimental data. The theoretical research indicated that cold compaction of titanium powder can be separated into two stages: a PR stage, which occurs in the compacting pressure range of 0-200MPa, followed by a PD initiated PR stage from

200-1000MPa. The existence of stage II is due to the low plastic deformability of titanium and the low density achieved at the end of stage I. Ti particles need to be plastically deformed, or even cracked into fragments, to fill the gaps between Ti particles. The use of internal lubrication improves density at compacting pressures from 200-600MPa due to its improvement on particle motion. On the basis of this discussion, the approaches for modifying the cold compaction behaviour of Ti powder were studied.

9.2 Recommendations

- An internal lubricant, with a new composition or a mixed lubricant with various components should be studied. SA and MgSt are very common lubricants for iron compaction, but may not be very good for titanium because they introduce carbon and oxygen. While the contamination is not harmful to ferrous parts it is a significant problem for titanium. Thus any lubricant component which is easy to remove should be applied. Camphor may be a good choice to replace a large percentage of SA, because it retains some of the lubrication effect of SA when added as a mixture and is easier to remove than SA.
- A friction measurement testing facility should be designed and set-up. The facility needs two load cells to be set up on the top and bottom plunger to record the pressure on each plunger. A die set with many holes on the die wall is also required. Strain gauges are inserted into holes to record the force on the die wall. As a result, the friction coefficient is determined. This work has already started by the design of a die set for making such measurements. However, it was cancelled because of a failure of some critical equipment. Further work should aim to investigate the influence of a lubricant on the friction coefficient between a powder compact and the die wall. Such experimental work will provide more data for a

more robust theoretical analysis.

- For RE metal addition, extrusion may be a good way to eliminate Er segregation, since this process completely changes the sintered microstructure. Extrusion deformation may allow the Er addition to be internally oxidised properly, so that it has the potential to absorb more interstial oxygen in a Ti matrix. A master alloy powder of RE (with Al or Cu) may be another choice.
- For RE composites, the influence of more components should be studied. Such components of potential interest contain YH_2, $CeSi_2$ and so on. YH_2 will not generate other secondary phases only Y_2O_3. $CeSi_2$ will act as strengthening reinforcement but without an acicular texture, which in the case of TiB_2 reduces ductility.

Appendix

The colour layers pictures of Ti compact with different lubricant conditions and their density profiles

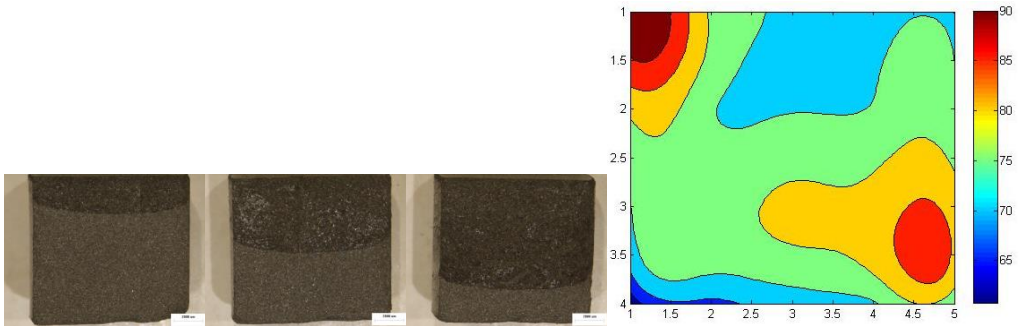

Pure Ti

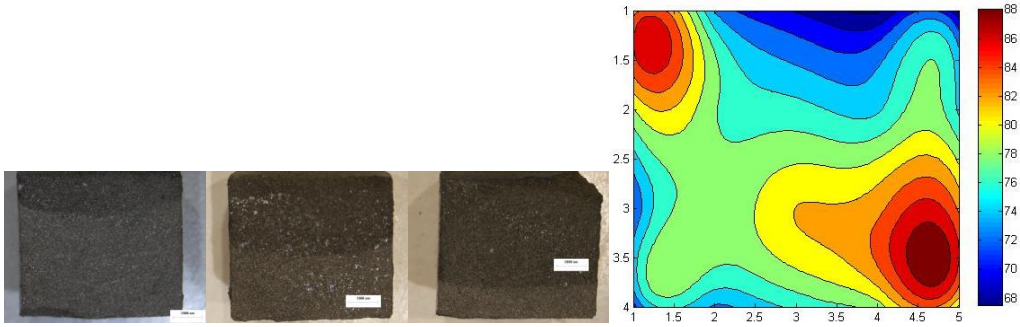

Ti-0.3SA

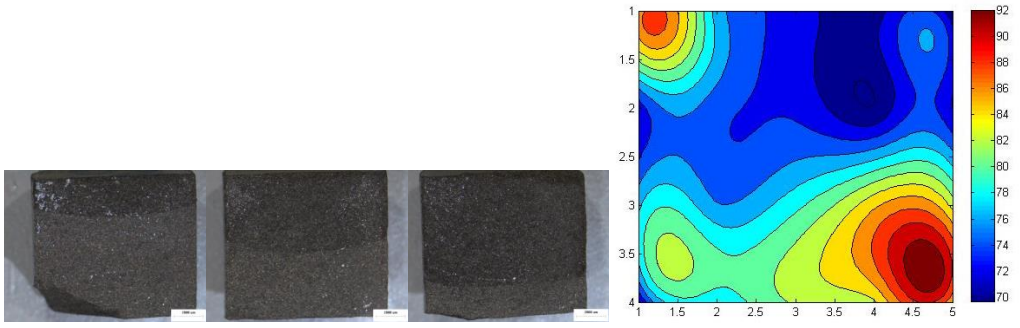

Ti-0.6SA

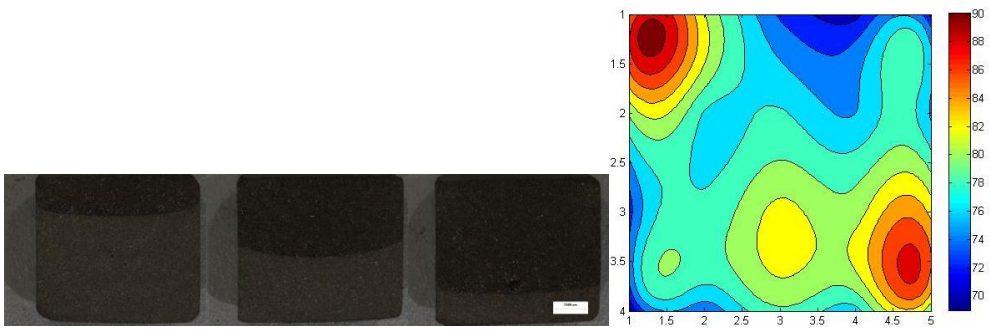

Ti-1SA

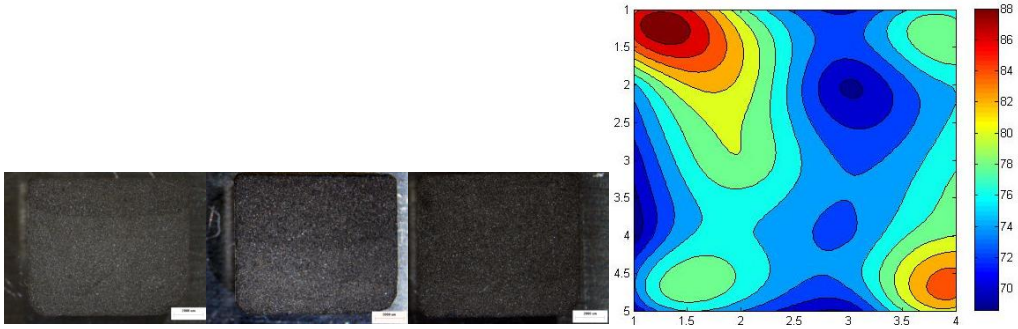

Ti-0.6SA (wet blended)

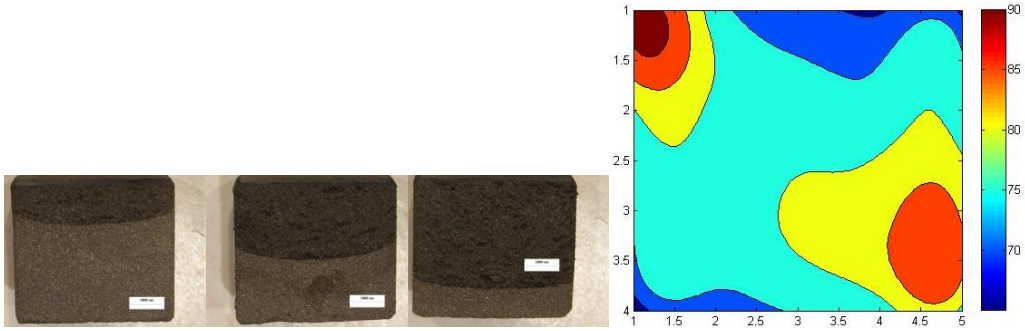

Ti-0.3MgSt

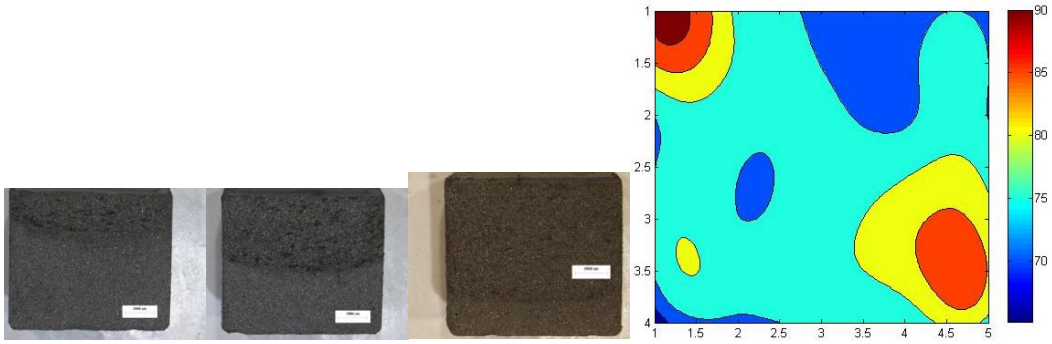

Ti-0.6MgSt

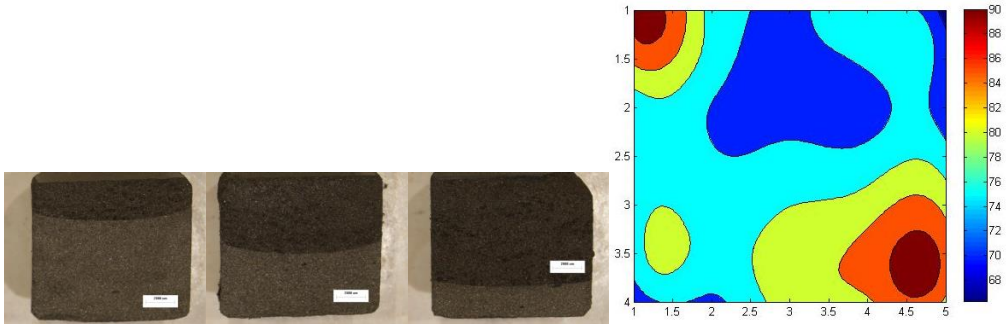

Ti-1MgSt

Reference

[1] D. R. Askeland, *Essentials of materials science and engineering*: Cengage Learning, 2012.

[2] C. Leyens and M. Peters, *Titanium and titanium alloys*: Wiley Online Library, 2003.

[3] M. Niinomi, "Recent Trends of Titanium Research and Development in Japan," presented at the The 12th World Conference on Titanium, Beijing, China, 2011.

[4] M. Qian, "Cold compaction and sintering of titanium and its alloys for near-net-shape or preform fabrication," *International journal of powder metallurgy,* vol. 46, pp. 29-44, 2010.

[5] GTBcomponents. *P/M process*. Available: http://www.gtbcomponents.co.uk/process.html

[6] G. Upadhyaya, *Powder metallurgy technology*: Cambridge Int Science Publ, 1997.

[7] P. Y. Huang, *FENMO YEJIN YUANLI, Second Edition,*. Beijing: Metallurgical Industry Press, 2008.

[8] A. Simchi, "Effects of lubrication procedure on the consolidation, sintering and microstructural features of powder compacts," *Materials & design,* vol. 24, pp. 585-594, 2003.

[9] U. Klemm, D. Sobek, and E. Forster, "Evaluation of New Types of Lubricants by an Instrumented Compacting Tool," *Advances in Powder Metallurgy & Particulate Materials--1993.*, vol. 2, pp. 51-61, 1993.

[10] K.-S. HWANG and K.-H. LIN, "Lubricant removal in metal powder compacts," *International journal of powder metallurgy,* vol. 28, pp. 353-360, 1992.

[11] Y. LIU, J.-h. FANG, Y.-r. WEN, N.-y. ZHANG, D.-h. LIU, and F. LIU, "Influences of die wall lubrication on mechanical properties of iron-based superalloy powder compacts," *Journal of Central South University (Science and Technology),* vol. 6, p. 003, 2007.

[12] ASTM-F2885-11, "Standard Specification for Metal Injection Molded Titanium-6Aluminum-4Vanadium Components for Surgical Implant Applications," ed, 2011.

[13] ASTM-WK35394, "Standard Specification for Metal Injection Molded Titanium-6Aluminum-4Vanadium Components for Surgical Implant Applications," ed, 2012.

[14] M. J. Donachie, *Titanium: a technical guide*: ASM international, 2000.

[15] P. Pérez, G. Salmi, A. Muñoz, and M. Monge, "Influence of yttria additions on the oxidation behaviour of titanium prepared by powder metallurgy," *Scripta Materialia,* vol. 60, pp. 1008-1011, 2009.

[16] S. Hotta, K. Yamada, T. Murakami, T. Narushima, Y. Iguchi, and C. Ouchi, ". BETA. Grain Refinement due to Small Amounts of Yttrium Addition in. ALPHA.+. BETA. Type Titanium Alloy, SP-700," *ISIJ international,* vol. 46, pp. 129-137, 2006.

[17] Y. Liu, Y. B. Liu, B. Wang, and H. P. Tang, "Rare Earth Element: Is it a Necessity for PM Ti Alloys?," *Key Engineering Materials,* vol. 520, pp. 41-48, 2012.

[18] A. Akisanya, A. Cocks, and N. Fleck, "The role of contact-contact interaction in the densification of powders," in *Powder Metallurgy World Congress(PM'94).* 1994, pp. 757-760.

[19] D. Gethin, A. Ariffin, D. Tran, and R. Lewis, "Compaction and ejection of green powder compacts," *Powder metallurgy,* vol. 37, pp. 42-52, 1994.

[20] P. Heyliger and R. McMeeking, "Cold plastic compaction of powders by a network model," *Journal of the Mechanics and Physics of Solids,* vol. 49, pp. 2031-2054, 2001.

[21] A. C. Cocks, "Constitutive modelling of powder compaction and sintering," *Progress in materials science,* vol. 46, pp. 201-229, 2001.

[22] A. Simchi and G. Veltl, "Behaviour of metal powders during cold and warm compaction," *Powder metallurgy,* vol. 49, pp. 281-287, 2006.

[23] D. Gethin, V. D. Tran, R. W. Lewis, and A. Ariffin, "An investigation of powder compaction processes," *International journal of powder metallurgy,* vol. 30, pp. 385-398, 1994.

[24] D. Poquillon, V. Baco-Carles, P. Tailhades, and E. Andrieu, "Cold compaction of iron powders—relations between powder morphology and mechanical properties: Part II. Bending tests: results and analysis," *Powder technology,* vol. 126, pp. 75-84, 2002.

[25] N. Solimanjad and R. Larsson, "Die wall friction and influence of some process parameters on friction in iron powder compaction," *Materials science and technology,* vol. 19, pp. 1777-1782, 2003.

[26] T. Ye, "Research in warm compaction behaviour of Power metallurgy materials and its densification mechanism," PhD Thesis, Central South University, Changsha, 2007.

[27] J. Oliver, S. Oller, and J. Cante, "A plasticity model for simulation of industrial powder compaction processes," *International Journal of Solids and Structures,* vol. 33, pp. 3161-3178, 1996.

[28] N. Özkan and B. J. Briscoe, "Characterization of die-pressed green compacts," *Journal of the European Ceramic Society,* vol. 17, pp. 697-711, 1997.

[29] S.-T. Hong, Y. Hovanski, C. A. Lavender, and K. S. Weil, "Investigation of die stress profiles during powder compaction using instrumented die," *Journal of Materials Engineering and Performance,* vol. 17, pp. 382-386, 2008.

[30] S. Nor, M. Rahman, F. Tarlochan, B. Shahida, and A. Ariffin, "The effect of lubrication in reducing net friction in warm powder compaction process," *Journal of Materials Processing Technology,* vol. 207, pp. 118-124, 2008.

[31] N. Solimanjad, "New method for measuring and characterisation of friction coefficient at wide range of densities in metal powder compaction," *Powder metallurgy,* vol. 46, pp. 49-54, 2003.

[32] K. E. Amin, "FRICTION IN METAL POWDERS," *International Journal of Powder Metallurgy (Princeton, New Jersey),* vol. 23, pp. 83-93, 1987.

[33] W. Li, J. Nam, and J. J. Lannutti, "Density gradients formed during compaction of bronze powders: the origins of part-to-part variation," *Metallurgical and Materials Transactions A,* vol. 33, pp. 165-170, 2002.

[34] R. Rossi, M. Alves, and H. Al-Qureshi, "A model for the simulation of powder compaction processes," *Journal of Materials Processing Technology,* vol. 182, pp. 286-296, 2007.

[35] M. Brochu and S. Turenne, "Experimental method for determining densification function of metal powder and its validity," *Powder metallurgy,* vol. 47, pp. 55-59, 2004.

[36] F. Han, F.K. Ma and Y.J. Cao, *China Engineering Materials Canon, Part 14: Engineering of Powder Metallurgy Materials*. Beijing: Chemical Industry Press, 2006.

[37] G. Jiang, G. Daehn, J. Lannutti, Y. Fu, and R. Wagoner, "Effects of lubrication and aspect ratio on the consolidation of metal matrix composites under cyclic pressure," *Acta materialia,* vol. 49, pp. 1471-1477, 2001.

[38] M. Ward and J. Billington, "Effect of zinc stearate on apparent density, mixing, and compaction/ejection of iron powder compacts," *Powder metallurgy,* vol. 22, pp. 201-208, 1979.

[39] A. Zhornyak and V. Oliker, "Pressing behavior of atomized iron powders," *Powder Metallurgy and Metal Ceramics,* vol. 20, pp. 323-328, 1981.

[40] L. Twiggs, E. Hartenbach, A. Saltzman, L. King, and J. Capus, "Die wall lubrication aids higher density," *Metal Powder Report,* vol. 53, pp. 28-28, 1998.

[41] X. Yang, S. Guo, B. Chen, F. Meng, and Y. Lian, "Electrostatic performance of various lubricant powders in P/M electrostatic die wall lubrication," *Powder technology,* vol. 164, pp. 75-81, 2006.

[42] B. Wikman, N. Solimannezhad, R. Larsson, M. Oldenburg, and H.-A. Häggblad, "Wall friction coefficient estimation through modelling of powder die pressing experiment," *Powder metallurgy,* vol. 43, pp. 132-138, 2000.

[43] M. Yang, "Research on Warm compaction of ferrous powders with new binders," MSE MSE, HeFei University of Technology, 2009.

[44] D. Guyoncourt, J. Tweed, A. Gough, J. Dawson, and L. Pater, "Constitutive data and friction measurements of powders using instrumented die," *Powder metallurgy,* vol. 44, pp. 25-33, 2001.

[45] M. Gagne, Y. Thomas, and L. Lefebvre, "Effect of Compaction Temperature on the Lubricant Distribution in Powder Metal Parts," *ADVANCES IN POWDER METALLURGY AND PARTICULATE MATERIALS,* vol. 3, pp. 11-39, 1998.

[46] Y. Li, T. L. Ngai, D. Zhang, Y. Long, and W. Xia, "Effect of die wall lubrication on warm compaction powder metallurgy," *Journal of Materials Processing Technology,* vol. 129, pp. 354-358, 2002.

[47] B. James, "Die wall lubrication for powder compaction: a feasible solution?," *Powder metallurgy,* vol. 30, pp. 273-280, 1987.

[48] W. G. Ball, P. Hibner, F. Hinger, J. Peterson, and R. Phillips, "New die wall lubrication system," *International journal of powder metallurgy,* vol. 33, pp. 23-30, 1997.

[49] J. Capus, "Die wall lubrication system launched," *Powder Metall,* vol. 39, p. 236, 1996.

[50] S. Turenne, C. Godère, Y. Thomas, and P.-É. Mongeon, "Evaluation of friction conditions in powder compaction for admixed and die wall lubrication," *Powder metallurgy,* vol. 42, pp. 263-268, 1999.

[51] S. Turenne, C. Godere, and Y. Thomas, "Effect of temperature on the behaviour of lubricants during powder compaction," *Powder metallurgy,* vol. 43, pp. 139-142, 2000.

[52] M. Siddiqui, "Effect of Lubricants and Compaction Pressure on Green Properties of Iron Powder Premixed," *Powder Metallurgy International(Germany),* vol. 24, pp. 79-83, 1992.

[53] T. Canta and D. Frunza, "Friction-assisted pressing of PM components," *Journal of Materials Processing Technology,* vol. 143, pp. 645-650, 2003.

[54] Y. Taniguchi, K. Dohda, and Z. Wang, "Effect of Lubrication on the Improvement of Uniformity in Uniaxial Powder Compaction," *JSME International Journal Series A,* vol. 48, pp. 393-398, 2005.

[55] E. Robert-Perron, C. Blais, Y. Thomas, S. Pelletier, and M. Dionne, "An integrated approach to the characterization of powder metallurgy components performance during green machining," *Materials Science and Engineering: A,* vol. 402, pp. 325-334, 2005.

[56] M. P. Wang, D. R. Faron, and B. J. Vaughan, "An X-Ray Computed Tomography(CT) Approach for Density Gradient Characterization of Powder Compacts," *Advances in Powder Metallurgy & Particulate Materials--1993.,* vol. 1, pp. 263-271, 1993.

[57] A. I. Lawrence, S. H. Luk, and J. A. Hamill, "A performance comparison of current P/M lubricants and routes to improvement," *Advances in Powder Metallurgy and Particulate Materials--1997.,* vol. 1, p. 4, 1997.

[58] Y. C. Lin, Y.Q. Lin and K.X. Huang, "Effect of Lubricant on Powder Properties and Compacting Performance of Iron and Stainless Steel Powders. Ⅱ, Compacting Performance," *Journal of materials science and engineering,* vol. 33, pp. 223-232, 2001.

[59] H. Takamiya, M. Kondoh, and T. Saito, "Ultra-high pressure warm compaction for P/M titanium components," *Cost-Affordable Titanium,* pp. 185-192, 2004.

[60] Y. Hovanski, K. S. Weil, and C. A. Lavender, "Developments in Die Pressing Strategies for Low-Cost Titanium Powders," Pacific Northwest National Laboratory (PNNL), Richland, WA (US)2009.

[61] Z. Hongqiang and C. Zhiqiang, "Warm Pressing with Admixed Powder Lubrication for Titanium Alloy Powder," *Rare Metal Materials and Engineering,* vol. 11, p. 031, 2008.

[62] W. Chen, Y. Yamamoto, W. H. Peter, S. B. Gorti, A. S. Sabau, M. B. Clark, *et al.*, "Cold compaction study of Armstrong Process® Ti–6Al–4V powders," *Powder technology,* vol. 214, pp. 194-199, 2011.

[63] C. Haase, R. Lapovok, H. P. Ng, and Y. Estrin, "Production of Ti-6Al-4V billet through compaction of blended elemental powders by equal-channel angular pressing," *Materials Science And Engineering a-Structural Materials Properties Microstructure And Processing,* vol. 550, pp. 263-272, Jul 30 2012.

[64] Z. Yan, F. Chen, and Y. Cai, "High-velocity compaction of titanium powder and process characterization," *Powder technology,* vol. 208, pp. 596-599, 2011.

[65] Y. Xia, S. Luo, X. Wu, G. Schaffer, and M. Qian, "The sintering densification, microstructure and mechanical properties of gamma Ti-48Al-2Cr-2Nb alloy with a small addition of copper," *Materials Science and Engineering: A,* 2012.

[66] R. Lapovok, D. Tomus, V. Skripnyuk, M. Barnett, and M. Gibson, "The effect of hydrogenation on the ECAP compaction of Ti–6Al–4V powder and the mechanical properties of compacts," *Materials Science and Engineering: A,* vol. 513, pp. 97-108, 2009.

[67] H. P. Ng, C. Haase, R. Lapovok, and Y. Estrin, "Improving sinterability of Ti-6Al-4V from blended elemental powders through equal channel angular pressing," *Materials Science and Engineering: A,* vol. 565, pp. 396-404, Mar 10 2013.

[68] T. Threrujirapapong, K. Kondoh, H. Imai, J. Umeda, and B. Fugetsu, "Mechanical Properties of a Titanium Matrix Composite Reinforced with Low Cost Carbon Black via Powder Metallurgy Processing," *Materials transactions,* vol. 50, p. 2757, 2009.

[69] J. Lou, B. Gabbitas, and D. L. Zhang, "Effects of Lubrication on the Powder Metallurgy Processing of Titanium," *Key Engineering Materials,* vol. 520, pp. 133-138, 2012.

[70] Y. Li and Y. Li, *Theory and application of metal injection molding*. Changsha: Press of Central South University, 2004.
[71] J. McGraw, M. Koczak, and A. Kao, "Investigation in the delubrication of P/M compacts," *International Journal of Powder Metallurgy and Powder Technology,* vol. 14, pp. 277-80, 1978.
[72] M. Renowden and P. Pourtalet, "Experimental studies on lubricant removal," *Metal Powder Report,* vol. 45, pp. 625-628, 1990.
[73] M. S. Nowotarski, "Atmosphere control in continuous furnaces," *Industrial Heating,* vol. 54, pp. 34-6, 1987.
[74] Y. Wu, R. German, D. Blaine, B. Marx, and C. Schlaefer, "Effects of residual carbon content on sintering shrinkage, microstructure and mechanical properties of injection molded 17-4 PH stainless steel," *Journal of materials science,* vol. 37, pp. 3573-3583, 2002.
[75] G. I. Friedman, "TITANIUM POWDER METALLURGY," Whittaker Corp., West Concord, Mass.1970.
[76] A. Heidloff, J. Rieken, I. Anderson, D. Byrd, J. Sears, M. Glynn, *et al.*, "Advanced gas atomization processing for Ti and Ti alloy powder manufacturing," *JOM Journal of the Minerals, Metals and Materials Society,* vol. 62, pp. 35-41, 2010.
[77] M. Peters, J. Kumpfert, C. H. Ward, and C. Leyens, "Titanium alloys for aerospace applications," *Advanced Engineering Materials,* vol. 5, pp. 419-427, 2003.
[78] V. N. Moiseyev, *Titanium alloys: Russian aircraft and aerospace applications* vol. 5: CRC, 2005.
[79] ASTM, "Specification for Metal Injection Molded Commercially Pure Titanium Components for Surgical Implant Applications," vol. WK35394, ed. West Conshohocken, PA: ASTM International, 2012.
[80] H. L. He, Y; Xiong, L; Zeng, J, "Effect of Neodymium Addition on Microstructure and Mechanical Properties of MIM Titanium " in *Proceedings of the PM2010 Powder Metallurgy World Congress*, Florence, Italy, 2010.
[81] B. B. Panigrahi and M. M. Godkhindi, "Sintering of titanium: Effect of particle size," *International journal of powder metallurgy,* vol. 42, pp. 35-42, 2006.
[82] B. Panigrahi, M. Godkhindi, K. Das, P. Mukunda, and P. Ramakrishnan, "Sintering kinetics of micrometric titanium powder," *Materials Science and Engineering: A,* vol. 396, pp. 255-262, 2005.
[83] B. B. Panigrahi, "Sintering behaviour of Ti–2Ni and Ti–5Ni elemental powders," *Materials Letters,* vol. 61, pp. 152-155, 2007.
[84] O. M. Ivasishin, D. Eylon, V. Bondarchuk, and D. G. Savvakin, "Diffusion during powder metallurgy synthesis of titanium alloys," in *Defect and Diffusion Forum*, 2008, pp. 177-185.

[85] Y. Mahajan, D. Eylon, R. Bacon, and F. Froes, "Microstructure Property Correlation in Cold Pressed and Sintered Elemental Ti--6 Al--4 V Powder Compacts," *Powder Metallurgy of Titanium Alloys*, pp. 189-202, 1980.

[86] I. Robertson and G. Schaffer, "Comparison of sintering of titanium and titanium hydride powders," *Powder metallurgy*, vol. 53, pp. 12-19, 2010.

[87] T. Watanabe and Y. Horikoshi, "The sintering phenomenon of titanium powders- A discussion," *International Journal of Powder Metallurgy and Powder Technology*, vol. 12, pp. 209-214, 1976.

[88] P. Andersen, V. Svoyatytsky, F. Froes, Y. MAHAJA, and D. Eylon, "Fracture behavior of blended elemental P/M titanium alloys," *Modern developments in powder metallurgy.*, vol. 13, pp. 537-549, 1981.

[89] H. T. Wang, M. Lefler, Z. Zak Fang, T. Lei, S. M. Fang, J. M. Zhang, *et al.*, "Titanium and Titanium Alloy via Sintering of TiH2," *Key Engineering Materials*, vol. 436, pp. 157-163, 2010.

[90] D. Konitzer, H. Fraser, and B. Muddle, "Formation and thermal stability of an oxide dispersion in a rapidly solidified Ti-Er alloy," *Scr. Metall.;(United States)*, vol. 17, 1983.

[91] B. Wang, "Effect of rare earth elements on the microstructures and properties of powder metallurgical titanium alloys," MSE Thesis, Central South University, Changsha, 2011.

[92] B. B. Rath, B. A. MACDONALD, and S. M. L. SASTRY, "influnce of erbium and yttrium additions on the microstructure and mechanical properties of titanium alloys," *Titanium '80 Science & Technology* vol. 2, pp. 1185-1196, 1980.

[93] P.-Y. Lee, C.-J. Yao, J.-S. Chen, L.-Y. Wang, R.-R. Jeng, and Y.-L. Lin, "Preparation and thermal stability of mechanically alloyed Cu–Zr–Ti–Y amorphous powders," *Materials Science and Engineering: A*, vol. 375, pp. 829-833, 2004.

[94] C. R. Whitsett, S. M. S. Sastry, J. E. O'Neal, and R. J. Lederich, "Influence of Rare-Earth Additions on Properties of Titanium Alloys Microstructures and Room-Temperature Tensile Properties of Ti-6A1-4V with Yttrium, Erbium, and Mischmetal Additions.," *Technical rept*, vol. 1, pp. 76-77, 1977.

[95] R. Tang and R. Tian, *ER YUAN HE JIN XIANG TU JI ZHONG JIAN XIANG JIN TI JIE GOU* Changsha: Press of Central South University, 2009.

[96] P. Trivedi, S. Patankar, F. Froes, E. Baburaj, A. Genç and L. Ovecoglu, "Grain-size control in Ti-48Al-2Cr-2Nb with yttrium additions," *Metallurgical and Materials Transactions A*, vol. 33, pp. 2729-2736, 2002.

[97] Y. Wu, K. Hagihara, and Y. Umakoshi, "Influence of Y-addition on the oxidation behavior of Al-rich γ-TiAl alloys," *Intermetallics*, vol. 12, pp. 519-532, 2004.

[98] Y. Chen, F. Kong, J. Han, Z. Chen, and J. Tian, "Influence of yttrium on microstructure, mechanical properties and deformability of Ti–43Al–9V alloy," *Intermetallics,* vol. 13, pp. 263-266, 2005.

[99] Y. Ke, H. Duan, and Y. Sun, "Effect of yttrium and erbium on the microstructure and mechanical properties of Ti–Al–Nb alloys," *Materials Science and Engineering: A,* vol. 528, pp. 220-225, 2010.

[100] Y. Wu, S. Hwang, and J. Morris, "Development and elemental powder metallurgy of a Y-containing two-phase TiAl alloy," *Metallurgical and Materials Transactions A,* vol. 34, pp. 2077-2087, 2003.

[101] J. Deng, Z. WU, g. yang, and d. Chen, "An advanced elevated temperature titanium alloy modified by a rare earth element," *Journal of Aeronautical Materials,* vol. 10, pp. 1-7, 1990.

[102] V. De Castro, T. Leguey, A. Muñoz, M. Monge, and R. Pareja, "Microstructure and tensile properties of Y< sub> 2</sub> O< sub> 3</sub>-dispersed titanium produced by arc melting," *Materials Science and Engineering: A,* vol. 422, pp. 189-197, 2006.

[103] W. Cui, C. Liu, L. Zhou, and G. Luo, "Characteristics of microstructures and second-phase particles in Y-bearing Ti-1100 alloy," *Materials Science and Engineering: A,* vol. 323, pp. 192-197, 2002.

[104] W. Lu, L. Xiao, D. Xu, J. Qin, and D. Zhang, "Microstructural characterization of Y< sub> 2</sub> O< sub> 3</sub> in< i> in situ</i> synthesized titanium matrix composites," *Journal of alloys and compounds,* vol. 433, pp. 140-146, 2007.

[105] A. Cooper and L. Eaton, "Compaction behavior of several ceramic powders," *Journal of the American Ceramic Society,* vol. 45, pp. 97-101, 1962.

[106] H. Ellingham, "Reducibility of oxides and sulfides in metallurgical processes," *J Soc Chem Ind,* vol. 63, pp. 125-133, 1944.

[107] S. Sastry, J. O'neal, R. Lederch, and B. Rath, "The effect of yttrium and erbium dispersoids on the deformation behaviour of titanium," *Journal of Materials Science,* vol. 14, pp. 179-183, 1979.

[108] S. M. Sastry, T. Peng, and L. Beckerman, "Structure and properties of rapidly solidified dispersion strengthened titanium alloys: Part II. tensile and creep properties," *Metallurgical and Materials Transactions A,* vol. 15, pp. 1465-1474, 1984.

[109] S. Naka, M. Marty, and H. Octor, "Oxide-dispersed titanium alloys Ti-Y prepared with the rotating electrode process," *Journal of Materials Science,* vol. 22, pp. 887-895, 1987.

[110] C. Perrier, S. Naka, and L. Kubin, "Plastic deformation behaviour of rapidly solidified Ti-Y alloys below 700oC," *Scripta metallurgica,* vol. 23, pp. 477-482, 1989.

[111] S. Naka, L. Kubin, and C. Perrier, "The plasticity of titanium at low and medium temperatures," *Philosophical Magazine A,* vol. 63, pp. 1035-1043, 1991.
[112] S. Naka, H. Octor, E. Bouchaud, and T. Khan, "Reprecipitation observed in Y2O3-dispersed titanium during heat treatment after cold rolling," *Scripta metallurgica,* vol. 23, pp. 501-505, 1989.
[113] J. Lofvander, R. Kirchheim, and H. Fraser, "Thermal stability of rare-earth oxides in Ti when annealed above the α/β transus," *Scripta metallurgica,* vol. 21, pp. 859-861, 1987.
[114] D. Konitzer, B. Muddle, and H. Fraser, "A comparison of the microstructures of as-cast and laser surface melted Ti-8Al-4Y," *Metallurgical and Materials Transactions A,* vol. 14, pp. 1979-1988, 1983.
[115] D. Konitzer, J. Stanley, M. Loretto, and H. Fraser, "The nature of dispersed phases in Ti-0.7 at.% Er prepared by rapid solidification processing," *Acta Metallurgica,* vol. 34, pp. 1269-1277, 1986.
[116] Z. Yang, W. Lu, L. Zhao, J. Qin, and D. Zhang, "Microstructure and mechanical property of in situ synthesized multiple-reinforced (TiB+ TiC+ La< sub> 2</sub> O< sub> 3</sub>)/Ti composites," *Journal of alloys and compounds,* vol. 455, pp. 210-214, 2008.
[117] D. Xu, W. Lu, Z. Yang, J. Qin, and D. Zhang, "In situ technique for synthesizing multiple ceramic particulates reinforced titanium matrix composites (TiB+ TiC+ Y_2O_3)/Ti," *Journal of alloys and compounds,* vol. 400, pp. 216-221, 2005.
[118] Y. Wu and S. Hwang, "The effect of yttrium on microstructure and dislocation behavior of elemental powder metallurgy processed TiAl-based intermetallics," *Materials Letters,* vol. 58, pp. 2067-2072, 2004.
[119] Y. Wu and S. Hwang, "Microstructural refinement and improvement of mechanical properties and oxidation resistance in EPM TiAl-based intermetallics with yttrium addition," *Acta materialia,* vol. 50, pp. 1479-1493, 2002.
[120] M. Aindow, H. FRASER, K. CHAUDHURI, and S. DAS, "On the influence of stoichiometry and purity on the deformation mechanisms in the intermetallic compound TiAl," *Scripta Metallurgica et Materialia,* vol. 24, pp. 1105-1108, 1990.
[121] V. Vasudevan, P. Kurath, and H. Fraser, "Effect of grain size and temperature on the yield stress of the intermetallic compound TiAl," *Scripta metallurgica,* vol. 23, pp. 467-469, 1989.
[122] Y. Wu, S. Hwang, S. Nam, and N. Kim, "The effect of yttrium addition on the oxidation resistance of EPM TiAl-based intermetallics," *Scripta Materialia,* vol. 48, pp. 1655-1660, 2003.
[123] Y. Wu, S. K. Hwang, and Y. Umakoshi, "High-temperature oxidation behavior of elemental powder metallurgy processed TiAl-Mn-Mo-C alloys

with yttrium addition," *Materials transactions*, vol. 45, pp. 1272-1281, 2004.
[124] S. J. Gerdemann and P. D. Jablonski, "Compaction of Titanium Powders," *Metallurgical and Materials Transactions A*, vol. 42, pp. 1325-1333, 2011.
[125] J. Lou, B. Gabbitas, and D. L. Zhang, "The Effects of Lubrication on the Density Gradient of Titanium Powder Compacts," *Key Engineering Materials*, vol. 551, pp. 86-91, 2013.
[126] M. Qian, G. Schaffer, and C. Bettles, "Sintering of titanium and its alloys Fang, ZZ," in *Sintereing of advanced materials: fundamentals and processes*, Z. S. o. a. m. f. a. p. Fang, Ed., ed Philadelphia: Woodhead, 2010, pp. 324-355.
[127] D. J. Green, O. Guillon, and J. Rödel, "Constrained sintering: A delicate balance of scales," *Journal of the European Ceramic Society*, vol. 28, pp. 1451-1466, 2008.
[128] E. Olevsky and R. German, "Effect of gravity on dimensional change during sintering—I. Shrinkage anisotropy," *Acta materialia*, vol. 48, pp. 1153-1166, 2000.
[129] O. Guillon, L. Weiler, and J. Rödel, "Anisotropic Microstructural Development During the Constrained Sintering of Dip‐Coated Alumina Thin Films," *Journal of the American Ceramic Society*, vol. 90, pp. 1394-1400, 2007.
[130] A. Evans, "Considerations of inhomogeneity effects in sintering," *Journal of the American Ceramic Society*, vol. 65, pp. 497-501, 1982.
[131] I. Cristofolini, C. Menapace, M. Cazzolli, A. Rao, W. Pahl, and A. Molinari, "The effect of anisotropic dimensional change on the precision of steel parts produced by powder metallurgy," *Journal of Materials Processing Technology*, vol. 212, pp. 1513-1519, 2012.
[132] D. Ravi and D. J. Green, "Sintering stresses and distortion produced by density differences in bi-layer structures," *Journal of the European Ceramic Society*, vol. 26, pp. 17-25, 2006.
[133] S. E. Schoenberg, D. J. Green, A. E. Segall, G. L. Messing, A. S. Grader, and P. M. Halleck, "Stresses and distortion due to green density gradients during densification," *Journal of the American Ceramic Society*, vol. 89, pp. 3027-3033, 2006.
[134] J. Lou, Y. Li, H. He, and L. Li, "Effect of atomisation medium on sintering properties of austenitic stainless steel by eliminating influence of particle shape and particle size," *Powder metallurgy*, vol. 53, pp. 112-117, 2010.
[135] F. Lange, "Processing‐Related Fracture Origins: I, Observations in Sintered and Isostatically Hot‐Pressed A12O3/ZrO2 Composites," *Journal of the American Ceramic Society*, vol. 66, pp. 396-398, 1983.

[136] A. T. Sidambe, F. Derguti, and I. Todd, "Metal Injection Moulding of Low Interstitial Titanium," *Key Engineering Materials,* vol. 520, pp. 145-152, 2012.

[137] I. Robertson and G. Schaffer, "Review of densification of titanium based powder systems in press and sinter processing," *Powder metallurgy,* vol. 53, pp. 146-162, 2010.

[138] M. Yan, Y. Liu, Y. Liu, C. Kong, G. Schaffer, and M. Qian, "Simultaneous gettering of oxygen and chlorine and homogenization of the β phase by rare earth hydride additions to a powder metallurgy Ti-2.25 Mo-1.5 Fe alloy," *Scripta Materialia,* vol. 67, pp. 491-494, 2012.

[139] M. Yan, Y. Liu, G. Schaffer, and M. Qian, "In situ synchrotron radiation to understand the pathways for the scavenging of oxygen in commercially-pure Ti and Ti-6Al-4V by yttrium hydride," *Scripta Materialia,* pp. 63-66, 2012.

[140] R. Low, M. Qian, and G. Schaffer, "Sintering of Titanium with Yttrium Oxide Additions for the Scavenging of Chlorine Impurities," *Metallurgical and Materials Transactions A,* vol. 43, pp. 5271-5278, 2012.

[141] Y. Yang, S. Luo, G. Schaffer, and M. Qian, "Impurity scavenging, microstructural refinement and mechanical properties of powder metallurgy Titanium and Titanium Alloys by a small addition of cerium Silicide," *Materials Science and Engineering: A,* pp. 166-174, 2013.

[142] H. He, Y. Li, X. Liang, and J. Zeng, "Effect of Neodymium Addition on Microstructure and Mechanical Properties of MIM Titanium," presented at the Proceedings of the PM2010 Powder Metallurgy World Congress, Florence, Italy, 2010.

[143] V. De Castro, T. Leguey, A. Muñoz, M. Monge, and R. Pareja, "Microstructure and tensile properties of Y_2O_3 dispersed titanium produced by arc melting," *Materials Science and Engineering: A,* vol. 422, pp. 189-197, 2006.

[144] G. Schaffer, T. Sercombe, and R. Lumley, "Liquid phase sintering of aluminium alloys," *Materials Chemistry and Physics,* vol. 67, pp. 85-91, 2001.

[145] Y. Ozaki, S. Uenosono, and K. Ogura, "An analysis of compaction behaviors of iron powder during warm compaction," *ADVANCES IN POWDER METALLURGY AND PARTICULATE MATERIALS,* vol. 1, pp. 2-109, 1999.

[146] Z. Razavi Hesabi, H. Hafizpour, and A. Simchi, "An investigation on the compressibility of aluminum/nano-alumina composite powder prepared by blending and mechanical milling," *Materials Science and Engineering: A,* vol. 454, pp. 89-98, 2007.

[147] J. Liu and P. David, "Particle rearrangement during powder compaction," *Metallurgical and Materials Transactions A,* vol. 32, pp. 3117-3124, 2001.

[148] R. M. German and M. Bulger, "A model for densification by sintering of bimodal particle size distributions," *International journal of powder metallurgy,* vol. 28, pp. 301-311, 1992.

[149] R. F. Boyer and E. Collings, *Materials properties handbook: titanium alloys*: ASM international, 1994.